

# A Modern Study of Extended Objects in Conformal Field Theory

Dissertation  
zur Erlangung des Doktorgrades  
an der Fakultät für Mathematik, Informatik und Naturwissenschaften  
Fachbereich Physik  
der Universität Hamburg

vorgelegt von

Philine Julia van Vliet

Hamburg

2023

Gutachter der Dissertation:

Dr. Pedro Liendo  
Prof. Dr. Timo Weigand

Zusammensetzung der Prüfungskommission:

Dr. Pedro Liendo  
Prof. Dr. Timo Weigand  
Prof. Dr. Gleb Arutyunov  
Dr. Juliette Simonet  
Prof. Dr. Sven-Olaf Moch

Vorsitzender der Prüfungskommission:

Prof. Dr. Sven-Olaf Moch

Datum der Disputation:

25. Juli 2023

Vorsitzender des Fach-Promotionsausschusses PHYSIK:

Prof. Dr. Günter H. W. Sigl

Leiter des Fachbereichs PHYSIK:

Prof. Dr. Wolfgang J. Parak

Dekan der Fakultät MIN:

Prof. Dr.-Ing. Norbert Ritter

# Abstract

Conformal Field Theories (CFTs) are ubiquitous in modern theoretical physics and play an important role in high-energy physics and condensed matter physics alike, describing the universal behavior of second-order phase transitions. The notion of a CFT can be generalized by introducing extended objects, or *defects*. These defects, breaking part of the conformal symmetry, give access to new observables, and provide interesting new dynamics. Conformal defects are those that preserve conformal symmetry on the defect, and can be studied with similar methods employed to study CFTs without extended objects. In particular, one can use well-known perturbative methods such as the  $\varepsilon$ -expansion to compute critical exponents, or employ a modern approach and use the conformal bootstrap to constrain bulk and defect CFT data. In this thesis we study a plethora of conformal defects, ranging from highly constraining supersymmetric setups to physical and experimentally realizable setups without supersymmetry, including interactions between scalars and fermions. We will use the  $\varepsilon$ -expansion and the conformal bootstrap, and in this way combine the old and the new.

# Zusammenfassung

Konforme Feldtheorien (KFT) sind allgegenwärtig in der moderne theoretischen Physik und spielen eine wichtige Rolle in der Hoch-Energiephysik und der Physik der kondensierten Materie, da sie das Universalverhalten von Phasenübergängen zweiter Ordnung beschreiben. Die Einführung von ausgedehnten Objekten, oder *Defekten*, generalisieren den Begriff einer konformen Feldtheorie. Solche Defekte gewähren uns Zugang zu neuen Messgrößen und bieten eine interessante, neue Dynamik, weil sie Teile der konformen Symmetrie brechen. Konforme Defekte sind Defekte, die die konforme Symmetrie auf dem Defekt erhalten. Um sie zu studieren, können ähnliche Methoden wie im Studium der KFTs ohne ausgedehnte Objekte verwendet werden. Vor allem kann man bekannte störungsbezogene Methoden, wie die  $\varepsilon$ -Expansion zur Berechnung der kritischer Exponenten, oder moderne Ansätze, zum Beispiel den konforme Bootstrap um Gros und Defekt KFT Daten einzuschränken, verwenden. In dieser Arbeit studieren wir eine Fülle von konformen Defekten, angefangen bei sehr einschränkenden, supersymmetrischen Modellen bis zu physischen und experimentell realisierbaren Modellen ohne Supersymmetrie mit Interaktionen zwischen skalaren und fermionischen Feldern. Wir benutzen die  $\varepsilon$ -Expansion und den konformen Bootstrap um auf diese Weise das Alte und Neue zu kombinieren.

It is invaluable to have a friend who  
shares your interests and helps you  
stay motivated

---

Maryam Mirzakhani

## Acknowledgments

A PhD thesis cannot be completed alone, and I would like to thank all the people who helped me the past four years and long before that.

Firstly, I am greatly indebted to my supervisor, Pedro Liendo, for his support during my PhD. Thank you for the many enlightening discussions and chats, for encouraging me to ask any question and share my ideas, and for teaching me to go from student to independent scientist. I am also grateful to my cosupervisor Volker Schomerus, for his support and inspiring discussions, and my Master supervisor Robert Fleischer, for his continued support and advice during the PhD.

Secondly, I want to thank my collaborators, Aleix, Ilija, Julien, Apratim, and Edo, from whom I have learned a lot. I had a great time working together so far, and am looking forward to continue that. My time at DESY wouldn't have been the same without my fellow students and postdocs in the group. I have had the pleasure to get to know both the "old" and the "new" cohort as colleagues and as friends. A PhD at DESY would not be complete without all the dinners at Samarkand, nice afternoons in the park, or evenings spent around the pool table or dancing.

I also want to thank my friends, both the ones from (long) before and the ones made during my PhD. Studying and working, even on such an interesting topic as the one of this thesis, is not the only thing in life and I am grateful for all the necessary distractions. I hope we will continue to spend many days and nights dancing, talking, drinking wine, and discussing physics, politics, literature, and the latest gossip. A special thank you to Yashoj, for getting me out of bed and keeping me active with early morning tennis sessions. See you at Roland Garros!

I would like to thank my family; my parents and my sister, for always supporting my plans and ideas, and for helping me become who I am today.

A special place in my heart is reserved for all the strong, independent women in my life: Jorinde, Anniek, Melin, Kendra, Astrid, Sophie, Tjaša, Lena, Lea, Marijn, Sylvia, and Sanne. Thank you for being there to celebrate and laugh and enjoy the highlights. And for being there to offer support, a place to rant, and inspiration during more difficult times.

And last but not least, thank you Kristian. Without your love (and the morning coffees) I would have had a significantly worse time getting through these four years. Thank you for all your support and for brightening my days. Tusen tak, kjaeresten min.

## Statement of Originality

This thesis is based on the following publications:

- A. Gimenez-Grau, P. Liendo, and P. van Vliet, *Superconformal boundaries in  $4 - \epsilon$  dimensions*, *JHEP* **04** (2021) 167, [[arXiv:2012.00018](#)].
- A. Gimenez-Grau, E. Lauria, P. Liendo, and P. van Vliet, *Bootstrapping line defects with  $O(2)$  global symmetry*, *JHEP* **11** (2022) 018, [[arXiv:2208.11715](#)].
- J. Barrat, P. Liendo, and P. van Vliet, *Line defect correlators in fermionic CFTs*, [arXiv:2304.13588](#).

All authors contributed equally to the above publications.

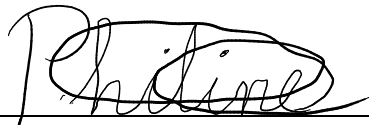
Other papers by the author not included in this thesis are:

- K. De Bruyn, F. Fleischer, M. Malami, and P. van Vliet, *Studies of New Physics in  $B_q^0 - \bar{B}_q^0$  Mixing and Implications for Leptonic Decays*, *8th Symposium on Prospects in the Physics of Discrete Symmetries* (2023), [[arXiv:2301.13649](#)].
- K. De Bruyn, F. Fleischer, M. Malami, and P. van Vliet, *New physics in  $B_q^0 - \bar{B}_q^0$  mixing: present challenges, prospects, and implications for  $B_q^0 \rightarrow \mu^+ \mu^-$* , *J. Phys. G* **50** (2023) 04, [[arXiv:2208.14910](#)].

## **Eidesstattliche Versicherung / Declaration on oath**

Hiermit versichere ich an Eides statt, die vorliegende Dissertationsschrift selbst verfasst und keine anderen als die angegebenen Hilfsmittel und Quellen benutzt zu haben.

Hamburg, den 24. Mai 2023

A handwritten signature in black ink, appearing to read 'Christine', written over a horizontal line.

Unterschrift der Doktorandin / des Doktoranden

# Contents

<b>1</b>	<b>Introduction</b>	<b>1</b>
1.1	Conformal defects . . . . .	4
1.2	Layout of the thesis . . . . .	6
<b>2</b>	<b>Conformal Field Theory</b>	<b>7</b>
2.1	Conformal Algebra . . . . .	7
2.2	Conformal kinematics . . . . .	11
2.3	The $\varepsilon$ -expansion . . . . .	14
2.4	Conformal bootstrap . . . . .	17
<b>3</b>	<b>Conformal defects</b>	<b>23</b>
3.1	Defect algebra . . . . .	23
3.2	Defect kinematics . . . . .	25
3.3	Defects in the $\varepsilon$ -expansion . . . . .	28
3.4	Defect bootstrap . . . . .	29
<b>4</b>	<b>Superconformal boundaries in <math>4 - \varepsilon</math> dimensions</b>	<b>33</b>
4.1	Introduction . . . . .	33
4.2	Preliminaries . . . . .	35
4.3	Boundaries in three dimensions . . . . .	38
4.4	Boundaries across dimensions . . . . .	50
4.5	Wess-Zumino model with a boundary . . . . .	61
<b>5</b>	<b>Bootstrapping line defects with <math>O(2)</math> global symmetry</b>	<b>69</b>
5.1	Introduction . . . . .	69
5.2	Line defects with global symmetry . . . . .	71
5.3	Defect theories in the $\varepsilon$ -expansion . . . . .	76
5.4	Numerical results . . . . .	88
<b>6</b>	<b>Line defect correlators in fermionic CFTs</b>	<b>103</b>
6.1	Introduction . . . . .	103
6.2	Yukawa CFTs with a line defect . . . . .	105
6.3	Correlators of defect operators . . . . .	109
6.4	Correlators of bulk operators with a defect . . . . .	121
<b>7</b>	<b>Conclusion</b>	<b>131</b>

<b>A</b>	<b>Details on three-dimensional boundaries</b>	<b>135</b>
A.1	Conventions . . . . .	135
A.2	Superconformal algebra . . . . .	135
A.3	Differential operators . . . . .	136
<b>B</b>	<b>Non-supersymmetric conformal blocks</b>	<b>137</b>
B.1	Two-point function . . . . .	137
B.2	Three-point bosonic blocks . . . . .	138
<b>C</b>	<b>More on blocks across dimensions</b>	<b>139</b>
<b>D</b>	<b>More data on the <math>O(N)</math> monodromy defect in 3d</b>	<b>141</b>
D.1	OPE coefficients with the displacement operator . . . . .	141
D.2	The leading singlet . . . . .	143
<b>E</b>	<b>Crossing vectors for <math>O(2)</math> line defects</b>	<b>145</b>
E.1	One complex scalar . . . . .	145
E.2	Tilt and displacement . . . . .	145
E.3	One real and one complex scalar . . . . .	146
E.4	Two complex scalars . . . . .	147
<b>F</b>	<b>Spinor conventions</b>	<b>149</b>
<b>G</b>	<b>More details on the <math>\beta</math>-functions for Yukawa CFTs</b>	<b>151</b>
G.1	Gross–Neveu–Yukawa model ( $N = 1$ ) . . . . .	152
G.2	Nambu–Jona-Lasinio–Yukawa model ( $N = 2$ ) . . . . .	153
G.3	Chiral Heisenberg model ( $N = 3$ ) . . . . .	154
<b>H</b>	<b>Integrals</b>	<b>157</b>



# Chapter 1

## Introduction

There is a natural distinction between long-distance (low energy) and short-distance (high energy) physics in theoretical physics. Low-energy physics is the domain of condensed matter physics, of effective field theories, and materials that often exhibit remarkable behavior. On the other side, high-energy physics encaptures fundamental interactions between elementary particles, string theory, and other theories of quantum gravity. A bridge between these two domains is formed by the Renormalization Group (RG) flow of Quantum Field Theories (QFTs). QFTs are evaluated at different energy scales, and coupling constants in the theory evolve or “run” with these energies. As such, the RG flow describes physics between the UV (high energy) and the IR (low energy).

The term *Renormalization Group flow* first appeared in a paper in 1955 by Bogoliubov and Shirkov [1], following earlier pioneering work by Stückelberg and Petermann, and Gell-Mann and Low [2, 3]. However, it was Kenneth Wilson who solidified the approach, and gave a more physical meaning to the abstract concept of renormalizing quantum field theories [4]. The RG flows of QFTs start or end in fixed points, which correspond to scale-invariant theories [4, 5]. These theories are in general also invariant under *special conformal symmetry*, which preserves the angles in a theory, and the fixed point corresponds to a *conformal field theory* (CFT).<sup>1</sup> CFTs describe second-order, continuous phase transitions, for which the correlation length goes to infinity. The requirement of scale and conformal invariance severely constrains the form of correlation functions between different operators. In particular, higher-point correlation functions are related to lower-point correlation functions through the Operator Product Expansion (OPE), and one considers a CFT to be “solved” if one knows its entire spectrum and the normalization of the three-point correlation functions. While not an easy task, this is already a simplification with respect to QFTs, where the OPE is not exact, and one would need to compute all correlation functions individually. In this way, CFTs can be a gateway to a better understanding of QFTs.

A well-known example is the conformal window of QCD. QCD is famously hard to solve, and it is hard to obtain reliable predictions through perturbative methods due to the strong coupling constant at low energies. Various nonperturbative techniques, the most well-established one being lattice QCD, have been used over the years to tackle this problem. Together with methods to improve perturbative studies of QCD, they

---

<sup>1</sup>The question whether scale invariance implies conformal invariance is an interesting and longstanding problem. Proof in  $2d$  was provided in [6], but counterexamples are also known, e.g. [7]. In higher dimensions, under certain assumptions such as unitarity, Poincaré invariance, a discrete spectrum, unbroken scale invariance in the vacuum, and the existence of a scale current, it seems that scale invariance implies conformal invariance and to date, no counterexamples have been found. See for a review [8].

have led to a greatly improved understanding of QCD. In addition, there is a “window” for a certain number of fermions  $N_f$ , given a certain amount of colors  $N_c$ , in which the theory becomes conformally invariant [citation!](#). Here, it is possible to use nonperturbative methods specific to CFTs and one might hope to gain even more insight in the full theory of QCD.

In condensed matter the examples of CFTs corresponding to interesting and often surprising behavior of materials, are ubiquitous. The most famous one is the critical point of water or other liquids, which exhibits *critical opalescence*, leading to the liquid becoming luminous. The CFT describing this phase transition, the critical point of the famous  $3d$  Ising model, also describes the second-order phase transition of ferromagnets at the Curie point. It is said that these phase transitions belong to the same *universality class*, and it becomes clear that the same underlying CFT can describe vastly different physical systems. The behavior of fields or operators and their correlation functions in the critical point are the same, and are given by *critical exponents*, e.g. the susceptibility exponent, the magnetisation exponent, or the specific heat exponent. These are related to CFT quantities such as conformal dimensions of operators and the dimension  $d$  of the CFT itself. Throughout this thesis, we encounter different examples of universality classes besides the  $3d$  Ising model, such as the  $O(N)$  CFTs, the Yukawa CFTs, and the Wess-Zumino CFTs. Distinctions between these universality classes of CFTs are given by e.g. the number of fundamental fields (scalars, fermions or gauge fields) in the theory, or the number of dimensions the theory is defined in. When studying CFTs, in general a distinction is made between CFTs in one dimension, CFTs in two dimensions, and CFTs in higher dimensions. In this thesis, we focus on CFTs in  $d > 2$ , however  $1d$  CFTs will appear as conformal line defects. They are further discussed in section 2.2.4.

CFTs can be studied either perturbatively or nonperturbatively. Perturbative approaches rely on the existence of a small parameter to expand in. In a scale invariant theory, it is sometimes difficult to find such a parameter. However, there are a few expansions that are often considered in the context of CFTs. Examples are the large- $N$  expansion, the weak coupling expansion, and the  $\varepsilon$ -expansion, where we deform the number of dimensions  $d$  in which the CFT is evaluated by a (small) parameter  $\varepsilon$ . In this thesis we use the  $\varepsilon$ -expansion to study CFTs across dimensions, and focus on CFTs with an upper critical dimension  $d = 4$ , such as the Ising model or  $\phi^4$  theory, and the  $O(N)$  models, for which perturbative results are known up to 7-loop order [9]. There are other well-studied CFTs whose upper critical dimension is higher, e.g. the Yang-Lee edge singularity with  $d_c = 6$ , corresponding to  $\phi^3$  theory, or lower, e.g. the purely fermionic Gross-Neveu or Nambu-Jona-Lasinio models with  $d_c = 2$ .

The  $d = 4 - \varepsilon$  expansion has a long history in QFT, and has been used in the context of *dimensional regularization* to renormalize theories such as QED and electroweak theories. There, one is interested in  $d = 4$  and the limit  $\varepsilon \rightarrow 0$  is taken after expanding in orders of  $\varepsilon$ . In the context of CFTs, it is often the  $3d$  physics that is the most interesting. Take again the example of the Ising model, which is a free theory in  $d = 4$  (its upper-critical dimension), but becomes interacting in  $d = 4 - \varepsilon$ . The corresponding fixed point is the famous Wilson-Fisher fixed point [10], proportional to  $\lambda \sim \mathcal{O}(\varepsilon)$ . In this case, we would like to set  $\varepsilon \rightarrow 1$ , which of course brings up the question of convergence of the perturbative expansion. The general technique of computing critical exponents in the  $\varepsilon$ -expansion and concerns like these will be discussed later in this thesis. There are many known interacting, conformal fixed points in the  $\varepsilon$ -expansion. Other well-known examples are the Wess-Zumino fixed point for superconformal Wess-Zumino models [11],

the Banks–Zaks fixed point for nonabelian CFTs such as conformal QCD [12], and the Wilson–Fisher–Yukawa fixed points for CFTs with scalar-fermion interactions. We will encounter some of them later in this thesis.

Although perturbative expansions give us a good grasp on the theory, some properties only become apparent in nonperturbative studies and some CFTs can only be studied nonperturbatively due to being strongly interacting/coupled. Nonperturbative results can in addition be used to compare with perturbative calculations, and can lead to an intriguing interplay between the two. Nonperturbative techniques for CFTs include e.g. Monte Carlo simulations, lattice calculations, and the conformal bootstrap. Monte Carlo simulations are an excellent way to study strongly coupled many-body systems, and with the advancement of computer power can obtain very precise results for various observables and critical exponents. One is not necessarily restricted to the critical point and can study a larger domain of phase transitions. Studying QFTs on a lattice is a widely applied technique in high-energy physics, and allows one to study strongly coupled theories such as QCD. For CFTs, they are mostly used to study them in two dimensions. In 1944, this method was used by Onsager to solve the  $2d$  Ising model [13].

The conformal bootstrap on the other hand is a method specifically tailored to CFTs. The idea is to constrain CFTs by only making use of their symmetry properties and a handful of assumptions such as associativity of the OPE, and sometimes unitarity, but to remain agnostic about microscopic details of the theory. By using this minimal input, one can then “pull oneself up by the bootstraps” and either constrain the space of possible CFTs, or determine critical exponents of a particular CFT of interest. This method is fully nonperturbative, and can also be applied to CFTs without a Lagrangian description. The conformal bootstrap, already formulated in the ’70s [14, 15], booked its first great success in 2 dimensions, when in 1984 the authors of [16] used it to solve a set of  $2d$  CFTs called the *minimal models*. However,  $2d$  CFTs are invariant under the severely constraining, infinite Virasoro algebra, while this algebra is not present in  $d > 2$ . In particular, the minimal models in two dimensions have a finite number of Virasoro primaries, operators from which all other operators can be constructed as infinite towers of descendants, while the number of conformal primaries is infinite in CFTs in  $d > 2$ . Hence, it proved more difficult to bootstrap interacting CFTs in higher dimensions and additional approaches and techniques were required. The first breakthrough for higher-dimensional CFTs came in 2008 [17], where they numerically computed bounds on conformal dimensions in four-dimensional CFTs. Since then, there has been a lot of developments, both in the numerical and the analytic conformal bootstrap.

The numerical conformal bootstrap has known great successes in determining conformal data to high precision in the last decade. A milestone was the Ising model “kink”: a feature in the numerical bound on the dimension of the lowest-lying operator in a scalar CFT in  $3d$ , that corresponds to the interacting  $3d$  Ising CFT [18]. The state-of-the-art for the numerical bootstrap nowadays is very precise *islands* for the Ising model and other  $O(N)$  models [19, 20], as well as for other CFTs [21, 22]. The precision has reached a point where it competes or surpasses other methods to study CFTs, and it can be used as an independent source to solve discrepancies between for example Monte Carlo studies and experiment, as was done in the case of the  $O(2)$  model [23].

The analytic conformal bootstrap for  $d > 2$  is generally considered to have started a few years later, in 2012, with the two works [24, 25]. Here, it was shown that there are families of operators parametrized by their spin, so-called *twist families* that exist in any CFT in  $d > 2$ . Another breakthrough came in 2017 with the work of Caron-Huot [26],

which introduced the *Lorentzian inversion formula*, neatly capturing and generalizing the analyticity in spin of the spectrum of CFTs. Other directions within the analytic conformal bootstrap include the large charge bootstrap [27, 28], analytic functionals [29–32], the Mellin space bootstrap [33–36], and the superconformal bootstrap for protected subsectors [37–39].

We cannot end our discussion of CFTs without mentioning the AdS/CFT correspondence [40]. It states that there is a one-to-one correspondence between quantities in Anti-de Sitter (AdS) spacetime in  $d + 1$  dimensions, and correlation functions in a  $d$ -dimensional CFT living on the boundary of the AdS space. The original setup was the large- $N$  superconformal field theory  $\mathcal{N} = 4$  SYM (with gauge group  $SU(N)$ ) in four dimensions on the boundary of  $\text{AdS}_5 \times S^5$ , where the bulk theory corresponds to type IIB string theory. Since then, the AdS/CFT correspondence has been established in many dimensions and extensively tested. It provides us with a way to understand quantum gravity if we have a good grasp on the CFT living on the boundary. The conformal algebra can be enhanced to a superconformal algebra by including supercharges, resulting in a *superconformal field theory* (SCFT). The addition of supersymmetry (SUSY) puts extra constraints on the CFT spectrum and on OPE coefficients of certain operators. On top of that, techniques such as localization can be used to compute SCFT data. We will not discuss SCFTs in the general introduction, but discuss a specific setup in section 4.

## 1.1 Conformal defects

Besides local operators, a CFT can contain extended operators or *defects*. These defects can break conformal symmetry in the bulk, relaxing the constraints on correlation functions of local operators. Hence, they provide access to observables which are normally hidden in CFTs, such as one-point functions of local operators in the presence of the defect, or the expectation value of the defect itself. Defects are important objects historically used to study confinement [41–43], to describe generalized symmetries [44], to investigate dualities between 4d gauge theories [45], and more. *Conformal defects* are a special class of defects which preserve a conformal subgroup on the defect. They can be studied perturbatively in various limits, similar to the bulk CFT. In this thesis the focus lies on the  $\varepsilon$ -expansion, where the defect can either change dimension with the bulk (fixed codimension), or have a fixed dimension while the codimension changes with  $\varepsilon$ . Both cases will be discussed later on in this thesis.

In addition, conformal defects can be included in the modern conformal bootstrap program, to extend it to the *defect bootstrap* [46, 47]. Using the defect bootstrap, one can constrain both bulk and defect CFT data in a nonperturbative way. The techniques that have been developed and used are similar to those of the conformal bootstrap, but there are some important differences that are highlighted in section 3.4. For example, even though a conformal symmetry group is preserved on the defect, the theory on the defect is not a local CFT due to the absence of a conserved stress-energy tensor. The breaking of the bulk conformal symmetry changes the kinematics of correlators of bulk operators in the presence of the defect, which has been developed in [48–52]. In particular, one can use the bootstrap to study two-point correlation functions of bulk operators, which are no longer fully fixed kinematically.

Defects also exist in superconformal field theories, and can either completely break or preserve part of the supersymmetry in the bulk. We can define the class of *superconformal*

defects as preserving a superalgebra on the defect. Often, one can have different superconformal defects in the same SCFT depending on which supercharges are left unbroken by the defect. We will see an example of this in chapter 4.

Conformal defects can be classified according to their dimension and codimension. *Boundaries* are codimension-1 objects and are somewhat special. They allow for only one defect cross-ratio, and do not admit transverse rotations, and thus operators do not have transverse spin. They have gotten a lot of attention in recent years [53–66], and have been studied for a variety of theories. In the two-dimensional minimal models, Cardy classified the conformal boundary conditions now known as Cardy boundary conditions [67]. Efforts to constrain the space of possible boundary theories in higher-dimensional bulk CFTs using the analytic defect bootstrap have also been made [56]. The boundary has also been studied using numerical bootstrap [68–70]. A closely related defect is the *interface*. Where the boundary only has a bulk CFT on one side and a trivial or non-physical theory on the other, the interface can connect two CFTs with each other. One can also study two boundaries or interfaces connected to each other, forming an edge [71, 72].

Higher-codimension defects can preserve transverse rotations in addition to conformal symmetry on the defect. A special class are *monodromy defects*, which are codimension-2 defects that can be interpreted as domain walls [73, 74]. Operators acquire a phase when going around the monodromy defect, resulting in fractional transverse spin. In the  $\varepsilon$ -expansion, since the codimension is fixed to  $q = 2$ , these defects change dimension with the bulk theory. Studies of these defects in the  $\varepsilon$ -expansion can be found in [75–79].

*Line defects* are one-dimensional defects of arbitrary codimension that can exist in any CFT with dimension  $d > 1$ . In  $d = 2$  they “coincide” with a boundary or interface. Since one-dimensional CFTs are non-local, the interpretation as conformal line defects comes very naturally. Well-known examples of conformal line defects in gauge theories are Wilson lines or loops [41]. They have been studied extensively in the literature, especially embedded in  $\mathcal{N} = 4$  SYM, where the conformal Wilson line or loop is dual to a string worldsheet in AdS<sub>2</sub> [80]. Another class are the localized magnetic field or pinning line defects, constructed by integrating over a scalar field [81–84]. These defects have been studied in the  $O(N)$  model [85–88] and generalized Yukawa CFTs [89–91]. Constraining line defects and one-dimensional CFTs using the modern conformal bootstrap has proven to be very successful in the case of  $\mathcal{N} = 4$  SYM due to the combination with integrability [92–94]. In addition the numerical bootstrap [95, 96, 85], and analytic bootstrap methods such as the inversion formula [97, 78, 98, 99] and analytic functionals [30, 32, 100, 101], have been used to study line defects and one-dimensional CFTs. They have also been tackled using perturbative techniques such as the  $\varepsilon$ -expansion or the large- $N$  expansion [84, 89, 90].

There are other defects with higher dimension and codimension. *Surface defects* are two-dimensional defects, which coincide with boundaries and interfaces in a  $3d$  CFT. They exist as an analog to the localized magnetic field line defect in the  $O(N)$  and Yukawa models in  $d = 4 - \varepsilon$ , where now a surface operator is inserted in a CFT in  $d = 6 - \varepsilon$  dimensions [102–105]. In the context of the AdS/CFT correspondence, they are dual to branes in different AdS backgrounds. In  $4d$  gauge theories they are studied in connection with the geometric Langlands program [106, 107]. Superconformal surface defects can also be defined in  $6d \mathcal{N} = (2, 0)$  theories [108], where notably, one can define another type of superconformal defect with codimension two [109]. These types of defects will not play a role in this thesis, with the exception of the monodromy defect, which is defined as a surface defect in  $4d$ .

There are many applications of conformal defects in different areas of theoretical physics. In the context of string theory and holography, they are related to D-branes and boundaries of open strings. They appear in the context of quantum information theory; codimension-2 twist defects in  $n$  copies of a CFT can be used to study the so-called Rényi entropy [48]. In condensed matter, they correspond to (magnetic) impurities, or boundaries of topological insulators. An interesting point of view is also provided by their interpretation as theories with long-range interactions [110, 111].

## 1.2 Layout of the thesis

The aim of this thesis is to study extended objects in CFTs using several approaches. The “old” method of perturbative  $d = 4 - \varepsilon$  expansion will play a central role, as does the “new” method of nonperturbative conformal bootstrap. Combining the two gives us more powerful constraints, and the  $\varepsilon$ -expansion provides us with guidance in a nonperturbative bootstrap study. As we combine the old with the new, we also move through different theories and go from a controlled, supersymmetric setup to a more and more realistic setup that describes many interesting materials and phenomena in condensed matter.

This work is structured as follows. In chapter 2, we discuss aspects of CFTs necessary to understand the main results of this thesis. We focus on CFTs in general higher dimensions ( $d > 2$ ), but also comment on one-dimensional CFTs. Furthermore, the  $\varepsilon$ -expansion is discussed as a perturbative method to study CFTs. The final part of the section introduces the conformal bootstrap program, and shows how one can use either numerical or analytical techniques to study CFTs nonperturbatively.

Chapter 3 is dedicated to conformal defects, and explains how the conformal algebra and correlation functions of conformal primaries get modified in the presence of a defect. Several types of defects are discussed, and it is shown how they can be studied in the  $\varepsilon$ -expansion. The *defect conformal bootstrap* is introduced as an analog of the conformal bootstrap to study CFTs including defects. There are some important differences with respect to the bootstrap for CFTs without defects, which are pointed out at the end of this chapter.

After the review of these concepts, the main results of the thesis will be presented. In chapter 4 (appeared as [62]), we study 1/2-BPS superconformal boundaries in  $3d\mathcal{N} = 2$  superconformal field theories. We analytically continue one such boundary to  $d = 4 - \varepsilon$  dimensions, and bootstrap correlators of bulk chiral fields in the  $4 - \varepsilon$  expansion. Then, in chapter 5 (appeared as [85]), we study line defects with additional  $O(2)$  global symmetry using the numerical conformal bootstrap. We take two specific line defects to compare with our general results: a monodromy line defect and a localized magnetic field line defect. The latter can also appear in Yukawa-type theories, and is the subject of the work presented in chapter 6 (appeared as [91]). We study correlation functions of both bulk and defect operators for general Yukawa CFTs with  $N$  scalars and  $N_f$  fermions in the  $d = 4 - \varepsilon$  expansion. We expand several of the obtained correlators in conformal blocks to extract the conformal data. The thesis concludes with a summary, conclusion, and outlook in chapter 7.

# Chapter 2

## Conformal Field Theory

In this chapter we introduce conformal field theories in general higher dimensions  $d > 2$ . The chapter starts with a discussion of the conformal algebra in section 2.1, where the notion of *conformal primaries* is introduced. The state-operator correspondence and unitarity bounds are also treated in this section. Section 2.2 contains a review of the structure of correlation functions of conformal primaries, the Operator Product Expansion, and the construction of conformal blocks. We briefly comment on CFTs in one dimension at the end of this section.

CFTs can be studied perturbatively across dimensions using the  $\varepsilon$ -expansion. In section 2.3 some aspects of Renormalization Group (RG) techniques are reviewed using the example of  $\phi^4$  theory in  $d = 4 - \varepsilon$  dimensions; in three dimensions this model corresponds to the  $3d$  Ising model. We show how to compute various critical exponents for this model in the  $\varepsilon$ -expansion.

Section 2.4 is dedicated to a nonperturbative method to study CFTs: the conformal bootstrap. The crossing equations for four-point correlation functions of scalars are given and the two main approaches within the conformal bootstrap are discussed: the numerical bootstrap in section 2.4.2 and the analytic conformal bootstrap in section 2.4.3.

There are many excellent reviews and lecture notes on CFTs and the conformal bootstrap, which are more detailed and complete than the introduction given in this thesis, serving merely as an overview and a reminder of concepts used later on. For CFTs and the conformal bootstrap, see for example [112–115].

### 2.1 Conformal Algebra

The conformal symmetry group in  $d$  spacetime dimensions is  $SO(d + 1, 1)$  for Euclidean CFTs and  $SO(d, 2)$  for Lorentzian CFTs. In this thesis we work with Euclidean CFTs, but in some cases, such as when considering the *lightcone limit* introduced in section 2.4.3, the Lorentzian signature is preferred. The conformal group contains the Poincaré symmetry group of QFT generated by translations and rotations, and in addition to that, CFTs are scale invariant and invariant under special conformal transformations. The generators of these symmetries together form the conformal algebra, and can be found by solving the appropriate Killing equations.

### 2.1.1 Killing equations

A local QFT should satisfy the condition that the stress-energy tensor  $T_{\mu\nu}$  is conserved:

$$\partial_\mu T^{\mu\nu}(x) = 0, \quad (2.1.1)$$

as long as there are no other operator insertions. A local *CFT* requires a stronger condition on the stress-energy tensor, namely that it is not only conserved, but also traceless:

$$T^\mu{}_\mu = 0. \quad (2.1.2)$$

This can be interpreted as the theory being invariant under a local rescaling of the metric:

$$\delta g_{\mu\nu} = \omega(x)g_{\mu\nu}. \quad (2.1.3)$$

The demand of conservation and tracelessness of the stress-energy tensor results in the *conformal Killing equation*:

$$\partial_\mu \epsilon_\nu + \partial_\nu \epsilon_\mu = c(x)\delta_{\mu\nu}, \quad (2.1.4)$$

where  $c(x)$  is a scalar, position-dependent function. This equation has the following solutions for the Killing vectors  $\epsilon_\mu$ :

$$\begin{aligned} p_\mu &= \partial_\mu, \\ m_{\mu\nu} &= x_\nu \partial_\mu - x_\mu \partial_\nu, \\ d &= x_\mu \partial_\mu, \\ k_\mu &= 2x_\mu(x \cdot \partial) - x^2 \partial_\mu, \end{aligned} \quad (2.1.5)$$

which are respectively translations, rotations, dilatations and special conformal transformations.

### 2.1.2 Conformal algebra in general $d$

Each of the Killing vectors in eq. (2.1.5) corresponds to a conserved charge:

$$Q_\epsilon(\Sigma) = - \int_\Sigma dS_\mu \epsilon_\nu(x) T^{\mu\nu}(x). \quad (2.1.6)$$

These conserved charges are momentum  $\mathcal{P}_\mu$ , angular momentum  $\mathcal{M}_{\mu\nu}$ , scaling  $\mathcal{D}$ , and special conformal symmetry  $\mathcal{K}_\mu$ . Their commutation relations form the *conformal algebra*, which in general spacetime dimensions  $d$  can be written as follows:

$$\begin{aligned} [\mathcal{P}_\mu, \mathcal{K}_\nu] &= 2\mathcal{M}_{\mu\nu} - 2\mathcal{D}\delta_{\mu\nu}, \\ [\mathcal{D}, \mathcal{P}_\mu] &= \mathcal{P}_\mu, \\ [\mathcal{D}, \mathcal{K}_\mu] &= -\mathcal{K}_\mu, \\ [\mathcal{M}_{\mu\nu}, \mathcal{P}_\rho] &= \delta_{\nu\rho}\mathcal{P}_\mu - \delta_{\mu\rho}\mathcal{P}_\nu, \\ [\mathcal{M}_{\mu\nu}, \mathcal{K}_\rho] &= \delta_{\nu\rho}\mathcal{K}_\mu - \delta_{\mu\rho}\mathcal{K}_\nu, \\ [\mathcal{M}_{\mu\nu}, \mathcal{M}_{\rho\sigma}] &= \delta_{\nu\rho}\mathcal{M}_{\mu\sigma} - \delta_{\mu\rho}\mathcal{M}_{\nu\sigma} + \delta_{\nu\sigma}\mathcal{M}_{\rho\mu} - \delta_{\mu\sigma}\mathcal{M}_{\rho\nu}, \end{aligned} \quad (2.1.7)$$

where  $\mu, \nu, \dots = 1, \dots, d$ . All other commutators vanish. The generators can be recast in a more compact form:

$$\begin{aligned} L_{d+1,\mu} &= \frac{1}{2}(\mathcal{P}_\mu - \mathcal{K}_\mu), \quad L_{d+2,\mu} = \frac{1}{2}(\mathcal{P}_\mu + \mathcal{K}_\mu), \quad L_{\mu\nu} = \mathcal{M}_{\mu\nu}, \quad L_{d+1,d+2} = \mathcal{D}, \\ [L_{AB}, L_{CD}] &= \eta_{BC}L_{AD} - \eta_{AC}L_{BD} + \eta_{BD}L_{CA} - \eta_{AD}L_{CB}, \end{aligned} \quad (2.1.8)$$



where  $\eta_{AB} = \text{diag}(1, 1, \dots, -1)$  is a  $d + 2$  dimensional metric. From this it is easily seen that the symmetry group is  $SO(d + 1, 1)$ . It also indicates that when considering a  $(d + 1)$ -dimensional space  $\mathbb{R}^{d+1}$  instead of  $\mathbb{R}^d$ , the conformal transformations act linearly on operators instead of quadratically. This is the idea of the *embedding space formalism*. Dating back to Dirac [116], who used it to generalize the Maxwell equations to conformal space, the embedding space formalism provides a compact way to construct correlation functions of operators. We will not encounter the embedding space formalism in this thesis. For the interested reader, reviews can be found in e.g. [113, 114].

### 2.1.3 Representations of the conformal algebra

Having established the form of the conformal algebra, we can focus on how its generators act on local operators  $\mathcal{O}^a$  and classify the operators in terms of different representations of the  $SO(d + 1, 1)$  symmetry. Local operators at the origin, denoted by  $\mathcal{O}^a(0)$ , transform as irreducible representations of the  $SO(d)$  rotation symmetry group:

$$[\mathcal{M}_{\mu\nu}, \mathcal{O}^a(0)] = (\mathcal{S}_{\mu\nu})_a^b \mathcal{O}^b(0). \quad (2.1.9)$$

The matrices  $\mathcal{S}_{\mu\nu}$  satisfy the same algebra as  $\mathcal{M}_{\mu\nu}$ . In the rest of this section, we use the example of scalar operators  $\mathcal{O}$ , which transform in the trivial representation of  $SO(d)$ . We can find the action on  $\mathcal{O}(x)$ , where the operator is no longer at the origin, by considering

$$\mathcal{O}(x) = e^{\mathcal{P}\cdot x} \mathcal{O}(0), \quad (2.1.10)$$

and using the commutation relations in eq. (2.1.7). Since a CFT is scale invariant, the dilatation operator can be diagonalized such that it acts on operators in the origin as:

$$[D, \mathcal{O}(0)] = \Delta \mathcal{O}(0). \quad (2.1.11)$$

The eigenvalue  $\Delta$  is called the *conformal dimension* of the operator  $\mathcal{O}(0)$ , and labels the operator in question.<sup>1</sup> In principle,  $\Delta$  can take arbitrary values, with the constraint that for unitary theories,  $\Delta \geq 0$ . However, we will see that there exist special operators called *protected operators*, which have fractional or integer values of  $\Delta$ . The unique operator with  $\Delta = 0$  is the identity.

If one acts with the generator of special conformal transformations  $\mathcal{K}_\mu$  on an operator with dimension  $\Delta$ ,  $\mathcal{K}_\mu$  becomes a lowering operator:<sup>2</sup>

$$\mathcal{D}\mathcal{K}_\mu \mathcal{O}(0) = (\Delta - 1) \mathcal{K}_\mu \mathcal{O}(0). \quad (2.1.12)$$

The equation above, together with the constraint that  $\Delta \geq 0$  for unitary theories, implies there is an operator for which

$$[\mathcal{K}_\mu, \mathcal{O}(0)] = 0. \quad (2.1.13)$$

We call these operators *conformal primaries*. In a similar way, the generator of translations  $\mathcal{P}_\mu$  acts as a raising operator:

$$\mathcal{D}\mathcal{P}_\mu \mathcal{O}(0) = (\Delta + 1) \mathcal{P}_\mu \mathcal{O}(0). \quad (2.1.14)$$

Other operators can then be constructed from the conformal primaries with conformal dimension  $\Delta_n = \Delta_{\mathcal{O}} + n$ ,  $n \in \mathbb{Z}$ , which are called *conformal descendants*. Usually, we are only concerned with correlation functions between conformal primaries, and from here on the operators considered are primary operators, unless specified otherwise.

<sup>1</sup>Spinning operators are labeled by both their conformal dimension and their spin  $\ell$ .

<sup>2</sup>Note that here we make use of the shorthand  $\mathcal{K}_\mu \mathcal{O}(0) \equiv [\mathcal{K}_\mu, \mathcal{O}(0)]$ .

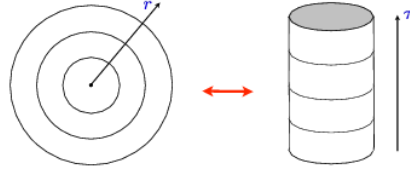


Figure 2.1: Radial quantization versus cylindrical quantization, figure from [113]

### 2.1.4 State-operator correspondence

So far we have studied how the conformal algebra acts on operators. We can also think of a particular quantization of the theory, and relate operators to states in a Hilbert space  $\mathcal{H}$ . A natural choice for scale-invariant theories is *radial quantization*, in which spacetime is foliated in concentric circles around the origin.<sup>3</sup> States evolve from one foliation or circle to the next by acting with an evolution operator  $\hat{U}$ . This evolution operator is constructed using the dilatation operator  $\mathcal{D}$ :

$$\hat{U} = e^{i\Delta \log r}, \quad (2.1.15)$$

where  $r$  is the radius of the circle. The evolution of states is then given by:

$$\langle \mathcal{O}_{\text{out}} | \hat{U} | \mathcal{O}_{\text{in}} \rangle. \quad (2.1.16)$$

In radial quantization,  $\mathcal{D}$  acts as a Hamiltonian and evolves an operator over time, and one can construct states with a defined conformal dimension  $\Delta$ . This is called the *state-operator correspondence*. Since the dilatation operator commutes with the generator of rotations  $\mathcal{M}_{\mu\nu}$ , states can also have a defined spin  $\ell$ .

For conformal theories, this picture can be expanded further, and one can consider the evolution of operators along a cylinder, see figure 2.1. The cylinder and flat space are conformally equivalent, since their metric is related by a Weyl transformation:

$$ds_{\text{cyl}}^2 = d\tau^2 + ds_{S^{d-1}}^2 = \frac{1}{r^2} ds_{\text{flat}}^2. \quad (2.1.17)$$

In the cylindrical picture, states now evolve along cylindrical time  $\tau$ , with  $\tau = \log r$ , and

$$\hat{U} = e^{i\Delta\tau}. \quad (2.1.18)$$

The equivalence between cylindrical and flat space plays a role in the AdS/CFT correspondence. If Anti-de Sitter spacetime is described in the usual, so-called “global coordinates”, it can be depicted as a cylinder. Time evolution along  $\tau$  in AdS is then conformally equivalent to radial quantization and evolution along  $r$  in the CFT.

<sup>3</sup>Of course, instead of the origin, one can take any arbitrary point.

### 2.1.5 Unitarity bounds

From the radial or cylindrical quantization and the “state” picture, we can derive bounds on conformal dimensions of operators in unitary theories.<sup>4</sup> It was already mentioned in section 2.1.3 that for unitary theories,  $\Delta$  needs to be zero (the identity) or positive. Let us derive this result, and find stronger constraints. Cylindrical quantization provides a natural inner product, and for unitary theories we can write:

$$|\mathcal{P}_0 |\mathcal{O}\rangle|^2 = \langle \mathcal{O} | \mathcal{K}_0 \mathcal{P}_0 | \mathcal{O} \rangle = 2\Delta \langle \mathcal{O} | \mathcal{O} \rangle \rightarrow \Delta \geq 0. \quad (2.1.19)$$

Here we have made use of the fact that  $\mathcal{P}_\mu^\dagger = \mathcal{K}_\mu$ , and  $\mathcal{O}$  is a primary such that  $\mathcal{K}_\mu |\mathcal{O}\rangle = 0$ . We can continue taking inner products, now including descendants defined by  $\mathcal{P}_{\mu_1} \cdots \mathcal{P}_{\mu_i} |\mathcal{O}\rangle$ :

$$|\mathcal{P}_\mu \mathcal{P}^\mu |\mathcal{O}\rangle|^2 = \langle \mathcal{O} | \mathcal{K}_\nu \mathcal{K}^\nu \mathcal{P}_\mu \mathcal{P}^\mu | \mathcal{O} \rangle = 4\Delta(2 + 2\Delta - 2) \langle \mathcal{O} | \mathcal{O} \rangle, \quad (2.1.20)$$

where the last equality is found by repeatedly using the commutation relations in eq. 2.1.7. This results in stronger bounds on  $\Delta$ , and one might wonder if, in order to find the strongest possible unitarity bound, one needs to consider infinitely many descendants. Fortunately, the equation above already results in the optimal unitarity bound for scalars. Repeating this exercise for spinning operators, one finds:<sup>5</sup>

$$\begin{aligned} \Delta &= 0 \text{ (identity) ,} \\ \Delta &\geq \frac{d-2}{2}, \quad \ell = 0, \\ \Delta &\geq \ell + d - 2, \quad \ell > 0. \end{aligned} \quad (2.1.21)$$

These bounds will play an important role in the numerical conformal bootstrap of section 2.4.2.

## 2.2 Conformal kinematics

### 2.2.1 Conformal correlators

The requirement of conformal symmetry heavily restricts the form of correlation functions between operators, and many correlation functions are fully fixed kinematically. In this section, we restrict ourselves to correlators of scalars. Correlation functions of spinning operators depend on additional tensor structures, and can be found in [117, 50]. In a CFT, one-point functions of conformal primaries are zero:

$$\langle \mathcal{O}(x) \rangle = 0. \quad (2.2.1)$$

Two-point functions between conformal primaries are not zero, but are completely fixed kinematically. For scalar operators, they take the form:

$$\langle \mathcal{O}_{\Delta_1}(x_1) \mathcal{O}_{\Delta_2}(x_2) \rangle = \frac{\delta_{\Delta_1 \Delta_2}}{|x_{12}|^{2\Delta_1}}, \quad (2.2.2)$$

<sup>4</sup>Below we are considering Euclidean CFTs.

<sup>5</sup>see for example [112] for a more extensive derivation.

where we have defined  $x_{ij} \equiv x_i - x_j$ . It follows that the two-point functions are only nonzero if the operators have equal conformal dimensions. The two-point functions are normalized to 1.

Three-point functions are also fixed kinematically, and for scalars, they are given by:

$$\langle \mathcal{O}_{\Delta_1}(x_1) \mathcal{O}_{\Delta_2}(x_2) \mathcal{O}_{\Delta_3}(x_3) \rangle = \frac{\lambda_{123}}{|x_{12}|^{\Delta_1+\Delta_{23}} |x_{23}|^{\Delta_2+\Delta_{31}} |x_{13}|^{\Delta_3+\Delta_{12}}}, \quad (2.2.3)$$

while for general spinning operators the three-point function depends on tensor structures, but is still fixed by conformal symmetry. We have defined  $\Delta_{ij} \equiv \Delta_i - \Delta_j$ . Since we have already normalized the two-point function, the three-point function will now depend on a constant  $\lambda_{123}$  which is theory dependent.

Four-point functions can no longer be fully determined kinematically, but depend on *conformal cross-ratios*:

$$u \equiv \frac{x_{12}^2 x_{34}^2}{x_{13}^2 x_{24}^2}, \quad v \equiv \frac{x_{14}^2 x_{23}^2}{x_{13}^2 x_{24}^2}. \quad (2.2.4)$$

Often, these cross-ratios are denoted as  $z$  and  $\bar{z}$ , where

$$u = z\bar{z}, \quad v = (1-z)(1-\bar{z}). \quad (2.2.5)$$

The correlation function of four scalar conformal primaries is then given by

$$\langle \mathcal{O}_{\Delta_1}(x_1) \mathcal{O}_{\Delta_2}(x_2) \mathcal{O}_{\Delta_3}(x_3) \mathcal{O}_{\Delta_4}(x_4) \rangle = \frac{f(u, v)}{|x_{12}|^{\Delta_1+\Delta_2} |x_{34}|^{\Delta_3+\Delta_4}} \left( \frac{|x_{24}|}{|x_{14}|} \right)^{\Delta_{12}} \left( \frac{|x_{14}|}{|x_{13}|} \right)^{\Delta_{34}}, \quad (2.2.6)$$

where  $f(u, v)$  is an unknown function depending on the cross-ratios of eq. (2.2.4). Eq. (2.2.6) simplifies significantly in the case of identical scalars, for which  $\Delta_{ij} = 0$ .

If we consider higher-point correlation functions, then the number of cross-ratios on which the correlator depends, will increase. This causes the correlation functions to become more complicated and hence more difficult objects to study using e.g. the conformal bootstrap. In this thesis we will not consider correlation functions of more than four operators.

## 2.2.2 Operator Product Expansion

Two operators brought close together can be expanded in an infinite sum of local operators, which is called the *Operator Product Expansion* (OPE). In ordinary QFT, the OPE is an approximation for operators at an infinitesimally small distance from each other. However, due to scale invariance, in CFTs the OPE converges everywhere as long as there are no other operators inserted in between the two operators involved in the OPE, that is, if a circle or sphere can be drawn around the two operators that does not intersect any other operator, see figure 2.2. The OPE between two conformal primaries is given by:

$$\mathcal{O}_{\Delta_1, \ell_1}(x) \mathcal{O}_{\Delta_2, \ell_2}(0) \sim \sum_k \lambda_{12k} \left[ C_\mu(x) \mathcal{O}_{\Delta_k, \ell_k}(0) + \dots \right]. \quad (2.2.7)$$

The function  $C_\mu(x)$  is known and can be written as

$$C_\mu(x) = \frac{x^{\mu_1} \dots x^{\mu_\ell}}{|x|^{\Delta_1+\Delta_2-\Delta_k+\ell}}. \quad (2.2.8)$$

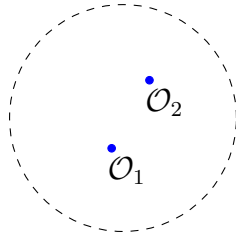


Figure 2.2: The OPE between two operators in a CFT converges as long as there are no other operator insertions.

The coefficients  $\lambda_{12k}$  are called *OPE coefficients*, and are real for unitary CFTs, such that  $\lambda_{12k}^2$  is always positive. Using the OPE we can write  $n + 1$ -point functions as an infinite sum of  $n$ -point functions. When applied to the three-point function in eq. (2.2.3), it is reduced to two-point functions, which are completely fixed by conformal invariance. It turns out that the constant  $\lambda_{123}$  in eq. (2.2.3) is given by the OPE coefficient in eq. (2.2.7) for an operator  $\mathcal{O}_3$  in the OPE of  $\mathcal{O}_1$  and  $\mathcal{O}_2$ . Hence, three-point functions give us direct access to the OPE coefficients between the external operators.

### 2.2.3 Conformal blocks

Using the OPE of eq. (2.2.7), we can rewrite the four-point function of eq. (2.2.6) as:

$$\langle \mathcal{O}_{\Delta_1}(x_1) \mathcal{O}_{\Delta_2}(x_2) \mathcal{O}_{\Delta_3}(x_3) \mathcal{O}_{\Delta_4}(x_4) \rangle = \sum_k \lambda_{12k} \lambda_{34k} g_k(u, v), \quad (2.2.9)$$

where  $u, v$  are the conformal cross-ratios given in eq. (2.2.4) and we have taken the OPE between operators  $\mathcal{O}_1, \mathcal{O}_2$ , and  $\mathcal{O}_3, \mathcal{O}_4$ . The functions  $g_k(u, v)$  are called *conformal blocks* and in general, they depend on the conformal dimension  $\Delta_k$  of the operator  $\mathcal{O}_k$ , on its spin  $\ell_k$ , and on the dimensions  $\Delta_i, i = 1, \dots, 4$  of the external operators. The work by Dolan and Osborn [118, 119] have been crucial for our understanding of these functions. They showed that the blocks are solutions to differential equations, which are obtained by acting with the Casimir of the conformal group  $SO(d + 1, 1)$  on the four-point function:

$$(\mathcal{C}^2 - c) \langle \mathcal{O}_{\Delta_1}(x_1) \mathcal{O}_{\Delta_2}(x_2) \mathcal{O}_{\Delta_3}(x_3) \mathcal{O}_{\Delta_4}(x_4) \rangle = 0. \quad (2.2.10)$$

The solutions to the resulting differential equations are unique when appropriate boundary conditions are chosen, given by the asymptotic behavior of the blocks found by looking at the leading term in the OPE.

In some cases, the differential equations have a closed-form solution. This is the case for even dimensions, and for  $d = 1$ , which we discuss below. The conformal blocks for scalars in even  $d \leq 4$  are given by:

$$d = 4 : \quad g_{\Delta, \ell}^{\Delta_{12}, \Delta_{34}}(z, \bar{z}) = \frac{1}{(-2)^\ell} \frac{z \bar{z}}{(z - \bar{z})} \left( k_{\Delta+\ell}^{\Delta_{12}, \Delta_{34}}(z) k_{\Delta-\ell-2}^{\Delta_{12}, \Delta_{34}}(\bar{z}) - z \leftrightarrow \bar{z} \right), \quad (2.2.11)$$

$$d = 2 : \quad g_{\Delta, \ell}^{\Delta_{12}, \Delta_{34}}(z, \bar{z}) = \frac{1}{(-2)^\ell} \frac{1}{1 + \delta_{\ell, 0}} \left( k_{\Delta+\ell}^{\Delta_{12}, \Delta_{34}}(z) k_{\Delta-\ell}^{\Delta_{12}, \Delta_{34}}(\bar{z}) + z \leftrightarrow \bar{z} \right), \quad (2.2.12)$$

$$k_{\beta}^{\Delta_{12}, \Delta_{34}}(x) = x^{\frac{\beta}{2}} {}_2F_1 \left( \frac{\beta - \Delta_{12}}{2}, \frac{\beta + \Delta_{34}}{2}, \beta, x \right). \quad (2.2.13)$$

For  $d = 3$  the blocks are not known in closed form, but can be written as an infinite series. The same series can also be used to write down conformal blocks analytic in  $d$ , which one can use to expand correlation functions across dimensions.

### 2.2.4 CFTs in 1d

Later on in this thesis we will encounter CFTs in one dimension, which are in some aspects different from CFTs in higher dimensions. In 1d, the theory is restricted to a line or a circle, and one needs to specify the ordering of the operators. The conformal blocks for the four-point function reduce to simple hypergeometric functions of a single variable:

$$d = 1 : \quad g_{\Delta}^{\Delta_{12}, \Delta_{34}}(z) = k_{2\Delta}^{\Delta_{12}, \Delta_{34}}(\xi), \quad (2.2.14)$$

where  $k_{\Delta}^{\Delta_{12}, \Delta_{34}}(\xi)$  is defined in eq. (2.2.13). The cross-ratio  $\xi$  differs slightly from  $u$  defined in eq. (2.2.5), and is given by:

$$\xi = \frac{x_{12}x_{34}}{x_{13}x_{24}}. \quad (2.2.15)$$

If one considers the ordering  $x_1 < x_2 < x_3 < x_4$ , the cross-ratio takes values between  $0 < \xi < 1$ . The equivalent of  $v$  is now given by:

$$1 - \xi = \frac{x_{14}x_{23}}{x_{13}x_{24}}, \quad (2.2.16)$$

and is no longer an independent variable. Another difference with respect to higher-dimensional CFTs is the absence of spin in one dimension. There is a notion of *parity*, which is more extensively discussed in chapter 5. Operators are classified according to their transformation under parity in parity-preserving CFTs, in analogy to the classification according to their spin.

One-dimensional CFTs are nonlocal, since there is no stress-tensor that can be written down in 1d. Hence, 1d CFTs are less intuitive than their higher-dimensional counterparts. We will encounter 1d CFTs as line defects in this thesis, for which the nonlocality follows naturally.

Considering one-dimensional CFTs often simplifies calculations. Conformal blocks are well-known functions of only one variable, making it straightforward to expand in them. On the other hand, 1d CFTs lack the structure that higher-dimensional CFTs have. Operators cannot be labeled according to their spin, and there is no protected stress-tensor or other tensor structures that define a certain class of operators. All in all, they are an excellent testing ground for various approaches such as analytic functionals, but need to be treated with care.

## 2.3 The $\varepsilon$ -expansion

Having determined the basic kinematics of CFTs, the next step is to extract dynamical information such as conformal dimensions, spins, and OPE coefficients of different operators. The set of these is called the *conformal data*:

$$\text{conformal data} = \{\Delta_i, \ell_i, \lambda_{ijk}\}. \quad (2.3.1)$$

As pointed out in the introduction, this data can either be determined perturbatively, or nonperturbatively. There are many perturbative approaches e.g. large- $N$ , weak coupling, which have been mentioned in the introduction, and which we will not review here. Instead, we will focus on the  $\varepsilon$ -expansion.

CFTs can be seen as the fixed points of renormalization group flows of QFTs. A few well-known examples that will be considered later in this thesis are the Wilson-Fisher

fixed point of the Ising model and the  $O(N)$  models, the Wess-Zumino fixed point for the supersymmetric Wess-Zumino models, and the Wilson-Fisher-Yukawa fixed point for the Yukawa CFTs. All these CFTs are free theories in  $d = 4$  dimensions, but become interacting if we consider the theory in  $d = 4 - \varepsilon$  dimensions. If we stay at the fixed point, the respective CFTs can be studied perturbatively using the  $\varepsilon$ -expansion. Setting  $\varepsilon \rightarrow 1$ , one obtains information about the fully interacting CFT in three dimensions. It is of course not necessary to start in four dimensions, and there exist fixed points with corresponding CFTs in  $d = 6 - \varepsilon$  and  $d = 2 + \tilde{\varepsilon}$  as well, examples of which were given in the introduction. However, in this section and thesis we will focus on the  $\varepsilon$ -expansion in  $d = 4 - \varepsilon$  dimensions, and below we give the example of  $\phi^4$  theory at the Wilson-Fisher fixed point, which corresponds to the Ising model.

### 2.3.1 The Wilson-Fisher fixed point

The Ising model in  $d = 4 - \varepsilon$  dimensions is described by the action of massless  $\phi^4$  theory:

$$\mathcal{S} = \int d^d x \left( (\partial_\mu \phi)^2 + \frac{\lambda}{4!} \phi^4 \right), \quad (2.3.2)$$

where the coupling  $\lambda$  describes a four-scalar interaction. The following Feynman rules are associated to this action. The free propagator of the scalar in  $d$  dimensions is given by:

$$\text{----} := \langle \phi(x_1) \phi(x_2) \rangle_{\lambda=g=0} = \delta_{ab} I_{12}. \quad (2.3.3)$$

where the scalar propagator function in  $d = 4 - \varepsilon$  dimensions is defined as:

$$I_{ij} := \frac{\Gamma(1 - \varepsilon/2)}{4\pi^{2-\varepsilon/2} x_{ij}^{2(1-\varepsilon/2)}}, \quad (2.3.4)$$

with  $x_{ij} := x_i - x_j$ . The scalar propagator satisfies the Green's equation:

$$\partial_i^2 I_{ij} = -\delta^{(d)}(x_{ij}), \quad (2.3.5)$$

where  $\delta^{(d)}(x)$  is the  $d$ -dimensional Dirac delta function.

The interaction terms yield the following vertices:

$$\text{---}\times\text{---} := -\lambda_0 \int d^d x_5 I_{15} I_{25} I_{35} I_{45}. \quad (2.3.6)$$

The fixed point describing the CFT is given by the value of the coupling  $\lambda$  for which the  $\beta$ -function associated to the action (2.3.2) is zero. To compute the  $\beta$ -function, we need to compute all corrections to the scalar interaction vertex up to a given order in  $\varepsilon$ , and require that this is finite when introducing the proper counterterms. From these counterterms the  $\beta$ -function can be derived, and equated to zero to find the fixed point. The coupling  $\lambda$  does not receive a correction at  $\mathcal{O}(\varepsilon)$ . The first contribution is at  $\mathcal{O}(\varepsilon^2)$  and is given by:

$$\lambda = \text{---}\times\text{---} + \text{---}\times\text{---} + \mathcal{O}(\varepsilon^4). \quad (2.3.7)$$

Their evaluation is well known (see e.g. [120]) and the diagrams diverge with  $1/\varepsilon$ . We can now introduce a *counterterm*  $Z_\lambda$  to absorb these divergences, and define:

$$Z_\lambda = \text{---}\star\text{---} = \mu^\varepsilon \lambda \left( 1 + \frac{\alpha\lambda}{\varepsilon} + \dots \right), \quad (2.3.8)$$

where the dots represent contributions that will appear at  $\mathcal{O}(1/\varepsilon^2)$ . The renormalization scale  $\mu$  is introduced to ensure that the coupling is dimensionless. It is unphysical, meaning that after proper renormalization it should drop out of the computations. Imposing that eq. (2.3.7) is finite gives us the following expression for  $Z_\lambda$ :

$$Z_\lambda = \mu^\varepsilon \lambda \left( 1 + \frac{3\lambda}{\varepsilon(4\pi)^2} - \frac{3\lambda^2}{\varepsilon(4\pi)^2} + \mathcal{O}(\lambda^3, 1/\varepsilon^2) \right). \quad (2.3.9)$$

The  $\beta$ -function can now be determined by requiring that  $Z_\lambda$  is independent of the renormalization scale  $\mu$ :

$$\beta_\lambda = \frac{dZ_\lambda}{d \log \mu} = -\varepsilon\lambda + \frac{3}{(4\pi)^2}\lambda - \frac{17}{3(4\pi)^4}\lambda^2 + \mathcal{O}(\lambda^3), \quad (2.3.10)$$

where we have redefined  $g \rightarrow g/(4\pi)^2$ . The Wilson-Fisher (WF) fixed point is given by the zeros of eq. (2.3.10):

$$\lambda_\star = \frac{16\pi^2\varepsilon}{3}. \quad (2.3.11)$$

The fixed point is of order  $\mathcal{O}(\varepsilon)$ . This means that up to  $\mathcal{O}(\varepsilon^a)$ , we only need to consider diagrams with a maximum of  $a$  scalar vertices.

### 2.3.2 Renormalization factors

We have used the renormalization factor for the coupling  $Z_\lambda$  to determine the  $\beta$ -function and the corresponding WF fixed point. We also need to renormalize the field  $\phi$  to describe the fully renormalized CFT. We proceed similarly as before, but now consider the two-point function  $\langle \phi(x)\phi(0) \rangle$  and require that it is finite when adding the appropriate counterterms. The diagrams contributing to the two-point function at  $\mathcal{O}(\varepsilon^2)$  are:

$$\langle \phi(x_1)\phi(x_2) \rangle = \text{---}\text{---} + \text{---}\text{---} + \mathcal{O}(\varepsilon^3). \quad (2.3.12)$$

Their evaluation is once again well known (see [120]) and divergent in  $1/\varepsilon$ . In order to cancel the divergences, we need the following counterterm:

$$Z_\phi = \text{---}\star\text{---} = \mu^\varepsilon \left( 1 - \frac{\lambda^2}{12(4\pi)^4} + \mathcal{O}(\lambda^4) \right). \quad (2.3.13)$$

From the renormalization factor of  $\phi$  we can determine the anomalous dimension, which is the correction to the conformal dimension:

$$\Delta_\phi = \frac{d-2}{2} + \gamma_\phi, \quad (2.3.14)$$

where  $\frac{d-2}{2}$  is the free theory dimension of a scalar field in  $d$  dimensions. The anomalous dimension is given by:

$$\gamma_\phi = \beta_\phi \frac{dZ_\phi}{d \log \mu} = \frac{\lambda^2}{12(4\pi)^4} + \mathcal{O}(\lambda^4). \quad (2.3.15)$$



### 2.3.3 More conformal data

Having determined the anomalous dimensions and renormalization factors, we are ready to compute higher-point functions. The three-point function of three operators  $\mathcal{O}_{1,2,3}$  contains the OPE coefficient  $\lambda_{123}$ . Note that there are no possible diagrams that would give us the three-point function  $\langle\phi(x_1)\phi(x_2)\phi(x_3)\rangle$ . For three scalars  $\phi, \phi, \phi^2$ , the three-point function can be expressed in Feynman diagrams as:

$$\langle\phi(x_1)\phi(x_2)\phi^2(x_3)\rangle = \text{diagram 1} + \text{diagram 2} + \mathcal{O}(\varepsilon^2). \quad (2.3.16)$$

Adding these diagrams, we find the three-point function and the OPE coefficient  $\lambda_{\phi\phi\phi^2}$ :

$$\langle\phi(x_1)\phi(x_2)\phi^2(x_3)\rangle = \frac{\mathcal{N}_\phi^2 \mathcal{N}_{\phi^2} \lambda_{\phi\phi\phi^2}}{|x_{12}|^{2\Delta_\phi - \Delta_{\phi^2}} |x_{23}|^{\Delta_{\phi^2}} |x_{13}|^{\Delta_{\phi^2}}}, \quad \lambda_{\phi\phi\phi^2} = \left(\sqrt{2} - \frac{\varepsilon}{3\sqrt{2}}\right). \quad (2.3.17)$$

The constants  $\mathcal{N}_\phi, \mathcal{N}_{\phi^2}$  are normalization constants that can be found from the two-point functions of  $\phi$  and  $\phi^2$  respectively.

Having found the CFT data at a given order in  $\varepsilon$ , we want to find the results at finite  $\varepsilon \rightarrow 1$  to obtain the CFT data for the  $3d$  Ising model. Unfortunately, an exact solution would require computing Feynman diagrams to infinite order in  $\varepsilon$ . There are other methods such as Padé approximation to find better estimates of the CFT data at finite order. This raises the question how well the  $\varepsilon$ -expansion converges. It turns out that the expansion is non-convergent, but *Borel summable* [121]. The Borel resummation consists of first finding the Borel transform of the series (in this case a series in  $\varepsilon$ ), and then Borel resumming this transformation by integrating over it. For this to be well defined, and hence for a series to be considered Borel summable, there are three properties that need to be satisfied: the Borel transformation itself is convergent, it does not have singularities when analytically continued in a certain chosen direction, and the final integration of the Borel transform is finite. All these properties are satisfied in the case of the  $\varepsilon$ -expansion.

Besides computing explicit Feynman diagrams, there is an additional method of obtaining CFT data up to  $\mathcal{O}(\varepsilon)$  in  $\phi^4$  theory, which relies on observations of multiplet recombination in the interacting theory. In the interacting theory, the equations of motion of the action in eq. (2.3.2) relate  $\phi$  to  $\phi^3$ , making  $\phi^3$  a conformal descendant of  $\phi$ . In contrast, in the free theory in  $4d$ , which does not have the four-scalar interaction term, both  $\phi$  and  $\phi^3$  are conformal primaries. This observation made in [122] leads to relations which can be used to determine conformal data up to a low order in  $\varepsilon$ . However, to go to higher order explicit Feynman diagram computations are required. A nice overview of results for the  $O(N)$  CFTs can be found in [123].

## 2.4 Conformal bootstrap

The conformal bootstrap is the idea that conformal field theories can be constrained by making use of the conformal symmetry and some additional assumptions, such as the associativity of the Operator Product Expansion. The goal is to use *crossing symmetry* to constrain *conformal data*, which determines the entire CFT. This is done without considering specific realizations of the theory, and the goal is to be able to find universally valid bounds on theories. It is a nonperturbative method to study CFTs and hence is not only valid in perturbative limits. The crossing equation can be derived from the fact that

$$\sum_{\mathcal{O}} (\lambda_{\mathcal{O}})^2 \Delta_{\mathcal{O}} = \sum_{\mathcal{O}} (\lambda_{\mathcal{O}})^2 \Delta_{\mathcal{O}}$$

Figure 2.3: The crossing equation for the four-point function of scalars.

when considering four operators, the OPEs between them can be taken in different ways. These are called s-channel, u-channel and t-channel expansions, after the Mandelstam variables  $s, t, u$  that capture different limits of scattering amplitudes.

The crossing equation gives us an infinite set of constraints on correlation functions. It is very hard to solve, which can be seen from the infinite number of operators contributing on both sides. However, in some limits the equations simplify, making it possible to solve for the conformal data. This happens in specific kinematic limits or when approaching the theory from a perturbative point of view. Another approach is to artificially truncate the sum and derive less optimal, but still valid bounds using numerical techniques. Both the analytic and numerical approach will be discussed below.

### 2.4.1 Crossing equation

In section 2.2.3 we have shown how the four-point function of scalars can be decomposed in conformal blocks by taking the OPE between the four operators. In that case, we took the OPE between  $\mathcal{O}_1, \mathcal{O}_2$  and  $\mathcal{O}_3, \mathcal{O}_4$ . We can repeat the process but now take the OPE in different combinations. Since the OPE is *associative*, this should result in the same expression. If we additionally take the OPE between  $\mathcal{O}_1, \mathcal{O}_4$  and  $\mathcal{O}_2, \mathcal{O}_3$ , we end up with the equation in figure 2.3. The crossing equation can be written as (for simplicity we take the external operators to be identical):

$$\sum_{\mathcal{O}_k} \lambda_{12k} \lambda_{34k} g(u, v) = \sum_{\mathcal{O}_i} \lambda_{14i} \lambda_{23i} \frac{u^{\Delta_{\mathcal{O}_i}}}{v^{\Delta_{\mathcal{O}_i}}} g(v, u). \quad (2.4.1)$$

Note that we can also consider  $x_1 \leftrightarrow x_2$ , which will give a trivial crossing equation where  $u \rightarrow u/v, v \rightarrow 1/v$ . The operators appearing in the two OPEs in principle differ from each other; they can have different spin and come in different representations of the global symmetries of the CFT. It turns out that not all combinations of  $\{\lambda, \Delta, \ell\}$  satisfy the crossing equation. It is the goal of the *conformal bootstrap* to determine the set of conformal data that does, or find exclusion regions and bounds on OPE coefficients and operator dimensions. We will review two methods: the numerical bootstrap and the analytic bootstrap. Both have different regions in the space of CFT data where they are best applicable. In this thesis, the numerical bootstrap will be used in chapter 5. The analytic bootstrap will be used in combination with the  $\varepsilon$ -expansion in chapter 4.

### 2.4.2 Numerical conformal bootstrap

The aim of the numerical conformal bootstrap is to put bounds - both upper and lower ones - on conformal data. In order to do this, one can make use of *semidefinite programming* to solve the crossing equations discussed in section 2.4.1. There are two main objectives: bounding conformal dimensions and bounding OPE coefficients.

In order to put bounds on a certain OPE coefficient  $\lambda_{\mathcal{O}}$  of an operator  $\mathcal{O}$  being the lowest-lying operator appearing in the OPE of two other, identical scalar operators  $\phi$ , we write the crossing equation (2.4.1) in the following way:

$$\lambda_{\mathcal{O}}^2 F_{\Delta_{\mathcal{O}}, \ell_{\mathcal{O}}}(u, v) = -F_{0,0}(u, v) - \sum_{\mathcal{O}_k \neq \mathcal{O}} \lambda_{\mathcal{O}_k}^2 F_{\Delta_k, \ell_k}(u, v), \quad (2.4.2)$$

$$F_{\Delta, \ell}(u, v) = \frac{v^{\Delta_{\phi}} g_{\Delta, \ell}^{0,0}(u, v) - u^{\Delta_{\phi}} g_{\Delta, \ell}^{0,0}(u, v)}{u^{\Delta_{\phi}} - v^{\Delta_{\phi}}}. \quad (2.4.3)$$

The contribution from the operator  $\mathcal{O}$  whose OPE coefficient we want to bound, is pulled out. The functions  $F_{\Delta, \ell}(u, v)$  are normalized such that the contribution of the identity  $F_{0,0}(u, v) = -1$ . Note that for a unitary CFT, the OPE coefficients  $\lambda$  are real and hence  $\lambda^2$  is positive. This is an important assumption in the numerical bootstrap, and we will restrict ourselves to unitary CFTs for the rest of this section.

The crossing equation is in fact an infinite set of constraints, one for each value of  $u$  and  $v$ . The crossing equation does not change when acting with a functional on  $F$ , and we can write

$$\lambda_{\mathcal{O}}^2 \alpha(F_{\Delta_{\mathcal{O}}, \ell_{\mathcal{O}}}(u, v)) = -\alpha(F_{0,0}(u, v)) - \sum_{\mathcal{O}_k \neq \mathcal{O}} \lambda_{\mathcal{O}_k}^2 \alpha(F_{\Delta_k, \ell_k}(u, v)). \quad (2.4.4)$$

The functional  $\alpha$  can be any linear functional, but is most often taken to be a number of derivatives in  $u$  and  $v$ . The functions  $F$ , which contain the conformal blocks, have certain positivity properties which makes it possible to find functionals  $\alpha$  such that:

$$\alpha(F_{\Delta_{\mathcal{O}}, \ell_{\mathcal{O}}}) = 1, \quad \alpha(F_{\Delta_k, \ell_k}) \geq 0. \quad (2.4.5)$$

It becomes clear that under these conditions, we obtain an upper bound on  $\lambda_{\mathcal{O}}^2$ :

$$\lambda_{\mathcal{O}}^2 = -\alpha(F_{0,0}(u, v)) - \sum_{\mathcal{O}_k} \lambda_{\mathcal{O}_k}^2 \alpha(F_{\Delta_k, \ell_k}(u, v)) \leq -\alpha(F_{0,0}(u, v)). \quad (2.4.6)$$

Finding an  $\alpha$  that satisfies eq. (2.4.5) is nontrivial and depends on the spectrum of the CFT under consideration. In particular, if one makes assumptions about the conformal dimension of the operators appearing in the OPE, and demands that no operators with dimension lower than  $\Delta_{\star}$  appear, the space of  $\alpha$ 's satisfying eq. (2.4.5) becomes larger. Having found such a functional  $\alpha$ , one can try to optimize the bound on  $\lambda_{\mathcal{O}}^2$  by minimizing  $\alpha(F_{0,0}(u, v))$ . If then it happens that  $\lambda_{\mathcal{O}}^2 \leq 0$ , the operator is excluded from the spectrum of the CFT.

The same logic can be applied to bound conformal dimensions, but the algorithm needs to be changed slightly. Instead of isolating an operator  $\mathcal{O}$ , we use the fact that the identity gives a nonzero contribution and we write:

$$\alpha(F_{0,0}(u, v)) = - \sum_{\mathcal{O}_k, \Delta_k \geq \Delta_{\star}} \lambda_{\mathcal{O}_k}^2 \alpha(F_{\Delta_k, \ell_k}(u, v)), \quad (2.4.7)$$

where the dimensions  $\Delta_k$  of the operators  $\mathcal{O}_k$  are taken to be larger than some minimal dimension  $\Delta_{\star}$ . Now the goal is to try to find a functional  $\alpha$  such that:

$$\alpha(F_{0,0}) = 1, \quad \alpha(F_{\Delta_k, \ell_k}) \geq 0. \quad (2.4.8)$$

If this  $\alpha$  exists, the crossing equation (2.4.7) cannot be satisfied and  $\Delta_*$  becomes an upper bound on the conformal dimensions. We call such a solution *dual feasible*. If there is no such  $\alpha$  (within a set precision), the solution is allowed and is named *primal feasible*. One can perform a bisection to find the exact value of  $\Delta_*$  where one jumps from primal feasible to dual feasible, and find the optimal upper bound on the conformal dimensions.

The problem of bounding the OPE coefficients or conformal dimensions is now turned into a problem of finding a set of functionals  $\alpha_i$  that satisfy either (2.4.5) or (2.4.8). However, there is still an infinite set of constraints, and in principle an infinite search space for  $\alpha$ . Hence, there are a few cutoffs that need to be made. First, the conformal blocks need to be expanded in polynomials in  $u, v$  up to a certain order, and are evaluated around  $u = v = 1/4$ . Second, we take  $\alpha$  to be derivatives in  $u, v$ , and impose a maximum number of derivatives  $\Lambda$ . Third, the search space for  $\alpha$  needs to be bounded when there is no  $\alpha$  satisfying (2.4.5) or (2.4.8). All these cutoffs affect the precision of the bounds. Luckily, due to the analytic properties of the conformal blocks, increasing the cutoffs only leads to stronger bounds, so at a certain precision the bound that is obtained is still valid, just not optimal. By looking at the convergence of the bound, one can estimate at which precision one needs to work.

The examples above treated correlation functions of identical scalars. If one includes multiple operators with different conformal dimensions, the crossing equations get modified and may involve contributions with  $\lambda_{\mathcal{O}_1}\lambda_{\mathcal{O}_2}$  instead of  $\lambda_{\mathcal{O}}^2$ . This requires the condition of positivity to be slightly relaxed to a condition of semidefinite positivity on matrices of polynomials. The state-of-the-art linear program SDPB [124] makes it possible and easy to implement such constraints as well.

Lastly, we have focused on obtaining upper bounds on conformal data. It is possible to obtain lower bounds as well, but one needs to make further assumptions about the CFT spectrum, and assume discreteness in the spectrum for low-lying operators. In some cases, this can lead to isolated “islands”, as is the case for the  $3d$  Ising model when one assumes only a limited number of relevant ( $\Delta < 3$ ) operators in the spectrum, and study multiple correlators of the lowest-lying operators in the spectrum [20]. High numerical precision combined with multi-operator and multi-correlator studies have led to the numerical bootstrap being able to obtain extremely precise results for various critical exponents. In some cases, it can also serve as an independent method to solve existing discrepancies between theory and experiment, for example in the case of the  $O(2)$  model [23], where Monte Carlo studies disagree with experimental measurements.

The numerical bootstrap focuses on bounding the lowest-lying operators in the spectrum in a region around  $u, v = 1/4$ . The precision of the results decreases significantly when trying to bound higher-dimensional operators, and hence the range of applicability is often limited to low  $\Delta$  and low  $\ell$ . The *extremal functional method* can be used to extract the spectrum of the lower-lying operators [125, 126]. More recently, a new method called the “Navigator” has been developed that allows for a more efficient search of islands in the parameter space of the CFT data [127, 128].

The numerical conformal bootstrap has been combined with the  $\varepsilon$ -expansion to study CFTs in fractional or non-integer dimensions. However, it can be shown that the CFT is no longer unitary [129]. This poses a problem for numerics, which heavily relies on unitarity and positivity of the OPE coefficients. Nevertheless, it can be successfully applied, since the operators which break unitarity only appear at very high dimension  $\Delta$ , and the numerical bootstrap is most sensitive to operators of low  $\Delta$  [130].

### 2.4.3 Analytic conformal bootstrap

The second pillar of the conformal bootstrap is the *analytical* conformal bootstrap. The development of especially Caron-Huot's *inversion formula* [26] has played a major role in the modern bootstrap, as have several other techniques such as Mellin space bootstrap, large charge expansion and analytic functionals. Although most of the analytical techniques available nowadays are not used in this thesis, we briefly review the highlights of the literature. More detailed overviews of recent progress can be found in [131, 132].

#### The lightcone bootstrap and the inversion formula

The analytic conformal bootstrap applies to *Lorentzian* CFTs, and the crossing equation is studied in what is known as the *lightcone limit*. In a Lorentzian CFT, the two cross-ratios  $(z, \bar{z})$  in eq. (2.2.5) are independent of each other, and it is possible to let  $z$  be small while keeping  $\bar{z}$  fixed. This is called the lightcone limit and is equivalent to sending  $x^2 \rightarrow 0$  while staying on the lightcone. The *double lightcone limit* requires one to take  $z \rightarrow 0$  and afterwards  $\bar{z} \rightarrow 1$ , such that  $z \ll 1 - \bar{z} \ll 1$ . In this limit, the crossing equation for identical scalars (2.4.1) is given by:

$$\left(\frac{z}{1-\bar{z}}\right)^{\Delta_\phi} \sim \sum_{\mathcal{O}} \frac{1}{(-2)^\ell} \lambda_{\phi\phi\mathcal{O}}^2 z^{\frac{\Delta-\ell}{2}} k_{\Delta+\ell}(\bar{z}), \quad 0 < 1 - \bar{z} \ll z \ll 1, \quad (2.4.9)$$

where the functions  $k_\Delta$  are given in eq. (2.2.13). For  $\bar{z} \rightarrow 1$ , it is clear that the left-hand side has a powerlaw divergence. On the right-hand side, it turns out that the divergence in this limit is logarithmic. Hence, there needs to be an infinite number of contributions on the right-hand side in this limit to reproduce the divergence on the left-hand side. It was shown in [24, 25] that there must exist an infinite family of operators with scaling dimensions

$$\Delta_{\ell,n} = 2\Delta_\phi + \ell + 2n + \gamma_\tau, \quad (2.4.10)$$

which are called *multi-twist operators*. The anomalous dimensions  $\gamma_\tau$  can be found with the *lightcone bootstrap* and are of the order of  $\mathcal{O}(1/\ell)$ . The crossing equation can be expanded around large spin  $\ell \rightarrow \infty$  and low *twist*  $\tau = \Delta - \ell$ . This gives access to a different regime than the numerical bootstrap, which is most efficient for operators with low  $\Delta$ .

The ideas of the lightcone bootstrap sketched above are elegantly and compactly generalized in the *Lorentzian inversion formula* [26]:

$$c^t(\Delta, \ell) = \frac{\kappa_{\ell+\Delta}}{4} \int_0^1 dz d\bar{z} \mu(z, \bar{z}) G_{\Delta+1-d, \ell+d-1}(z, \bar{z}) d\text{Disc}[\mathcal{G}(z, \bar{z})], \quad (2.4.11)$$

where  $\mu(z, \bar{z})$  is the appropriate measure for the integral,  $G_{\Delta, \ell}(z, \bar{z})$  are the conformal blocks,  $d\text{Disc}[\mathcal{G}(z, \bar{z})]$  is the double discontinuity of a four-point correlation function, and the coefficient  $\kappa_{\ell+\Delta}$  is given by:

$$\kappa_{\Delta+\ell} = \frac{(1 + (-1)^\ell) \Gamma\left(\frac{\Delta+\ell}{2}\right)^4}{2\pi^2 \Gamma(\Delta + \ell - 1) \Gamma(\Delta + \ell)}. \quad (2.4.12)$$

The coefficient  $c^t(\Delta, \ell)$  is the *t*-channel contribution to the full OPE coefficient  $c(\Delta, \ell) = c^t(\Delta, \ell) + c^u(\Delta, \ell)$ , and the *u*-channel contribution can be written in the same way as

eq. (2.4.11) but with the range of integration being  $(-\infty, 0)$  instead of  $(0, 1)$  and the double discontinuity is taken around  $\infty$ . The Lorentzian inversion formula provides a way to construct OPE coefficients from the double discontinuity of the correlator, which is in general a simpler object than the full correlator itself. However, one needs to be careful for operators of low spin. Specifically, eq. (2.4.11) cannot be trusted for operators with spin  $l < l_*$ , where  $l_*$  is theory-dependent but is at most  $l_* = 2$ .

### Other analytic approaches

Another development is the understanding of analytic functionals. The conformal bootstrap has taught us that some interesting CFTs (e.g. the 3d Ising model), are close to saturating the bound found by the numerical bootstrap. The exact solution to the numerical bound is given by *extremal functionals* [133], which often contain enough information to reconstruct a solution to crossing. To obtain an analytic solution instead of a numerical bound, one would need to analytically construct these extremal functionals. This was first done in [29] and further developed in [30–32] in 1d.<sup>6</sup> A generalization to higher  $d$  has been made in [135]. Examples of analytic functionals have been found for generalized free theories, and the goal is to obtain such functionals for interacting CFTs and hence solve crossing exactly by perturbing the free theory solutions.

Both the Lorentzian inversion formula and analytic functionals for generalized free theories lead to so-called *conformal dispersion relations*. A third method can also be used as a basis to derive these relations: the Polyakov bootstrap [14]. In later work [33–36], Mellin space was used to recast the Polyakov bootstrap in the language of Witten exchange diagrams.

A fourth noteworthy development is the large global charge expansion in CFTs. Besides large spin, one can also expand in large global charge  $J$  [27]. This gives access to CFT data of CFTs with global symmetry that might be strongly coupled and cannot be computed in other perturbative regimes. The large charge limit corresponds to specific phases, such as a superfluid phase, of the theory, and allows one to construct an *effective field theory* (EFT) for this phase. Computations can be done explicitly in the EFT framework, but can also be combined with bootstrap techniques as was done in [28].

The above techniques will play no further role in this thesis. However, it is also possible to combine the conformal bootstrap with perturbative expansions such as large- $N$ , weak coupling, and the  $\varepsilon$ -expansion and solve the bootstrap equations order by order in perturbation theory. In this thesis we will combine the conformal bootstrap with the  $d = 4 - \varepsilon$  expansion, both for the analytic bootstrap and the numerical bootstrap. In this way, we combine the old and the new in a modern approach to solving CFTs.

---

<sup>6</sup>Remarkably, these analytic functionals can also be applied to the problem of sphere packing in pure mathematics [134].

# Chapter 3

## Conformal defects

One can extend the notion of a conformal field theory by allowing the presence of extended objects, also commonly called *defects*. Extended objects, such as line operators, boundaries, interfaces and surface operators, break part of the conformal symmetry of the original CFT, which we refer to as the *bulk* CFT from now on. Correlation functions between operators are no longer invariant under the full bulk conformal algebra, but only under the reduced algebra preserved by the defect. There are many types of extended operators, but we focus on the special class of *conformal defects*.

In section 3.1 we show how such defects break the bulk conformal algebra, and which symmetries will be preserved by conformal defects. In addition, we highlight special defect operators that appear as a result of the symmetry breaking. The bulk-to-defect OPE and correlation functions of bulk and defect operators are treated in section 3.2. Defects can also be studied perturbatively. Explicit calculations in the  $\varepsilon$ -expansion for a line defect in  $\phi^4$  theory are shown in section 3.3. Lastly, in section 3.4, we introduce the *defect bootstrap* and highlight similarities and differences with the conformal bootstrap covered in section 2.4.

### 3.1 Defect algebra

A general  $p$ -dimensional, non-spinning conformal defect will break the  $d$ -dimensional bulk conformal algebra in the following way:

$$SO(d+1,1) \rightarrow SO(p+1,1) \times SO(q), \quad (3.1.1)$$

where  $q \equiv d - p$  is the codimension of the defect. If  $q = 1$ , the defect is a boundary or an interface, while monodromy defects have codimension  $q = 2$ . The group  $SO(p+1,1)$  is the conformal symmetry group preserved on the defect, and  $SO(q)$  is the symmetry group of the preserved rotations around the defect.

The defect conformal algebra is given by the bulk algebra restricted to the defect, and

the transverse rotations as a disconnected part of the algebra:

$$\begin{aligned}
[\mathcal{P}_{\hat{a}}, \mathcal{K}_{\hat{b}}] &= -2\mathcal{D}\delta_{\hat{a}\hat{b}}, \\
[\mathcal{D}, \mathcal{P}_{\hat{a}}] &= \mathcal{P}_{\hat{a}}, \\
[\mathcal{D}, \mathcal{K}_{\hat{b}}] &= -\mathcal{K}_{\hat{b}}, \\
[\mathcal{M}_{\hat{a}\hat{b}}, \mathcal{P}_{\hat{c}}] &= \delta_{\hat{b}\hat{c}}\mathcal{P}_{\hat{a}} - \delta_{\hat{a}\hat{c}}\mathcal{P}_{\hat{b}}, \\
[\mathcal{M}_{\hat{a}\hat{b}}, \mathcal{K}_{\hat{c}}] &= \delta_{\hat{b}\hat{c}}\mathcal{K}_{\hat{a}} - \delta_{\hat{a}\hat{c}}\mathcal{K}_{\hat{b}}, \\
[\mathcal{M}_{\hat{a}\hat{b}}, \mathcal{M}_{\hat{c}\hat{d}}] &= \delta_{\hat{b}\hat{c}}\mathcal{M}_{\hat{a}\hat{d}} - \delta_{\hat{a}\hat{c}}\mathcal{M}_{\hat{b}\hat{d}} + \delta_{\hat{b}\hat{d}}\mathcal{M}_{\hat{c}\hat{a}} - \delta_{\hat{a}\hat{d}}\mathcal{M}_{\hat{c}\hat{b}}, \\
[\mathcal{M}_{ij}, \mathcal{M}_{kl}] &= \delta_{jk}\mathcal{M}_{il} - \delta_{ik}\mathcal{M}_{jl} + \delta_{jl}\mathcal{M}_{ki} - \delta_{il}\mathcal{M}_{kj}.
\end{aligned} \tag{3.1.2}$$

The indices running over the dimension of the defect are denoted with a hat, while  $i, j$  are the directions perpendicular to the defect. In the rest of this thesis, we will extend this notation to operators, and denote operators restricted to the defect with a hat to distinguish them from bulk operators. Defect conformal primaries are defined similarly to bulk conformal primaries, that is:

$$[\mathcal{K}_{\hat{a}}, \hat{\mathcal{O}}(0)] = 0. \tag{3.1.3}$$

Descendants are constructed by acting with  $\mathcal{P}_{\hat{a}}$  on a defect conformal primary.

There are now two types of generators of rotations: those that generate the rotations on the defect and those generating the rotations around the defect. The generators of rotations on the defect,  $\mathcal{M}_{\hat{a}\hat{b}}$ , commute with the generator of dilatations,  $\mathcal{D}$ , and as such we can label defect operators by their conformal dimension  $\hat{\Delta}$  and spin  $\hat{j}$ . The generators of rotations around the defect,  $\mathcal{M}_{i,j}$ , also commute with  $\mathcal{D}$  since they form a disconnected part of the algebra. Hence, we can add an extra label to  $\hat{\mathcal{O}}$ , which is the *transverse spin*  $s$ . Here,  $s$  denotes the charge under the  $SO(q)$  symmetry group.

Because the defect breaks the bulk conformal symmetry, and in particular the translational symmetry, the stress-energy tensor  $T_{\mu\nu}$  is no longer locally conserved. This gives rise to a defect operator called the *displacement*, which is defined through the following Ward identity [47]:

$$\partial_{\mu}T_{\mu i} = -\delta^{(q)}(\mathcal{D})D^i, \tag{3.1.4}$$

where the defect is denoted by  $\mathcal{D}$ . The displacement is a protected operator with conformal dimension  $\Delta_{\mathcal{D}} = p + 1$ , and transverse spin  $s = 1$ . It is a canonical defect operator which appears in the defect spectrum when translational symmetry is broken in the bulk.<sup>1</sup>

So far we have not included additional flavor symmetries in the bulk, which can either be preserved or broken by the presence of a conformal defect. If the flavor symmetry is partly broken, it will give rise to a protected operator associated to the broken flavor current in the bulk, analogous to the displacement operator [136]. The defect operator is commonly referred to as the *tilt* and is defined as:

$$\partial_{\mu}J_A^{\mu} = \delta^{(q)}(\mathcal{D})t_A. \tag{3.1.5}$$

It has a protected conformal dimension  $\Delta_t = p$ . It is also charged under the flavor symmetry preserved by the defect, but does not have transverse spin.

---

<sup>1</sup>Trivial and topological defects do not have a displacement operator.



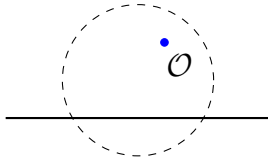


Figure 3.1: The OPE between a bulk operator  $\mathcal{O}$  and the defect, depicted by a solid line. The OPE converges as long as there are no other operator insertions within the circle.

## 3.2 Defect kinematics

The presence of a conformal defect influences the kinematics of the CFT. In particular, one-point functions of bulk operators are no longer necessarily zero by symmetry requirements, and two-point functions depend on defect cross-ratios instead of being completely fixed kinematically. Furthermore, there exist correlators between bulk and defect operators. Note that all correlators involving only defect operators still obey the usual CFT constraints, but now in  $p$  dimensions, and hence are given by the expressions in section 2.2.

To write down the general form of the correlation functions between bulk and defect operators, let us introduce the *bulk-to-defect OPE*. Bulk operators close to the defect can be expanded in an infinite series of defect operators. This expansion takes the following form [47]:

$$\mathcal{O}(x) \sim \sum \frac{b_{\mathcal{O}\hat{\mathcal{O}}}}{|x^\perp|^{\Delta-\hat{\Delta}}} C_{\hat{\mathcal{O}}} (|x^\perp|^2 \partial_\parallel^2) \frac{x_{i_1} \cdots x_{i_s}}{|x^\perp|^s} \hat{\mathcal{O}}^{i_1, \dots, i_s}(\hat{x}), \quad (3.2.1)$$

where  $x^\perp$  are the directions perpendicular to the defect, and  $\hat{x} \equiv x^{\hat{a}}$  are the directions parallel to the defect. The bulk-to-defect OPE converges if one considers a sphere drawn around the bulk operator, intersecting the defect, in which no other operator insertions are present. Then, following the state-operator correspondence, the bulk operator can be expressed as an infinite sum of defect states as in eq. (3.2.1). This is depicted in figure 3.1. Using eq. (3.2.1), the one-point function of a bulk scalar in the presence of a conformal defect is given by:

$$\langle\langle \mathcal{O}(x) \rangle\rangle = \frac{a_{\mathcal{O}}}{|x^\perp|^{\Delta_{\mathcal{O}}}}. \quad (3.2.2)$$

We have used the notation

$$\langle\langle \cdots \rangle\rangle \equiv \frac{\langle \mathcal{D} \cdots \rangle}{\langle \mathcal{D} \rangle}, \quad (3.2.3)$$

to denote a correlation function of bulk operators in the presence of a defect, normalized by the expectation value of the defect itself. The two-point function between bulk and defect scalar operators is given by:

$$\langle\langle \mathcal{O}(x_1) \hat{\mathcal{O}}(\hat{x}_2) \rangle\rangle = \frac{b_{\mathcal{O}\hat{\mathcal{O}}}}{|x_1^\perp|^{\Delta_1 - \hat{\Delta}_2} |x_{12}^\mu|^{2\hat{\Delta}_2}}. \quad (3.2.4)$$

In the case of spinning or fermionic operators, additional tensor structures will appear in eq. (3.2.4). These are all the correlation functions involving bulk operators that are kinematically fixed. Two-point functions between bulk operators are the first correlators that depend on the *defect cross-ratios*:

$$r + \frac{1}{r} = \frac{\hat{x}_{12}^2 + x_1^\perp + x_2^\perp}{|x_1^\perp| |x_2^\perp|}, \quad w + \frac{1}{w} = \frac{2x_1^\perp \cdot x_2^\perp}{|x_1^\perp| |x_2^\perp|}. \quad (3.2.5)$$

They are often rewritten as  $(z, \bar{z})$ , where<sup>2</sup>

$$z = rw, \bar{z} = \frac{r}{w}. \quad (3.2.6)$$

A third variable  $\chi$  is also used, with

$$\chi = \frac{(1 - rw)(w - r)}{rw} = \frac{x_{12}^2}{|x_1^\perp||x_2^\perp|}. \quad (3.2.7)$$

In terms of these cross-ratios, the two-point function of two bulk scalar operators can be written as follows:

$$\langle\langle \mathcal{O}_{\Delta_1}(x_1)\mathcal{O}_{\Delta_2}(x_2) \rangle\rangle = \frac{\mathcal{F}(r, w)}{|x_1^\perp|^{\Delta_1}|x_2^\perp|^{\Delta_2}}. \quad (3.2.8)$$

One can also consider three-point functions between bulk and defect operators, which in general depend on more cross-ratios. Expressions for general, spinning three-point functions between one or two bulk operators and a defect operator can be found in [52]. Three-point functions of a bulk and two boundary operators are derived in appendix B.2.

An additional piece of defect CFT data is provided by the normalization of the two-point function of the displacement. Usually, the normalization of the two-point function is non-physical data, but because of the relation of the displacement to the bulk stress-tensor, this coefficient becomes meaningful [47]:

$$\langle D_i(\hat{x}_1)D_j(\hat{x}_2) \rangle = c_D \frac{\delta_{ij}}{(\hat{x}^2)^{p+1}}. \quad (3.2.9)$$

The bulk-to-defect coupling of the stress-tensor  $T_{\mu\nu}$  and the displacement is fully fixed in terms of this coefficient  $c_D$  and the one-point function coefficient of the stress-tensor  $a_T$ .

### 3.2.1 Conformal blocks

We have seen in the previous subsection that two-point functions of bulk operators in the presence of a defect depend on defect cross ratios  $r, w$ . They admit a conformal block expansion, similar to the four-point functions in CFTs without defects, or far away from the defect, described in section 2.2. In the presence of a defect, there are two different OPEs one can exploit: the ‘‘ordinary’’ bulk OPE of eq. (2.2.7) between two bulk operators away from the defect, and the bulk-to-defect OPE in eq. (3.2.1). Choosing either one or the other allows us to expand eq. (3.2.8) in *bulk* or *defect* blocks.

**Bulk channel.** The expansion of eq. (3.2.8) in bulk blocks is obtained by acting with the bulk OPE (2.2.7) first. This results in an infinite sum of local bulk operators, which can acquire a one-point function when brought close to the defect. Hence, the expansion in bulk channel conformal blocks provides information on the bulk OPE coefficient  $\lambda_{ijk}$  as well as on the one-point function coefficient  $a_k$ :

$$\langle\langle \mathcal{O}_1(x_1)\mathcal{O}_2(x_2) \rangle\rangle = \sum_{\mathcal{O}_k} \lambda_{12k} a_k f_{\Delta_k, \ell_k}^{\Delta_{12}}(r, w). \quad (3.2.10)$$

---

<sup>2</sup>Not to be confused with the bulk cross-ratios defined in eq. (2.2.5). It will be clear from the context whether bulk or defect cross-ratios are meant.

The blocks  $f_{\Delta_k, \ell_k}^{\Delta_{12}}(r, w)$  can be found by acting with the quadratic Casimir of the bulk algebra and solving the corresponding differential equation.

The bulk channel blocks are not known in closed form for arbitrary defect dimension  $p$  and codimension  $q$ . They can be written down as an infinite sum over hypergeometrics instead [47, 137]:

$$\begin{aligned}
f_{\Delta, \ell}^{\Delta_{12}}(r, w) = & r^{-\frac{\Delta_{12}}{2}} \sum_{m, n=0}^{\infty} \frac{4^{m-n} \left(-\frac{\ell}{2}\right)_m \left(\frac{1-\ell-p}{2}\right)_m \left(\frac{-\ell+\Delta+2+\Delta_{12}}{2}\right)_m}{m!n! \left(2-\frac{d}{2}-\ell\right)_m \left(\frac{3-\Delta-\ell}{2}\right)_m} \times \\
& \frac{\left(\frac{\Delta-1}{2}\right)_n \left(\frac{\Delta-p}{2}\right)_n \left(\frac{\ell+\Delta+\Delta_{12}}{2}\right)_{n-m} (1-r^2)^{\ell-2m} \left(\frac{(w-r)(1-rw)}{w}\right)^{\frac{\Delta-\ell}{2}+m+n}}{\left(1+\Delta-\frac{d}{2}\right)_n \left(\frac{1+\Delta+\ell}{2}\right)_n \left(\frac{\ell+\Delta-1}{2}\right)_{n-m}} \times \\
& {}_2F_1\left(\frac{\Delta+\ell-\Delta_{12}}{2}-m+n, \frac{\Delta+\ell}{2}-m+n, \Delta+\ell-2m+2n; 1-r^2\right) \times \\
& {}_4F_3\left(-n, \frac{\Delta_{12}-\Delta-\ell-2n+2}{2}, -m, \frac{\Delta_{12}+\Delta+\ell-2m}{2}, \frac{1+\Delta_{12}}{2}, \frac{\Delta_{12}+\Delta-\ell-d+2}{2}; 1\right), \tag{3.2.11}
\end{aligned}$$

In special cases it is possible to write down a closed form expression, for example for the case of a boundary or interface, which will be discussed in more detail below.

**Defect channel.** Another way to expand eq. (3.2.8) is by taking the bulk-to-defect OPE twice, resulting in a (normalized) two-point function on the defect. In this case, the expansion in defect channel blocks provides us with the bulk-to-defect OPE coefficients  $\hat{b}_{ij}$ :

$$\langle\langle \mathcal{O}_1(x_1) \mathcal{O}_2(x_2) \rangle\rangle = \sum_{\hat{\mathcal{O}}_k} \hat{b}_{1k} \hat{b}_{2k} \hat{f}_{\hat{\Delta}_k, \hat{j}_k, s_k}(r, w). \tag{3.2.12}$$

The defect blocks  $\hat{f}_{\hat{\Delta}_k, \hat{j}_k, s_k}(r, w)$  are obtained by acting with the quadratic Casimir of the defect algebra (3.1.2). Solving the resulting differential equations, we find the following formula for the conformal blocks [47]:

$$\begin{aligned}
\hat{f}_{\hat{\Delta}, s}(\chi, \phi) = & 2^{-s} \frac{\Gamma(q+s-2)\Gamma\left(\frac{q}{2}-1\right)}{\Gamma\left(\frac{q}{2}+s-1\right)\Gamma(q-2)} \chi^{-\hat{\Delta}} {}_2F_1\left(\frac{q+s}{2}-1, -\frac{s}{2}; \frac{q-1}{2}; \sin^2\phi\right) \\
& \times {}_2F_1\left(\frac{\hat{\Delta}+1}{2}, \frac{\hat{\Delta}}{2}; \hat{\Delta}+1-\frac{p}{2}; \frac{4}{\chi^2}\right), \tag{3.2.13}
\end{aligned}$$

where  $p$  is the dimension of the defect and  $q$  the codimension.

Conformal blocks for two-point functions of spinning operators in the presence of a defect were computed in [50], where they also found a closed-form expression for the blocks in the defect channel.

### 3.2.2 Boundary CFT

Let us look further into the case of a codimension-1 defect. We specifically consider boundaries, but the discussion below also applies to interfaces. There are some similarities with one-dimensional CFTs in the way that they differ from higher-codimensional defects. Firstly, there are no rotations possible around a boundary or interface, and hence bulk operators cannot acquire transverse spin. Secondly, for a CFT with a boundary there is

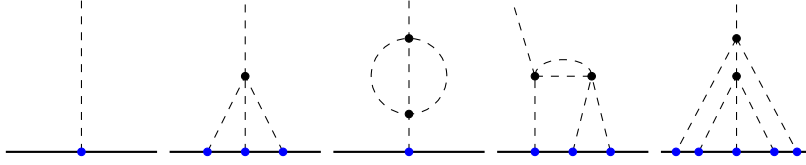


Figure 3.2: Diagrams contributing to the one-point function  $\langle\langle\phi\rangle\rangle$  up to  $\mathcal{O}(\varepsilon^2)$ . The defect is denoted by a solid line, scalars by a dotted line, and fermions by solid arrowed lines. Bulk scalar couplings  $\lambda_0$  are represented by a black dot, and defect couplings  $h_0$  by a blue dot.

only one direction perpendicular to the defect. Because of this, the two-point function of bulk operators shown in eq. (3.2.8) no longer depends on two independent cross-ratios, but only on  $\chi$  defined in eq. (3.2.7). This makes the expressions for the conformal blocks simpler, and in particular makes it possible to find a closed form expression for the bulk channel blocks:

$$g_{\Delta}^{\Delta_{12}}(\chi) = \chi^{\Delta/2} {}_2F_1\left(\frac{\Delta + \Delta_{12}}{2}, \frac{\Delta - \Delta_{12}}{2}; \Delta + 1 - \frac{d}{2}; -\chi\right). \quad (3.2.14)$$

More details on the derivation can be found in appendix B. Lastly, boundary CFTs only admit one-point functions of scalar operators. Spinning operators, including the stress-tensor, do not have a one-point function.

### 3.3 Defects in the $\varepsilon$ -expansion

CFTs with defects can also be studied in the  $\varepsilon$ -expansion, where both the bulk and the defect need to be tuned to the fixed point. There are two different types of defects one can study: those with a fixed dimension  $p$  or those with a fixed codimension  $q$ . Examples of defects with a fixed codimension are boundaries ( $q = 1$ ) or monodromy defects ( $q = 2$ ). As a result of having  $q$  fixed, the defect changes dimension with the bulk. Calculations in the  $\varepsilon$ -expansion for these types of defects are given in section 4.5 for a superconformal field theory with a boundary, and in section 5.3.1 for a monodromy defect with  $O(N)$  flavor symmetry.

Defects with a fixed dimension are e.g. surface or line defects. Let us look at the example of a line defect in the  $\phi^4$  model we studied in section 2.3. We take the localized magnetic field line defect studied in [81, 84] and section 5.3 for the  $O(N)$  model, and focus on the case  $N = 1$ . The action of eq. (2.3.2) is modified with the field  $\phi$  integrated over a line:

$$S_{\phi^4} \rightarrow S_{\phi^4} + h \int d\tau \phi(x). \quad (3.3.1)$$

Because  $\phi$  has dimension  $\Delta_{\phi} = 1$  in four dimensions, it is a marginal operator in  $1d$ . The action in eq. (3.3.1) describes a CFT if we tune both the bulk coupling  $\lambda$  and the defect coupling  $h$  to their fixed points. This requires us to find the fixed point  $h_*$ , which is given by the zero of the  $\beta$ -function  $\beta_h$ . In the bulk, we obtained  $\beta_{\lambda}$  by requiring that the four-point interaction vertex is finite. To obtain  $\beta_h$ , we require that the one-point function of  $\phi$  is finite. The corresponding Feynman diagrams up to  $\mathcal{O}(\varepsilon^2)$  are given in figure 3.2. Their evaluation can be found in [81]. Note that even though we can work perturbatively in the bulk coupling  $\lambda$ , this is not the case for the defect coupling  $h$  and we need to consider diagrams to all orders in  $h$ . However, it becomes immediately clear

that for a given number of bulk couplings  $\lambda$ , there are only finitely many defect diagrams. Extracting the divergences, we find the following expression for  $Z_h$ :

$$Z_h = \mu^{\varepsilon/2} h \left\{ 1 + \frac{1}{\varepsilon(4\pi)^2} \left( \frac{\lambda h^3}{12} + \frac{\lambda^2 h}{24(4\pi)^2} - \frac{\lambda^2 h^3}{12(4\pi)^2} - \frac{\lambda^2 h^5}{48(4\pi)^2} + \mathcal{O}(\lambda^3) \right) + \dots \right\}, \quad (3.3.2)$$

where the dots indicate terms of order  $1/\varepsilon^2$ . The  $\beta$ -function is obtained in the same way we found  $\beta_\lambda$  in section 2.3:

$$\beta_h = \frac{dZ_h}{d \log \mu} = -\frac{\varepsilon}{2} h + \frac{\lambda h^3}{6(4\pi)^2} + \frac{\lambda^2 h}{12(4\pi)^4} - \frac{\lambda^2 h^3}{4(4\pi)^4} - \frac{\lambda^2 h^5}{12(4\pi)^4} + \mathcal{O}(\lambda^3). \quad (3.3.3)$$

The fixed point is given by the zero of eq. (3.3.3) for  $\lambda = \lambda_*$  given in eq. (2.3.11):

$$h_*^2 = 9 + \frac{73\varepsilon}{6} + \mathcal{O}(\varepsilon^2). \quad (3.3.4)$$

Notice that we only find the fixed point up to  $\mathcal{O}(\varepsilon)$ . To go to  $\mathcal{O}(\varepsilon^2)$ , we would need to know the  $\beta$ -function at  $\mathcal{O}(\varepsilon^3)$ .

When we also consider the finite part of the diagrams in figure 3.2, we find the complete one-point function:

$$\langle\langle \phi(x) \rangle\rangle = \frac{\mathcal{N}_\phi a_\phi}{|x|^{\Delta_\phi}}, \quad a_\phi^2 = \frac{9}{4} + \varepsilon \frac{81 \log 4 - 24}{56} + \mathcal{O}(\varepsilon^2), \quad (3.3.5)$$

where the normalization factor  $\mathcal{N}_\phi$  comes from the normalization of  $\langle \phi(x_1) \phi(x_2) \rangle$  away from the defect.

The anomalous dimension of the first operator in the bulk-to-defect expansion, which we denote as  $\hat{\phi}$ , can be computed in the usual way by looking at the divergence of its two-point function on the defect. However, in this case we can also extract it directly from the  $\beta$ -function  $\beta_h$ . The reason is that one can define a *defect stress-tensor*  $\hat{T}_D$ , which here is proportional to  $\beta_h$  [84]:

$$\hat{T}_D(\tau) = \beta_h \hat{\phi}(\tau), \quad (3.3.6)$$

with protected dimension  $\Delta_{\hat{T}_D} = 1$ . Hence, the conformal dimension of  $\hat{\phi}$  is given by:

$$\hat{\Delta}_{\hat{\phi}} = 1 + \frac{\partial \beta_h}{\partial h} = 1 + \frac{6\varepsilon}{7} + \mathcal{O}(\varepsilon^2). \quad (3.3.7)$$

For the  $O(N)$  model (note that the defect above is the case  $N = 1$ ), correlation functions between defect operators can be found in section 5.3.2, while correlators between bulk and defect operators, and bulk operators in the presence of a defect were recently computed in [86, 87]. A generalization to Yukawa CFTs, which include interactions between fermions and scalars, is given in chapter 6.

## 3.4 Defect bootstrap

We have seen in section 3.2 that two-point functions of bulk operators in the presence of a defect are no longer fully fixed by conformal symmetry. Instead, they depend on the defect cross-ratios  $r$  and  $w$ . In section 3.2, it was shown that the two-point functions can be expanded in either bulk or defect conformal blocks, depending on which OPE one

$$\sum_{\mathcal{O}} \lambda_{\mathcal{O}} a_{\mathcal{O}} \Delta_{\mathcal{O}} = \sum_{\hat{\mathcal{O}}} (\hat{b}_{\hat{\mathcal{O}}})^2 \Delta_{\hat{\mathcal{O}}}$$

Figure 3.3: The defect crossing equation. On the left the bulk channel is shown, while the right-hand side corresponds to the defect channel.

uses: the bulk OPE between the two operators and subsequently bringing the resulting local operators to the defect, or the bulk-to-defect OPE for each operator, resulting in a two-point function of two defect operators. The first expansion is called the *bulk channel*, and the second expansion the *defect channel*. Demanding that these two expansions are equivalent if we are close enough to the defect (and there are no insertions of other operators), results in the *defect crossing equation*, depicted in figure 3.3, which takes the following form:

$$\sum_{\mathcal{O}_k} \lambda_{12k} a_{\mathcal{O}_k} f(r, w) = \sum_{\hat{\mathcal{O}}_i} \hat{b}_{1i} \hat{b}_{2i} \hat{f}(r, w), \quad (3.4.1)$$

where  $\lambda_{ijk}$  is the bulk OPE coefficient,  $a_{\mathcal{O}}$  the one-point function coefficient,  $\hat{b}_{ij}$  the bulk-to-boundary OPE coefficients,  $f(r, w)$  the bulk channel conformal blocks and  $\hat{f}(r, w)$  the defect channel conformal blocks. Note that while on the defect side the square of the bulk-to-defect OPE coefficients appears, on the bulk side it is the product of the bulk OPE coefficient and the one-point function coefficient.

One might wonder if eq. (3.4.1) is the most fundamental crossing equation for defect CFTs that one can write down, and defect data, and the answer is no. While this crossing equation includes information on bulk OPE coefficients, one-point function coefficients, and bulk-to-defect OPE coefficients, as well as the bulk and defect spectrum, it does not rely on defect OPE coefficients and hence cannot be used to constrain those. The true parallel with the four-point function of bulk operators far away from the defect appearing in the bulk crossing equation in eq. (2.4.1), would be the correlator  $\langle\langle \phi\phi\hat{\phi} \rangle\rangle$ . Knowing all the correlators of this form would be enough to completely determine the bulk and defect CFT data. However, it was already pointed out in section 3.2 that the correlation function depends on multiple cross-ratios, which makes it harder to use them in the defect bootstrap, and most results in the defect bootstrap rely on the study of two-point functions between bulk operators in the presence of the defect, which already constrain a significant part of the bulk and defect CFT data.

### 3.4.1 Numerical versus analytic bootstrap

The defect crossing equation in eq. (3.4.1) contains information on both the defect and the bulk CFT. Hence, having knowledge about the bulk conformal data can be beneficial to find constraints on defect data, but it is also possible to obtain information about the bulk using the defect bootstrap. In this way, the defect bootstrap enriches the usual conformal bootstrap program, but at the same time comes with additional challenges.

One main challenge is the lack of positivity, even for unitary theories. As said earlier, on the bulk channel side the bulk OPE coefficient appears together with the one-point function coefficient, and there is no guarantee that this combination will be a positive number. Hence, solving eq. (3.4.1) with the modern numerical conformal bootstrap tech-

niques outlined in section 2.4.2 is currently not possible. It is, however, possible to look at the CFT on the defect and study it as an “ordinary” CFT using the numerical bootstrap. This approach is used in chapter 5. Since it is equivalent to using numerical techniques described in section 2.4.2, we will not further elaborate here. The same philosophy has also been applied to other setups, for example to find the space of allowed conformal boundary conditions of a free bulk theory [68, 69]. Another possibility is to assume positivity in the defect crossing equation, based on for example results for the OPE coefficients and one-point coefficients from various perturbative expansions, as was done in [70].

A noteworthy method to bootstrap theories without positivity is the method of determinants, also known as Gliozzi’s method [138, 139]. Instead of considering the full crossing equations with an infinite number of conformal primaries exchanged in the OPEs, one studies a truncated version where only a few exchanged operators contribute. If one assumes that  $N$  operators contribute, and considers  $M$  linear functionals (derivatives of conformal blocks), with  $M > N$ , and there are  $n < N$  free parameters, the system is overdetermined and it might be possible to find a unique solution. The main advantage is that no unitarity is required, and one can find the spectrum of theories not saturating the numerical bound. Indeed, this method was used in [53] to bootstrap codimension-1 defects. However, the assumptions of a finite spectrum are very strong, and it is in general difficult to estimate the error on the obtained spectrum.

Let us now turn to the analytic bootstrap, which does not require positivity. Similar to the bulk CFT, it is possible to construct a *Lorentzian defect inversion formula* [51, 97]. Starting from the lightcone limit and performing the lightcone bootstrap for two-point functions of bulk operators in the presence of a defect, it can be shown [51] that in the defect spectrum, there are conformal primaries with dimension

$$\hat{\Delta} = \Delta_\phi + s + 2m + \mathcal{O}\left(\frac{1}{s}\right), \quad (3.4.2)$$

where  $s$  denotes the *transverse* spin. Hence, an expansion in large transverse spin is possible, and the analogy with the bulk case without defects, discussed in section 2.4.3, becomes clear. A Lorentzian inversion formula for the defect channel was then constructed in [51], and later for the bulk channel as well in [97], following an improved understanding of the bulk conformal blocks [137].

Other analytical methods that we encountered in section 2.4.3 can also be applied to or adapted for the case of defect CFTs. The analytic functionals used to study  $1d$  CFTs can be directly applied to constrain four-point functions of defect operators confined to a line. In addition, the functional bootstrap has been set up for the case of a boundary [57, 58], which as we have seen shares many similarities with the  $1d$  bootstrap.

The large charge expansion has also been used in the context of defects to study new, strongly coupled regions not accessible by perturbative methods. In the case of a boundary, [140] showed that if a *bulk* operator at large charge corresponds to a superfluid state, then the large charge sector of *boundary* operators will also be in a superfluid state, and an effective field theory can be constructed. From the EFT, the large charge spectrum of boundary operators can be determined.

Another possibility, as for bulk CFTs, is to combine perturbative expansions with the analytic bootstrap. In the next chapter 4 we will bootstrap bulk and boundary CFT data of superconformal boundaries in the  $\varepsilon$ -expansion.





# Chapter 4

## Superconformal boundaries in $4 - \varepsilon$ dimensions

### 4.1 Introduction

The conformal algebra shown in section 2.1 can be extended to a *superconformal algebra* by including anticommuting supersymmetry generators. Theories invariant under this algebra are called *superconformal field theories* (SCFTs). The amount of supersymmetry is usually denoted by  $\mathcal{N}$  and corresponds to the number of *supercharges* present in the superconformal algebra. Which superconformal algebra is considered depends on  $\mathcal{N}$  and on the dimension of the SCFT. In this chapter we consider  $3d \mathcal{N} = 2$  SCFTs with a boundary, where the bulk superconformal algebra is  $OSP(2|4)$  and contains the supercharges  $\mathcal{Q}_\alpha, \bar{\mathcal{Q}}_\alpha, \alpha = 1, 2$  as well as their superpartners  $\mathcal{S}^\alpha, \bar{\mathcal{S}}^\alpha, \alpha = 1, 2$ .

We have seen that the presence of conformal symmetry severely constrains the kinematics of correlation functions and makes it possible to constrain the spectrum of a CFT based on symmetry arguments and basic assumptions alone, using the conformal bootstrap. Adding additional symmetry constraints could then lead to even stronger bounds on CFTs. However, the Coleman–Mandula theorem [141] states that spacetime and internal symmetries can only combine trivially. Conformal symmetry is still allowed because of the lack of a mass gap, which is one of the assumptions of the Coleman–Mandula theorem. Supersymmetry is the other exception, which has been solidified in the Haag–Łopuszański–Sohnius theorem [142], generalizing the Coleman–Mandula theorem by allowing anticommuting generators of the symmetry algebra. Hence, supersymmetry (SUSY) seems to be the only possibility to further constrain correlation functions in the theory, which can be exploited to find stronger bounds on the CFT data.

Adding a boundary to the bulk SCFT breaks part of the conformal symmetry and of the supersymmetry. We will consider 1/2-BPS superconformal boundaries, which preserve a superconformal algebra on the boundary with half the amount of SUSY of the bulk. Such a setup has received particular attention in the context of infrared dualities [143–146], and localization [147, 148].

There are two ways in which supersymmetry can be preserved when a boundary is introduced: one choice preserves supercharges of the same chirality which define a  $2d \mathcal{N} = (0, 2)$  subalgebra, while the other choice is non-chiral and describes a  $2d \mathcal{N} = (1, 1)$  subalgebra. We will study the kinematical constraints on correlators for both choices, with a particular emphasis on two-point functions. As explained in section 3.2, in the presence of a boundary two-point correlators of bulk fields are not fixed by symmetry, but

depend on a conformal invariant. They contain non-trivial dynamics akin to four-point functions in homogeneous CFTs, which is captured by the existence of two inequivalent conformal block expansions: the bulk and defect expansions. Consistency between the two decompositions is the starting point of the bootstrap program for BCFT.

Our main focus will be chiral fields, which are short operators of the bulk superconformal algebra killed by half of the supercharges, and whose conformal dimension is fixed by the  $R$ -symmetry. As usual in the bootstrap, it is essential to calculate the relevant superconformal blocks. Bosonic blocks for BCFT two-point functions have been known for a long time [149], however less work has been done on supersymmetric models, the sole exception being boundaries in  $\mathcal{N} = 4$  SYM [150]. Attempts to formalize the study of superconformal blocks include analytic superspace [151] and the connection to Calogero-Sutherland models [152, 153]. Here we start our analysis using standard superspace techniques, and calculate superblocs using the Casimir approach [119]. The superspace analysis will be uniform for the  $\mathcal{N} = (0, 2)$  and  $\mathcal{N} = (1, 1)$  subalgebras, but it turns out that the  $\mathcal{N} = (1, 1)$  blocks have the interesting property that they can be analytically continued across dimensions. In more detail, there is a unique half-BPS boundary in  $4d$   $\mathcal{N} = 1$  which is non-chiral, and that can be interpolated to the  $\mathcal{N} = (1, 1)$  boundary in  $3d$ . This is the BCFT counterpart of the results obtained in [154], where the bulk superconformal blocks were continued in  $d$ . Even though conformal symmetry is subtle in non-integer dimensions,<sup>1</sup> conformal blocks are usually analytic in all their quantum numbers.<sup>2</sup>

Armed with the analytic continuation we tackle the  $\varepsilon$ -expansion for models that satisfy our constraints. Using minimal assumptions, we prove that two-point functions of free chiral and antichiral fields are completely fixed. At leading order in  $\varepsilon$ , which already corresponds to an interacting fixed point, we prove that the two-point functions are universal up to two free parameters: the anomalous dimension of the lowest-lying bulk field, and the anomalous dimension of the lowest-lying boundary field. The solution is non-trivial and contains an infinite number of conformal blocks, and therefore can be used to extract an infinite amount of CFT data.

As a check of our general order  $\varepsilon$  result, we concentrate on the Wess-Zumino model with cubic superpotential, which is a prime example of a critical system that preserves four supercharges. Using the results of [156], we construct an explicit Lagrangian model with boundary degrees of freedom that exhibits all the symmetries of our setup. We use this model to perform a Feynman diagram calculation at one-loop order, and confirm that the perturbative result is in perfect agreement with our bootstrap prediction.

The outline of this chapter is as follows. In section 4.2 we summarize the differences between the  $\mathcal{N} = (0, 2)$  and  $\mathcal{N} = (1, 1)$  boundaries and introduce the crossing equations for BCFT. In section 4.3 we carry out a detailed study of correlation functions and superconformal blocks of these  $3d$  models. In section 4.4 we rederive the superconformal blocks with a new method that is applicable to any  $3 \leq d \leq 4$ , and use them to bootstrap two-point functions of chiral operators in the  $\varepsilon$  expansion. Finally, in section 4.5 we compute the same two-point functions for the Wess-Zumino model using Feynman diagrams.

---

<sup>1</sup>See [129] for discussions on non-integer  $d$  and [155] for non-integer  $N$  (in the context of  $O(N)$  models).

<sup>2</sup>In the case of the defects both dimension and codimension appear as parameters in the blocks [47, 137] as was shown in section 3.2.

## 4.2 Preliminaries

In this preliminary section we introduce the symmetry algebra in the bulk, and the two possible half-BPS subalgebras preserved by a supersymmetric boundary. We also introduce chiral fields and review the standard bootstrap equations for two-point functions in BCFT.

### 4.2.1 Superconformal boundaries in $3d$

There are two inequivalent half-BPS boundaries that one can consider in  $3d$   $\mathcal{N} = 2$  superconformal theories, which are commonly denoted as  $\mathcal{N} = (0, 2)$  and  $\mathcal{N} = (1, 1)$  boundaries (see [147, 148, 143–146, 157] for related work). The cleanest way to understand their differences is at the level of the commutation relations of their algebras.

Let us start by reminding the reader about the main features of  $3d$   $\mathcal{N} = 2$  superconformal symmetry. Besides the conformal generators  $\mathcal{D}, \mathcal{P}_\mu, \mathcal{K}_\mu, \mathcal{M}_{\mu\nu}$ , the superconformal algebra has four Poincaré supercharges  $\mathcal{Q}_\alpha, \bar{\mathcal{Q}}_\alpha$ , and four superconformal partners  $\mathcal{S}_\alpha, \bar{\mathcal{S}}_\alpha$ . There is an extra  $U(1)$  symmetry generated by  $\mathcal{R}$  under which  $\mathcal{Q}_\alpha, \mathcal{S}_\alpha$  have charge  $-1$ , and  $\bar{\mathcal{Q}}_\alpha, \bar{\mathcal{S}}_\alpha$  have charge  $+1$ . The precise commutation relations with a summary of our conventions are presented in appendix A. The representation theory of  $3d$   $\mathcal{N} = 2$  is well known and can be found for example in [158].

When we restrict ourselves to three dimensions, we take the superconformal boundary to be located at  $x_2 \equiv x_\perp = 0$ . It is clear that the bosonic subalgebra is generated by  $\mathcal{P}_a, \mathcal{K}_a, \mathcal{M}_{ab}$ , and  $\mathcal{D}$ , where  $a = 0, 1$  runs over directions parallel to the boundary. We are now ready to introduce the two inequivalent boundary-preserving superalgebras, which differ only by the choice of fermionic generators.

**The  $\mathcal{N} = (0, 2)$  boundary:** The first possibility is to choose the following fermionic generators:  $\mathcal{Q}_2, \bar{\mathcal{Q}}_2, \mathcal{S}^2, \bar{\mathcal{S}}^2$ . The precise commutation relations can be obtained by restricting the full superconformal algebra presented in appendix A.2. The following ones are of particular importance:

$$\begin{aligned} \{\mathcal{Q}_2, \bar{\mathcal{Q}}_2\} &= -2(\mathcal{P}_0 + \mathcal{P}_1), \\ \{\mathcal{Q}_2, \bar{\mathcal{S}}^2\} &= -2i\mathcal{D} + 2\mathcal{R} + 2i\mathcal{M}_{01}, \\ \{\bar{\mathcal{Q}}_2, \mathcal{S}^2\} &= -2i\mathcal{D} - 2\mathcal{R} + 2i\mathcal{M}_{01}. \end{aligned} \tag{4.2.1}$$

From the first equation, we notice that  $\mathcal{P}_2$  does not appear on the right-hand side. This was to be expected, since translations in the  $x_2 = x_\perp$  direction are not preserved. Regarding the second and third equations, it is crucial to notice the appearance of  $\mathcal{R}$ . Physically, it means that the  $\mathcal{N} = (0, 2)$  boundary preserves  $R$ -symmetry, a property that strongly constrains which correlation functions are non-vanishing. For example, we will often be concerned with bulk operators  $\mathcal{O}_r$  with charge  $r$ . From the above discussion, it follows that one-point functions  $\langle \mathcal{O}_r \rangle = 0$  unless  $r = 0$ , and similarly two-point functions  $\langle \mathcal{O}_{r_1} \mathcal{O}_{r_2} \rangle = 0$  unless  $r_1 + r_2 = 0$ .

**The  $\mathcal{N} = (1, 1)$  boundary:** The second possibility is to choose the following fermionic generators:

$$\begin{aligned}\tilde{\mathcal{Q}}_1 &\equiv \frac{1}{\sqrt{2}} (\mathcal{Q}_1 + \bar{\mathcal{Q}}_1), & \tilde{\mathcal{Q}}_2 &\equiv \frac{i}{\sqrt{2}} (\mathcal{Q}_2 - \bar{\mathcal{Q}}_2), \\ \tilde{\mathcal{S}}^1 &\equiv \frac{1}{\sqrt{2}} (\mathcal{S}^1 + \bar{\mathcal{S}}^1), & \tilde{\mathcal{S}}^2 &\equiv \frac{i}{\sqrt{2}} (\mathcal{S}^2 - \bar{\mathcal{S}}^2).\end{aligned}\tag{4.2.2}$$

Once again, the full set of commutation relations can be obtained from the formulas in appendix A.2. The non-vanishing anticommutators are

$$\begin{aligned}\{\tilde{\mathcal{Q}}_\alpha, \tilde{\mathcal{Q}}_\beta\} &= 2(\gamma^a)_{\alpha\beta} \mathcal{P}_a, \\ \{\tilde{\mathcal{Q}}_1, \tilde{\mathcal{S}}^1\} &= -2i(\mathcal{D} + \mathcal{M}_{01}), \\ \{\tilde{\mathcal{Q}}_2, \tilde{\mathcal{S}}^2\} &= -2i(\mathcal{D} - \mathcal{M}_{01}).\end{aligned}\tag{4.2.3}$$

As before,  $\mathcal{P}_2$  is not part of the algebra since  $a = 0, 1$ . Interestingly, the second anticommutator does not contain  $\mathcal{R}$ , since  $R$ -symmetry is broken by the  $\mathcal{N} = (1, 1)$  boundary. In this case, charged bulk operators can have one- and two-point functions that would be forbidden by charge conservation, namely  $\langle \mathcal{O}_r \rangle \neq 0 \neq \langle \mathcal{O}_{r_1} \mathcal{O}_{r_2} \rangle$  for any values of the charges.

## 4.2.2 Chiral primaries in superconformal theories

As announced before, we will mostly focus on chiral primary operators  $\phi$  and their complex conjugates. Often, we will call these operators “chirals” and “antichirals” for simplicity. These are short multiplets of the superconformal algebra killed by half of the supercharges:

$$[\bar{\mathcal{Q}}_\alpha, \phi(0)] = 0, \quad [\mathcal{Q}_\alpha, \bar{\phi}(0)] = 0,\tag{4.2.4}$$

and whose conformal dimension and  $R$ -charge are related to each other. For general spacetime dimension one obtains

$$\Delta_\phi = \frac{d-1}{2} r_\phi, \quad \Delta_{\bar{\phi}} = -\frac{d-1}{2} r_{\bar{\phi}}.\tag{4.2.5}$$

There is a consistent way to define chiral multiplets in any, in principle continuous, number of dimensions, a fact that will play a significant role in section 4.4.

Chiral operators are ubiquitous in the study of SCFTs and they are present in most known models. A textbook example of a  $4d$  Lagrangian with  $\mathcal{N} = 1$  supersymmetry is to consider chiral fields in superspace with some non-linear interaction. We will consider a simple example of this in section 4.5, where we study the Wess-Zumino model, i.e. a single chiral multiplet with a cubic superpotential. This model flows to an interacting fixed point, which can be described perturbatively in the  $\varepsilon$ -expansion using weakly-coupled chiral fields. It turns out that the  $\varepsilon$ -expansion can be generalized to include boundaries, a fact that we will explore using the bootstrap results obtained in this work.

An important property of chiral operators is that they often satisfy non-trivial chiral-ring relations. These relations are dynamic and imply that certain chiral operators might disappear from an OPE, for example  $\phi_3 \notin \phi_1 \times \phi_2$ , even if this is not forbidden by superconformal symmetry. The Wess-Zumino model in  $3d$  is a simple SCFT with chiral-ring relations. The chiral ring of this model is generated by  $\phi$  together with the relation

$\phi^2 \notin \phi \times \phi$ . In the numerical bootstrap analysis of [159, 154], the chiral-ring relation provided strong evidence that a kink in the numerical plots described the Wess-Zumino model. In section 4.5.3 we will notice that our perturbative results are also consistent with the same chiral-ring relation. More complicated examples of chiral-ring relations can be found in [160] where the authors studied numerically a  $3d$  conformal manifold parametrized by the complex gauge coupling  $\tau$ . Chiral-ring relations of bulk operators could also be used to extract information of a theory living on the boundary, similar in spirit to the work of [52, 68].<sup>3</sup>

In this work we will not explore all these questions yet, but they motivated us to study this setup. Here we will work out basic kinematical constraints and use the bootstrap to study the dynamics of a single chiral field. Possible future directions and applications of our results will be discussed in the conclusions. Before we jump to the main analysis, let us first review the bootstrap approach for BCFT, which will be one of our main tools.

### 4.2.3 Crossing symmetry in BCFT

In this section we will review crossing symmetry for generic, non-supersymmetric boundary CFTs. There are two relevant symmetry algebras to study BCFT. The first one contains the  $d$ -dimensional conformal group, and it describes physics far away from the boundary. In particular, bulk local operators  $\mathcal{O}(x)$  transform in irreducible representations of this algebra, and are labeled by a conformal dimension  $\Delta$  and spin  $\ell$ . There can also be physical excitations localized on the boundary, which are represented by local operators  $\hat{\mathcal{O}}(x_a, x^\perp = 0)$ . These boundary operators transform as irreducible representations of the symmetry algebra that preserves the boundary, namely they have conformal dimension  $\hat{\Delta}$  and  $d - 1$  dimensional spin  $j$ .

Correlation functions can be constructed with arbitrary combinations of bulk and boundary operators. As usual, conformal symmetry puts strong constraints on the form of these correlation functions. For example, the one-point function and the bulk-to-boundary correlator of a bulk scalar are fixed up to a constant [149]

$$\langle \mathcal{O}(x) \rangle = \frac{a_{\mathcal{O}}}{(2x^\perp)^\Delta}, \quad \langle \mathcal{O}(x_1) \hat{\mathcal{O}}(x_2^a) \rangle = \frac{b_{\mathcal{O}\hat{\mathcal{O}}}}{(2x_1^\perp)^{\Delta-\hat{\Delta}} ((x_{12}^a)^2 + (x_1^\perp)^2)^{\hat{\Delta}}}. \quad (4.2.6)$$

For more general correlation functions the situation is more involved, because they can depend on conformal invariants. For example, a two-point function of bulk scalars depends on an arbitrary function of the invariant  $\xi$ :

$$\langle \mathcal{O}_1(x_1) \mathcal{O}_2(x_2) \rangle = \frac{\mathcal{F}(\xi)}{(2x_1^\perp)^{\Delta_1} (2x_2^\perp)^{\Delta_2}}, \quad \xi = \frac{(x_1 - x_2)^2}{4x_1^\perp x_2^\perp}. \quad (4.2.7)$$

Knowledge of  $\mathcal{F}(\xi)$  is equivalent to knowing the full two-point correlator. The function  $\mathcal{F}(\xi)$  is far from arbitrary; it is heavily constrained by crossing symmetry and it is the main subject of study in the bootstrap program for BCFT.

The main ingredient to derive the crossing equation is the operator product expansion (OPE). It is well known that one can rewrite a product of two bulk local operators as an infinite sum of individual bulk local operators using the standard OPE. In the presence of a boundary there is a second possible expansion, the boundary operator expansion

---

<sup>3</sup>We thank Edo Lauria for discussions on this idea.

(BOE), in which one bulk local operator is replaced by a sum of operators that are localized in the boundary. In terms of equations, these two OPEs are

$$\begin{aligned}\mathcal{O}_1(x)\mathcal{O}_2(0) &= \frac{1}{x^{2\Delta}} + \sum_{\mathcal{O}} \lambda_{\mathcal{O}_1\mathcal{O}_2\mathcal{O}} C[x, \partial_x] \mathcal{O}(0), \\ \mathcal{O}(x) &= \frac{a_{\mathcal{O}}}{(2x_{\perp})^{\Delta}} + \sum_{\hat{\mathcal{O}}} b_{\mathcal{O}\hat{\mathcal{O}}} D[x_{\perp}, \partial_a] \hat{\mathcal{O}}(x^a).\end{aligned}\tag{4.2.8}$$

The sums run only over conformal primaries, and the contributions of the descendants are captured by the differential operators  $C$  and  $D$  which are completely fixed by conformal symmetry.

The power of the OPE is that it allows us to evaluate higher-point functions using lower-point correlators, provided we know the spectrum of the theory and all the OPE coefficients  $a$ ,  $b$  and  $\lambda$ . In the example of a bulk two-point function, there are two different decompositions possible:

$$\mathcal{F}(\xi) = \sum_{\mathcal{O}} a_{\mathcal{O}} \lambda_{\mathcal{O}_1\mathcal{O}_2\mathcal{O}} f_{\Delta}(\xi) = \sum_{\hat{\mathcal{O}}} b_{\mathcal{O}_1\hat{\mathcal{O}}} b_{\mathcal{O}_2\hat{\mathcal{O}}} \hat{f}_{\hat{\Delta}}(\xi).\tag{4.2.9}$$

The objects  $f_{\Delta}(\xi)$  and  $\hat{f}_{\hat{\Delta}}(\xi)$  are called conformal blocks, which we review in appendix B. Equation (4.2.9) is called the ‘‘crossing equation’’, and it provides non-trivial constraints on the spectrum and CFT data of boundary conformal field theories.

The above discussion was completely general, and it applies to any conformal field theory with a conformal boundary. The main goal of this work is to specialize it to superconformal boundaries, in which case the crossing equation (4.2.9) can be constrained even further. The reason is that supersymmetry relates the OPE coefficients of different conformal primaries that belong to the same supermultiplet, which means that we can organize the expansion in terms of superconformal blocks  $F_{\Delta}(\xi)$  and  $\hat{F}_{\hat{\Delta}}(\xi)$ . These new objects are linear combinations of the bosonic blocks  $f_{\Delta}(\xi)$  and  $\hat{f}_{\hat{\Delta}}(\xi)$  with coefficients fixed by supersymmetry. In sections 4.3 and 4.4 we will compute these objects in  $d = 3$  and in  $3 \leq d \leq 4$  respectively, which will allow us to study the bootstrap equations analytically in section 4.4.4.

## 4.3 Boundaries in three dimensions

### 4.3.1 Superspace analysis

Let us start by studying correlators for both types of boundary conditions using superspace techniques. We introduce a standard Minkowski superspace in which each supercharge  $\mathcal{Q}_{\alpha}$ ,  $\bar{\mathcal{Q}}_{\alpha}$ , where  $\alpha = (1, 2) = (-, +)$ , has a Grassmann variable  $\theta^{\alpha}$ ,  $\bar{\theta}^{\alpha}$  associated to it. This setup is enough for our purposes, because we will mostly study correlators of scalar operators in a system with minimal supersymmetry.<sup>4</sup> Our superspace then consists of three spacetime coordinates  $x^{\mu}$  and four Grassmann coordinates  $\theta^{\alpha}$  and  $\bar{\theta}^{\alpha}$  which we collect as follows:

$$z = (x^{\mu}, \theta^{\alpha}, \bar{\theta}^{\alpha}),\tag{4.3.1}$$

<sup>4</sup>See [50, 161] for studies of non-supersymmetric two-point functions of arbitrary spin.

where  $\mu = 0, 1, 2$ . We can convert spinor indices  $\alpha, \beta$  into vector indices  $\mu, \nu$  by means of the gamma matrices  $(\gamma^\mu)_{\alpha\beta}$ . The form of these matrices, together with further conventions regarding raising, lowering and contracting indices, can be found in appendix A.1.

The differential form of the (super)translations acting on fields  $\mathcal{O}(z)$  is standard

$$[\mathcal{P}_\mu, \mathcal{O}(z)] = i\partial_\mu \mathcal{O}(z), \quad (4.3.2)$$

$$[\mathcal{Q}_\alpha, \mathcal{O}(z)] = (\partial_\alpha + i(\gamma^\mu)_{\alpha\beta} \bar{\theta}^\beta \partial_\mu) \mathcal{O}(z), \quad (4.3.3)$$

$$[\bar{\mathcal{Q}}_\alpha, \mathcal{O}(z)] = -(\bar{\partial}_\alpha + i(\gamma^\mu)_{\alpha\beta} \theta^\beta \partial_\mu) \mathcal{O}(z). \quad (4.3.4)$$

From the bulk algebra it is easy to derive the form of all the other differential operators, which we list in appendix A.3. The action of the covariant derivatives is also standard

$$D_\alpha \mathcal{O}(z) = (\partial_\alpha - i(\gamma^\mu)_{\alpha\beta} \bar{\theta}^\beta \partial_\mu) \mathcal{O}(z), \quad \bar{D}_\alpha \mathcal{O}(z) = -(\bar{\partial}_\alpha - i(\gamma^\mu)_{\alpha\beta} \theta^\beta \partial_\mu) \mathcal{O}(z), \quad (4.3.5)$$

and as usual, they anticommute with the action of supertranslations. The main focus of this work is on chiral and antichiral operators (see section 4.2), which are defined in superspace as

$$\bar{D}_\alpha \Phi(z) = 0, \quad D_\alpha \bar{\Phi}(z) = 0. \quad (4.3.6)$$

In order to work with chiral operators it is useful to work with chiral/antichiral coordinates defined as

$$y^\mu = x^\mu - i\gamma_{\alpha\beta}^\mu \theta^\alpha \bar{\theta}^\beta, \quad \bar{y}^\mu = x^\mu + i\gamma_{\alpha\beta}^\mu \theta^\alpha \bar{\theta}^\beta. \quad (4.3.7)$$

In terms of these coordinates, a chiral field depends only on  $\Phi(y, \theta)$  and similarly for the antichiral field  $\bar{\Phi}(\bar{y}, \bar{\theta})$ . If we consider two points, we can also define supersymmetric invariant distances with well-defined chirality:<sup>5</sup>

$$y_{12}^\mu = x_{12}^\mu - i(\gamma^\mu)_{\alpha\beta} \left( \theta_1^\alpha \bar{\theta}_1^\beta + \theta_2^\alpha \bar{\theta}_2^\beta - 2\theta_1^\alpha \bar{\theta}_2^\beta \right), \quad (4.3.8)$$

$$\bar{y}_{12}^\mu = x_{12}^\mu + i(\gamma^\mu)_{\alpha\beta} \left( \theta_1^\alpha \bar{\theta}_1^\beta + \theta_2^\alpha \bar{\theta}_2^\beta + 2\bar{\theta}_1^\alpha \theta_2^\beta \right). \quad (4.3.9)$$

These distances are chiral at one point and antichiral at the other, namely

$$\bar{D}_\alpha^{(1)} y_{12}^\mu = D_\alpha^{(2)} y_{12}^\mu = 0, \quad D_\alpha^{(1)} \bar{y}_{12}^\mu = \bar{D}_\alpha^{(2)} \bar{y}_{12}^\mu = 0. \quad (4.3.10)$$

Introducing a boundary will generally break supersymmetry in the bulk. In this chapter we study a special class of boundaries that preserve one half of the supersymmetry. As already discussed, they are characterized by  $2d$  algebras with  $\mathcal{N} = (0, 2)$  and  $\mathcal{N} = (1, 1)$  supersymmetry respectively. The two boundaries have distinct features that we discuss in detail below, the most prominent being that the  $\mathcal{N} = (1, 1)$  boundary breaks  $R$ -symmetry, while it is kept intact in the  $\mathcal{N} = (0, 2)$  case.

### 4.3.2 The $\mathcal{N} = (0, 2)$ boundary

The  $\mathcal{N} = (0, 2)$  boundary preserves the supercharges  $\mathcal{Q}_+, \bar{\mathcal{Q}}_+$ , resulting in the algebra given in (4.2.1). The bulk superspace can be split into coordinates parallel and perpendicular to the boundary. The parallel coordinates are

$$(\theta^+, \bar{\theta}^+, x^a), \quad a = 0, 1, \quad (4.3.11)$$

<sup>5</sup>Note that  $y_{12}^\mu \neq y_1^\mu - y_2^\mu$ , we hope the notation will not create confusion.

while the perpendicular coordinates read

$$(\theta^-, \bar{\theta}^-, x^\perp \equiv x^2). \quad (4.3.12)$$

As was the case for the bulk theory, it is convenient to define supersymmetric, chiral, and antichiral perpendicular distances. The supersymmetric distance is

$$z^\perp = x^\perp - i\theta^\alpha \bar{\theta}_\alpha \quad (4.3.13)$$

and the chiral  $y^\perp \equiv y^2$  and antichiral  $\bar{y}^\perp \equiv \bar{y}^2$  perpendicular distances can be read off from eq. (4.3.7). Note that  $z^\perp$  is invariant under the boundary (super)translations  $\mathcal{P}_a$ ,  $\mathcal{Q}_+$  and  $\bar{\mathcal{Q}}_+$ , while  $y^\perp$  and  $\bar{y}^\perp$  are not. The component expansion of a chiral field  $\Phi$  takes the familiar form

$$\Phi(y, \theta) = \phi(y) + \theta^+ \psi_+(y) + \theta^- \psi_-(y) + \theta^+ \theta^- F(y), \quad (4.3.14)$$

where  $\phi$  is a complex boson,  $\psi_\alpha$  a complex fermion, and  $F$  a complex auxiliary field. It will be convenient to decompose this bulk chiral supermultiplet  $\Phi$  in terms boundary supermultiplets, that transform irreducibly under the  $(0, 2)$  subalgebra [157, 146]

$$\Phi = \hat{\Phi} + \theta^- \hat{\Psi} + \dots, \quad (4.3.15)$$

where  $\hat{\Phi}$  is a boundary chiral field,  $\hat{\Psi}$  a boundary Fermi field, and the  $\dots$  stand for derivatives of  $\hat{\Phi}$  parallel to the boundary. A similar expansion can be written for the antichiral bulk supermultiplet  $\bar{\Phi}$ . From now on, we will denote boundary multiplets and boundary fields with a hat. One can straightforwardly derive a similar expansion for  $\bar{\Phi}$  and  $\hat{\Psi}$ :

$$\hat{\Phi} = \Phi \Big|_{\theta^- = \bar{\theta}^- = 0} = \phi + \theta^+ \psi_+ + \dots, \quad (4.3.16)$$

$$\hat{\Psi} = D_- \Phi \Big|_{\theta^- = \bar{\theta}^- = 0} = \psi_- + \theta^+ F + \dots, \quad (4.3.17)$$

where  $F \sim \partial_\perp \phi$  on-shell and the  $\dots$  stand for terms with derivatives. The usual Neumann and Dirichlet boundary conditions can be neatly represented in terms of these superfields:

$$\text{Neumann:} \quad \partial_\perp \phi \Big|_\partial = 0, \quad \psi_- \Big|_\partial = 0 \quad \rightarrow \quad \hat{\Psi} \Big|_\partial = 0, \quad (4.3.18)$$

$$\text{Dirichlet:} \quad \phi \Big|_\partial = 0, \quad \psi_+ \Big|_\partial = 0 \quad \rightarrow \quad \hat{\Phi} \Big|_\partial = 0. \quad (4.3.19)$$

### One-point functions

As reviewed in section 4.2, scalar bulk operators can acquire a one-point function in the presence of a boundary. In the superspace setup we are considering, we expect on general grounds one-point functions of the form

$$\langle \mathcal{O}(z) \rangle = \frac{a_{\mathcal{O}}}{(z^\perp)^\Delta}, \quad (4.3.20)$$

where  $z^\perp$  is given in eq. (4.3.13). For chiral fields, the chirality condition (4.3.6) and conservation of  $R$ -symmetry imply that the one-point function vanishes:  $a_\Phi = 0$ .



### Bulk-to-boundary correlator

Similarly to the one-point function, we expect bulk-to-boundary correlators to be of the form

$$\langle \mathcal{O}(z_1) \hat{\mathcal{O}}(z_2) \rangle = \frac{1}{(z_1^\perp)^{\Delta - \hat{\Delta}} |y_{12}^2 \bar{y}_{12}^2|^{\hat{\Delta}/2}} g(\Theta_i), \quad (4.3.21)$$

where  $g$  is a function of possible nilpotent invariants  $\Theta_i$ .

Again, the chirality condition (4.3.6) is extremely powerful and severely constrains the possible defect operators that can appear in the boundary OPE of a chiral field. From the expansion in (4.3.15) we expect two types of boundary multiplets, and indeed there are two possible correlators consistent with all the symmetry constraints. One choice involves a scalar boundary multiplet<sup>6</sup>

$$\langle \Phi(y, \theta) \hat{\Phi}_r(0) \rangle = \frac{b_{\Phi \hat{\Phi}}}{|y^\mu|^{2\Delta}}, \quad (4.3.22)$$

where  $|y^\mu|$  is the norm of the chiral distance (4.3.7), and the conformal dimensions are constrained by conservation of  $R$ -symmetry  $\hat{\Delta} = \Delta_\phi = r_\phi = r_{\hat{\phi}}$ .

The other bulk-to-boundary two-point function involves the Fermi multiplet  $\hat{\Psi}$  whose highest weight carries spin:

$$\langle \Phi(y, \theta) \hat{\Psi}(0) \rangle = \frac{b_{\Phi \hat{\Psi}} \gamma_{1\beta}^\mu y_\mu \theta^\beta}{(y^\perp)^{\Delta - \hat{\Delta} + \frac{1}{2}} |y^\mu|^{2(\hat{\Delta} + \frac{1}{2})}}. \quad (4.3.23)$$

Charge conservation implies  $r_\psi = 1 - r_\phi$  but  $\hat{\Delta}$  is not constrained to take a specific value, which means these multiplets are responsible for most of the operators that appear in the boundary block expansion of the two-point function of chiral fields. The power  $\hat{\Delta} + \frac{1}{2}$  indicates that the contributing field is not the primary, but a descendant (see eq. (4.3.36) below).

### Two-point functions

As reviewed in section 4.2, bosonic two-point functions depend on a conformal invariant and therefore contain a large amount of dynamical information through their conformal block decompositions. As evident from our analysis so far, correlators of chiral fields are severely constrained by superconformal symmetry and their chirality condition. There is actually only one possible two-point invariant that satisfies all the superspace constraints:

$$\xi = \frac{y_{12}^2}{4y_1^\perp \bar{y}_2^\perp} \left( 1 + 2i \frac{(y_{12}^0 + y_{12}^1) \theta_1^- \bar{\theta}_2^-}{y_1^\perp \bar{y}_2^\perp} + 2i \frac{\theta_1^+ \bar{\theta}_2^-}{\bar{y}_2^\perp} \right). \quad (4.3.24)$$

This is the unique ‘‘supersymmetrization’’ of the standard bosonic invariant. The most general two-point function of a chiral and an antichiral field then reads

$$\langle \Phi(y_1, \theta_1) \bar{\Phi}(0, \bar{y}_2^\perp, \bar{\theta}_2^-) \rangle = \left( \frac{\xi}{y_{12}^2} \right)^\Delta \mathcal{F}(\xi), \quad (4.3.25)$$

where  $\mathcal{F}$  is an arbitrary function of the superconformal invariant  $\xi$ . In eqs. (4.3.24) and (4.3.25) we work in a frame where  $\bar{y}_2^a = \bar{\theta}_2^+ = 0$ , ( $a = 0, 1$ ), but we keep the

---

<sup>6</sup>Whenever possible we supertranslate point 2 to the origin to simplify our formulas, but if necessary one can easily supertranslate back to a general frame.

dependence on  $\bar{y}_2^\perp$  and  $\bar{\theta}_2^-$ , since they are perpendicular coordinates and cannot be set to zero. Using a supertranslation one can find the two-point function in a frame with completely general  $z_1$  and  $z_2$ , as will be needed below. Two-point functions of two chiral (or two antichiral) fields are zero due to  $R$ -symmetry. For more general external operators, for example long multiplets of the superconformal algebra, we expect a more complicated correlator involving nilpotent invariants, which then translates into superconformal blocks that have free parameters (see for example [162]). We will not consider more general correlators in this work, however our superspace setup could be used to study them in the future.

### Superconformal blocks

We are now ready to obtain one of the main results of this section: the superconformal blocks associated to the two-point correlator  $\mathcal{F}(\xi)$ . As reviewed in section 4.2, there are two conformal block expansions associated to the bulk and defect channel respectively. Bulk conformal blocks are eigenfunctions of the two-point bulk Casimir operator, while defect blocks are eigenfunctions of the defect Casimir.

**Bulk channel:** Let us start with the bulk channel,

$$\mathcal{C}_{\text{susy}}^{(12)} \langle \Phi(z_1) \bar{\Phi}(z_2) \rangle = C_{\Delta, \ell, r} \langle \Phi(z_1) \bar{\Phi}(z_2) \rangle, \quad (4.3.26)$$

where the supersymmetric bulk Casimir is given by

$$\mathcal{C}_{\text{susy}}^{(12)} = -\mathcal{D}^2 - \frac{1}{2} \{ \mathcal{K}^\mu, \mathcal{P}_\mu \} + \frac{1}{2} \mathcal{M}^{\mu\nu} \mathcal{M}_{\mu\nu} - \frac{1}{2} \mathcal{R}^2 + \frac{1}{4} [\mathcal{S}^\alpha, \bar{\mathcal{Q}}_\alpha] + \frac{1}{4} [\bar{\mathcal{S}}^\alpha, \mathcal{Q}_\alpha]. \quad (4.3.27)$$

The superscript (12) indicates that the operator acts on points  $z_1$  and  $z_2$ . To avoid cluttering we wrote the superscript only on the Casimir, and omit it from the operators on the RHS. The eigenvalue reads

$$C_{\Delta, \ell, r} = \Delta(\Delta - 1) + \ell(\ell + 1) - \frac{r^2}{2}. \quad (4.3.28)$$

Evaluating (4.3.26) leads to a differential equation for the corresponding block  $F_\Delta(\xi)$ . Our analysis implies the absence of nilpotent invariants when chiral fields are involved. This means that full superspace correlators can be reconstructed from those of the superprimaries and implies that a multiplet contributes only if its superprimary contributes. Because only scalars can acquire a one-point function in BCFT, we can safely set  $\ell = 0$  when looking for solutions to the Casimir equation. A standard approach to solve these equations is to recognize that superconformal blocks can be written as linear combinations of bosonic blocks. The superdescendants of a field  $\mathcal{O}(z)$  can be generated by acting on the superprimary  $\mathcal{O}(z)$  with the supercharges  $\mathcal{Q}, \bar{\mathcal{Q}}$ . This creates superdescendants of the schematic form  $\mathcal{Q}_1 \dots \bar{\mathcal{Q}}_n \mathcal{O}(z)$ .<sup>7</sup> We therefore make the following ansatz

$$F_\Delta(\xi) = f_\Delta(\xi) + c_0 f_{\Delta+\frac{1}{2}} + c_1 f_{\Delta+1}(\xi) + c_2 f_{\Delta+\frac{3}{2}}(\xi) + c_3 f_{\Delta+2}(\xi), \quad (4.3.29)$$

where  $f_\Delta(\xi)$  are the bosonic blocks given in eq. (B.1.3), and we fix the relative coefficients using eq. (4.3.26). The solution is easy to find

$$F_\Delta(\xi) = f_\Delta(\xi) - \frac{(\Delta - 1)\Delta}{(2\Delta - 1)(2\Delta + 1)} f_{\Delta+2}(\xi), \quad (4.3.30)$$

---

<sup>7</sup>In order to obtain proper conformal primaries (killed by  $\mathcal{K}$ ) the action of the  $\mathcal{Q}_i$  has to be corrected by terms containing the momentum generator  $\mathcal{P}$ .

which corresponds to a long operator being exchanged in the  $\phi \times \bar{\phi}$  OPE. There are also contributions from short multiplets, but they can be obtained from eq. (4.3.30) evaluating  $\Delta$  at the unitarity bound. The selection rules of this OPE have been studied in the context of bulk four-point functions [154] and our results are in perfect agreement with the literature. The block in eq. (4.3.30) can be written as a single hypergeometric function

$$F_{\Delta}(\xi) = \xi^{\Delta/2} {}_2F_1\left(1 + \frac{\Delta}{2}, \frac{\Delta}{2}; \Delta + \frac{1}{2}; -\xi\right). \quad (4.3.31)$$

We will see that all of the two-point blocks derived in this section have this feature.

**Boundary channel:** In the boundary channel the blocks are eigenfunctions of the boundary Casimir

$$\hat{\mathcal{C}}_{\text{susy}} = -\mathcal{D}^2 - \frac{1}{2} \{\mathcal{K}^a, \mathcal{P}_a\} + \frac{1}{2} \mathcal{M}^{ab} \mathcal{M}_{ab} - \frac{1}{2} \mathcal{R}^2 + \frac{1}{4} ([\bar{\mathcal{S}}^+, \mathcal{Q}_+] + [\mathcal{S}^+, \bar{\mathcal{Q}}_+]), \quad (4.3.32)$$

where now the operator acts at a single point:

$$\hat{\mathcal{C}}_{\text{susy}}^{(1)} \langle \Phi(z_1) \bar{\Phi}(z_2) \rangle = \hat{C}_{\hat{\Delta}, j, r} \langle \Phi(z_1) \bar{\Phi}(z_2) \rangle. \quad (4.3.33)$$

The eigenvalue depends on the conformal dimension  $\hat{\Delta}$  of the exchanged boundary operator, as well as its parallel spin  $j$  and its  $R$ -charge:

$$\hat{C}_{\hat{\Delta}, j, r} = \hat{\Delta}(\hat{\Delta} - 1) + j(j - 1) - \frac{r^2}{2}. \quad (4.3.34)$$

Proceeding as before we make an ansatz for  $\hat{F}_{\hat{\Delta}}$  in terms of bosonic blocks and fix the relative coefficients using eq. (4.3.33). Note that we only have to include conformal blocks up to dimension  $\hat{\Delta} + 1$  in our ansatz, since the boundary only preserves half of the supercharges. From section 4.3.2 we know there are two types of boundary multiplets that can appear in the boundary expansion of a chiral field: a scalar  $\hat{\Phi}$  and the Fermi multiplet  $\hat{\Psi}$ . We therefore expect two classes of solutions to the Casimir equation. Indeed, the solution corresponding to a chiral primary with  $r = r_{\phi}$ ,  $j = 0$  and  $\hat{\Delta} = \Delta_{\phi} = r_{\phi}$ , is given by

$$\hat{F}_{\hat{\Delta}}^{\hat{\Phi}}(\xi) = \hat{f}_{\Delta_{\phi}}(\xi). \quad (4.3.35)$$

The second solution, with  $r = r_{\phi} - 1$ ,  $j = \frac{1}{2}$  corresponds to the Fermi field

$$\hat{F}_{\hat{\Delta}}^{\hat{\Psi}}(\xi) = \hat{f}_{\hat{\Delta} + \frac{1}{2}}(\xi). \quad (4.3.36)$$

Notice that the  $\frac{1}{2}$  in the argument indicates that the highest weight does not contribute, but a descendant (as expected).

### Three-point functions

Although not our main topic, let us also analyze three-point correlators involving one bulk field and two boundary fields. An interesting application for these correlators is to impose that the bulk field is free, and to study the corresponding constraints on the boundary three-point couplings [52, 68]. For the rest of this section we will choose a

frame where  $x_2^a = \theta_2^+ = \bar{\theta}_2^+ = \theta_3^+ = \bar{\theta}_3^+ = 0, x_3^a \rightarrow \infty$ . By imposing that the bulk field is chiral we obtain

$$\langle \Phi(y, \theta) \hat{\mathcal{O}}_{2,j}(0, \omega) \hat{\mathcal{O}}_3(\infty) \rangle = \frac{(y^a \omega_a)^j}{(y^\perp)^{\Delta + \hat{\Delta}_{23}} |y^a|^j} \mathcal{F}^{3\text{pt}}(\chi). \quad (4.3.37)$$

The second operator has arbitrary parallel spin  $j$ , and we use an index-free notation where  $\hat{\mathcal{O}}_{2,j}(z, \omega) = \hat{\mathcal{O}}_{2,j}(z)^{a_1 \dots a_j} \omega_{a_1} \dots \omega_{a_j}$  and  $\omega_a$  is a null vector in the parallel directions. For brevity we define  $\hat{\Delta}_{23} \equiv \hat{\Delta}_2 - \hat{\Delta}_3$ , and  $y^a$  is defined in eq. (4.3.7), where one should remember that  $a = 0, 1$  are the parallel coordinates. Conservation of  $R$ -symmetry implies  $r_\phi + r_2 + r_3 = 0$ . The function  $\mathcal{F}^{3\text{pt}}(\chi)$  depends on the superconformal three-point invariant  $\chi$ . Like in the two-point function case, there is a unique, non-nilpotent, three-point invariant:

$$\chi = \frac{|y^a|^2}{(y^\perp)^2}. \quad (4.3.38)$$

The function  $\mathcal{F}_{3\text{pt}}(\chi)$  can be expanded in three-point superconformal blocks which are in turn sums of three-point bosonic blocks (reviewed in appendix B.2). Notice that there is no crossing equation for this correlator. We can act with the boundary Casimir on point  $z_1$  and obtain the eigenvalue equation

$$\hat{C}_{\text{susy}}^{(1)} \langle \Phi(y, \theta) \hat{\mathcal{O}}_{2,j}(0, \omega) \hat{\mathcal{O}}_3(\infty) \rangle = \hat{C}_{\hat{\Delta}, j, r} \langle \Phi(y, \theta) \hat{\mathcal{O}}_{2,j}(0, \omega) \hat{\mathcal{O}}_3(\infty) \rangle. \quad (4.3.39)$$

By now the story is familiar; we give an ansatz in terms of bosonic blocks and obtain a solution with  $r = r_\phi, j_{\text{chiral}} = 0, \hat{\Delta} = \Delta_\phi = r_\phi$ :

$$\hat{F}_{\Delta_\phi}^{3\text{pt}}(\chi) = \hat{f}_{\Delta_\phi, j}^{3\text{pt}, \hat{\Delta}_{23}}(\chi), \quad (4.3.40)$$

which describes the exchange of a boundary chiral field. The other possible solution has  $r = r_\phi - 1, j_{\text{fermi}} = \frac{1}{2}$  and generic  $\hat{\Delta}$ :

$$\hat{F}_{\hat{\Delta}}^{3\text{pt}}(\chi) = \hat{f}_{\hat{\Delta} + \frac{1}{2}, j}^{3\text{pt}, \hat{\Delta}_{23}}(\chi), \quad (4.3.41)$$

and corresponds to the exchange of a Fermi multiplet. Let us also consider the case where the second operator is a Fermi field. The three-point function is given by

$$\langle \Phi(y, \theta) \hat{\Psi}(0) \hat{\mathcal{O}}(\infty) \rangle = \frac{(\gamma_{1\beta})^\mu y_\mu \theta^\beta}{(y^\perp)^{\Delta + \hat{\Delta}_{23} + \frac{3}{2}}} \mathcal{F}_{3\text{pt}}(\chi), \quad (4.3.42)$$

where  $\chi$  is the same invariant as before. There are again two solutions to the eigenvalue equation, the first one corresponds to the exchange of a boundary chiral

$$\hat{F}_{\Delta_\phi}^{3\text{pt}}(\chi) = \hat{f}_{\Delta_\phi, 0}^{3\text{pt}, \hat{\Delta}_{23} + \frac{1}{2}}(\chi), \quad (4.3.43)$$

while the second describes a Fermi field

$$\hat{F}_{\hat{\Delta}}^{3\text{pt}}(\chi) = \hat{f}_{\hat{\Delta} + \frac{1}{2}, 0}^{3\text{pt}, \hat{\Delta}_{23} + \frac{1}{2}}(\chi). \quad (4.3.44)$$

The supersymmetric block corresponds to a bosonic block with shifted external conformal dimensions  $\hat{\Delta}_{23} \rightarrow \hat{\Delta}_{23} + \frac{1}{2}$  and with spin  $j = 0$ . Like in the two-point case, the shift can be understood as a contribution coming from a superconformal descendant of  $\hat{\Psi}$ .

### Free theory in the bulk

Having obtained a handful of correlators, let us investigate the possible constraints that a free theory in the bulk imposes on the boundary data. In superspace the free field equations of motion take the form

$$D^\alpha D_\alpha \Phi(y, \theta) = 0, \quad (4.3.45)$$

which is the supersymmetric version of the more familiar  $\partial^2 \phi(x) = 0$ . As usual, a free chiral field has dimension  $\Delta_\phi = r_\phi = \frac{1}{2}$ . Imposing this condition on the two bulk-to-boundary correlators (4.3.22) and (4.3.23), we obtain two solutions:

$$\langle \Phi(y, \theta) \hat{\Phi}_{\hat{\Delta}=\frac{1}{2}}(0) \rangle = \frac{b_{\Phi\hat{\Phi}}}{|y^\mu|}, \quad \langle \Phi(y, \theta) \hat{\Psi}_{\hat{\Delta}=1}(0) \rangle = \frac{b_{\Phi\hat{\Psi}} \gamma_{1\beta}^\mu y_\mu \theta^\beta}{|y^\mu|^3}. \quad (4.3.46)$$

This is not surprising. The first solution corresponds to a boundary chiral field of dimension  $\hat{\Delta} = \frac{1}{2}$ , which corresponds to the operator  $\hat{\phi}$  and describes Neumann boundary conditions. The second solution is a Fermi field with  $\hat{\Delta} = 1$ , which has a scalar descendant with dimension  $\hat{\Delta} + \frac{1}{2} = \frac{3}{2}$  (recall the discussion below eq. (4.3.23)). The descendant can be identified with  $\partial_\perp \hat{\phi}$  as expected for Dirichlet boundary conditions. We have therefore proven that the boundary expansion of a bulk free field has a finite number of contributions.

We now turn to the three-point function to see if there are extra constraints on the boundary operators from a free bulk chiral field. Let us expand the correlation function (4.3.37) in bosonic blocks, where we take  $\Phi$  to be a free bulk chiral. From eq. (4.3.46) we know that there are two independent contributions coming from a chiral and a Fermi boundary field:

$$\mathcal{F}^{3\text{pt}}(\chi) = b_{\phi\hat{\phi}} \lambda_{\hat{\phi}\hat{\phi}\hat{\phi}} \hat{f}_{\hat{\Delta}=\frac{1}{2},j}^{3\text{pt},\hat{\Delta}_{23}}(\chi) + b_{\phi\partial_\perp\hat{\phi}} \lambda_{\partial_\perp\hat{\phi}\hat{\phi}} \hat{f}_{\hat{\Delta}=\frac{3}{2},j}^{3\text{pt},\hat{\Delta}_{23}}(\chi). \quad (4.3.47)$$

Note that we have written the OPE coefficients explicitly in terms of the operators that appear in the OPE and not in terms of the superprimaries. Eq. (4.3.47) is identical to the conformal block expansion of a non-supersymmetric free scalar in the bulk, which has been studied in detail in [52, 68]. In the limit  $\chi \rightarrow 0$  there are unphysical singularities, which can only be removed provided the OPE coefficients satisfy the following relation:

$$b_{\phi\partial_\perp\hat{\phi}} \lambda_{\partial_\perp\hat{\phi}\hat{\phi}} = - \frac{2\Gamma\left(\frac{2j-2\hat{\Delta}_{23}+3}{4}\right) \Gamma\left(\frac{2j+2\hat{\Delta}_{23}+3}{4}\right)}{\Gamma\left(\frac{2j-2\hat{\Delta}_{23}+1}{4}\right) \Gamma\left(\frac{2j+2\hat{\Delta}_{23}+1}{4}\right)} b_{\phi\hat{\phi}} \lambda_{\hat{\phi}\hat{\phi}}. \quad (4.3.48)$$

This constraint is equivalent to the constraints on non-supersymmetric three-point functions with a free bulk. We can go one step further and look at the three-point function involving a boundary Fermi multiplet (4.3.42) in the hope that we will find additional constraints on the CFT data from supersymmetry. Once again, we expect the two solutions in eq. (4.3.46) to contribute to the Fermi three-point function. If we act with the equations of motion, the resulting differential equation can only be solved if  $\hat{\Delta}_{23} = 1$ , excluding the solution  $\hat{\Delta} = \frac{1}{2}$ . The resulting correlator corresponds to a single bosonic block

$$\mathcal{F}_{3\text{pt}}(\chi) \propto \hat{f}_{\hat{\Delta}=\frac{3}{2},0}^{3\text{pt},\frac{3}{2}}(\chi) = \frac{1}{(\chi+1)^{\frac{3}{2}}}. \quad (4.3.49)$$

In this case the correlator is manifestly non-singular as  $\chi \rightarrow 0$ . Having a free bulk implies that there is only one operator in the OPE  $\hat{\phi} \times \hat{\psi}$ , which has fixed dimension  $\hat{\Delta}_3 = \hat{\Delta}_2 - 1$ . This is a new, additional constraint coming from the superspace analysis that was not present in the non-supersymmetric case. It would be interesting to see if a more systematic analysis allows us to find more general constraints.

### 4.3.3 The $\mathcal{N} = (1, 1)$ boundary

We now present the superspace analysis for the  $\mathcal{N} = (1, 1)$  boundary, and since it is quite similar to what we have done so far, we will mostly state the results. We again divide the superspace into parallel and perpendicular coordinates, the bosonic coordinates are split as usual, and for the fermionic variables we define

$$\text{parallel: } \tilde{\theta}^1 \equiv \tilde{\theta}^- = -i(\theta^- - \bar{\theta}^-), \quad \tilde{\theta}^2 \equiv \tilde{\theta}^+ = -(\theta^+ + \bar{\theta}^+), \quad (4.3.50)$$

$$\text{perpendicular: } \theta_{\perp}^1 \equiv \theta_{\perp}^- = -(\theta^- + \bar{\theta}^-), \quad \theta_{\perp}^2 \equiv \theta_{\perp}^+ = -i(\theta^+ - \bar{\theta}^+), \quad (4.3.51)$$

There are two useful ways to construct supersymmetric perpendicular distances

$$z^{\perp} = y^{\perp} + 2i\theta^-\theta^+, \quad \bar{z}^{\perp} = \bar{y}^{\perp} + 2i\bar{\theta}^-\bar{\theta}^+, \quad (4.3.52)$$

with the property that they are chiral and antichiral respectively  $\bar{D}_{\alpha}z^{\perp} = D_{\alpha}\bar{z}^{\perp} = 0$ . These distances will be the natural objects to appear in correlators of (anti)chiral fields. The decomposition of a bulk (anti)chiral field for the  $\mathcal{N} = (1, 1)$  boundary contains only one boundary supermultiplet instead of the two possibilities present in the  $(0, 2)$  boundary

$$\Phi = \hat{\Phi} + \dots, \quad (4.3.53)$$

where the dots stand for derivatives of  $\hat{\Phi}$ . The field  $\hat{\Phi}$  can be decomposed into bosonic components, schematically (see [157] for the precise coefficients)

$$\hat{\Phi} = \hat{\phi} + \tilde{\theta}^+\hat{\psi}_+ + \tilde{\theta}^-\hat{\psi}_- + \tilde{\theta}^2\partial_{\perp}\hat{\phi} + \tilde{\theta}^2\hat{F}. \quad (4.3.54)$$

We see that  $\hat{\phi}$  and  $\partial_{\perp}\hat{\phi}$  belong to the same boundary multiplet, which implies the unexpected feature that Neumann and Dirichlet boundary conditions are related by supersymmetry.

#### One-point functions

Due to the absence of  $R$ -symmetry, (anti)chiral bulk fields can now acquire a one-point function. The only correlators consistent with the symmetry constraints are given by

$$\langle \Phi(y, \theta) \rangle = \frac{a_{\Phi}}{(2z^{\perp})^{\Delta}}, \quad \langle \bar{\Phi}(\bar{y}, \bar{\theta}) \rangle = \frac{a_{\bar{\Phi}}}{(2\bar{z}^{\perp})^{\Delta}}, \quad (4.3.55)$$

where  $z^{\perp}, \bar{z}^{\perp}$  were defined in eq. (4.3.52), and  $a_{\Phi}$  is the one-point coupling that appears as the coefficient of the ‘‘boundary identity’’ in the conformal block expansion.

#### Bulk-to-boundary correlator

Since a chiral bulk supermultiplet decomposes into one boundary supermultiplet, we expect only one correlator:

$$\langle \Phi(y, \theta)\hat{\mathcal{O}}(0) \rangle = \frac{b_{\Phi\hat{\mathcal{O}}}}{(2z^{\perp})^{\Delta-\hat{\Delta}}|y^{\mu}|^{2\hat{\Delta}}}, \quad (4.3.56)$$

where  $z^\perp$  is the same as above and  $|y^\mu|$  is the norm of the chiral coordinate (4.3.7). Notice that  $\hat{\Delta}$  is unconstrained so these are the operators captured by the boundary conformal blocks to be calculated below.

### Two-point functions

Due to the broken  $R$ -symmetry there is now no selection rule implying that correlators with fields of the same chirality vanish. Thus, we should consider the two-point functions  $\langle \Phi_1 \bar{\Phi}_2 \rangle$  and  $\langle \Phi_1 \Phi_2 \rangle$  where the  $R$ -charges are arbitrary. The two-point functions in the presence of the  $\mathcal{N} = (1, 1)$  boundary have the same structure as in the  $\mathcal{N} = (0, 2)$  case. Each of them depends on a single superconformal invariant  $\xi$  which has the appropriate chirality properties:

$$\langle \Phi_1(y_1, \theta_1) \bar{\Phi}_2(\bar{y}_2, \bar{\theta}_2) \rangle = \frac{\mathcal{F}^{\phi\bar{\phi}}(\xi)}{(2z_1^\perp)^{\Delta_1} (2\bar{z}_2^\perp)^{\Delta_2}}, \quad \xi = \frac{(y_{12})^2}{4z_1^\perp \bar{z}_2^\perp}, \quad (4.3.57)$$

$$\langle \Phi_1(y_1, \theta_1) \Phi_2(y_2, \theta_2) \rangle = \frac{\mathcal{F}^{\phi\phi}(\xi)}{(2z_1^\perp)^{\Delta_1} (2z_2^\perp)^{\Delta_2}}, \quad \xi = \frac{(\tilde{y}_{12})^2 + 2i\theta_{12}^2(z_1^\perp + z_2^\perp)}{4z_1^\perp z_2^\perp}. \quad (4.3.58)$$

The perpendicular distances  $z^\perp, \bar{z}^\perp$  are given in eq. (4.3.52), the chiral-antichiral distance  $y_{12}^\mu$  can be found in eq. (4.3.8), and we have defined the following chiral-chiral distance:

$$\begin{aligned} \tilde{y}_{12}^0 &= y_1^0 - y_2^0 - 2i(\theta_1^+ \theta_2^+ - \theta_1^- \theta_2^-), \\ \tilde{y}_{12}^1 &= y_1^1 - y_2^1 - 2i(\theta_1^+ \theta_2^+ + \theta_1^- \theta_2^-), \\ \tilde{y}_{12}^2 &= z_1^\perp - z_2^\perp. \end{aligned} \quad (4.3.59)$$

Let us now calculate the corresponding superblocks for the functions  $\mathcal{F}^{\phi\bar{\phi}}(\xi)$  and  $\mathcal{F}^{\phi\phi}(\xi)$ .

### Superconformal blocks

We now calculate the superconformal blocks using the same approach we used in the  $\mathcal{N} = (0, 2)$  case in section 4.3.2. We use the Casimir to obtain a differential equation that we then solve using a finite combination of bosonic blocks.

**Bulk channel.** We first act with the bulk Casimir

$$\mathcal{C}_{\text{susy}}^{(12)} \langle \Phi_1(y_1, \theta_1) \bar{\Phi}_2(\bar{y}_2, \bar{\theta}_2) \rangle = C_{\Delta, \ell, r} \langle \Phi_1(y_1, \theta_1) \bar{\Phi}_2(\bar{y}_2, \bar{\theta}_2) \rangle, \quad (4.3.60)$$

where  $\mathcal{C}_{\text{susy}}^{(12)}$  and  $C_{\Delta, \ell, r}$  were already given in eqs. (4.3.27) and (4.3.28) respectively. The solution to this equation in terms of bosonic blocks is easy to find. Only  $\ell = 0$  and  $r = r_1 - r_2$  contributes

$$\begin{aligned} F_{\Delta}^{\phi_1 \bar{\phi}_2}(\xi) &= f_{\Delta}^{\Delta_{12}}(\xi) + \frac{(\Delta - \Delta_{12})(\Delta + \Delta_{12})}{(2\Delta - 1)(2\Delta + 1)} f_{\Delta+2}^{\Delta_{12}}(\xi) \\ &= \xi^{\frac{\Delta - \Delta_1 - \Delta_2}{2}} {}_2F_1\left(\frac{\Delta - \Delta_{12}}{2}, \frac{\Delta + \Delta_{12}}{2}; \Delta + \frac{1}{2}; -\xi\right), \end{aligned} \quad (4.3.61)$$

which in general corresponds to a long operator being exchanged in the  $\phi_1 \times \bar{\phi}_2$  OPE. The contributions of short operators can be found by evaluating  $\Delta$  at the unitarity bound, as

discussed below eq. (4.3.30). For the two-point function  $\langle \Phi_1 \Phi_2 \rangle$ , which was not present in the  $\mathcal{N} = (0, 2)$  case, the solution to the Casimir equation

$$\mathcal{C}_{\text{susy}}^{(12)} \langle \Phi_1(y_1, \theta_1) \Phi_2(y_2, \theta_2) \rangle = C_{\Delta, \ell, r} \langle \Phi_1(y_1, \theta_1) \Phi_2(y_2, \theta_2) \rangle, \quad (4.3.62)$$

can be written in terms of single bosonic blocks with shifted arguments  $F_{\Delta}^{\phi\phi} = f_{\Delta + \frac{n}{2}}$ . This is a well-known result which has been described in detail for  $d = 3$  in [154]. We will review the analysis in detail in section 4.4.1.

**Boundary channel.** Let us now move on to the boundary channel. The boundary Casimir is now given by

$$\hat{\mathcal{C}}_{\text{susy}} = -\mathcal{D}^2 - \frac{1}{2} \{ \mathcal{K}^a, \mathcal{P}_a \} + \frac{1}{2} \mathcal{M}^{ab} \mathcal{M}_{ab} + \frac{1}{4} [ \tilde{\mathcal{S}}^\alpha, \tilde{\mathcal{Q}}_\alpha ], \quad (4.3.63)$$

with eigenvalue

$$\hat{C}_{\hat{\Delta}, j} = \hat{\Delta}(\hat{\Delta} - 1) + j^2. \quad (4.3.64)$$

We can only find consistent solutions when the superprimary has no parallel spin:  $j = 0$ . For the chiral-antichiral correlator we find

$$\begin{aligned} \hat{F}_{\hat{\Delta}}^{\phi_1 \bar{\phi}_2}(\xi) &= \hat{f}_{\hat{\Delta}}(\xi) + \frac{1}{4} \hat{f}_{\hat{\Delta}+1}(\xi) \\ &= \xi^{-\hat{\Delta}} {}_2F_1\left(\hat{\Delta} - \frac{1}{2}, \hat{\Delta}; 2\hat{\Delta}; -\frac{1}{\xi}\right). \end{aligned} \quad (4.3.65)$$

while for the chiral-chiral correlator we have

$$\begin{aligned} \hat{F}_{\hat{\Delta}}^{\phi_1 \phi_2}(\xi) &= \hat{f}_{\hat{\Delta}}(\xi) - \frac{1}{4} \hat{f}_{\hat{\Delta}+1}(\xi) \\ &= \xi^{-\hat{\Delta}} {}_2F_1\left(\hat{\Delta} + \frac{1}{2}, \hat{\Delta}; 2\hat{\Delta}; -\frac{1}{\xi}\right). \end{aligned} \quad (4.3.66)$$

These two blocks describe the exchange of operators whose correlator (4.3.56) is non-vanishing. This concludes our analysis of two-point blocks in the  $\mathcal{N} = (1, 1)$  boundary. We will generalize these results for arbitrary  $3 \leq d \leq 4$  in section 4.4. The superspace analysis of this section will give supporting evidence that the blocks of section 4.4 are a consistent continuation of the  $3d$  results presented here.

### Three-point functions

Let us now study the correlator of a chiral bulk field and two boundary fields. We allow the first boundary operator to have arbitrary spin  $j$ , and we will work in a frame where we set  $x_2^a, \tilde{\theta}_2^a, \tilde{\theta}_3^a$  to zero, and  $x_3^a$  to infinity. Unlike the situations studied so far, there is a nilpotent invariant consistent with all the symmetries, which implies the following structure

$$\langle \Phi(y, \theta) \hat{\mathcal{O}}_{2,j}(0, \omega) \hat{\mathcal{O}}_3(\infty) \rangle = \frac{(y^a \omega_a)^j}{(y^\perp)^{\Delta_\phi + \hat{\Delta}_{23}} |y^a|^j} \left( \mathcal{F}_1^{\text{3pt}}(\chi) + \frac{\theta^+ \theta^-}{y^\perp} \mathcal{F}_2^{\text{3pt}}(\chi) \right). \quad (4.3.67)$$

All the dependence of the correlator is in terms of the chiral coordinates  $y$  and  $\theta$ , see (4.3.7). The superconformal invariant  $\chi$  is the same as for the  $\mathcal{N} = (0, 2)$  boundary in eq. (4.3.38). The superfields  $\Phi, \hat{\mathcal{O}}_i$  appearing in the three-point function can be expanded



into bosonic components, whose correlators are captured by  $\mathcal{F}_i^{3\text{pt}}$ . Let us look at this expansion with more details. Since we chose a frame where  $\theta_2 = \bar{\theta}_2 = \theta_3 = \bar{\theta}_3 = 0$ , only the superprimary in the  $\theta$ -expansion of  $\hat{\mathcal{O}}_i$  will contribute, then

$$\Phi(y, \theta) = \phi(y) + \theta^\alpha \psi_\alpha(y) + \theta^+ \theta^- F(y), \quad \hat{\mathcal{O}}_2(0, \omega) = \hat{\mathcal{O}}_2(0, \omega), \quad \hat{\mathcal{O}}_3(\infty) = \hat{\mathcal{O}}_3(\infty). \quad (4.3.68)$$

Comparing the correlator (4.3.67) with the expansion (4.3.68) we read off

$$\langle \phi(x) \hat{\mathcal{O}}_2(0, \omega) \hat{\mathcal{O}}_3(\infty) \rangle = \frac{(x^a w_a)^j}{(x^\perp)^{\Delta_\phi + \hat{\Delta}_{23}} |x^\mu|^j} \mathcal{F}_1^{3\text{pt}}(\chi), \quad (4.3.69)$$

$$\langle \psi_\alpha(x) \hat{\mathcal{O}}_2(0, \omega) \hat{\mathcal{O}}_3(\infty) \rangle = 0, \quad (4.3.70)$$

$$\langle F(x) \hat{\mathcal{O}}_2(0, \omega) \hat{\mathcal{O}}_3(\infty) \rangle = \frac{(x^a w_a)^j}{(x^\perp)^{(\Delta_\phi + 1) + \hat{\Delta}_{23}} |x^\mu|^j} \mathcal{F}_2^{3\text{pt}}(\chi), \quad (4.3.71)$$

so indeed  $\mathcal{F}_{1,2}^{3\text{pt}}$  capture the correlators of the top and bottom components of the chiral multiplet. To find the corresponding superconformal blocks we act with the boundary supersymmetric Casimir in point  $z_1$ :

$$\hat{\mathcal{C}}_{\text{susy}}^{(1)} \langle \Phi(y, \theta) \hat{\mathcal{O}}_{2,j}(0, \omega) \hat{\mathcal{O}}_3(\infty) \rangle = \hat{C}_{\hat{\Delta}, 0, r} \langle \Phi(y, \theta) \hat{\mathcal{O}}_{2,j}(0, \omega) \hat{\mathcal{O}}_3(\infty) \rangle, \quad (4.3.72)$$

where  $\hat{C}_{\hat{\Delta}, 0, r}$  is given in eq. (4.3.64). This results in two coupled differential equations, which we can solve by assuming that the superconformal blocks are given in terms of the bosonic blocks  $\hat{f}_{\hat{\Delta}}^{3\text{pt}}$  given in eq. (B.2.4). The final result reads

$$\begin{aligned} F_{1, \hat{\Delta}}^{3\text{pt}}(\chi) &= f_{\hat{\Delta}, j}^{3\text{pt}, \hat{\Delta}_{23}}(\chi) + c_{\hat{\Delta}} f_{\hat{\Delta}+1, j}^{3\text{pt}, \hat{\Delta}_{23}}(\chi), \\ F_{2, \hat{\Delta}}^{3\text{pt}}(\chi) &= -2i(r_\phi - \hat{\Delta}) f_{\hat{\Delta}, j}^{3\text{pt}, \hat{\Delta}_{23}}(\chi) + 2ic_{\hat{\Delta}}(r_\phi + \hat{\Delta} - 1) f_{\hat{\Delta}+1, j}^{3\text{pt}, \hat{\Delta}_{23}}(\chi), \end{aligned} \quad (4.3.73)$$

where  $c_{\hat{\Delta}}$  is a free parameter, related to the OPE coefficients of the exchanged operator, see eq. (4.3.74) below.

### Free bulk theory

We now repeat the analysis of section 4.3.2, and see how the bulk equations of motion constrain the spectrum of boundary operators. Imposing that the chiral field is free in eq. (4.3.56) fixes the dimension of the boundary field to  $\hat{\Delta} = \frac{1}{2}$ . Unlike in the  $\mathcal{N} = (0, 2)$  case there is only solution, since both Neumann and Dirichlet boundary conditions are related by supersymmetry, and belong to the same supermultiplet.

Let us now focus on to the three-point function (4.3.67). It is well known that the free equations of motion for a chiral field imply  $F(x) = 0$ , so it is sufficient to focus on  $\mathcal{F}_1^{3\text{pt}}(\chi)$ . From the analysis of the free bulk-to-boundary correlator we conclude that there can only be one multiplet in the bulk-to-boundary OPE. The superprimary has dimension  $\hat{\Delta} = \frac{1}{2}$ , which we will call  $\hat{\phi}$ . The multiplet also contains a superdescendant of dimension  $\hat{\Delta} + 1 = \frac{3}{2}$ , which we denote by  $\partial_\perp \hat{\phi}$ . Both operators contribute to the superconformal block (4.3.73), and the resulting correlation function is

$$\mathcal{F}_1^{3\text{pt}}(\chi) = b_{\phi \hat{\phi}} \lambda_{\hat{\phi} \hat{\mathcal{O}}_2 \hat{\mathcal{O}}_3} \hat{f}_{\hat{\Delta}=\frac{1}{2}, j}^{3\text{pt}, \hat{\Delta}_{23}}(\chi) + b_{\phi \partial_\perp \hat{\phi}} \lambda_{\partial_\perp \hat{\phi} \hat{\mathcal{O}}_2 \hat{\mathcal{O}}_3} \hat{f}_{\hat{\Delta}=\frac{3}{2}, j}^{3\text{pt}, \hat{\Delta}_{23}}(\chi), \quad (4.3.74)$$

where the OPE coefficients are written in terms of the superdescendants, not the superprimaries. Due to the presence of a free coefficient  $c_{\hat{\Delta}}$  in the superconformal block (4.3.73), the relative coefficient in this expansion is not fixed by supersymmetry. Eq. (4.3.74) is identical to the non-supersymmetric case of a free scalar in the bulk and to eq. (4.3.47) for the  $\mathcal{N} = (0, 2)$  boundary. Thus, the analysis below eq. (4.3.47) applies here as well and we find the same OPE relations (4.3.48). There are no extra constraints coming from supersymmetry.

## 4.4 Boundaries across dimensions

In this section we study superconformal theories with boundaries in any, in principle continuous, number of dimensions  $3 \leq d \leq 4$ , keeping the codimension fixed. We obtain superconformal blocks using similar techniques as were developed originally for bulk four-point functions in [154, 163].<sup>8</sup> Conformal blocks in an arbitrary number of dimensions allow us to use analytical techniques like the  $\varepsilon$ -expansion, a subject that we explore in this section inspired by previous work [46, 56].

### 4.4.1 Superconformal blocks

#### Superconformal algebra

In the entire section we follow the same conventions as [154], which we review briefly. The notation will differ from the one in section 4.3, but our main results, the superconformal blocks, will be convention-independent. We hope this does not cause too much confusion. The reader is welcome to look at the original reference for more details. The conformal part of the algebra is generated by the usual operators  $D$ ,  $P_i$ ,  $K_i$  and  $M_{ij}$ . We also have four Poincaré supercharges  $Q_{\alpha}^{+}$  and  $Q_{\dot{\alpha}}^{-}$  and four conformal supercharges  $S^{\dot{\alpha}+}$  and  $S^{\alpha-}$  with anticommutation relations

$$\{Q_{\alpha}^{+}, Q_{\dot{\alpha}}^{-}\} = \Sigma_{\alpha\dot{\alpha}}^i P_i, \quad \{S^{\dot{\alpha}+}, S^{\alpha-}\} = \bar{\Sigma}_i^{\dot{\alpha}\alpha} P_i, \quad i = 1, \dots, d. \quad (4.4.1)$$

Finally, there is a generator  $R$  of  $U(1)_R$  symmetry, under which  $Q_{\alpha}^{+}$  and  $Q_{\dot{\alpha}}^{-}$  have charge  $+1$  and  $-1$  respectively. Provided that  $\Sigma_{\alpha\dot{\alpha}}^i$  satisfies certain formal identities, the super-jacobi identities are satisfied for arbitrary  $d$ . The full set of commutation relations, the Casimir operator  $C_{\text{bulk}}$ , and many other important relations can be found in [154].

In what follows, we will focus our attention on chiral primary operators  $\phi$  and their complex conjugates  $\bar{\phi}$ . These operators are killed by supercharges of the same chirality, and using the superconformal algebra their conformal dimension is related to the  $R$ -charge:

$$[Q_{\alpha}^{+}, \phi(0)] = [Q_{\dot{\alpha}}^{-}, \bar{\phi}(0)] = 0 \quad \Rightarrow \quad \Delta_{\phi} = \Delta_{\bar{\phi}} = \frac{d-1}{2} r_{\phi} = -\frac{d-1}{2} r_{\bar{\phi}}. \quad (4.4.2)$$

The chirality property, as well as the relation between  $\Delta$  and  $r$ , will be important in the calculation of superconformal blocks in the next section.

The subalgebra of conformal transformations that preserve the boundary is generated by  $D$ ,  $P_a$ ,  $K_a$  and  $M_{ab}$ , where  $a, b = 2, \dots, d$ . We chose  $P_1$  not to be part of this

---

<sup>8</sup>Another example of blocks across dimensions was uncovered in the context of Parisi-Sourlas supersymmetry [164, 165].

subalgebra, which physically means that the boundary sits at  $x_1 \equiv x^\perp = 0$ . Only half of the original supercharges belong to the algebra, and they anticommute as:

$$\{Q_A^{\text{bdy}}, Q_B^{\text{bdy}}\} = (\Sigma_{\text{bdy}}^a)_{AB} P_a, \quad \{S_A^{\text{bdy}}, S_B^{\text{bdy}}\} = (\Sigma_{\text{bdy}}^a)_{AB} K_a, \quad A, B = 1, 2. \quad (4.4.3)$$

For arbitrary  $d$  we embed the boundary subalgebra into the full superconformal algebra as

$$Q_1^{\text{bdy}} = Q_1^+ + Q_2^-, \quad Q_2^{\text{bdy}} = Q_2^+ + Q_1^-, \quad S_1^{\text{bdy}} = S_2^+ + S_1^-, \quad S_2^{\text{bdy}} = S_1^+ + S_2^-. \quad (4.4.4)$$

It is easy to check explicitly in  $d = 3$  and  $d = 4$  that eq. (4.4.4) indeed generates a subalgebra and that all the superjacobian identities are satisfied, provided that we use the following Clifford algebra representation:

$$\Sigma_{\alpha\dot{\alpha}}^i = (\bar{\Sigma}_i^{\dot{\alpha}\alpha})^* = (\sigma_3, \sigma_1, \sigma_2, i\mathbb{1}). \quad (4.4.5)$$

Notice that the generator  $R$  is not part of the boundary superalgebra. In physical terms the  $R$  charge is not conserved near the boundary, and both  $\langle\phi_1\phi_2\rangle$  and  $\langle\phi_1\bar{\phi}_2\rangle$  are non-vanishing two-point functions for any  $r_{1,2}$ . These two-point functions have different superconformal block decompositions that we treat separately in the next section.

In order to compute superconformal blocks, we will need the explicit form of the superconformal Casimir of the boundary superalgebra:

$$C_{\text{bdy}} = -D^2 - \frac{1}{2}\{P_a, K^a\} + \frac{1}{2}M_{ab}M^{ab} + \frac{1}{4}[S_A^{\text{bdy}}, Q_A^{\text{bdy}}]. \quad (4.4.6)$$

If we consider a boundary operator with quantum numbers  $\hat{\Delta}, j$ , then it will be an eigenstate of the superconformal Casimir with eigenvalue

$$\hat{C}_{\hat{\Delta}, j} = \hat{\Delta}(\hat{\Delta} - d + 2) + j(j - d + 3). \quad (4.4.7)$$

### Boundary channel

As discussed at length in the superspace section, the boundary channel blocks for a two-point function are eigenfunctions of the boundary superconformal Casimir (4.4.6). We can naturally split the Casimir operator into a non-supersymmetric piece and a contribution coming from supersymmetry:

$$C_{\text{bdy}} = C_{\text{bdy, non-susy}} + C_{\text{bdy, susy}}, \quad C_{\text{bdy, susy}} \equiv \frac{1}{4}[S_A^{\text{bdy}}, Q_A^{\text{bdy}}]. \quad (4.4.8)$$

We worked out the non-supersymmetric contribution in eq. (B.1.4). Focusing only on the supersymmetric part and using the anticommutation relations we obtain:

$$\begin{aligned} [C_{\text{bdy, susy}}, \phi_1(x)]|0\rangle &= \left( \frac{d-1}{2} [R, \phi_1(x)] - \frac{1}{2} \{Q_2^-, [S^{1-}, \phi_1(x)]\} \right) |0\rangle \\ &= \left( \Delta_1 \phi_1(x) + ix^\perp \{Q_1^-, [Q_2^-, \phi_1(x)]\} \right) |0\rangle. \end{aligned} \quad (4.4.9)$$

In appendix C we use superconformal Ward identities to rewrite the piece with  $Q_1^- Q_2^-$  as a term that can be included in a differential equation. Unfortunately, we have not been able to find a strategy to use these Ward identities for general  $d$ . Instead, we focus on the particular cases of  $d = 3, 4$  where the explicit Clifford algebra representation (4.4.5) is

valid. Since the final result does not depend on  $d$ , we claim it is also valid for  $3 \leq d \leq 4$ .<sup>9</sup> The fact that we can find solutions to the Casimir equations with the expected properties for any continuous  $d$  confirms that our assumption is justified. The  $\varepsilon$ -expansion results, to be described below and in the next section, also give supporting evidence that the whole picture is consistent.

**$\langle \phi_1 \bar{\phi}_2 \rangle$  correlator:** When we consider the two-point function of a chiral and antichiral operator, the contribution from supersymmetry is given by

$$\frac{C_{\text{bdy,susy}} \langle \phi_1(x_1) \bar{\phi}_2(x_2) \rangle}{(2x_1^\perp)^{-\Delta_1} (2x_2^\perp)^{-\Delta_2}} = -\xi \partial_\xi \hat{F}_{\hat{\Delta}}^{\phi_1 \bar{\phi}_2}(\xi). \quad (4.4.10)$$

Combining the supersymmetric and non-supersymmetric pieces, and using the appropriate value of the Casimir, we get the following differential equation:

$$\left[ \xi(\xi + 1) \partial_\xi^2 + \left( \frac{d}{2} + (d-1)\xi \right) \partial_\xi - (\hat{\Delta}(\hat{\Delta} - d + 2) + j(j - d + 3)) \right] \hat{F}_{\hat{\Delta}}^{\phi_1 \bar{\phi}_2}(\xi) = 0. \quad (4.4.11)$$

A priori, there are two independent solutions of this equation for arbitrary values  $\hat{\Delta}$  and  $j$ . However, we must also require that the solutions can be decomposed into non-supersymmetric blocks, and we find that this is only possible whenever  $j = 0$  for arbitrary  $\hat{\Delta}$ . The solution can be expressed either as a linear combination of bosonic blocks, or as a single hypergeometric function with a prefactor:

$$\begin{aligned} \hat{F}_{\hat{\Delta}}^{\phi_1 \bar{\phi}_2}(\xi) &= \hat{f}_{\hat{\Delta}}(\xi) + \frac{\hat{\Delta}}{2(2\hat{\Delta} - d + 3)} \hat{f}_{\hat{\Delta}+1}(\xi), \\ &= \xi^{-\hat{\Delta}} {}_2F_1\left(\hat{\Delta}, \hat{\Delta} + 1 - \frac{d}{2}; 2\hat{\Delta} - d + 3; -\frac{1}{\xi}\right). \end{aligned} \quad (4.4.12)$$

Even though we considered a general two-point function  $\langle \phi_1 \bar{\phi}_2 \rangle$ , the superconformal blocks are the same as for a two-point function of identical (anti)chiral operators  $\langle \phi \bar{\phi} \rangle$ . A nice consistency check is that the relative coefficient between the non-supersymmetric blocks is positive, as we expect in the defect channel of  $\langle \phi \bar{\phi} \rangle$ , because the coefficients that appear in the OPE are  $|b_{\phi\bar{\phi}}|^2$ . When we restrict to  $d = 3$  we find perfect agreement with the explicit superspace calculation (4.3.65).

**$\langle \phi_1 \phi_2 \rangle$  correlator:** In a similar way, we can work out the Ward identities for the  $\langle \phi_1 \phi_2 \rangle$  two-point function. The new contribution to the Casimir equation is:

$$\frac{C_{\text{bdy,susy}} \langle \phi_1(x_1) \phi_2(x_2) \rangle}{(2x_1^\perp)^{-\Delta_1} (2x_2^\perp)^{-\Delta_2}} = -(\xi + 1) \partial_\xi \hat{F}_{\hat{\Delta}}^{\phi_1 \phi_2}(\xi). \quad (4.4.13)$$

Combining the non-supersymmetric and supersymmetric pieces with the eigenvalue (4.4.7), the Casimir equation reads

$$\left[ \xi(\xi + 1) \partial_\xi^2 + \left( \frac{d-2}{2} + (d-1)\xi \right) \partial_\xi - (\hat{\Delta}(\hat{\Delta} - d + 2) + j(j - d + 3)) \right] \hat{F}_{\hat{\Delta}}^{\phi_1 \phi_2}(\xi) = 0. \quad (4.4.14)$$

<sup>9</sup>It is likely that our blocks are valid for  $2 \leq d \leq 4$  but we have not checked explicitly the  $d = 2$  case. Notice that below  $d \leq 3$  one has to take into account the operators  $M_{\hat{i}, \hat{j}}$  with  $\hat{i}, \hat{j} = d, \dots, 4$ , and the calculation is slightly more complicated.

Once again, we only find physically acceptable solutions whenever  $j = 0$ :

$$\begin{aligned}\hat{F}_{\hat{\Delta}}^{\phi_1\phi_2}(\xi) &= \hat{f}_{\hat{\Delta}}(\xi) - \frac{\hat{\Delta}}{2(2\hat{\Delta} - d + 3)} \hat{f}_{\hat{\Delta}+1}(\xi), \\ &= \xi^{-\Delta} {}_2F_1\left(\hat{\Delta}, \hat{\Delta} + 2 - \frac{d}{2}; 2\hat{\Delta} - d + 3; -\frac{1}{\xi}\right).\end{aligned}\tag{4.4.15}$$

The decompositions into non-supersymmetric blocks in eqs. (4.4.15) and (4.4.12) are identical up to a relative minus sign. We know this must be the case, since the boundary OPE of  $\langle\phi\phi\rangle$  contains  $b_{\phi\hat{\mathcal{O}}}^2$ , which is not necessarily positive definite, but instead  $b_{\phi\hat{\mathcal{O}}}^2 = \pm|b_{\phi\hat{\mathcal{O}}}|^2$ . When we restrict to  $d = 3$  we find perfect agreement with the explicit superspace calculation (4.3.66).

### Bulk channel

Now we proceed to calculate the blocks that appear in the bulk decomposition using the bulk Casimir.

**$\langle\phi_1\bar{\phi}_2\rangle$  correlator:** To obtain bulk channel blocks we act with the full Casimir once more focusing on the part that is new from supersymmetry:

$$C_{\text{bulk,susy}} = -\frac{d-1}{2}R^2 + \frac{1}{2}[S^{\dot{\alpha}+}, Q_{\dot{\alpha}}^-] + \frac{1}{2}[S^{\alpha-}, Q_{\alpha}^+].\tag{4.4.16}$$

We can simplify the action of the superconformal Casimir using the commutation relations, the chirality properties of  $\phi_1$  and  $\bar{\phi}_2$ , and equation (51) from [154]:

$$\begin{aligned}[C_{\text{bulk,susy}}, \phi_1(x_1)\bar{\phi}_2(x_2)]|0\rangle &= ix_{12}^{\mu}\bar{\Sigma}_{\mu}^{\dot{\alpha}\alpha}[Q_{\dot{\alpha}}^-, \phi_1(x_1)][Q_{\alpha}^+, \bar{\phi}_2(x_2)]|0\rangle \\ &\quad + \left(2(\Delta_1 + \Delta_2) - \frac{d-1}{4}r_{12}^2\right)\phi_1(x_1)\bar{\phi}_2(x_2)|0\rangle.\end{aligned}\tag{4.4.17}$$

Here we assume  $\phi_i$  has charge  $r_i$ , we define  $r_{12} = r_1 - r_2$  and we use chirality to relate  $\Delta_i = \frac{1}{2}(d-1)r_i$ . We can use Ward identities to rewrite the  $Q$ -dependent part in a way that can be put in a Casimir equation. After some algebra we get<sup>10</sup>

$$\frac{C_{\text{bulk,susy}}\langle\phi_1(x_1)\bar{\phi}_2(x_2)\rangle}{(2x_1^{\perp})^{-\Delta_1}(2x_2^{\perp})^{-\Delta_2}\xi^{-(\Delta_1+\Delta_2)/2}} = \left(4\xi\partial_{\xi} - \frac{d-1}{4}r_{12}^2\right)G_{\Delta}^{\phi_1\bar{\phi}_2}(\xi).\tag{4.4.18}$$

Now we can combine all the pieces to form the differential equation

$$\begin{aligned}\left[4\xi^2(\xi+1)\partial_{\xi}^2 + 2\xi(2\xi-d+4)\partial_{\xi} - \Delta(\Delta-d+2)\right. \\ \left. - \ell(\ell+d-2) - \frac{d-1}{4}(r_{12}^2 - r^2) - \Delta_{12}^2\xi\right]G_{\Delta}^{\phi_1\bar{\phi}_2}(\xi) = 0.\end{aligned}\tag{4.4.19}$$

The superselection rules in the  $\phi_1 \times \bar{\phi}_2$  OPE were worked out in four dimensions [166] and in any  $d$  [154]. For our setup, they imply that only superprimaries with  $r = r_{12}$  and

<sup>10</sup>We find it more convenient to work in terms of  $G(\xi) = \xi^{(\Delta_1+\Delta_2)/2}F(\xi)$ , but one can easily map the results between the two conventions.

$\ell = 0$  can appear<sup>11</sup>. Indeed, we can solve the Casimir equation in this case to find:

$$\begin{aligned} G_{\Delta}^{\phi_1 \bar{\phi}_2}(\xi) &= g_{\Delta}^{\Delta_{12}}(\xi) + \frac{(\Delta - \Delta_{12})(\Delta + \Delta_{12})}{(2\Delta - d + 2)(2\Delta - d + 4)} g_{\Delta+2}^{\Delta_{12}}(\xi) \\ &= \xi^{\Delta/2} {}_2F_1\left(\frac{\Delta + \Delta_{12}}{2}, \frac{\Delta - \Delta_{12}}{2}; \Delta + 2 - \frac{d}{2}; -\xi\right). \end{aligned} \quad (4.4.20)$$

For generic values of  $\Delta$  these blocks capture the exchange of a long operator, while they can be interpreted as short operators when  $\Delta$  saturates the unitarity bounds. The classification of possible short multiplets in  $d = 3, 4$  is well known and can be found for example in [167, 158].

**$\langle \phi_1 \phi_2 \rangle$  correlator:** It is well known that when the two operators are chiral the bulk blocks are equal to non-supersymmetric blocks. The precise selection rules for  $\phi_1 \times \phi_2$  are known [154], but we review them here for convenience:

- Consider a superprimary  $\mathcal{O}$  that has  $R$ -charge  $r = r_1 + r_2 - 2$  and dimension  $\Delta$ . The descendant  $(Q^+)^2 \mathcal{O}$  has charge  $r_1 + r_2$ , dimension  $\Delta + 1$  and is killed by  $Q_{\alpha}^+$ , so it appears in the  $\phi_1 \times \phi_2$  OPE.
- Alternatively, consider the chiral superprimary operator  $(\phi_1 \phi_2)$ , with  $r = r_1 + r_2$  and  $\Delta = \Delta_1 + \Delta_2$ . In this case the superprimary itself is exchanged in the OPE.
- Finally, consider an anti-chiral superprimary operator  $\bar{\Psi}$  whose dimension is related to its charge and given by  $\Delta = -\frac{d-1}{2}r = d-1 - (\Delta_1 + \Delta_2)$ . The descendant operator  $(Q^+)^2 \bar{\Psi}$  is exchanged in the OPE.

In what follows, whenever we consider bulk channel  $\phi\phi$  superconformal blocks,  $\Delta$  will be the dimension of the actual exchanged operator, and not the dimension of the superprimary.

#### 4.4.2 An aside: codimension-two defects

In this work we are mostly concerned with boundaries that interpolate between  $3 \leq d \leq 4$  models. In the same way there exist codimension-two defects that interpolate between a line in  $d = 3$  and a surface in  $d = 4$ . A familiar example is the  $3d$  Ising twist defect, which was studied using Feynman diagrams in  $4 - \varepsilon$  dimensions [74] (see also [73] for a Monte-Carlo analysis in exactly  $d = 3$ ). These results were later reproduced and generalized using analytic bootstrap technology [97]. Similar techniques should be applicable to half-BPS codimension-two defects in supersymmetric theories like the Wess-Zumino model. We plan to come back to this problem in the future, but for now we describe how the superconformal blocks can be obtained within our framework.

The notation in this subsection will be different from the rest of the section; we hope this does not cause confusion. We insert the codimension-two defect at  $x_i = 0$  for  $i = 1, 2$  and label the parallel directions as  $x_a$  for  $a = 3, \dots, d$ . The defect will naturally preserve parallel translations and special conformal transformations  $P_a, K_a$ , dilatations  $D$ , as well as parallel and perpendicular rotations  $M_{ab}, M_{ij}$ . The two-point function of

---

<sup>11</sup>Superprimaries with  $\ell \geq 1$  also appear in the OPE but they have zero one-point function, so they are not relevant in our analysis.

local operators depends on two cross-ratios. To study the defect channel it is convenient to use coordinates  $(\chi, \phi)$ , while the bulk channel simplifies using coordinates  $(x, \bar{x})$ :<sup>12</sup>

$$\begin{aligned} \frac{|x_{12}^a|^2 + |x_1^i|^2 + |x_2^i|^2}{|x_1^i||x_2^i|} &= \chi = \frac{2 - x - \bar{x}}{\sqrt{(1-x)(1-\bar{x})}}, \\ \frac{x_1^i x_2^i}{|x_1^i||x_2^i|} &= \cos \phi = \frac{2 - x - \bar{x} + x\bar{x}}{2\sqrt{(1-x)(1-\bar{x})}}. \end{aligned} \quad (4.4.21)$$

The non-supersymmetric as well as the superconformal blocks are given below.

Besides the bosonic generators described above, a half-BPS defect preserves two Poincaré supercharges:

$$Q_1^{\text{defect}} = Q_1^+, \quad Q_2^{\text{defect}} = Q_1^-, \quad S_1^{\text{defect}} = S^{1+}, \quad S_2^{\text{defect}} = S^{1-}. \quad (4.4.22)$$

Our system does not preserve  $R$ -symmetry or transverse rotations independently, but only a linear combination of them that we call twisted transverse rotations:<sup>13</sup>

$$M^{\text{defect}} = M_{12} + \frac{d-1}{2}R. \quad (4.4.23)$$

With these conventions in mind, we proceed to obtain the superconformal blocks.

### Defect channel

When supersymmetry is not present, the defect operators are labeled by the conformal dimension  $\hat{\Delta}$  and the transverse spin  $s$ . One can write down a Casimir equation which is solved by the following conformal blocks [47]:

$$\hat{f}_{\hat{\Delta},s}(\chi, \phi) = e^{is\phi} \chi^{-\hat{\Delta}} {}_2F_1\left(\frac{\hat{\Delta}}{2}, \frac{\hat{\Delta}+1}{2}; \hat{\Delta}+2 - \frac{d}{2}; \frac{4}{\chi^2}\right). \quad (4.4.24)$$

In the supersymmetric case the only difference is that  $s$  denotes the twisted transverse spin (4.4.23). One can work out the selection rules, and find that only one operator in each multiplet contributes to the OPE, so the superconformal blocks are just eq. (4.4.24) with the arguments shifted appropriately.

### Bulk channel

Similarly, one can obtain a Casimir equation for the non-supersymmetric bulk channel. It was observed in [47] that for codimension-two the Casimir equation is identical to the one found by Dolan and Osborn (D&O) for bulk four-point functions [119]. Therefore, the bulk-channel blocks of a defect two-point function are equal to the familiar four-point blocks:

$$f_{\Delta,\ell}(x, \bar{x}) = G_{\Delta,\ell,\text{D\&O}}^{0,0}(x, \bar{x}). \quad (4.4.25)$$

When supersymmetry is included, the Casimir equation has an extra term  $C_{\text{bulk,susy}}$  that can be simplified using Ward identities, as described in appendix C. When the dust

<sup>12</sup>Our cross-ratios are related to the ones in [51] by  $z = 1 - x$  and  $\bar{z} = (1 - \bar{x})^{-1}$ .

<sup>13</sup>For the particular case of a line defect in  $d = 3$ , the subalgebra has been written explicitly in [168].

settles, it turns out that the blocks are described by non-supersymmetric blocks with shifted arguments:

$$F_{\Delta,\ell}(x, \bar{x}) = (x\bar{x})^{-\frac{1}{2}} G_{\Delta+1,\ell,D\&O}^{-1,-1}(x, \bar{x}). \quad (4.4.26)$$

Even more surprisingly, these blocks are exactly the same that were found in [154] for a four-point function of chiral and antichiral operators!

### 4.4.3 Free theory

After the small codimension-two detour let us come back to the boundary setup. As a first consistency check of our superconformal blocks, we consider a free chiral multiplet in the bulk in the presence of a half-BPS boundary. It is well known that a free scalar has dimension  $\Delta_\phi = \frac{d-2}{2}$ , and the bulk equations of motion have a simple solution:

$$\partial_x^2 \langle \phi(x) \bar{\phi}(x') \rangle = 0 \quad \Rightarrow \quad \mathcal{F}^{\phi\bar{\phi}}(\xi) = \frac{c_1^{\phi\bar{\phi}}}{\xi^{(d-2)/2}} + \frac{c_2^{\phi\bar{\phi}}}{(\xi+1)^{(d-2)/2}}. \quad (4.4.27)$$

For the two-point function  $\langle \phi\phi \rangle$  we find the same solution with free coefficients  $c_{1,2}^{\phi\phi}$ . In order to impose supersymmetry, we must require that these correlators have consistent superconformal block decompositions in the bulk and boundary channels. It is a simple exercise to show that this fixes  $c_1^{\phi\phi} = c_2^{\phi\bar{\phi}} = 0$ . We can also fix  $c_1^{\phi\bar{\phi}} = 1$  requiring that far away from the boundary, the two-point function  $\langle \phi\bar{\phi} \rangle$  is unit normalized: it is normalized such that the OPE coefficient of the bulk identity block is 1. Finally, after an appropriate redefinition  $\phi \rightarrow e^{i\delta}\phi$  we can always choose the normalization  $c_2^{\phi\phi} = 1$ . All in all,

$$\begin{aligned} \mathcal{F}^{\phi\bar{\phi}}(\xi) &= \frac{1}{\xi^{(d-2)/2}} = F_{\text{Id}}^{\phi\bar{\phi}}(\xi) = \hat{F}_{(d-2)/2}^{\phi\bar{\phi}}(\xi), \\ \mathcal{F}^{\phi\phi}(\xi) &= \frac{1}{(\xi+1)^{(d-2)/2}} = F_{d-2}^{\phi\phi}(\xi) = \hat{F}_{(d-2)/2}^{\phi\phi}(\xi). \end{aligned} \quad (4.4.28)$$

In the above equation we also present the expansion of the correlation functions in terms of superconformal blocks. Interestingly, only one superconformal block contributes to each channel, and with our normalization conventions all OPE coefficients are equal to one.

The above solution to crossing has a clear physical interpretation if we split the chiral primary operator in terms of its real and imaginary parts  $\phi = \phi_1 + i\phi_2$ . Then we see that  $\phi_1$  satisfies Neumann boundary conditions, whereas  $\phi_2$  satisfies Dirichlet boundary conditions. Indeed, from eq. (4.4.28) we obtain

$$\lim_{x \rightarrow \text{bdy}} \langle \partial_\perp \phi_1(x) \phi_1(x') \rangle = 0, \quad \lim_{x \rightarrow \text{bdy}} \langle \phi_2(x) \phi_2(x') \rangle = 0. \quad (4.4.29)$$

We can think of our free correlation functions as linear combinations of the Neumann and Dirichlet boundary CFTs studied in [46], with the precise relative coefficients fixed by supersymmetry.

### 4.4.4 The $\varepsilon$ -expansion bootstrap

It was originally observed in [46] that the crossing equation for boundary CFTs can be used to extract information about the Wilson-Fischer fixed point in the epsilon expansion.



In particular, they bootstrapped the one-loop correlators at order  $\mathcal{O}(\varepsilon)$ , and the analysis was generalized to  $\mathcal{O}(\varepsilon^2)$  using different techniques in later works [56, 57, 169]. In this section we apply the same ideas to our supersymmetric two-point functions, and we obtain the full correlation functions at order  $\mathcal{O}(\varepsilon)$ .

In the supersymmetric setup there are two relevant crossing equations, one for  $\phi\bar{\phi}$  and the other for  $\phi\phi$ :

$$F_{\text{Id}}^{\phi\bar{\phi}}(\xi) + \sum_n c_n F_{\hat{\Delta}_n}^{\phi\bar{\phi}}(\xi) = \sum_n \mu_n \hat{F}_{\hat{\Delta}_n}^{\phi\bar{\phi}}(\xi), \quad \sum_n d_n F_{\Delta_n}^{\phi\phi}(\xi) = \sum_n \rho_n \hat{F}_{\hat{\Delta}_n}^{\phi\phi}(\xi). \quad (4.4.30)$$

Notice that the spectrum of operators in the boundary channel is the same for the two correlators. The boundary OPE coefficients are given in terms of bulk-to-boundary coefficients as  $\mu_n = |b_{\phi\mathcal{O}_n}|^2$  and  $\rho_n = b_{\phi\mathcal{O}_n}^2$ , so they must be equal up to possible signs  $\mu_n = \pm\rho_n$ . The precise signs as a function of  $n$  will be an outcome of our bootstrap analysis. The bulk channel OPE coefficients are products of one- and three-point coefficients  $c_n = a_{\mathcal{O}_n} \lambda_{\phi\bar{\phi}\mathcal{O}_n}$  and  $d_n = a_{\mathcal{O}_n} \lambda_{\phi\phi\mathcal{O}_n}$  so we do not expect any relations between them.

Our analysis starts in  $d = 4$ , where the SCFT is free and the correlators are given in eq. (4.4.28). We assume that the coupling of the theory is of order  $g \sim \varepsilon$ , so as we lower the dimension to  $d = 4 - \varepsilon$  the CFT data acquires small corrections. In particular, we expect the external chiral operator to acquire an anomalous dimension:

$$\Delta_\phi = \frac{d-2}{2} + \Delta_\phi^{(1)}\varepsilon + \Delta_\phi^{(2)}\varepsilon^2 + \dots \quad (4.4.31)$$

We should think of  $\Delta_\phi^{(1)}$  as being related to the strength of the coupling  $g \propto \Delta_\phi^{(1)}\varepsilon$ , and the precise constant depends on the model under consideration. In the bulk four-point function  $\varepsilon$ -expansion bootstrap, see for example [170], conservation of the stress tensor allows one to fix the precise value of  $\Delta_\phi^{(1)}$ . Unfortunately this will not be possible in our setup because the stress-tensor multiplet does not appear in the bulk OPE.

Another consequence of turning on the couplings is that we expect that new infinite families of operators will enter our crossing equations. In the bulk channel, from the intuition gained from the usual four-point function analytic bootstrap, we expect double-trace operators of the form  $\phi\Box^n\phi$  with dimensions

$$\Delta_n = d - 2 + 2n + \Delta_n^{(1)}\varepsilon + \Delta_n^{(2)}\varepsilon^2 + \dots, \quad (4.4.32)$$

and similarly operators  $\phi\Box^n\bar{\phi}$  with dimensions  $\tilde{\Delta}_n$ . In the boundary channel, we expect operators of the schematic form  $\Box^m\partial_\perp^{n-2m}\phi$  so they have dimension

$$\hat{\Delta}_n = \frac{d-2}{2} + n + \hat{\Delta}_n^{(1)}\varepsilon + \hat{\Delta}_n^{(2)}\varepsilon^2 + \dots \quad (4.4.33)$$

Finally, the OPE coefficients will also get corrections as a power series in  $\varepsilon$ , namely

$$c_n = c_n^{(0)} + c_n^{(1)}\varepsilon + c_n^{(2)}\varepsilon^2 + \dots, \quad (4.4.34)$$

and similarly for  $d_n$ ,  $\mu_n$  and  $\rho_n$ . With the above conventions, the free theory solution when  $d = 4$  is given by

$$d_0^{(0)} = \mu_0^{(0)} = \rho_0^{(0)} = 1, \quad c_{n \geq 0}^{(0)} = d_{n \geq 1}^{(0)} = \mu_{n \geq 1}^{(0)} = \rho_{n \geq 1}^{(0)} = 0. \quad (4.4.35)$$

In what follows we derive the first order correction to the CFT data.

**$\langle \phi\phi \rangle$  correlator**

We start by studying the two-point function  $\langle \phi\phi \rangle$ , because in this case we can reuse many results from [56]. We will very closely follow the notation and manipulations from this reference, and we refer the reader there for further details. The similarity is a consequence of the  $\phi\phi$  bulk channel superconformal blocks being equal to non-supersymmetric ones:  $F_{\Delta}^{\phi\phi} = f_{\Delta}$ .

The first step in the construction of [56] is to divide the crossing equation in two terms called  $G$  and  $H$ :

$$\mathcal{F}^{\phi\phi}(\xi) = G_{\text{blk}}(\xi) + H_{\text{blk}}(\xi) = G_{\text{bdy}}(\xi) + H_{\text{bdy}}(\xi). \quad (4.4.36)$$

In  $G$  we collect the contributions that appeared at order  $\varepsilon^0$ , but we allow them to acquire anomalous dimensions:

$$\begin{aligned} G_{\text{blk}}(\xi) &= F_{2-\varepsilon+\Delta_0^{(1)}\varepsilon}^{\phi\phi}(\xi) = \frac{1}{\xi+1} + \frac{(\Delta_0^{(1)} - 2\Delta_{\phi}^{(1)})\log\xi + \log(\xi+1)}{2(\xi+1)}\varepsilon + \mathcal{O}(\varepsilon^2), \\ G_{\text{bdy}}(\xi) &= \hat{F}_{1-\frac{\varepsilon}{2}+\varepsilon\hat{\Delta}_0^{(1)}}^{\phi\phi}(\xi) = \frac{1}{\xi+1} + \frac{\log(\xi+1) - 2\hat{\Delta}_0^{(1)}\log\xi}{2(\xi+1)}\varepsilon + \mathcal{O}(\varepsilon^2). \end{aligned} \quad (4.4.37)$$

On the other hand, we collect in  $H$  all the contributions where the anomalous dimensions do not contribute, so the blocks are evaluated at integer values of the dimensions:

$$H_{\text{blk}}(\xi) = \varepsilon \sum_{n=0}^{\infty} d_n^{(1)} F_{2n+2}^{\phi\phi}(\xi), \quad H_{\text{bdy}}(\xi) = \varepsilon \sum_{n=0}^{\infty} \rho_n^{(1)} \hat{F}_{n+1}^{\phi\phi}(\xi). \quad (4.4.38)$$

Note that an operator can contribute to both  $G$  and  $H$ , for instance the anomalous dimension  $\Delta_0^{(1)}$  of the leading bulk operator  $\mathcal{O}_0$  appears in  $G_{\text{blk}}$ , while the correction to its OPE coefficient  $d_0^{(1)}$  appears in  $H_{\text{blk}}$ .

The key observation of [56] was that one can eliminate  $H_{\text{bdy}}$  from the crossing equation by applying the following discontinuity:

$$\text{Disc } f(z) = f(ze^{i\pi}) - f(ze^{-i\pi}), \quad z \equiv \xi + \frac{1}{2} \in \left(\frac{1}{2}, \infty\right). \quad (4.4.39)$$

Indeed, from (4.4.39) one sees that  $\text{Disc } \hat{f}_n(\xi) = 0$  for integer  $n$ , which implies  $\text{Disc } H_{\text{bdy}}(\xi) = 0$ . It is an easy exercise to take the discontinuity of eq. (4.4.37), and using the crossing equation we find

$$\text{Disc } H_{\text{blk}}(\xi) = \text{Disc } G_{\text{bdy}}(\xi) - \text{Disc } G_{\text{blk}}(\xi) = \frac{i\pi\varepsilon}{\xi} \left( 2\hat{\Delta}_0^{(1)} - 2\Delta_{\phi}^{(1)} + \Delta_0^{(1)} \right). \quad (4.4.40)$$

The authors of [56] reconstructed the full correlator by expanding eq. (4.4.40) in terms of discontinuities of bulk blocks, extracting the CFT data, and then resumming the bulk OPE expansion. Note that since our expansion in the bulk has non-supersymmetric blocks, we can reuse their results without problems. In particular, comparing their equations (4.8) and (4.14) with our expression we obtain

$$H_{\text{blk}}(\xi) = -\frac{\varepsilon \log(\xi+1)}{2(\xi+1)} \left( 2\hat{\Delta}_0^{(1)} - 2\Delta_{\phi}^{(1)} + \Delta_0^{(1)} \right). \quad (4.4.41)$$

From this calculation we can reconstruct the full correlator  $\mathcal{F}^{\phi\phi}(\xi) = G_{\text{blk}}(\xi) + H_{\text{blk}}(\xi)$  and extract CFT data to  $\mathcal{O}(\varepsilon)$ . Before we do that, however, let us also reconstruct the  $\langle \phi\bar{\phi} \rangle$  correlator using the same technique.

$\langle \phi \bar{\phi} \rangle$  correlator

As before, let us divide the contributions of the crossing equations into two pieces, where

$$\begin{aligned} G_{\text{blk}}(\xi) &= F_{\text{Id}}^{\phi \bar{\phi}}(\xi) = \frac{1}{\xi} + \frac{(1 - 2\Delta_\phi^{(1)}) \log \xi}{2\xi} \varepsilon + \mathcal{O}(\varepsilon^2), \\ G_{\text{bdy}}(\xi) &= \hat{F}_{1-\frac{\varepsilon}{2} + \varepsilon \hat{\Delta}_0^{(1)}}^{\phi \bar{\phi}}(\xi) = \frac{1}{\xi} + \frac{\log \xi - 2\hat{\Delta}_0^{(1)} \log(\xi + 1)}{2\xi} \varepsilon + \mathcal{O}(\varepsilon^2), \end{aligned} \quad (4.4.42)$$

and the functions  $H$  are the same we defined in eq. (4.4.38), replacing  $(d_n, \rho_n) \rightarrow (c_n, \mu_n)$  and using the appropriate superconformal blocks for  $\phi \bar{\phi}$ . Again, the discontinuity removes  $H_{\text{bdy}}(\xi)$  and we are left with

$$\text{Disc } H_{\text{blk}}(\xi) = \text{Disc } G_{\text{bdy}}(\xi) - \text{Disc } G_{\text{blk}}(\xi) = -\frac{2\pi i \varepsilon}{\xi + 1} \left( \Delta_\phi^{(1)} - \hat{\Delta}_0^{(1)} \right). \quad (4.4.43)$$

This can be expanded in terms of discontinuities of superconformal blocks. In principle, we should repeat the analysis of [56] using our superconformal blocks. However, the first term in the expansion captures the entire correlator:

$$\text{Disc } F_2^{\phi \bar{\phi}}(\xi) = -\frac{2\pi i}{\xi + 1} = \frac{\text{Disc } H_{\text{blk}}(\xi)}{\varepsilon \left( \Delta_\phi^{(1)} - \hat{\Delta}_0^{(1)} \right)}. \quad (4.4.44)$$

We can remove the discontinuity from this equation<sup>14</sup> to obtain

$$H_{\text{blk}}(\xi) = \varepsilon \left( \Delta_\phi^{(1)} - \hat{\Delta}_0^{(1)} \right) F_2^{\phi \bar{\phi}} = \varepsilon \left( \Delta_\phi^{(1)} - \hat{\Delta}_0^{(1)} \right) \frac{\log(\xi + 1)}{\xi}. \quad (4.4.45)$$

The full correlator is  $\mathcal{F}^{\phi \bar{\phi}}(\xi) = G_{\text{blk}}(\xi) + H_{\text{blk}}(\xi)$ . Equation (4.4.44) implies that the bulk channel of  $\phi \bar{\phi}$  contains only the identity and another block, unlike the  $\phi \phi$  expansion which contained infinitely many blocks.

**Correlation functions and CFT data**

The solution of crossing we have found to  $\mathcal{O}(\varepsilon)$  has three free parameters. However, as discussed below eq. (4.4.30), the boundary OPE coefficients in the two channels should be equal up to a sign  $\rho_n = \pm \mu_n$ . Expanding  $\mathcal{F}^{\phi \phi}(\xi)$  and  $\mathcal{F}^{\phi \bar{\phi}}(\xi)$  in boundary superblocks and comparing the expansions we find one last constraint:

$$\Delta_0^{(1)} = 2 \left( (s + 1) \Delta_\phi^{(1)} - \hat{\Delta}_0^{(1)} \right), \quad s = \pm. \quad (4.4.46)$$

Hence, our solution depends on the anomalous dimension  $\Delta_\phi^{(1)}$  of the external chiral operator, the anomalous dimension of the leading boundary operator  $\hat{\Delta}_0^{(1)}$ , and a choice of signs  $s = \pm$ . Using this relation, the one-loop correlation functions take a very simple

---

<sup>14</sup>The discontinuities of superblocks are schematically  $\text{Disc } F_{2n}^{\phi \bar{\phi}} \sim P_n$ , where  $P_n$  are certain orthogonal polynomials. Since any function has a unique expansion in terms of  $P_n$ , it is safe to remove Disc from (4.4.44).

form<sup>15</sup>

$$\begin{aligned}\mathcal{F}^{\phi\bar{\phi}}(\xi) &= \frac{1}{\xi} + \frac{\left(1 - 2\Delta_\phi^{(1)}\right) \log \xi + 2\left(\Delta_\phi^{(1)} - \hat{\Delta}_0^{(1)}\right) \log(\xi + 1)}{2\xi} \varepsilon + \mathcal{O}(\varepsilon^2), \\ \mathcal{F}^{\phi\phi}(\xi) &= \frac{1}{\xi + 1} + \frac{\left(1 - 2s\Delta_\phi^{(1)}\right) \log(\xi + 1) + 2\left(s\Delta_\phi^{(1)} - \hat{\Delta}_0^{(1)}\right) \log \xi}{2(\xi + 1)} \varepsilon + \mathcal{O}(\varepsilon^2).\end{aligned}\tag{4.4.47}$$

From the correlation functions we can extract the CFT data at one-loop:<sup>16</sup>

$$\begin{aligned}c_0^{(1)} &= \Delta_\phi^{(1)} - \hat{\Delta}_0^{(1)}, & c_{n \geq 1}^{(1)} &= 0, & d_0^{(1)} &= 0, & \mu_0^{(1)} &= \rho_0^{(1)} = 0, \\ \mu_n^{(1)} &= s(-1)^n \rho_n^{(1)} = s(-1)^n d_n^{(1)} = \frac{(n-1)!}{2^{n-1}(2n-1)!!} \Delta_\phi^{(1)}, & n &\geq 1.\end{aligned}\tag{4.4.48}$$

Although we lack a conclusive proof, we believe it is very likely that the unfixed sign is always  $s = +1$ . One argument is that the correlators (4.4.47) are related to each other under  $\xi \leftrightarrow \xi + 1$ , provided  $s = +1$ . Another argument is that only for  $s = +1$  the signs of the coefficients in the BOE are alternating, namely  $(\rho_0, \rho_1, \rho_2, \dots) = (\mu_0, -\mu_1, \mu_2, \dots)$ , and otherwise they are alternating only for  $n \geq 1$ . Finally, we will do an explicit perturbative calculation for a specific model in the next section and we will find again that  $s = +1$ .

An interesting feature of the CFT data (4.4.48) is that the bulk and boundary OPE coefficients are identical for the two-point function  $\langle \phi\phi \rangle$ . This is a very non-trivial relation, since  $\rho_n = b_{\phi\mathcal{O}_n}^2$ , but  $d_n = a_{\mathcal{O}_n} \lambda_{\phi\phi\mathcal{O}_n}$ . It would be interesting to see if this is just a coincidence of the order  $\mathcal{O}(\varepsilon)$  result, or if it actually persists at higher orders in perturbation theory.

### Going to order $\varepsilon^2$

From the structure of the order  $\varepsilon$  CFT data (4.4.48), there is hope that one can push the bootstrap analysis to order  $\varepsilon^2$ . Indeed, only two blocks contribute at order  $\varepsilon$  in the  $\phi\bar{\phi}$  bulk channel. We expect infinitely many operators at order  $\varepsilon^2$ , but the majority of them will contribute as conformal blocks of even dimension  $F_{2n+2}(\xi)$ . One can construct a discontinuity, different than (4.4.39), that kills bulk blocks  $\widetilde{\text{Disc}} F_{2n+2} = 0$ , see [58]. From here there are several possible directions one can pursue:

- Following the ideas of the present section and [56], one can calculate  $\widetilde{\text{Disc}} H_{\text{bdy}} = \widetilde{\text{Disc}} G_{\text{blk}} - \widetilde{\text{Disc}} G_{\text{bdy}}$ . One should now expand  $\widetilde{\text{Disc}} H_{\text{bdy}}$  in terms of discontinuities of boundary blocks to extract the relevant CFT data. However, at this order in  $\varepsilon$ , the discontinuities of the blocks cannot be easily rewritten in terms orthogonal polynomials, and it is not clear how to proceed.

<sup>15</sup>We can also write  $\langle \phi(x)\bar{\phi}(y) \rangle = (x-y)^{-2\Delta_\phi} (\xi+1)^{\varepsilon(\Delta_\phi^{(1)} - \hat{\Delta}_0^{(1)})}$  and similarly for  $\langle \phi\phi \rangle$ . This is very similar to the non-supersymmetric case, see equation (2.32) of [171]. We thank A. Söderberg for pointing this out.

<sup>16</sup>Our solution of crossing splits naturally into a piece involving only boundary blocks with  $n = 0$  and a piece that includes all  $n \geq 1$ . This resembles the four-point analytic bootstrap where our  $n$  plays the role of the bulk spin  $\ell$ . In particular, our  $n = 0$  solution corresponds to the solutions with finite support in spin found in [172]. We thank F. Alday for pointing this out.

- The authors of [58] studied an inversion formula that would reconstruct the boundary data from the two discontinuities  $\text{Disc } \mathcal{F}$  and  $\widetilde{\text{Disc } \mathcal{F}}$  of a correlator. Unfortunately, they were unable to determine its precise form for the case of interest here, and even if the relevant inversion formula is found, calculating  $\text{Disc } \mathcal{F}^{\phi\bar{\phi}}$  in our setup would be challenging.
- Finally, one can make an ansatz for the full correlator based on transcendentality and demand consistency with the above discontinuities to fix coefficients. With this approach it is possible to rederive the order  $\varepsilon^2$  correlator of the Wilson-Fischer fixed point calculated in [56]. In our supersymmetric setup, we have found a consistent solution to crossing at order  $\varepsilon^2$  that depends on a number of free parameters. However, it is not clear to us yet whether this correlator is physical or whether it is part of a more general solution of crossing yet to be found.

## 4.5 Wess-Zumino model with a boundary

In this section we study the Wess-Zumino (WZ) model with a cubic superpotential in the presence of half-BPS boundary conditions. The WZ model has a stable fixed point in  $4 - \varepsilon$  dimensions, which has been studied in the context of emergent supersymmetry [173, 174]. The two-loop calculation of [175] showed that supersymmetry is preserved perturbatively, provided the gamma matrix algebra is evaluated in  $d = 4$ , but using a  $4 - \varepsilon$  dimensional spacetime otherwise. Here we adopt the same regularization procedure, which is reminiscent of the way we obtained the blocks in section 4.4, using a superconformal algebra with  $4d$  spinor representations, but allowing arbitrary  $d \leq 4$  spacetime dimensions. Furthermore, we assume that the boundary is exactly codimension-one for any  $d$ .

### 4.5.1 Action and boundary conditions

Our model consists of a single chiral multiplet interacting with a cubic superpotential, so the degrees of freedom are the real and imaginary parts of  $\phi = \phi_1 + i\phi_2$ , a four-component Majorana fermion  $\Psi$ , and the real and imaginary parts of the auxiliary fields  $F = F_1 + iF_2$ . The action is obtained by integrating the Lagrangian density over a half-space, with parallel coordinates  $\mathbf{x} \in \mathbb{R}^{d-1}$  and perpendicular coordinate  $y \in \mathbb{R}^+$ :<sup>17</sup>

$$S_{blk} = \int d^{d-1}\mathbf{x} dy \left( \frac{1}{2}(\partial_\mu \phi_1)^2 + \frac{1}{2}(\partial_\mu \phi_2)^2 + \frac{1}{2}\bar{\Psi}\gamma^\mu \partial_\mu \Psi - \frac{1}{2}F_1^2 - \frac{1}{2}F_2^2 - \frac{\lambda}{2\sqrt{2}} \left( F_1(\phi_1^2 - \phi_2^2) + 2F_2\phi_1\phi_2 - \bar{\Psi}(\phi_1 + i\gamma_5\phi_2)\Psi \right) \right). \quad (4.5.1)$$

In order to compute Feynman diagrams, it will be simpler to integrate out the auxiliary fields  $F_i$ , producing the following interaction vertices:

$$S_{int} = \int d^{d-1}\mathbf{x} dy \left( \frac{1}{16}\lambda^2 (\phi_1^2 + \phi_2^2)^2 + \frac{\lambda}{2\sqrt{2}}\bar{\Psi}(\phi_1 + i\gamma_5\phi_2)\Psi \right). \quad (4.5.2)$$

<sup>17</sup>We work in Euclidean signature with  $\{\gamma^\mu, \gamma^\nu\} = 2\delta^{\mu\nu}$  and  $\gamma_5 = \gamma^1\gamma^2\gamma^3\gamma^4$ . The Majorana reality condition is  $\Psi^T \mathcal{C} = \bar{\Psi}$ , where the charge conjugation matrix satisfies  $\gamma^\mu = -\mathcal{C}^{-1}(\gamma^\mu)^T \mathcal{C}$ .

However, it is easier to work with the off-shell action to study how the boundary breaks supersymmetry. The supersymmetry transformations are parametrized by a Majorana spinor  $\varepsilon$  and they are well known:

$$\begin{aligned} \delta\phi_1 &= -\bar{\varepsilon}\Psi, & \delta\Psi &= (-\not{\partial}\phi_1 - i\gamma_5\not{\partial}\phi_2 - F_1 + i\gamma_5F_2)\varepsilon, & \delta F_1 &= -\bar{\varepsilon}\not{\partial}\Psi, \\ \delta\phi_2 &= i\bar{\varepsilon}\gamma_5\Psi, & \delta\bar{\Psi} &= \bar{\varepsilon}(\not{\partial}\phi_1 - i\gamma_5\not{\partial}\phi_2 - F_1 + i\gamma_5F_2), & \delta F_2 &= i\bar{\varepsilon}\gamma_5\not{\partial}\Psi. \end{aligned} \quad (4.5.3)$$

If we integrated the Lagrangian (4.5.1) over  $\mathbb{R}^d$ , the supersymmetry transformations (4.5.3) would be an exact symmetry of the action. However, the situation is more complicated in the presence of the boundary. On the one hand, we know that not all supersymmetries can be preserved, because that would imply that translations orthogonal to the boundary are also preserved. We can preserve at most half of the supersymmetry, namely the transformations generated by spinors satisfying [176]

$$\Pi_+\varepsilon = \varepsilon \quad \Leftrightarrow \quad \Pi_-\varepsilon = 0, \quad \Pi_{\pm} \equiv \frac{1}{2}(1 \pm i\gamma_5\gamma^n). \quad (4.5.4)$$

On the other hand, to check invariance under supersymmetry of (4.5.1), we have to integrate by parts, which generates extra boundary terms. Supersymmetry will only be preserved for an action containing extra boundary degrees of freedom  $S = S_{blk} + S_{bdy}$ , provided we choose  $S_{bdy}$  to cancel the terms generated by the supersymmetry variation of  $S_{blk}$ . A systematic study of all possible boundary actions for a generic  $4d$   $\mathcal{N} = 1$  theory appeared in [156], and we can easily translate their results to our conventions. For the purposes of this section, we will pick the minimal boundary action that preserves supersymmetry, although more general options would be possible:

$$S_{bdy} = \int d^{d-1}\mathbf{x} \left( \frac{1}{2}(\phi_1\partial_n\phi_1 + \phi_2\partial_n\phi_2 + \phi_1F_2 + \phi_2F_1) - \frac{\lambda}{2\sqrt{2}}\left(\frac{1}{3}\phi_2^3 - \phi_1^2\phi_2\right) \right). \quad (4.5.5)$$

It is an easy but tedious exercise to check that the combination of bulk and boundary actions indeed preserves half of the original supersymmetries.

Next we address the problem of determining the boundary conditions of our fields. Demanding that the Euler-Lagrange variation of the total action vanishes produces a bulk term which is zero, provided that the fields satisfy the equations of motion (EOM). However, we also get terms localized in the boundary

$$\begin{aligned} \delta(S_{bulk} + S_{bdy}) &= \int d^{d-1}\mathbf{x} dy (\text{EOM}) + \int d^{d-1}\mathbf{x} \left( \frac{1}{2}\phi_1\delta(F_2 + \partial_n\phi_1) \right. \\ &\quad \left. + \frac{1}{2}\phi_2\delta(F_1 + \partial_n\phi_2) - \frac{1}{2}\delta\phi_1(F_2 + \partial_n\phi_1) - \frac{1}{2}\delta\phi_2(F_1 + \partial_n\phi_2) + \frac{1}{2}\delta\bar{\Psi}\gamma^n\Psi \right), \end{aligned} \quad (4.5.6)$$

and the boundary conditions must be chosen such that they are zero. Moreover, one must check that the boundary conditions are closed under the supersymmetry transformations (4.5.3). In [156] it was shown that there is only one possible supersymmetric boundary condition, up to  $R$ -symmetry redefinitions  $\phi \rightarrow e^{i\delta}\phi$ . In conventions that match the bootstrap analysis of section 4.4 this boundary condition is

$$\partial_n\phi_1 = -F_2 = \frac{\lambda}{\sqrt{2}}\phi_1\phi_2, \quad \phi_2 = 0, \quad \Pi_-\Psi = 0. \quad (4.5.7)$$

In equations (4.5.6) and (4.5.7) we used the bulk equations of motion that relate  $F \sim \lambda\phi^2$ . Since we will work in perturbation theory, the free propagators are obtained for  $\lambda = 0$ , where  $\phi_1$  satisfies Neumann boundary conditions  $\partial_n\phi_1 = 0$ . As pointed out in [177], these boundary conditions are a good description near the free theory, but are not meant to describe the boundary condition of the fields at the interacting fixed point.

## 4.5.2 Using susceptibility

The calculation of correlation functions in the presence of boundaries using Feynman diagrams is typically challenging. An important observation that dates back to the work of McAvity and Osborn [149, 178] is that the calculations simplify in terms of susceptibilities, defined as

$$\chi_{\mathcal{O}_1\mathcal{O}_2}(y, y') = \int d^{d-1}\mathbf{x} \langle \mathcal{O}_1(\mathbf{x}, y) \mathcal{O}_2(0, y') \rangle. \quad (4.5.8)$$

Crucially, this integral transform is invertible and one can recover the two-point function in terms of the susceptibility. This idea has been recently used to compute the one-loop two-point function of the order parameter in the extraordinary phase transition of the  $O(N)$  model [179, 61]. One can also apply it to the  $O(N)$  model in the large- $N$  limit, see [180] for the three-dimensional case with a  $\phi^6$  potential.

In susceptibility space the role of the cross ratio  $\xi$  is played by a new object  $\zeta$ , which is defined as follows:

$$\zeta = \frac{\min(y, y')}{\max(y, y')}. \quad (4.5.9)$$

The importance of  $\zeta$  was noted in [61], where they observed that the contribution of a single conformal block in the boundary expansion is proportional to  $\zeta^{\hat{\Delta} - \frac{d-1}{2}}$ . This allows one to extract the boundary CFT data directly from the susceptibility without the need to reexpress everything in terms of the correlation function  $F(\xi)$ . To be more precise, the susceptibility can be expanded as

$$\chi_{\mathcal{O}\mathcal{O}}(y, y') = (4yy')^{\frac{d-1}{2} - \Delta_{\mathcal{O}}} \sum_{\hat{\mathcal{O}}} \mu_{\hat{\mathcal{O}}} \pi^{\frac{d-1}{2}} \frac{\Gamma\left(\hat{\Delta} - \frac{d-1}{2}\right)}{\Gamma(\hat{\Delta})} (4\zeta)^{\hat{\Delta} - \frac{d-1}{2}}, \quad (4.5.10)$$

where  $\Delta_{\mathcal{O}}$  is the dimension of the external operator,  $\mu_{\hat{\mathcal{O}}}$  is the boundary OPE coefficient and  $\hat{\Delta}$  is the dimension of the exchanged operator.

Even though the bootstrap analysis used the chiral field and its complex conjugate, for the purposes of the current section it is more convenient to work with its real and imaginary parts  $\phi = \phi_1 + i\phi_2$ . The susceptibilities of the two descriptions are related by

$$\begin{aligned} \chi^+(y, y') &\equiv \chi_{\phi_1\phi_1}(y, y') = \frac{1 + \frac{\varepsilon}{2}(\gamma + \log \pi)}{4\pi^2} (\chi_{\phi\bar{\phi}}(y, y') + \chi_{\phi\phi}(y, y')), \\ \chi^-(y, y') &\equiv \chi_{\phi_2\phi_2}(y, y') = \frac{1 + \frac{\varepsilon}{2}(\gamma + \log \pi)}{4\pi^2} (\chi_{\phi\bar{\phi}}(y, y') - \chi_{\phi\phi}(y, y')), \end{aligned} \quad (4.5.11)$$

where the prefactor translates from the natural normalization in the bootstrap calculation to the natural normalization using Lagrangians. It is an easy exercise to check that our

prediction for the order  $\varepsilon$  correlator (4.4.47) leads to

$$\begin{aligned}\chi^+(y, y') &= \frac{-1}{2\sqrt{\zeta}}(4yy')^{\frac{1}{2}-\Delta_\phi^{(1)}\varepsilon} \left[ 1 + 2\hat{\Delta}_0^{(1)}\varepsilon + \hat{\Delta}_0^{(1)}\varepsilon \log \zeta \right. \\ &\quad \left. - \Delta_\phi^{(1)}\varepsilon \left( (1+\zeta) \log(1+\zeta) + (1-\zeta) \log(1-\zeta) \right) + \mathcal{O}(\varepsilon^2) \right], \\ \chi^-(y, y') &= \frac{\sqrt{\zeta}}{2}(4yy')^{\frac{1}{2}-\Delta_\phi^{(1)}\varepsilon} \left[ 1 + 2 \left( 2\Delta_\phi^{(1)} - \hat{\Delta}_0^{(1)} \right) \varepsilon + \hat{\Delta}_0^{(1)}\varepsilon \log \zeta \right. \\ &\quad \left. - \Delta_\phi^{(1)}\varepsilon \left( \frac{(1+\zeta)}{\zeta} \log(1+\zeta) - \frac{(1-\zeta)}{\zeta} \log(1-\zeta) \right) + \mathcal{O}(\varepsilon^2) \right].\end{aligned}\tag{4.5.12}$$

In the rest of this section we will check that perturbation theory gives a result consistent with this prediction, and we will find the explicit values of  $\Delta_\phi^{(1)}$  and  $\hat{\Delta}_0^{(1)}$  for the Wess-Zumino model.

### 4.5.3 Susceptibility at one-loop

#### Tree level

To compute the scalar propagators we have to solve the Klein-Gordon equation in position space. It is well known that in the presence of a boundary one has to add a “mirror” term to the propagator to satisfy the correct boundary conditions at  $y = 0$ . Since  $\phi_1/\phi_2$  satisfy Neumann/Dirichlet boundary conditions we have:

$$\begin{aligned}\langle \phi_1(x)\phi_1(x') \rangle_0 &= \kappa_s \left( \frac{1}{|x-x'|^{d-2}} + \frac{1}{|\bar{x}-x'|^{d-2}} \right), \\ \langle \phi_2(x)\phi_2(x') \rangle_0 &= \kappa_s \left( \frac{1}{|x-x'|^{d-2}} - \frac{1}{|\bar{x}-x'|^{d-2}} \right).\end{aligned}\tag{4.5.13}$$

Here  $\langle \dots \rangle_0$  indicates the two-point functions are evaluated in the free theory. For each  $x = (\mathbf{x}, y)$  we defined the mirror point  $\bar{x} = (\mathbf{x}, -y)$ , and the overall normalization is  $\kappa_s = \frac{\Gamma(\frac{d}{2})}{(d-2)2\pi^{d/2}}$ . We will be mostly interested in the susceptibilities, which can be readily obtained from eqs. (4.5.8) and (4.5.13):

$$\begin{aligned}\chi_0^+(y, y') &= \chi_{\langle \phi_1 \phi_1 \rangle_0}(y, y') = -\max(y, y'), \\ \chi_0^-(y, y') &= \chi_{\langle \phi_2 \phi_2 \rangle_0}(y, y') = +\min(y, y').\end{aligned}\tag{4.5.14}$$

Similarly, solving the Dirac equation and adding a “mirror” term dictated by the boundary conditions one gets [176]

$$\langle \Psi(x)\bar{\Psi}(x') \rangle_0 = \kappa_f \left( \frac{\gamma \cdot (x-x')}{|x-x'|^d} + i\gamma_5 \gamma^n \frac{\gamma \cdot (\bar{x}-x')}{|\bar{x}-x'|^d} \right), \quad \kappa_f = \frac{\Gamma(\frac{d}{2})}{2\pi^{d/2}}.\tag{4.5.15}$$

It is not hard to check that the fermion propagator satisfies the correct boundary conditions:

$$\Pi_- \langle \Psi(\mathbf{x}, 0)\bar{\Psi}(\mathbf{x}', y') \rangle_0 = \langle \Psi(\mathbf{x}, y)\bar{\Psi}(\mathbf{x}', 0) \rangle_0 \Pi_- = 0.\tag{4.5.16}$$



### Tadpole diagram

First we consider the quartic interaction terms in eq. (4.5.2) and we use them to form loop diagrams with either  $\phi_1$  or  $\phi_2$  running in the loop. These diagrams would vanish if the boundary was not present, or equivalently if we studied physics far away from the boundary. As a result, we expect them to be finite in the limit  $\varepsilon \rightarrow 0$ . Taking symmetry factors into account the total contribution is

$$\chi^\pm(y, y')|_{\text{tadpole}} = \text{---}\text{---}\text{---}\text{---}\text{---}\text{---}\text{---} = \mp 2^{-3+\varepsilon} \lambda^2 \kappa_s I_b^\pm(y, y'). \quad (4.5.17)$$

The propagator that runs in the loop is defined as the finite part of  $\langle \phi_i(\mathbf{x}, y) \phi_i(\mathbf{x}', y') \rangle_0$  when  $\mathbf{x}' \rightarrow \mathbf{x}$ , and can be obtained from (4.5.13). With this prescription, the Feynman integrals we must compute are [179]

$$\begin{aligned} I_b^+(y, y') &= \int_0^\infty dz \chi_0^+(y, z) z^{-2+\varepsilon} \chi_0^+(z, y') = \frac{y^\varepsilon y'}{\varepsilon - 1} - \frac{y'(y^\varepsilon - y'^\varepsilon)}{\varepsilon} - \frac{y'^{\varepsilon+1}}{\varepsilon + 1}, \\ I_b^-(y, y') &= \int_0^\infty dz \chi_0^-(y, z) z^{-2+\varepsilon} \chi_0^-(z, y') = -\frac{yy'^\varepsilon}{\varepsilon - 1} - \frac{y(y^\varepsilon - y'^\varepsilon)}{\varepsilon} + \frac{y^{\varepsilon+1}}{\varepsilon + 1}. \end{aligned} \quad (4.5.18)$$

For simplicity we assumed here and in the rest of the section that  $y < y'$ , but one can obtain the integral for  $y > y'$  replacing  $y \leftrightarrow y'$ .

### Fermion bubble

Similarly, we can use the Yukawa interactions in eq. (4.5.2) to form diagrams with fermions running in the loop. If the boundary was not present, these diagrams would be UV divergent and would contribute to the renormalization of  $\phi$ . Since the boundary does not change the UV behaviour of the theory, we expect a divergence as  $\varepsilon \rightarrow 0$  which is canceled by the counterterm  $\delta_\phi$ :

$$\begin{aligned} \chi^\pm(y, y')|_{\text{bubble}} &= \text{---}\text{---}\text{---}\text{---}\text{---}\text{---}\text{---} + \text{---}\text{---}\text{---}\text{---}\text{---}\text{---}\text{---} \\ &= \lambda^2 \kappa_f^2 I_f^\pm(y, y') - \delta_\phi \chi_0^\pm(y, y'). \end{aligned} \quad (4.5.19)$$

Using the identities

$$\begin{aligned} \text{tr} \left[ \langle \Psi(x) \bar{\Psi}(x') \rangle_0 \langle \Psi(x') \bar{\Psi}(x) \rangle_0 \right] &= -4\kappa_f^2 \left( \frac{1}{|x - x'|^{2(d-1)}} + \frac{1}{|\bar{x} - x'|^{2(d-1)}} \right), \\ \text{tr} \left[ \langle \Psi(x) \bar{\Psi}(x') \rangle_0 \gamma_5 \langle \Psi(x') \bar{\Psi}(x) \rangle_0 \gamma_5 \right] &= 4\kappa_f^2 \left( \frac{1}{|x - x'|^{2(d-1)}} - \frac{1}{|\bar{x} - x'|^{2(d-1)}} \right), \end{aligned} \quad (4.5.20)$$

we see that the Feynman integral is

$$I_f^\pm(y, y') = \int_0^\infty dz \int_0^\infty dz' \chi^\pm(y, z) b^\pm(z, z') \chi^\pm(z', y'), \quad (4.5.21)$$

where we have defined

$$\begin{aligned} b^\pm(z, z') &= \int d^{d-1} \mathbf{r} \left( \frac{1}{(\mathbf{r}^2 + (z - z')^2)^{d-1}} \pm \frac{1}{(\mathbf{r}^2 + (z + z')^2)^{d-1}} \right) \\ &= \frac{2^{2-d} \pi^{d/2}}{\Gamma(\frac{d}{2})} (|z - z'|^{-3+\varepsilon} \pm |z + z'|^{-3+\varepsilon}). \end{aligned} \quad (4.5.22)$$

We will evaluate this integral with a trick that has been used in the literature in similar situations [181, 179, 61]. The idea is to split the integration region between  $z > z'$  and  $z < z'$ . By changing variables to  $Z = \frac{z}{z'}$  and  $Z = \frac{z'}{z}$ , one can carry out the first integration in terms of  $I_b^\pm$  defined in the previous section. The result is:

$$I_f^\pm(y, y') = y^{\varepsilon+1} \left[ \int_1^\infty dZ I_b^\pm(1, Z/\zeta) b^\pm(1, Z) Z^{-\varepsilon} + \int_1^{1/\zeta} dZ I_b^\pm(1, (Z\zeta)^{-1}) b^\pm(1, Z) Z \right. \\ \left. + \zeta^{-1-\varepsilon} \int_{1/\zeta}^\infty dZ I_b^\pm(1, \zeta Z) b^\pm(1, Z) Z^{-\varepsilon} \right]. \quad (4.5.23)$$

Remember that we are assuming  $y < y'$ , such that  $\zeta = y/y'$ . Finally, all terms in eq. (4.5.23) can be integrated using `Mathematica`<sup>18</sup>. The result for general  $\varepsilon$  is not particularly illuminating and will not be needed later, instead we focus on the result in the limit  $\varepsilon \rightarrow 0$ . First, the divergent piece is canceled in  $\overline{\text{MS}}$  with the following counterterm:

$$\delta_\phi = -\frac{\lambda^2}{(4\pi)^2} \left( \frac{1}{\varepsilon} + \frac{1}{2}(\gamma + \log \pi) + 1 \right). \quad (4.5.24)$$

The total diagram is now finite:

$$\chi^+(y, y')|_{\text{bubble}} = \frac{\lambda^2}{64\pi^2} \frac{\sqrt{4yy'}}{\sqrt{\zeta}} \left( \log(4yy') - \log \zeta - 2 \right. \\ \left. + (1 + \zeta) \log(1 + \zeta) + (1 - \zeta) \log(1 - \zeta) \right) + \mathcal{O}(\varepsilon), \\ \chi^-(y, y')|_{\text{bubble}} = \frac{-\lambda^2}{64\pi^2} \sqrt{4yy'\zeta} \left( \log(4yy') - \log \zeta - 2 \right. \\ \left. + \frac{(1 + \zeta)}{\zeta} \log(1 + \zeta) - \frac{(1 - \zeta)}{\zeta} \log(1 - \zeta) \right) + \mathcal{O}(\varepsilon). \quad (4.5.25)$$

## Final result

We can obtain the full susceptibility at order  $\varepsilon$  by combining the tree-level result (4.5.14), the tadpole diagram (4.5.18), and the fermion bubble (4.5.25). We should evaluate the sum at the fixed point coupling  $\lambda_*^2 = \frac{16\pi^2}{3}\varepsilon$ , and keep only terms up to order  $\varepsilon$ . The result is perfectly consistent with the bootstrap prediction (4.5.12), and we identify

$$\Delta_\phi^{(1)} = \frac{1}{6}, \quad \hat{\Delta}_0^{(1)} = 0, \quad s = +1. \quad (4.5.26)$$

The anomalous dimension of  $\phi$  in the Wess-Zumino model is well known in the literature. One can obtain it by demanding that the superpotential has  $R$ -charge  $R(W) = 3r_\phi = 2$ , so we find that  $r_\phi = 2/3$ . Using the relation between the  $R$ -charge and conformal dimension we find  $\Delta_\phi = \frac{d-1}{3}$ , in perfect agreement with eq. (4.5.26). From this argument it is clear that  $\Delta_\phi$  is one-loop exact.

<sup>18</sup>The only exception are integrals of the form  $\int_1^\infty dZ (Z-1)^a$ , but they are zero in dimensional regularization.

An interesting prediction of our calculation is the anomalous dimension of the leading bulk operator in the OPE  $\phi \times \phi \sim \mathcal{O}_0 + \dots$ . We calculated this for a general model in (4.4.46), and for the Wess-Zumino case we get

$$\Delta_0^{(1)} = \frac{2}{3} \quad \Rightarrow \quad \Delta_0 = \frac{d+2}{3} = d - 2\Delta_\phi. \quad (4.5.27)$$

Recalling the selection rules of section 4.4.1, we see that the exchanged operator is of the form  $\mathcal{O}_0 \sim (Q^+)^2 \bar{\Psi}$  where  $\bar{\Psi}$  is an antichiral primary operator. Indeed, the numerical bootstrap applied to the Wess-Zumino model in [159, 154] also provides strong evidence that the leading operator in the  $\phi \times \phi$  OPE is of this form. The agreement of our results with the predictions from [159, 154] provides a non-trivial sanity check of our perturbative calculation. It would be interesting to consider other particular models, for instance with extra boundary interactions or a more complicated bulk, and see whether the anomalous dimension of the defect operator changes. We hope to come back to this question in the future.



# Chapter 5

## Bootstrapping line defects with $O(2)$ global symmetry

### 5.1 Introduction

The presence of supersymmetry in the previous chapter provided us with better control over the setup of a SCFT with a boundary. However, if we want to consider applications of defects in physical setups, then supersymmetry is often not present. Hence, we will trade the increased control for more realistic setups, and study defects without SUSY, but with an additional global or flavor symmetry.

In this chapter we explore the space of codimension two conformal line defects with  $O(N)$  global symmetry. We base our approach on the modern numerical conformal bootstrap discussed in section 2.4.2, and we focus exclusively on the  $1d$  theory living on the line defect. This work is then a natural extension of [74], where line defects with a  $\mathbb{Z}_2$  global symmetry were studied using similar techniques. Other setups where this strategy has been successful include line defects in supersymmetric models in [182, 95] and in the study of the long-range Ising model in various dimensions in [183]. More recently it has also been employed in order to carve out the space of conformal boundary conditions for a free massless scalar in [68, 69].

By definition, a codimension two conformal line defect with  $O(N)$  global symmetry preserves a ‘little’ conformal group  $SL(2, \mathbb{R})$  along the line times a residual ‘transverse rotations’ group  $SO(2)_T$  about the line.<sup>1</sup> We can think of  $O(N)$  to be the remnant bulk global symmetry after the introduction of the defect in the homogeneous  $3d$  CFT with a global symmetry  $G$  so that

$$SO(4, 1) \times G \longrightarrow SL(2, \mathbb{R}) \times SO(2)_T \times O(N) , \quad O(N) \subseteq G . \quad (5.1.1)$$

The residual symmetry of the theory allows us to define local defect operators that are primaries with respect to the ‘little’ conformal group. Such operators will then be conveniently labeled by their scaling dimensions  $\Delta$ , which are non-negative in unitary theories, their transverse  $SO(2)_T$  spins  $s$  and their  $SO(N)$  charges  $r_i$ . Since all connected rotations along the line are trivial, we just need to distinguish between parity-odd and parity-even scalar defect operators, whenever parity on the line is preserved.<sup>2</sup>

Correlation functions between defect operators are akin to those of a one-dimensional CFT and must be crossing symmetric in the usual sense. Hence, while on the one hand

---

<sup>1</sup>Such ‘transverse rotations’ may be broken e.g. by spinning conformal defects, see e.g. [184].

<sup>2</sup>In the context of the 3d Ising model, this parity has been called  $\mathcal{S}$ -parity [74, 73].

these correlation functions enjoy ‘positivity’ in unitary theories and so they can be bootstrapped using semi-definite programming, on the other hand they know little about the bulk. While it remains a very interesting open problem to understand how, for generic bulk CFTs, the bulk information can be encoded into defect correlation functions,<sup>3</sup> at the same time we find that a systematic exploration of codimension two line defects with  $O(N)$  global symmetry purely based on the numerical conformal bootstrap technique is still missing.<sup>4</sup> In the present chapter we aim at filling this gap, and in doing so we will be starting from codimension two defects with  $O(2)_F$  global symmetry.<sup>5</sup>

In section 5.4 we will present a systematic bootstrap study of certain universal defect observables such as mixed correlation functions involving the displacement operator and the tilt operator, which capture the breaking of certain bulk local symmetries by the presence of the defect. Along with the agnostic bootstrap and whenever possible, we will try to isolate known defect theories by making gap assumptions inspired by  $\varepsilon$ -expansion predictions in specific models. There are indeed quite a few instances of interesting conformal defects of this sort which should be allowed by our bootstrap bounds. The preeminent example is the so-called localized magnetic field line defect or magnetic line defect (see [83, 84] and references therein), which for our purposes can be defined in the  $O(3)$  CFT and breaks the bulk global symmetry down to  $O(2)_F$ , i.e.

$$S_{\text{LML}} = S_{O(3)} + h \int_{-\infty}^{\infty} d\tau \phi_1(\tau) , \quad (5.1.2)$$

where  $\phi_1$  is one component of the fundamental  $O(3)$  vector. This symmetry breaking implies the existence of a tilt in the spectrum, namely the defect primary operator with protected scaling dimension  $\Delta_t = 1$  and transforming as a vector of  $O(2)_F$  discussed earlier in section 3.1. A review of known results on the magnetic line defect, along with original computations of correlators relevant to our study in the  $\varepsilon$ -expansion will be presented in section 5.3. Other interesting known examples of codimension two line defects with continuous global symmetry are of the monodromy type, i.e. they can be thought of as boundaries of codimension one topological operators that implement a bulk global symmetry transformation  $g \in G$ , see e.g. [73, 74]. For our purposes we can consider a bulk CFT with global symmetry  $G$  and a complex scalar field  $\Phi$  charged under  $U(1)_F \in G$ . We can then define an  $U(1)_F$ -preserving monodromy defect for any element  $g = e^{2\pi i v} \in U(1)_F$  by requiring  $\Phi$  to be single valued after a  $SO(2)_T$  rotation only up to  $g$ , i.e. [76, 77, 79]

$$\Phi(r, \theta + 2\pi, \vec{x}) = e^{2\pi i v} \Phi(r, \theta, \vec{x}) , \quad v \sim v + 1 , \quad v \in [0, 1) , \quad (5.1.3)$$

where  $(r, \theta)$  are the polar coordinates in the transverse plane with respect to the defect. For both  $v = 0$  (i.e. no monodromy) and  $v = 1/2$ , the internal  $U(1)_F$  symmetry of  $\Phi$  will get enhanced to  $O(2)_F$ , which includes complex conjugation of  $\Phi$ . Now, the specific choice for the monodromy has broken the original symmetry  $G$  down to  $U(1)_F$ , and therefore the resulting defect may feature a tilt operator as well. In our study however we will

---

<sup>3</sup>Some progress in this direction can be found in [52, 68, 69] in the context of conformal boundaries and defects for the free massless scalar field and in [185] in the context of surface defects for the 4d Maxwell field.

<sup>4</sup>See [32] and references therein for works that combine analytic functionals in 1d with the numerical conformal bootstrap.

<sup>5</sup>Here and below (whenever necessary) we will denote the global symmetry group as  $O(2)_F$ , to be distinguished from the group of transverse rotations about the defect that is denoted as  $SO(2)_T$ .

focus on the  $O(2)$  bulk global symmetry, for which the defect spectrum does not contain a tilt operator.

This chapter is organized as follows. In section 5.2, we discuss properties of codimension two line defects with global symmetries, covering the discrete symmetries of the defect, the two canonical defect operators, and in the end showing the crossing equations for correlators studied in section 5.4. Then, in section 5.3, we present a small review on  $\varepsilon$ -expansion results relevant to our numerical study and focus on the monodromy defect and the localized magnetic field line defect. The results of the numerical conformal bootstrap for the  $O(2)$  line defect will be presented in section 5.4.

## 5.2 Line defects with global symmetry

In this section we discuss some universal properties of co-dimension two line defects with global symmetry. We start our analysis with a discussion of the discrete symmetries that characterize a line defect. We then introduce the two main characters of our bootstrap analysis: the displacement operator and the tilt operator. We conclude by presenting the crossing equations for the correlators that we will study in section 5.4.

### 5.2.1 Discrete symmetries and parity

In addition to the continuous part of the symmetry, e.g. the group in eq. (5.1.1), we are also interested in the case where the symmetry group involves improper reflections along the parallel or transverse directions with respect to the line, i.e.

$$O^+(2,1) \times O(2)_T \times O(2)_F, \quad O^+(2,1) \times SO(2)_T \times O(2)_F. \quad (5.2.1)$$

We can think about the  $O^+(2,1)$  parity as the improper rotations in 1d, such that spin-odd primaries in higher dimensions become parity-odd in 1d. This is the  $\mathcal{S}$ -parity of [73, 74],

$$\mathcal{S}: \quad \tau \rightarrow -\tau, \quad \mathcal{S}(\psi(\tau)) = (-1)^{S_\psi} \psi(-\tau), \quad S_\psi = 0, 1, \quad (5.2.2)$$

so that invariance under  $\mathcal{S}$ -parity of defect correlation functions implies that ( $\tau_i < \tau_{i+1}$ )

$$\langle \psi_1(\tau_1) \psi_2(\tau_2) \psi_3(\tau_3) \rangle = (-1)^{S_1+S_2+S_3} \langle \psi_3(-\tau_3) \psi_2(-\tau_2) \psi_1(-\tau_1) \rangle. \quad (5.2.3)$$

For the conformal three-point correlation functions, invariance under  $\mathcal{S}$ -parity means that [74]

$$\lambda_{123} = (-1)^{S_1+S_2+S_3} \lambda_{213}. \quad (5.2.4)$$

Hence, only  $\mathcal{S}$ -parity even operators are allowed to appear in the fusion of two identical local defect operators.<sup>6</sup> Throughout this chapter we will assume  $\mathcal{S}$ -parity invariant defects and so  $\mathcal{S}$  will play an important role in our numerical bootstrap study of section 5.4.

The second parity assignment is for  $O(2)_T$ . We will adopt the convention of [74] and denote the action of the  $O(2)_T$ -parity with  $\mathcal{B}$ . The action  $\mathcal{B}$  is a reflection in a plane perpendicular to the defect [73] which flips the sign of one of the transverse coordinates<sup>7</sup>

<sup>6</sup>Note that the connected component of the conformal group does not change the cyclic order of operators insertions, so  $\lambda_{123} = \lambda_{231} = \lambda_{312}$ .

<sup>7</sup>Flipping the sign of both transverse coordinates would be a transformation with  $\det(\mathcal{B}') = 1$  and is part of the connected part of the group  $O(2)_T$  instead of the disconnected part.

and reverses the  $O(2)_T$  charge (as it follows from the anti-symmetric properties of the generator of the rotations around the defect,  $\mathcal{M}_{xy}$ )

$$\mathcal{B} : \quad (x, y) \rightarrow (-x, y) , \quad \mathcal{B}(\psi_s(\tau)) = b_{\psi_s} \psi_{-s}(\tau) . \quad (5.2.5)$$

The coefficient  $b_{\psi_s}$  determines the parity of the operator. Without loss of generality we can choose a basis of operators such that operators with  $s \neq 0$  are even under  $O(2)_T$ -parity, while operators with  $s = 0$  can be both even or odd [74]. In this chapter we will not require  $O(2)_T$  parity to be a symmetry of the defect CFT.

## 5.2.2 Universal defect operators

### The displacement operator

When considering a local  $d$ -dimensional bulk CFT, i.e. with a stress-energy tensor  $T^{\mu\nu}$ , conservation of  $T^{\mu\nu}$  is generically violated by terms localized on the defect [74, 47]:

$$\partial_\mu T^{\mu i} = -\delta^{(q)}(\mathcal{D}) D^i . \quad (5.2.6)$$

Here  $\delta^{(q)}(\mathcal{D})$  is a Dirac delta function with support on the co-dimension  $q = d - p$  defect, and  $i = 1, \dots, q$  is an index in the directions orthogonal to the defect. The operator  $D$  on the right-hand side of the eq. (5.2.6) is the displacement operator, i.e. a defect primary operator of scaling dimension  $\Delta = p + 1$  and a vector under  $SO(2)_T$ . For the co-dimension two case we use the notation

$$D \equiv D^1 + iD^2 , \quad \bar{D} \equiv D^1 - iD^2 , \quad (5.2.7)$$

to denote the positive and negative spin components.

When taking the correlator of four displacement operators, there are two OPEs that we need to consider. In a theory where  $\mathcal{S}$ -parity is preserved, the  $D \times \bar{D}$  OPE contains the identity operator  $\mathbf{1}$ , as well as  $SO(2)_T$  singlet operators, which can be either even or odd under  $\mathcal{S}$ -parity as dictated by eq. (5.2.4). We denote these operators as  $(D\bar{D})^\pm$ . The  $D \times D$  OPE exchanges operators with transverse spin  $s = 2$  and positive  $\mathcal{S}$ -parity, denoted  $D^2$ . All in all, we get

$$D \times \bar{D} \sim \mathbf{1} + (D\bar{D})^+ + (D\bar{D})^- + \dots , \quad D \times D \sim D^2 + \dots . \quad (5.2.8)$$

### The tilt operator

In analogy to the case of the displacement operator, a conformal defect that breaks a local continuous global symmetry of the bulk must feature a tilt operator.<sup>8</sup> Consider the case where the bulk global symmetry  $G$  is broken down to a subgroup  $H$ . If  $J_A^\mu$  is the conserved current of the symmetry  $G$ , then for each symmetry generator broken by the defect we have [136, 140, 70]

$$\partial_\mu J_A^\mu = \delta^{(q)}(\mathcal{D}) t_A , \quad A \in G/H . \quad (5.2.9)$$

The tilt  $t_A$  has protected scaling dimension  $\Delta_t = p$  and is a scalar under rotations. Furthermore, the tilt consists of  $\dim(G) - \dim(H)$  components, which are organized into

---

<sup>8</sup>Here the term ‘local’ refers to the existence of a conserved current in the bulk that can be used to define conserved charges.



irreducible representations of the preserved subgroup  $H$ . The example we consider in this work is  $G = O(N)$  and  $H = O(N - 1)$ , when the tilt transforms in the vector representation of  $H$ . For the particular case  $N = 3$ , such that the preserved subgroup is  $O(2)_F$ , the tilt consists of two components  $t^1$  and  $t^2$ , which can be expressed in complex notation as

$$t \equiv t^1 + it^2, \quad \bar{t} \equiv t^1 - it^2. \quad (5.2.10)$$

The symmetries allow us to define the following OPEs:

$$t \times \bar{t} \sim \mathbb{1} + (t\bar{t})^+ + (t\bar{t})^- + \dots, \quad t \times t \sim t^2 + \dots. \quad (5.2.11)$$

In the expressions above, the operators  $(t\bar{t})^\pm$  are  $O(2)_F \times SO(2)_T$  singlets and even (odd) under  $\mathcal{S}$ -parity. The operators  $t^2$  are charged under  $O(2)_F$ , and they are even under  $\mathcal{S}$ -parity.

### 5.2.3 Crossing equations

We are interested in the study of one-dimensional conformal defects in three-dimensional bulk CFTs, but because we restrict our attention to four-point functions on the defect, the crossing equations are identical to the ones for regular one-dimensional CFTs. In particular, a general four-point function takes the form

$$\langle \phi_i(\tau_1) \phi_j(\tau_2) \phi_k(\tau_3) \phi_l(\tau_4) \rangle = \frac{G_{ijkl}(\xi)}{|\tau_{12}|^{\Delta_i + \Delta_j} |\tau_{34}|^{\Delta_k + \Delta_l}} \left( \frac{|\tau_{24}|}{|\tau_{14}|} \right)^{\Delta_i - \Delta_j} \left( \frac{|\tau_{14}|}{|\tau_{13}|} \right)^{\Delta_k - \Delta_l}, \quad (5.2.12)$$

where  $\tau$  is the coordinate along the defect, and we introduced the cross-ratio

$$\xi = \frac{\tau_{12}\tau_{34}}{\tau_{13}\tau_{24}}. \quad (5.2.13)$$

The external operators are ordered along the line  $\tau_1 < \tau_2 < \tau_3 < \tau_4$ , such that the cross-ratio takes the values  $0 < \xi < 1$ . In the limit when  $\tau_1$  approaches  $\tau_2$ , or equivalently when  $\xi \rightarrow 0$ , the correlation function  $G_{ijkl}(\xi)$  admits an expansion in s-channel conformal blocks [186]

$$G_{ijkl}(\xi) = \sum_{\mathcal{O}} \lambda_{ij\mathcal{O}} \lambda_{kl\mathcal{O}} g_{\Delta}^{\Delta_{ij}, \Delta_{kl}}(\xi), \quad g_{\Delta}^{\Delta_{ij}, \Delta_{kl}}(\xi) = \xi^{\Delta} {}_2F_1(\Delta - \Delta_{ij}, \Delta + \Delta_{kl}; 2\Delta; \xi), \quad (5.2.14)$$

where  $\lambda_{ij\mathcal{O}}$  are three-point OPE coefficients. It is natural to think of the one-dimensional CFT as living on a circle, which is the conformal compactification of the real line. On the circle, it is clear that the correlator should respect cyclicity  $\langle \phi_i \phi_j \phi_k \phi_l \rangle = \langle \phi_l \phi_i \phi_j \phi_k \rangle$ , which, including the prefactor in eq. (5.2.12), leads to

$$(1 - \xi)^{\Delta_j + \Delta_k} G_{ijkl}(\xi) = \xi^{\Delta_i + \Delta_j} G_{lijk}(1 - \xi). \quad (5.2.15)$$

The crossing equation is obtained by requiring consistency between cyclicity and the conformal block decomposition. Using standard manipulations, see for example [187], we can write the crossing equations as

$$\sum_{\mathcal{O}} \left[ \lambda_{ij\mathcal{O}} \lambda_{kl\mathcal{O}} F_{\mp, \Delta}^{ij, kl}(\xi) \pm \lambda_{kj\mathcal{O}} \lambda_{il\mathcal{O}} F_{\mp, \Delta}^{kj, il}(\xi) \right] = 0, \quad (5.2.16)$$

where  $F_{\pm,\Delta}^{ij,kl}$  are defined similarly as for higher-dimensional CFTs:

$$F_{\pm,\Delta}^{ij,kl}(\xi) \equiv (1 - \xi)^{\Delta_k + \Delta_j} g_{\Delta}^{\Delta_{ij}, \Delta_{kl}}(\xi) \pm \xi^{\Delta_k + \Delta_j} g_{\Delta}^{\Delta_{ij}, \Delta_{kl}}(1 - \xi). \quad (5.2.17)$$

With the help of these results, the process of writing all crossing equations becomes straightforward. Given a set of external operators, one simply lists all non-vanishing four-point functions. Then, for each inequivalent ordering, eq. (5.2.16) gives the relevant crossing equations.

### Comment on complex notation

In this work we consider scalar operators charged under  $O(2)$  symmetry, so in order to write the crossing equations we should take global-symmetry tensor structures into account. Alternatively, we can exploit complex notation, which means that for an  $O(2)$  vector instead of working with a real field  $\phi^i$  with a two-valued index  $i = 1, 2$ , we work with a single complex field  $\phi = \phi^1 + i\phi^2$  and its complex conjugate  $\bar{\phi} \equiv \phi^*$ . In a completely analogous way, we can construct operators with arbitrary charge. The advantage of complex notation is that it eliminates the need to keep track of global-symmetry indices and tensor structures. Using again the example of a vector under  $O(2)$ , the OPE  $\phi^i \times \phi^j$  contains the singlet representation ( $S$ ), the antisymmetric representation ( $A$ ), and the symmetric-traceless representation ( $T$ ), each with an associated tensor structure. Instead, in complex notation we have the OPE  $\phi \times \bar{\phi}$  with  $\mathcal{S}$ -parity even operators corresponding to ( $S$ ), the OPE  $\phi \times \bar{\phi}$  with  $\mathcal{S}$ -parity odd operators corresponding to ( $A$ ), and the OPE  $\phi \times \phi$  with  $\mathcal{S}$ -parity even operators corresponding to ( $T$ ).

### One complex scalar

The simplest case of crossing that we can consider is for one complex scalar  $\phi$ . From the defect CFT perspective, this setup has three applications depending on the interpretation given to  $\phi$ . In the first application, which we consider in section 5.4.1, we take  $\Delta_{\phi} = 2$  and interpret  $\phi = D^1 + iD^2 \equiv D$  as the displacement operator of a co-dimension two defect. In the second application, which we consider in section 5.4.1, we take  $\Delta_{\phi} = 1$  and interpret  $\phi = t^1 + it^2 \equiv t$  as the tilt operator. In the third application, which we consider in section 5.3.1, we can think of  $\phi = \psi_{n+v}$  with  $n \in \mathbb{Z}$  as a defect mode in a monodromy defect.

Regardless of the interpretation of  $\phi$ , we can use eq. (5.2.16) on the orderings  $\langle \phi \bar{\phi} \phi \bar{\phi} \rangle$  and  $\langle \phi \phi \bar{\phi} \bar{\phi} \rangle$ . We find a system of three crossing equations which in vector notation read [188]

$$\sum_{\mathcal{O}^{\pm}} (\lambda_{\phi \bar{\phi} \mathcal{O}})^2 \vec{V}_{\Delta, S}^{\phi \bar{\phi}} + \sum_{\mathcal{O}^+} |\lambda_{\phi \phi \mathcal{O}}|^2 \vec{V}_{\Delta}^{\phi \phi} = 0, \quad (5.2.18)$$

where the crossing vectors are given explicitly in eq. (E.1.1). The leftmost sum runs over defect primaries of both  $\mathcal{S}$ -parities, while the rightmost one include only  $\mathcal{S}$ -parity even defect primaries. The contribution of the identity operator has not been separated explicitly, but is given by  $\vec{V}_{0,0}^{\phi \bar{\phi}}$ .

**One complex generalized free field.** A notable solution to the crossing equations in eq. (5.2.18) is complex generalized free field theory, based on a complex scalar field

$\phi$  with scaling dimension  $\Delta_\phi$ , and its complex conjugate  $\bar{\phi}$ . Using Wick's theorem, the four-point function in the notation of eq. (5.2.12) reads

$$G_{\phi\bar{\phi}\phi\bar{\phi}}(\xi) = 1 + \left(\frac{\xi}{1-\xi}\right)^{2\Delta_\phi} = 1 + \sum_{p=0}^{\infty} c_p(\Delta_\phi, \Delta_\phi) g_{2\Delta_\phi+p}^{0,0}(\xi), \quad (5.2.19)$$

$$G_{\phi\bar{\phi}\bar{\phi}\phi}(\xi) = \alpha \xi^{2\Delta_\phi} + \left(\frac{\xi}{1-\xi}\right)^{2\Delta_\phi} = \sum_{p=0}^{\infty} (1 + \alpha(-1)^p) c_p(\Delta_\phi, \Delta_\phi) g_{2\Delta_\phi+p}^{0,0}(\xi), \quad (5.2.20)$$

with [189, 74]

$$c_p(\Delta_1, \Delta_2) = \frac{(2\Delta_1)_p (2\Delta_2)_p}{p! (2\Delta_1 + 2\Delta_2 + p - 1)_p}. \quad (5.2.21)$$

The second correlator above contains a parameter  $\alpha$ , such that  $-1 \leq \alpha \leq 1$  in unitary theories. For  $\alpha = 1$  the solution corresponds to a generalized free boson (GFB), while for  $\alpha = -1$  it corresponds to a generalized free fermion (GFF).

It was noted in [74] that the solution to the crossing equation of the generalized real free fermion  $\langle \psi(\tau_1)\psi(\tau_2)\psi(\tau_3)\psi(\tau_4) \rangle$  can be extended to a solution of the crossing equations in eq. (5.2.18), if the gap on the scaling dimension of the first operator in the traceless-symmetric representation does not exceed  $2\Delta_\psi$ . The spectra for the  $\mathcal{S}$ -parity even and odd operators are equal in this case. For the displacement operator, this happens for  $\Delta_{D^2} < 2 \times 2 = 4$ , while for the tilt operator the solution appears for  $\Delta_{t^2} < 2 \times 1 = 2$ .

### Tilt and displacement

Next we consider a mixed system between the tilt operator  $t$  and the displacement operator  $D$ , where we again use complex notation. In order to write down the crossing equations we note that the  $\mathcal{S}$ -parity even singlets can appear both in  $t \times \bar{t}$  and  $D \times \bar{D}$ , while the  $\mathcal{S}$ -parity odd channels are different in the two OPEs, because the tilt and displacement transform under different  $O(2)$  groups. All in all, crossing reads

$$\begin{aligned} \sum_{\mathcal{O}^+} (\lambda_{t\bar{t}\mathcal{O}} \lambda_{D\bar{D}\mathcal{O}}) \vec{V}_\Delta^+ \begin{pmatrix} \lambda_{t\bar{t}\mathcal{O}} \\ \lambda_{D\bar{D}\mathcal{O}} \end{pmatrix} + \sum_{\mathcal{O}^-} |\lambda_{t\bar{t}\mathcal{O}}|^2 \vec{V}_\Delta^{\vec{t}\bar{t},-} + \sum_{\mathcal{O}^-} |\lambda_{D\bar{D}\mathcal{O}}|^2 \vec{V}_\Delta^{\vec{D}\bar{D},-} \\ + \sum_{\mathcal{O}^+} |\lambda_{tt\mathcal{O}}|^2 \vec{V}_\Delta^{\vec{t}t} + \sum_{\mathcal{O}^+} |\lambda_{DD\mathcal{O}}|^2 \vec{V}_\Delta^{\vec{D}D} + \sum_{\mathcal{O}^\pm} |\lambda_{tD\mathcal{O}}|^2 \vec{V}_{\Delta,S}^{\vec{t}D} = 0. \end{aligned} \quad (5.2.22)$$

Once again the crossing vectors are presented in appendix E.2.

### One real scalar and the tilt

The third setup we study is crossing for one real scalar  $\phi_1$  and a tilt operator  $t$ , for which we use complex notation. This has applications to the magnetic line defect of section 5.3.2, where  $\phi_1$  corresponds to the scalar that breaks the bulk symmetry, and the tilt operator must be present due to the symmetry breaking. The numerical results for this setup will be discussed in section 5.4.3. The crossing equations can be obtain in a similar way as before, but we now obtain seven independent equations that in vector notation read

$$\sum_{\mathcal{O}^+} (\lambda_{\phi_1\phi_1\mathcal{O}} \lambda_{t\bar{t}\mathcal{O}}) \vec{V}_\Delta^+ \begin{pmatrix} \lambda_{\phi_1\phi_1\mathcal{O}} \\ \lambda_{t\bar{t}\mathcal{O}} \end{pmatrix} + \sum_{\mathcal{O}^-} (\lambda_{t\bar{t}\mathcal{O}})^2 \vec{V}_\Delta^- + \sum_{\mathcal{O}^+} |\lambda_{tt\mathcal{O}}|^2 \vec{V}_\Delta^{\vec{t}t} + \sum_{\mathcal{O}^\pm} |\lambda_{\phi_1 t\mathcal{O}}|^2 \vec{V}_{\Delta,S}^{\phi_1 t} = 0. \quad (5.2.23)$$

The crossing vectors are found in appendix E.3. *Mutatis mutandis*, the same system of crossing equations can be used to study the mixed correlators of  $\phi_1$  and  $D$ . We will leave this idea for future exploration.

### Two complex scalars

Finally we study the crossing equations of two unequal complex scalars  $\phi_1$  and  $\phi_2$ . We apply this to monodromy defects, see section 5.4.2, where  $\phi_1 = \psi_{n_1+v}$  and  $\phi_2 = \psi_{n_2+v}$  are two different defect modes of a bulk scalar field. In total there are twelve crossing equations and five different OPE channels [190]

$$\begin{aligned} \sum_{\mathcal{O}^\pm} (\lambda_{\phi_1 \bar{\phi}_1 \mathcal{O}} \lambda_{\phi_2 \bar{\phi}_2 \mathcal{O}}) \vec{V}_{\Delta,S} \begin{pmatrix} \lambda_{\phi_1 \bar{\phi}_1 \mathcal{O}} \\ \lambda_{\phi_2 \bar{\phi}_2 \mathcal{O}} \end{pmatrix} + \sum_{\mathcal{O}^+} |\lambda_{\phi_1 \phi_1 \mathcal{O}}|^2 \vec{V}_{\Delta}^{11} + \sum_{\mathcal{O}^+} |\lambda_{\phi_2 \phi_2 \mathcal{O}}|^2 \vec{V}_{\Delta}^{22} \\ + \sum_{\mathcal{O}^\pm} |\lambda_{\phi_1 \phi_2 \mathcal{O}}|^2 \vec{V}_{\Delta,S}^{12} + \sum_{\mathcal{O}^\pm} |\lambda_{\phi_1 \bar{\phi}_2 \mathcal{O}}|^2 \vec{V}_{\Delta,S}^{1\bar{2}} = 0. \end{aligned} \quad (5.2.24)$$

The crossing vectors can be found in appendix E.4.

**Two complex generalized free fields.** The OPE coefficients that contain only  $\phi_1$  or only  $\phi_2$  follow from our discussion above. The new information is contained in the  $\phi_1 \times \phi_2$  OPE, which can be analyzed from the following four-point function

$$G_{\phi_1 \phi_2 \bar{\phi}_2 \bar{\phi}_1}(\xi) = \frac{\xi^{\Delta_1 + \Delta_2}}{(1 - \xi)^{2\Delta_2}} = \sum_{p=0}^{\infty} c_p(\Delta_1, \Delta_2) g_{\Delta_1 + \Delta_2 + p}^{\Delta_{12}, \Delta_{21}}(\xi). \quad (5.2.25)$$

From here we immediately read off  $|\lambda_{\phi_1 \phi_2 \mathcal{O}}|^2$ , and by sending  $\phi_2 \rightarrow \bar{\phi}_2$  we find that the same formula applies to  $|\lambda_{\phi_1 \bar{\phi}_2 \mathcal{O}}|^2$ .

## 5.3 Defect theories in the $\varepsilon$ -expansion

In this section we use perturbation theory to study two important examples of conformal line defects: the  $SO(2)_F$ -preserving monodromy defect and the  $O(3)$ -breaking magnetic line defect. We start by reviewing known results on the  $SO(2)_F$  monodromy defect in the  $\varepsilon$ -expansion, which has been studied in great detail in [76, 77, 79]. In view of the comparison to the numerical bootstrap results, we add a few OPE coefficients to the CFT data already available in the literature, which can be straightforwardly extracted from the results of [77]. Then, we study the magnetic line defect in the  $\varepsilon$ -expansion, and present new results which complement the study performed in [84]. We compare these perturbative results with the predictions from the numerical conformal bootstrap in section 5.4.

### 5.3.1 Monodromy defects with $SO(2)_F$ symmetry

**Monodromy defects in the free  $O(2)$  model.** The first example we discuss is a  $U(1)_F$ -preserving monodromy defect in free theory. This defect, first considered in [76, 77, 79], generalizes the  $\mathbb{Z}_2$  twist defect defined in [73, 74]. Following [76], we start from a set of  $N = 2$  free real scalars  $\phi^i$  in the bulk that satisfy

$$\phi^i(r, \theta + 2\pi, \vec{x}) = g^{ij} \phi^j(r, \theta, \vec{x}), \quad g^{ij} \in O(2)_F. \quad (5.3.1)$$

The scalars  $\phi^i$  either get mixed into each other, obtain a minus sign, or remain unchanged when going around the monodromy defect. In terms of the complex combination

$$\Phi = \phi^1 + i\phi^2, \quad (5.3.2)$$

the most general  $U(1)_F$  monodromy becomes<sup>9</sup>

$$\Phi(r, \theta + 2\pi, \vec{x}) = e^{2\pi i v} \Phi(r, \theta, \vec{x}), \quad v \sim v + 1, \quad v \in [0, 1). \quad (5.3.3)$$

The complex scalar  $\Phi$  has an internal  $U(1)_F$  symmetry that gets enhanced to  $O(2)_F$  for  $v = 0$  (the trivial defect) and for  $v = \frac{1}{2}$  (the  $\mathbb{Z}_2$  monodromy defect). For these values of  $v$ , the transformation  $\Phi \rightarrow \bar{\Phi}$ , which belongs to  $O(2)_F$  but not  $U(1) \simeq SO(2)_F$ , is a symmetry. As a consequence of the monodromy, the local primary operators allowed to appear in the bulk-defect expansion of  $\Phi$  will generically have non-integer spin  $s \in \mathbb{Z} + v$ , i.e.

$$\Phi(r, \theta, \vec{x}) \underset{r \rightarrow 0}{\sim} \sum_{\Psi_s} \sum_{s \in \mathbb{Z} + v} \frac{e^{-i\theta s}}{r^{\Delta_\Phi - \Delta_{\Psi_s}}} \Psi_s(\vec{x}) + \text{c.c.} \quad (5.3.4)$$

The scaling dimensions of the defect modes of  $\Phi$  are completely fixed as a consequence of the bulk free equation of motion, and read (see e.g. [73, 74, 47])

$$\Delta_{\Psi_s} = \Delta_\Phi + |s| = \frac{d-2}{2} + |s|. \quad (5.3.5)$$

In terms of real bulk scalar  $\phi^i \sim \sum_s e^{is\theta} \psi_s^i + \text{c.c.}$ , the reality condition is that  $\bar{\psi}_s^i = \psi_{-s}^i$  and so  $\Psi_s = \psi_s^1 + i\psi_s^2$  satisfies  $\bar{\Psi}_s \equiv \bar{\psi}_s^1 - i\bar{\psi}_s^2 = \psi_{-s}^1 - i\psi_{-s}^2$ .

**Monodromy defects in the interacting  $O(2)$  model.** The simplest example of an interacting  $U(1)_F$  monodromy defect is obtained by imposing the condition of eq. (5.3.3) on the fundamental vector of the critical 3d  $O(2)$  vector model. In perturbation theory this example is tractable in the standard framework of  $\varepsilon$ -expansion (with fixed co-dimension  $q = 2$ ). The bulk is tuned to the Wilson-Fisher fixed point with coupling<sup>10</sup>

$$\lambda^* = \frac{8\pi^2}{10} + \mathcal{O}(\varepsilon^2). \quad (5.3.6)$$

The scaling dimensions of the defect modes  $\Psi_s$  are found to be [76, 77]

$$\Delta_{\Psi_s} = 1 + |s| - \frac{\varepsilon}{2} + \frac{1}{5} \frac{v(v-1)}{|s|} \varepsilon + \mathcal{O}(\varepsilon^2). \quad (5.3.7)$$

For the monodromy defect, the displacement operator  $D$  appears in the OPE of two defect modes with spins  $|s| = v$  and  $|s| = v - 1$ :

$$\Psi_v \times \bar{\Psi}_{v-1} \sim D, \quad \bar{\Psi}_v \times \Psi_{v-1} \sim \bar{D}. \quad (5.3.8)$$

<sup>9</sup>As explained in [79] this monodromy can be thought of as a large and constant  $U(1)$  background gauge transformation for  $\Phi$ .

<sup>10</sup>There is a slight difference in notation with respect to [77], where the symmetry group in the bulk and on the defect is  $O(2N)$ , while we will denote it by  $O(N)$  with  $N = \text{even}$ , and in particular take  $N = 2$ , to avoid differences in notation throughout this thesis.

In appendix D we show that it appears in the  $\Psi_v \times \bar{\Psi}_{v-1}$  OPE with (squared) OPE coefficient

$$|\lambda_{\Psi_v \bar{\Psi}_{v-1} \mathbb{D}}|^2 = 1 + \frac{\varepsilon}{10} (2H^{1-v} + 2H^v - 3), \quad (5.3.9)$$

where  $H^v$  is the analytic continuation of the harmonic number. We will also need the scaling dimensions and corresponding OPE coefficients of the leading singlets in

$$\Psi_v \times \bar{\Psi}_v \sim \mathbb{1} + \mathcal{O}_0 + \dots, \quad \Psi_{v-1} \times \bar{\Psi}_{v-1} \sim \mathbb{1} + \mathcal{O}_0 + \dots \quad (5.3.10)$$

In appendix D we show that

$$\Delta_{\mathcal{O}_0} = 2 + 2v - \varepsilon + \varepsilon \left( \frac{4}{5(1+2v)} + \frac{2(v-1)}{5} \right). \quad (5.3.11)$$

In section 5.4.2 we will compare the  $\varepsilon$ -expansion predictions to the numerical bootstrap results.

It would be interesting to compute the correlator  $\langle \text{DD}\bar{\text{D}}\bar{\text{D}} \rangle$  at the first non-trivial order in  $\varepsilon$ -expansion to compare this to our single-correlator numerical bounds for the displacement operator. We will leave this for future work.

### 5.3.2 Localized magnetic field line defect

Let us continue with the determination of three-point OPE coefficients of defect operators for the magnetic line defect. The calculation is based on and extends the work [84], which focused on the scaling dimensions of low-lying defect operators. We obtain these results from a Feynman diagram expansion, keeping terms up to order  $\mathcal{O}(\varepsilon)$  in the  $\varepsilon$ -expansion. In order to obtain properly normalized OPE coefficients, we need to determine both two- and three-point functions. At the end, we also calculate several four-point functions, that by means of the conformal block decomposition allow us to check our results and obtain further coefficients.

#### Overview

To study the magnetic line defect we use a Lagrangian description that couples the  $O(N)$  model to a magnetic field localized along an infinite line. Using rotation invariance we take the line to be oriented as  $x^\mu(\tau) = (\tau, \vec{0})$ , while using  $O(N)$  invariance, we choose the magnetic field to be in the  $\phi_1$  direction. All in all, the action is

$$S = \int d^d x \left( \frac{1}{2} (\partial_\mu \phi_a)^2 + \frac{\lambda_0}{4!} (\phi_a^2)^2 \right) + h_0 \int_{-\infty}^{\infty} d\tau \phi_1(x(\tau)), \quad a = 1, \dots, N. \quad (5.3.12)$$

Let us start reviewing the results of [84], which motivate our bootstrap setup in section 5.4.3. Because the defect in eq. (5.3.12) breaks the global symmetry  $O(N) \rightarrow O(N-1)$ , there exists a tilt operator besides the displacement operator. In perturbation theory, the tilt and displacement operators are identified as

$$t_{\hat{a}} \propto \phi_{\hat{a}}, \quad \text{D} \propto \nabla \phi_1, \quad \hat{a} = 2, \dots, N, \quad (5.3.13)$$

and as usual they have protected dimension  $\Delta_t = 1$  and  $\Delta_{\text{D}} = 2$ . After the tilt, the operator with the second-lowest dimension is the localized magnetic field  $\phi_1$ . The scaling dimension of  $\phi_1$  to two-loop order in the  $\varepsilon$ -expansion reads

$$\Delta_{\phi_1} = 1 + \varepsilon - \frac{3N^2 + 49N + 194}{2(N+8)^2} \varepsilon^2 + \mathcal{O}(\varepsilon^3) \xrightarrow{\text{Padé}} 1.55. \quad (5.3.14)$$

$\lambda_{\phi_1\phi_1\phi_1}$	$\lambda_{t\phi_1}$	$\lambda_{\phi_1\phi_1s_{\pm}}$	$\lambda_{tts_{\pm}}$	$\lambda_{\phi_1tV}$	$\lambda_{t\phi_1A}$	$\lambda_{t\phi_1T}$
(5.3.46)	(5.3.46)	(5.3.51)	(5.3.52)	(5.3.53)	(5.3.58)	(5.3.53)

Table 5.1: Summary of the most important OPE coefficients computed in this section. Further coefficients appear in (5.3.48) or can be extracted from the four-point functions in section 5.3.2.

Furthermore, inputting information from  $d = 2$  in a Padé approximant, the authors of [84] estimated the value  $\Delta_{\phi_1} \approx 1.55$ , which is also consistent with their  $1/N$  results and Monte-Carlo simulations [191, 192].

Since the two lowest-dimensional operators on the defect are  $t_{\hat{a}}$  and  $\phi_1$ , a natural candidate for a bootstrap study is the mixed correlator involving them, which is the one-dimensional analog of [19, 20]. In order to motivate gap assumptions in the numerical study, let us look at the lowest-lying operators in the different OPE channels. In the singlet channel ( $S$ ), which appears for  $\phi_1 \times \phi_1$  or  $(t_{\hat{a}} \times t_{\hat{b}})_S$ , the lowest dimension operators are  $\phi_1 + s_- + s_+ + \dots$ . Here  $s_{\pm}$  are linear combinations of  $\phi_1^2$  and  $\phi_{\hat{a}}^2$  with scaling dimension

$$\Delta_{s_{\pm}} = 2 + \varepsilon \frac{3N + 20 \pm \sqrt{N^2 + 40N + 320}}{2(N + 8)} + \mathcal{O}(\varepsilon^2). \quad (5.3.15)$$

Similarly, vector operators appear in the OPE  $\phi_1 \times t_{\hat{a}} = t_{\hat{a}} + V_{\hat{a}} + \dots$ . The leading vector is  $V_{\hat{a}} \propto \phi_1 \phi_{\hat{a}}$ , and its dimension reads

$$\Delta_V = 2 + \varepsilon \frac{N + 10}{N + 8} + \mathcal{O}(\varepsilon^2). \quad (5.3.16)$$

Finally, in the OPE  $t_{\hat{a}} \times t_{\hat{b}}$  there is an antisymmetric channel ( $A$ ), where the lowest-dimensional operator is  $A_{\hat{a}\hat{b}} \propto \phi_{[\hat{a}}\phi_{\hat{b}]}$ , and a symmetric-traceless channel ( $T$ ) with the lowest-lying operator  $T_{\hat{a}\hat{b}} \propto \phi_{\hat{a}}\phi_{\hat{b}}$ . Their dimensions are given by

$$\Delta_A = 3 + \mathcal{O}(\varepsilon^2), \quad \Delta_T = 2 + \frac{2\varepsilon}{N + 8} + \mathcal{O}(\varepsilon^2). \quad (5.3.17)$$

Besides scaling dimensions, the numerical conformal bootstrap can also probe the three-point OPE coefficients of these operators. The goal of the rest of the section will be to compute these OPE coefficients to leading order in the  $\varepsilon$ -expansion, see table 5.1 for a summary of the main results. Besides two- and three-point functions, we also compute several four-point functions, which thanks to the conformal block decomposition, contain information of many other OPE coefficients.

### Conventions

Throughout this section we follow the conventions of [84], so in particular the action is given by eq. (5.3.12) and the scalar propagator in free theory is

$$---- \equiv \langle \phi_a(x_1)\phi_b(x_2) \rangle_{\lambda_0=h_0=0} = \frac{\kappa\delta_{ab}}{(x_{12}^2)^{1-\frac{\varepsilon}{2}}}, \quad \kappa = \frac{\Gamma(\frac{d}{2})}{2\pi^{d/2}(d-2)}. \quad (5.3.18)$$

In perturbative expansions there is a bulk four-point vertex and a vertex that couples a bulk operator to the defect

$$\begin{array}{c} \diagup \\ \bullet \\ \diagdown \end{array} \equiv -\lambda_0 \int d^d x \dots, \quad \begin{array}{c} | \\ \bullet \\ | \end{array} \equiv -h_0 \int_{-\infty}^{\infty} d\tau \dots \quad (5.3.19)$$

Notice that only  $\phi_1$  couples to the line, and not all  $\phi_{\hat{a}}$  for  $\hat{a} = 2, \dots, N$ . We work in dimensional regularization with minimal subtraction, so the bare couplings  $\lambda_0$  and  $h_0$  are related to the renormalized ones as

$$\lambda_0 = \lambda M^\varepsilon \left( 1 + \frac{\lambda}{(4\pi)^2} \frac{N+8}{3\varepsilon} + \mathcal{O}(\lambda^2) \right), \quad h_0 = h M^{\varepsilon/2} \left( 1 + \frac{\lambda}{(4\pi)^2} \frac{h^2}{12\varepsilon} + \mathcal{O}(\lambda^2) \right). \quad (5.3.20)$$

The renormalized couplings depend on the renormalization scale  $M$  as

$$\begin{aligned} \beta_\lambda &= M \frac{d\lambda}{dM} = -\lambda\varepsilon + \frac{\lambda^2}{(4\pi)^2} \frac{N+8}{3} + \mathcal{O}(\lambda^3), \\ \beta_h &= M \frac{dh}{dM} = -\frac{h\varepsilon}{2} + \frac{\lambda}{(4\pi)^2} \frac{h^3}{6} + \mathcal{O}(\lambda^2), \end{aligned} \quad (5.3.21)$$

so there exists a non-trivial fixed point where we evaluate most of our results:

$$\frac{\lambda_*}{(4\pi)^2} = \frac{3\varepsilon}{N+8} + \mathcal{O}(\varepsilon^2), \quad h_*^2 = N+8 + \mathcal{O}(\varepsilon). \quad (5.3.22)$$

Since we are interested in obtaining OPE coefficients at order  $\mathcal{O}(\varepsilon)$ , we shall consider diagrams with at most one bulk vertex insertion  $\lambda_* \sim \mathcal{O}(\varepsilon)$ . On the other hand, we have to allow an arbitrary number of defect insertions because  $h_* \sim \mathcal{O}(1)$ . However, in practice only a finite number of diagrams will contribute at any given order in  $\varepsilon$ .

We often split the coordinates into a direction  $\tau$  parallel to the defect and  $\vec{x} \in \mathbb{R}^{d-1}$  directions orthogonal to the defect. We shall only consider correlation functions of operators that live on the defect, for which we use the shorthand notation  $\mathcal{O}(\tau) = \mathcal{O}(\tau, \vec{x} = 0)$ .

## Two-point functions

We obtain all two-point functions of operators of the schematic form  $\phi, \phi^2, \nabla\phi$ , where  $\phi$  is the fundamental scalar and  $\nabla$  are derivatives orthogonal to the defect. Besides rederiving their scaling dimensions, which appeared previously in [84], we obtain the overall normalization, which is needed in the calculation of higher-point functions.

### The correlator $\langle \phi \phi \rangle$

Let us start with the simplest example: the two-point function of the fundamental field. To order  $\mathcal{O}(\varepsilon)$  only two diagrams contribute:

$$\langle \phi_a(\tau) \phi_b(0) \rangle = \text{---} + \text{---} + \dots \quad (5.3.23)$$

The first diagram is obtained setting  $\vec{x}_1 = \vec{x}_2 = 0$  in the free propagator (5.3.18). For the integral that enters the second diagram, we first integrate the two defect insertions using

$$\int_{-\infty}^{\infty} \frac{d\tau}{(|\vec{x}|^2 + \tau^2)^\Delta} = \frac{\sqrt{\pi} \Gamma(\Delta - \frac{1}{2})}{\Gamma(\Delta)} \frac{1}{|\vec{x}^2|^{\Delta - \frac{1}{2}}}, \quad (5.3.24)$$

and then the bulk vertex using

$$\int d^d x_3 \frac{|\vec{x}_3|^\varepsilon}{(x_{13}^2 x_{23}^2)^{1 - \frac{\varepsilon}{2}}} = \frac{\sqrt{\pi} \Gamma(1 - \frac{3\varepsilon}{2}) \Gamma(\varepsilon)^2 \Gamma(\frac{\varepsilon+1}{2})}{2\Gamma(1 - \frac{\varepsilon}{2})^2 \Gamma(2\varepsilon)} \frac{1}{|\tau_{12}^2|^{1 - \frac{3\varepsilon}{2}}}, \quad (5.3.25)$$



which follows from Schwinger parametrization. Using these results, it is a simple book-keeping exercise to obtain the contribution of each diagram:

$$\begin{aligned} \text{---} \overbrace{\text{---}}^{\text{---}} &= \frac{\kappa \delta_{ab}}{\tau^{2-\varepsilon}}, \\ \text{---} \overbrace{\text{---}}^{\text{---}} &= -\frac{\lambda_0 h_0^2}{(4\pi)^4} \frac{2\delta_{1a}\delta_{1b} + \delta_{ab}}{\tau^{2-3\varepsilon}} \left( \frac{2}{3\varepsilon} - \frac{1}{3} + \aleph + \mathcal{O}(\varepsilon) \right). \end{aligned} \quad (5.3.26)$$

To simplify the notation, we have introduced the constant

$$\aleph \equiv 1 + \gamma_E + \log \pi, \quad (5.3.27)$$

which appears repeatedly in the calculations below but drops out of physical quantities such as scaling dimensions and OPE coefficients. We now introduce renormalized fields, which transform irreducibly under the unbroken symmetry group  $O(N-1)$ :

$$\phi_1 \equiv Z_{\phi_1}[\phi_1], \quad \phi_{\hat{a}} \equiv Z_t t_{\hat{a}}. \quad (5.3.28)$$

The operator  $t_{\hat{a}}$  is the tilt operator from section 5.2.2. The two renormalization factors are obtained demanding that poles in  $\varepsilon$  cancel in (5.3.23), giving

$$Z_{\phi_1} = 1 - \frac{\lambda}{(4\pi)^2} \frac{h^2}{4\varepsilon} + \mathcal{O}(\lambda^2), \quad Z_t = 1 - \frac{\lambda}{(4\pi)^2} \frac{h^2}{12\varepsilon} + \mathcal{O}(\lambda^2). \quad (5.3.29)$$

From the renormalization factor one can immediately obtain the anomalous dimension at the critical point using  $\gamma_{\mathcal{O}} = M \frac{d}{dM} \log Z_{\mathcal{O}}$ . The results have been summarized in section 5.3.2, and are in perfect agreement with [84]. Finally, note that the two-point functions at the critical point read

$$\begin{aligned} \langle [\phi_1](\tau) [\phi_1](0) \rangle &= \frac{\mathcal{N}_{\phi_1}^2}{\tau^{2\Delta_{\phi_1}}}, & \mathcal{N}_{\phi_1}^2 &= \kappa \left( 1 - \frac{3\aleph}{2} \varepsilon + \mathcal{O}(\varepsilon^2) \right), \\ \langle t_{\hat{a}}(\tau) t_{\hat{b}}(0) \rangle &= \delta_{\hat{a}\hat{b}} \frac{\mathcal{N}_t^2}{\tau^2}, & \mathcal{N}_t^2 &= \kappa \left( 1 - \frac{\aleph}{2} \varepsilon + \mathcal{O}(\varepsilon^2) \right). \end{aligned} \quad (5.3.30)$$

### The correlator $\langle \nabla \phi \nabla \phi \rangle$

Similarly, we can consider the two-point function  $\langle \nabla_i \phi_a \nabla_j \phi_b \rangle$ , which again consists of two diagrams at this order:

$$\begin{aligned} \text{---} \overbrace{\text{---}}^{\text{---}} &= \kappa(d-2) \frac{\delta_{ij} \delta_{ab}}{\tau^{4-\varepsilon}}, \\ \text{---} \overbrace{\text{---}}^{\text{---}} &= -\frac{\lambda_0 h_0^2}{(4\pi)^4} \frac{\delta_{ij} (2\delta_{1a}\delta_{1b} + \delta_{ab})}{\tau^{4-3\varepsilon}} \left( \frac{4}{9\varepsilon} - \frac{8}{27} + \frac{2}{3}\aleph + \mathcal{O}(\varepsilon) \right). \end{aligned}$$

The integrals are computed as before, but one needs to be careful to first take transverse derivatives with respect to  $\vec{x}_1$  and  $\vec{x}_2$  and then sending  $\vec{x}_1, \vec{x}_2 \rightarrow 0$ . Once again we introduce renormalized fields

$$\nabla \phi_1 \equiv Z_D D, \quad \nabla \phi_{\hat{a}} \equiv Z_{\nabla \phi} [\nabla \phi_{\hat{a}}], \quad (5.3.31)$$

where  $D$  is the displacement operator which transforms as a vector under  $SO(d-1)$  transverse rotations. Cancelling poles in  $\varepsilon$  we find

$$Z_D = 1 - \frac{\lambda}{(4\pi)^2} \frac{h^2}{12\varepsilon} + \mathcal{O}(\lambda^2), \quad Z_{\nabla\phi} = 1 - \frac{\lambda}{(4\pi)^2} \frac{h^2}{36\varepsilon} + \mathcal{O}(\lambda^2). \quad (5.3.32)$$

It follows that the scaling dimension of the displacement is protected, and we obtain the scaling dimension  $\Delta_{\nabla\phi} = 2 - \frac{1}{3}\varepsilon + \mathcal{O}(\varepsilon^2)$ , in agreement with [84]. The defect-defect two-point functions at the critical point read

$$\begin{aligned} \langle D_i(\tau) D_j(0) \rangle &= \delta_{ij} \frac{\mathcal{N}_D^2}{\tau^4}, & \mathcal{N}_D^2 &= 2\kappa \left( 1 - \frac{4+3\aleph}{6} \varepsilon + \mathcal{O}(\varepsilon^2) \right), \\ \langle [\nabla_i \phi_{\hat{a}}](\tau) [\nabla_j \phi_{\hat{b}}](0) \rangle &= \delta_{\hat{a}\hat{b}} \delta_{ij} \frac{\mathcal{N}_{\nabla\phi}^2}{\tau^{2\Delta_{\nabla\phi}}}, & \mathcal{N}_{\nabla\phi}^2 &= 2\kappa \left( 1 - \frac{10+3\aleph}{18} \varepsilon + \mathcal{O}(\varepsilon^2) \right). \end{aligned}$$

### The correlator $\langle \phi^2 \phi^2 \rangle$

Finally, the last type of operators we are interested in are composites of two fundamental fields:

$$\langle \phi_a \phi_b(\tau) \phi_c \phi_d(\tau) \rangle = \text{diagram 1} + \text{diagram 2} + \text{diagram 3} + \dots \quad (5.3.33)$$

The first and third diagrams are computed as in section 5.3.2, whereas the second is a chain diagram, for which the integral is well known (see e.g. [120]):

$$\int \frac{d^d x_3}{(x_{13}^2)^{\Delta_1} (x_{23}^2)^{\Delta_2}} = \frac{\pi^{\frac{d}{2}}}{(x_{12}^2)^{\Delta_1 + \Delta_2 - \frac{d}{2}}} \frac{\Gamma(\frac{d}{2} - \Delta_1)}{\Gamma(\Delta_1)} \frac{\Gamma(\frac{d}{2} - \Delta_2)}{\Gamma(\Delta_2)} \frac{\Gamma(\Delta_1 + \Delta_2 - \frac{d}{2})}{\Gamma(d - \Delta_1 - \Delta_2)}. \quad (5.3.34)$$

Once again, we are interested in reducing  $\phi_a \phi_b$  into irreducible components. On one hand, we can form a vector and a symmetric-traceless operator as follows:

$$Z_V V_{\hat{a}} = \phi_1 \phi_{\hat{a}}, \quad Z_T T_{\hat{a}\hat{b}} = \phi_{\hat{a}} \phi_{\hat{b}} - \frac{\delta_{\hat{a}\hat{b}}}{N-1} \phi_{\hat{c}}^2, \quad (5.3.35)$$

with the following renormalization factors:

$$Z_V = 1 - \frac{\lambda}{(4\pi)^2} \frac{h^2 + 2}{3\varepsilon} + \mathcal{O}(\lambda^2), \quad Z_T = 1 - \frac{\lambda}{(4\pi)^2} \frac{h^2 + 4}{6\varepsilon} + \mathcal{O}(\lambda^2). \quad (5.3.36)$$

Again, it is straightforward to extract the anomalous dimensions at the critical point and the normalization of the two-point functions:

$$\begin{aligned} \langle V_{\hat{a}}(\tau) V_{\hat{b}}(0) \rangle &= \delta_{\hat{a}\hat{b}} \frac{\mathcal{N}_V^2}{\tau^{2\Delta_V}}, & \mathcal{N}_V^2 &= \kappa^2 \left( 1 - \frac{2N+18}{N+8} \aleph \varepsilon + \mathcal{O}(\varepsilon^2) \right), \\ \langle T_{\hat{a}\hat{b}}(\tau) T_{\hat{c}\hat{d}}(0) \rangle &= \mathbf{T}_{\hat{a}\hat{b},\hat{c}\hat{d}} \frac{\mathcal{N}_T^2}{\tau^{2\Delta_T}}, & \mathcal{N}_T^2 &= 2\kappa^2 \left( 1 - \frac{N+10}{N+8} \aleph \varepsilon + \mathcal{O}(\varepsilon^2) \right). \end{aligned} \quad (5.3.37)$$

Here we have introduced a symmetric-traceless tensor which will be useful later:

$$\mathbf{T}_{\hat{a}\hat{b},\hat{c}\hat{d}} = \frac{1}{2} \delta_{\hat{a}\hat{c}} \delta_{\hat{b}\hat{d}} + \frac{1}{2} \delta_{\hat{a}\hat{d}} \delta_{\hat{b}\hat{c}} - \frac{\delta_{\hat{a}\hat{b}} \delta_{\hat{c}\hat{d}}}{N-1}. \quad (5.3.38)$$

On the other hand, we can form two independent scalars  $\phi_1^2$  and  $\phi_a^2$ , which mix at  $\mathcal{O}(\varepsilon)$  due to quantum corrections. The renormalized fields  $s_\pm$  are defined as

$$\begin{pmatrix} \phi_1^2 \\ \phi_a^2 \end{pmatrix} = Z_s \begin{pmatrix} s_- \\ s_+ \end{pmatrix}, \quad (5.3.39)$$

where the renormalization factor  $Z_s$  is a two-by-two matrix. To determine  $Z_s$  one requires that three-point functions of renormalized fields

$$\langle [\phi_1] [\phi_1] s_\pm \rangle, \quad \langle [\phi_1] t_{\hat{a}} s_\pm \rangle, \quad \langle t_{\hat{a}} t_{\hat{b}} s_\pm \rangle, \quad (5.3.40)$$

have no poles in  $\varepsilon$ . We explain how to compute these three-point functions in section 5.3.2. Furthermore, one should require that  $Z_s$  is such that  $s_\pm$  have anomalous dimensions that do not mix. Demanding this we find the anomalous-dimension matrix

$$\gamma = Z_s^{-1} \frac{\partial Z_s}{\partial \log M} \Big|_{\text{fixed point}} = \begin{pmatrix} \frac{5N+36-\sqrt{N^2+40N+320}}{2N+16} & 0 \\ 0 & \frac{5N+36+\sqrt{N^2+40N+320}}{2N+16} \end{pmatrix} \varepsilon + \mathcal{O}(\varepsilon^2). \quad (5.3.41)$$

Our choice of  $Z_s$  guarantees that the two-point functions are orthogonal, as one usually requires in CFT:

$$\langle s_\pm(\tau) s_\pm(0) \rangle = \frac{\mathcal{N}_{s_\pm}^2}{\tau^{2\Delta_{s_\pm}}}, \quad \langle s_\pm(\tau) s_\mp(0) \rangle = 0. \quad (5.3.42)$$

The formulas for  $Z_s$  and  $\mathcal{N}_{s_\pm}^2$  are somewhat complicated and not particularly illuminating, so instead of writing them explicitly we attach them in a notebook.

### Three-point functions

Having determined the scaling dimension and normalization of the defect operators of interest, we are ready to compute some of their three-point OPE coefficients  $\lambda_{\mathcal{O}_1\mathcal{O}_2\mathcal{O}_3}$ . Here we shall focus on parity-even operators, that have three-point functions of the form

$$\langle \mathcal{O}_1(\tau_1)\mathcal{O}_2(\tau_2)\mathcal{O}_3(\tau_3) \rangle = \frac{\mathcal{N}_{\mathcal{O}_1}\mathcal{N}_{\mathcal{O}_2}\mathcal{N}_{\mathcal{O}_3} \lambda_{\mathcal{O}_1\mathcal{O}_2\mathcal{O}_3}}{|\tau_{12}|^{\Delta_1+\Delta_2-\Delta_3} |\tau_{13}|^{\Delta_1+\Delta_3-\Delta_2} |\tau_{23}|^{\Delta_2+\Delta_3-\Delta_1}}. \quad (5.3.43)$$

By choosing different external operators there are many three-point functions that can be computed. Here we focus on a subset of them, which can be compared to our numerical study or in future works.

### The correlator $\langle \phi\phi\phi \rangle$

The simplest three-point functions are the ones that involve only the fundamental scalar. These are zero at tree level, but receive a contribution at order  $\mathcal{O}(\varepsilon)$  from the following diagram:

$$\langle \phi_a(\tau_1) \phi_b(\tau_2) \phi_c(\tau_3) \rangle = \text{diagram} + \dots \quad (5.3.44)$$

Because this diagram is proportional to a factor  $\lambda_* \propto \varepsilon$ , it suffices to evaluate the integral in exactly  $d = 4$ :

$$\int \frac{d\tau_4 d^4x_5}{x_{15}^2 x_{25}^2 x_{35}^2 x_{45}^2} = \frac{2\pi^4}{\sqrt{\tau_{12}^2 \tau_{13}^2 \tau_{23}^2}}. \quad (5.3.45)$$

To compute this integral, we exploit that it is invariant under the one-dimensional conformal group, so we use a frame where  $\tau_1 = 0$ ,  $\tau_2 = 1$  and  $\tau_3 = \infty$ . We start integrating over  $\tau_4$ , then the orthogonal directions  $\vec{x}_5^2$ , and finally over  $\tau_5$ , all the steps being elementary. Splitting the diagram (5.3.44) into irreducible components under  $O(N-1)$ , and keeping track of all normalization factors, we find the two OPE coefficients

$$\lambda_{\phi_1\phi_1\phi_1} = \frac{3\pi\varepsilon}{\sqrt{N+8}} + \mathcal{O}(\varepsilon^2), \quad \lambda_{tt\phi_1} = \frac{\pi\varepsilon}{\sqrt{N+8}} + \mathcal{O}(\varepsilon^2). \quad (5.3.46)$$

### The correlator $\langle \nabla\phi\nabla\phi\phi \rangle$

We can also consider a three-point function where two of the external operators are orthogonal derivatives  $\langle \nabla\phi_a(\tau_1)\nabla\phi_b(\tau_2)\phi_c(\tau_3) \rangle$ . The same diagram as in (5.3.44) contributes, but now it leads to the integral

$$\lim_{\vec{x}_1, \vec{x}_2 \rightarrow 0} \frac{\partial}{\partial \vec{x}_{1,i}} \frac{\partial}{\partial \vec{x}_{2,j}} \int \frac{d\tau_4 d^4x_5}{x_{15}^2 x_{25}^2 x_{35}^2 x_{45}^2} = \frac{4\pi^4/3}{\sqrt{\tau_{12}^6 \tau_{13}^2 \tau_{23}^2}}, \quad (5.3.47)$$

which has been computed as before in eq. (5.3.45). Splitting the result into irreducible components under  $O(N-1)$  and keeping track of all normalization factors, we find the three OPE coefficients

$$\lambda_{DD\phi_1} = \frac{\pi\varepsilon}{\sqrt{N+8}} + \mathcal{O}(\varepsilon^2), \quad \lambda_{D\nabla\phi t} = \frac{\pi\varepsilon}{3\sqrt{N+8}} + \mathcal{O}(\varepsilon^2), \quad \lambda_{\nabla\phi\nabla\phi\phi_1} = \frac{\pi\varepsilon}{3\sqrt{N+8}} + \mathcal{O}(\varepsilon^2). \quad (5.3.48)$$

### The correlator $\langle \phi\phi\phi^2 \rangle$

The last type of OPE coefficient we consider involves two fundamental fields and a composite one:

$$\langle \phi_a(\tau_1)\phi_b(\tau_2)\phi_c\phi_d(\tau_3) \rangle = \text{diagram 1} + \text{diagram 2} + \text{diagram 3} + \dots \quad (5.3.49)$$

The first and third diagrams are elementary, and have been computed in section 5.3.2. The second diagram contains a new integral that reads

$$\int \frac{d^d x_4}{(x_{14}^2 x_{24}^2)^{1-\frac{\varepsilon}{2}} (x_{34}^2)^{2-\varepsilon}} = \frac{\pi^2}{\tau_{13}^2 \tau_{23}^2} \left( \frac{2}{\varepsilon} + 3 - \aleph + \log \left( \frac{\tau_{13}^4 \tau_{23}^4}{\tau_{12}^2} \right) + \mathcal{O}(\varepsilon) \right). \quad (5.3.50)$$

To compute it, we first rewrite the integral in parametric form using Schwinger's representation, and then we partial integrate as described in [193, 194].<sup>11</sup> The result is expanded to order  $\mathcal{O}(\varepsilon^0)$ , and each of the terms in the expansion is a convergent integral that can be solved with elementary methods.

Once again, the correlator in eq. (5.3.49) contains several OPE coefficients. If we let the third operator be a scalar under  $O(N-1)$ , then we have the following OPE

<sup>11</sup>Although we have not used `HyperInt` [195], the package automatizes this in the function `dimregPartial`.

coefficients:

$$\lambda_{\phi_1\phi_1s_\pm} = \frac{\pm 2\sqrt{N-1}}{\sqrt{N^2+40N+320 \mp (N+18)\sqrt{N^2+40N+320}}} \left( 1 \pm \frac{(95N-640)\varepsilon}{64\sqrt{N^2+40N+320}} \right. \\ \left. \pm \frac{17\varepsilon\sqrt{N^2+40N+320}}{64(N+8)} - \frac{7N^3+182N^2+1160N+2280}{4(N+8)(N^2+40N+320)}\varepsilon + \mathcal{O}(\varepsilon^2) \right), \quad (5.3.51)$$

$$\lambda_{tts_\pm} = \frac{(\mp(N+18) + \sqrt{N^2+40N+320})(N-1)^{-1/2}}{\sqrt{N^2+40N+320 \mp (N+18)\sqrt{N^2+40N+320}}} \left( 1 \mp \frac{(95N-640)\varepsilon}{64\sqrt{N^2+40N+320}} \right. \\ \left. \mp \frac{49\varepsilon\sqrt{N^2+40N+320}}{64(N+8)} - \frac{(11N^3+374N^2+3720N+12520)\varepsilon}{4(N+8)(N^2+40N+320)} + \mathcal{O}(\varepsilon^2) \right). \quad (5.3.52)$$

If we instead let the third operator be a vector or a symmetric-traceless tensor, we find:

$$\lambda_{\phi_1tV} = 1 - \frac{\varepsilon}{N+8} + \mathcal{O}(\varepsilon^2), \quad \lambda_{ttT} = \sqrt{2} \left( 1 - \frac{\varepsilon}{N+8} + \mathcal{O}(\varepsilon^2) \right). \quad (5.3.53)$$

The normalization of  $\lambda_{ttT}$  is chosen such that the tensor structure in eq. (5.3.38) multiplies the three-point function in eq. (5.3.43).

### Four-point functions

In this final section, we turn our attention to four-point functions of operators formed by the fundamental field and possibly one transverse derivative. Because of the OPE, four-point functions contain information about three-point OPE coefficients, so we will be able to check some calculations of section 5.3.2 and obtain new results.

#### The correlator $\langle \phi \phi \phi \phi \rangle$

The simplest four-point function is that of the fundamental field:

$$\langle \phi_a(\tau_1) \phi_b(\tau_2) \phi_c(\tau_3) \phi_d(\tau_4) \rangle = \text{---} + \text{---} + \text{---} + \dots \quad (5.3.54)$$

The first and third contributions lead to the disconnected part of the correlator, while the non-trivial part is given by the second diagram. Since the second diagram is multiplied by a coupling  $\lambda_* = \mathcal{O}(\varepsilon)$ , it suffices to evaluate the integral in  $d = 4$ :

$$\lim_{\vec{x}_n \rightarrow 0} \int \frac{d^4x_5}{x_{15}^2 x_{25}^2 x_{35}^2 x_{45}^2} = -2\pi^2 \frac{I_1(\xi)}{\tau_{12}^2 \tau_{34}^2}. \quad (5.3.55)$$

Since this integral preserves the one-dimensional conformal group, we can evaluate it in the frame  $(\tau_1, \tau_2, \tau_3, \tau_4) = (0, \xi, 1, \infty)$ , where the cross-ratio  $\xi$  is defined in eq. (5.2.13). We integrate first over orthogonal directions  $\vec{x}_5^2$  and then over  $\tau_5$ , considering separately the intervals  $\tau_5 \in (-\infty, 0)$ ,  $\tau_5 \in (0, \xi)$ ,  $\tau_5 \in (\xi, 1)$  and  $\tau_5 \in (1, \infty)$ . The final result reads

$$I_1(\xi) = \xi \log(1-\xi) + \frac{\xi^2}{1-\xi} \log \xi. \quad (5.3.56)$$

As usual, we decompose the correlator in eq. (5.3.54) into irreducible components, and using the appropriate renormalization factors we obtain three inequivalent correlators:

$$\begin{aligned}
G_{\phi_1\phi_1\phi_1\phi_1}(\xi) &= 1 + \xi^{2\Delta_{\phi_1}} + \left(\frac{\xi}{1-\xi}\right)^{2\Delta_{\phi_1}} + \frac{6\varepsilon I_1(\xi)}{N+8} + \mathcal{O}(\varepsilon^2), \\
G_{\phi_1\phi_1 t_{\hat{a}} t_{\hat{b}}}(\xi) &= \delta_{\hat{a}\hat{b}} + \varepsilon \frac{2\delta_{\hat{a}\hat{b}}}{N+8} I_1(\xi) + \mathcal{O}(\varepsilon^2), \\
G_{t_{\hat{a}} t_{\hat{b}} t_{\hat{c}} t_{\hat{d}}}(\xi) &= \delta_{\hat{a}\hat{b}} \delta_{\hat{c}\hat{d}} + \delta_{\hat{a}\hat{c}} \delta_{\hat{b}\hat{d}} \xi^2 + \delta_{\hat{a}\hat{d}} \delta_{\hat{b}\hat{c}} \left(\frac{\xi}{1-\xi}\right)^2 + \frac{2\varepsilon I_1(\xi)}{N+8} (\delta_{\hat{a}\hat{b}} \delta_{\hat{c}\hat{d}} + \text{perms}) + \mathcal{O}(\varepsilon^2) \\
&= \delta_{\hat{a}\hat{b}} \delta_{\hat{c}\hat{d}} G_{tttt}^S(\xi) + (\delta_{\hat{a}\hat{d}} \delta_{\hat{b}\hat{c}} - \delta_{\hat{a}\hat{c}} \delta_{\hat{b}\hat{d}}) G_{tttt}^A(\xi) + \mathbf{T}_{\hat{a}\hat{b}, \hat{c}\hat{d}} G_{tttt}^T(\xi).
\end{aligned} \tag{5.3.57}$$

The correlator of four tilt operators decomposes into singlet ( $S$ ), antisymmetric ( $A$ ) and symmetric-traceless ( $T$ ) channels with respect to the  $O(N-1)$  symmetry, where the last tensor structure is shown in eq. (5.3.38).

The virtue of having four-point functions is that they can be expanded in conformal blocks to obtain anomalous dimensions and three-point coefficients. For the vector, symmetric-traceless and antisymmetric channels we find:

$$\begin{aligned}
G_{t\phi_1\phi_1 t}(\xi) &= \left(1 - \frac{2\varepsilon}{N+8}\right) g_2^{\Delta_{t\phi_1}, \Delta_{\phi_1 t}}(\xi) + \varepsilon \frac{N+10}{N+8} \partial_{\Delta} g_2^{\Delta_{t\phi_1}, \Delta_{\phi_1 t}}(\xi) + \dots, \\
G_{tttt}^S(\xi) &= \left(2 - \frac{4\varepsilon}{N+8}\right) g_2(\xi) + \frac{4\varepsilon}{N+8} \partial_{\Delta} g_2(\xi) + \dots, \\
G_{tttt}^A(\xi) &= g_3(\xi) + \dots.
\end{aligned} \tag{5.3.58}$$

The ellipses stand for higher dimensional operators, as well as higher order corrections in  $\varepsilon$ . The first two lines confirm our computations of  $\Delta_V$ ,  $\Delta_T$ ,  $\lambda_{\phi_1 t V}$  and  $\lambda_{tt T}$ . From the third line, we conclude that the antisymmetric operator  $A_{ab} \sim \phi_{[a} \partial_{\tau} \phi_{b]}$  has scaling dimension  $\Delta_A = 3 + \mathcal{O}(\varepsilon^2)$  and three-point coefficient  $\lambda_{tt A} = 1 + \mathcal{O}(\varepsilon^2)$ .

Of course, we can also expand correlators in the singlet channel, for example

$$G_{\phi_1\phi_1\phi_1\phi_1}(\xi) = 1 + \left(2 - \frac{6\varepsilon}{N+8}\right) g_2(\xi) + \varepsilon \frac{4N+38}{N+8} \partial_{\Delta} g_2(\xi) + \dots \tag{5.3.59}$$

However, the above contributions are due to two operators  $s_{\pm}$  with nearly-degenerate dimension, so the expansion does not fix the scaling dimension or OPE coefficient, but instead it relates them in a non-trivial way:

$$\begin{aligned}
(\Delta_{s_+} - 2) \lambda_{\phi_1\phi_1 s_+}^2 + (\Delta_{s_-} - 2) \lambda_{\phi_1\phi_1 s_-}^2 &= \varepsilon \frac{4N+38}{N+8} + \mathcal{O}(\varepsilon^2), \\
\lambda_{\phi_1\phi_1 s_+}^2 + \lambda_{\phi_1\phi_1 s_-}^2 &= 2 - \frac{6\varepsilon}{N+8} + \mathcal{O}(\varepsilon^2).
\end{aligned} \tag{5.3.60}$$

It is reassuring that eq. (5.3.15) and eq. (5.3.51) indeed satisfy these relations. In a similar way, we can expand  $G_{tttt}^{\text{sing}}$  and  $G_{\phi_1\phi_1 tt}$ , finding again perfect agreement with our results. Note that the four-point functions do not capture the OPE coefficients in eq. (5.3.46) at this order in  $\varepsilon$ .

**The correlators**  $\langle \nabla\phi\nabla\phi\phi\phi \rangle$  and  $\langle \nabla\phi\nabla\phi\nabla\phi\nabla\phi \rangle$

In a similar way, one can consider four-point functions that include derivative operators  $\nabla\phi_a$ , and the only non-trivial contribution is a contact diagram. For the case of two derivative operators, the relevant integral is

$$\lim_{\vec{x}_n \rightarrow 0} \frac{\partial^2}{\partial \vec{x}_{3,i} \partial \vec{x}_{4,j}} \int \frac{d^4 x_5}{x_{15}^2 x_{25}^2 x_{35}^2 x_{45}^2} = \frac{2\pi^2}{3} \frac{I_2(\xi)}{\tau_{12}^2 \tau_{34}^4} \delta^{ij}, \quad (5.3.61)$$

$$I_2(\xi) = \frac{\xi^2}{1-\xi} - (\xi+2)\xi \log(1-\xi) + \frac{\xi^4}{(1-\xi)^2} \log \xi,$$

which has been computed using the same technique as in eq. (5.3.56). From this, we can read off several correlators, for example

$$G_{\phi_1 \phi_1 D_i D_j}(\xi) = \delta_{ij} \left( 1 - \frac{\varepsilon I_2(\xi)}{N+8} + \mathcal{O}(\varepsilon^2) \right), \quad (5.3.62)$$

$$G_{t_{\hat{a}} t_{\hat{b}} D_i D_j}(\xi) = \delta_{\hat{a}\hat{b}} \delta_{ij} \left( 1 - \frac{\varepsilon I_2(\xi)}{3(N+8)} + \mathcal{O}(\varepsilon^2) \right).$$

We can also obtain correlators with  $\nabla\phi_{\hat{a}}$ , but we do not write them for compactness. Finally, if we consider four derivative operators the relevant integral is

$$\lim_{\vec{x}_n \rightarrow 0} \frac{\partial^4}{\partial \vec{x}_{1,i} \partial \vec{x}_{2,j} \partial \vec{x}_{3,k} \partial \vec{x}_{4,l}} \int \frac{d^4 x_5}{x_{15}^2 x_{25}^2 x_{35}^2 x_{45}^2} = -\frac{8\pi^2}{15} \frac{I_3(\xi)}{\tau_{12}^4 \tau_{34}^4} \left( \delta_{ij} \delta_{kl} + \delta_{ik} \delta_{jl} + \delta_{il} \delta_{jk} \right),$$

$$I_3(\xi) = \frac{(\xi^2 - \xi + 1)\xi^2}{(1-\xi)^2} + \frac{1}{2} (2\xi^2 + \xi + 2) \xi \log(1-\xi) + \frac{(2\xi^2 - 5\xi + 5)\xi^4}{2(1-\xi)^3} \log \xi. \quad (5.3.63)$$

From here we extract the four-point function of the displacement operator

$$G_{D^i D^j D^k D^l}(\xi) = \delta^{ij} \delta^{kl} + \delta^{ik} \delta^{jl} \xi^4 + \delta^{il} \delta^{jk} \left( \frac{\xi}{1-\xi} \right)^4 + \frac{2\varepsilon I_3(\xi)}{5(N+8)} \left( \delta^{ij} \delta^{kl} + \text{perms} \right) + \mathcal{O}(\varepsilon^2). \quad (5.3.64)$$

In order to extract CFT data from this correlator, we decompose it in terms of singlet ( $S$ ), antisymmetric ( $A$ ) and symmetric-traceless ( $T$ ) channels under  $SO(d-1)_T$ :

$$G_{\text{DDDD}}^S(\xi) = 1 + \left( \frac{2}{3} + \frac{(4N+37)\varepsilon}{18(N+8)} \right) f_4(\xi) + \frac{5\varepsilon}{3(N+8)} \partial_\Delta f_4(\xi) + \dots,$$

$$G_{\text{DDDD}}^A(\xi) = 2f_5(\xi) + \dots, \quad (5.3.65)$$

$$G_{\text{DDDD}}^T(\xi) = \left( 2 + \frac{\varepsilon}{3(N+8)} \right) f_4(\xi) + \frac{2\varepsilon}{N+8} \partial_\Delta f_4(\xi) + \dots$$

Notice that these operators are not necessarily the lowest-dimensional operators in each channel. For instance, in the  $(D \times D)_S$  channel we have  $\phi_1$  with  $\Delta_{\phi_1} = 1 + \varepsilon + \mathcal{O}(\varepsilon^2)$ , but it does not appear because  $\lambda_{DD\phi_1}^2 = \mathcal{O}(\varepsilon^2)$ , see eq. (5.3.48). Similarly, in the  $(D \times D)_T$  channel the lowest-dimension operator is  $\partial_i \partial_j \phi_1$  with  $\Delta = 3 + \mathcal{O}(\varepsilon)$ , but it is invisible in the four-point function at this order. Only in the channel  $(D \times D)_A$  we expect the lowest-lying operators to be  $\partial_{[i} \phi_1 \partial_\tau \partial_{j]} \phi_1$  and  $\partial_{[i} \phi_a \partial_\tau \partial_{j]} \phi_a$ , with nearly-degenerate dimension  $\Delta = 5 + \dots$ . However, in order to disentangle these operators one should do an analysis similar to the one we did for  $s_\pm$  below eq. (5.3.39).

## 5.4 Numerical results

In this section we use numerical conformal bootstrap and the semidefinite program solver SDPB [196] to carve out the space of line defects with  $O(2)_F$  global symmetry. We consider:

1. Line defects without a tilt operator ( $t$ ) that preserve a  $U(1)_F$  subgroup of the  $O(2)_F$  symmetry in the bulk;
2. Line defects that break local  $O(3)_F$  to  $U(1)_F \simeq SO(2)_F$  and therefore feature a tilt operator transforming in the vector representation of  $U(1)_F$ .

In section 5.4.1 we study correlation functions involving  $D$  and  $t$ . Due to the universal nature of these operators, the numerical bounds presented in section 5.4.1 are valid for a large class of conformal defects. In sections 5.4.2 and 5.4.3 we focus on the specific models already announced in section 5.3: the magnetic line defect and the monodromy line defect. Here we use the  $\varepsilon$ -expansion results of section 5.3 as guidance, in order to zoom in on specific regions of the parameter space, where we expect these models to live.

### 5.4.1 Bounds on universal correlators

#### Single-correlator with the displacement operator

We start bootstrapping correlation functions of the displacement operator  $D$ . Recall from section 5.2.2 that  $D$  is a defect primary of scaling dimension  $\Delta_D = 2$ , transforming as a vector under  $SO(2)_T$  and neutral under  $O(2)_F$ . Hence, while we cannot impose the global symmetry  $O(2)_F$ , the charge of the displacement under  $SO(2)_T$  implies we restrict to defects of co-dimension  $q \geq 2$ . In the complex notation introduced in section 5.2.2, there are two non-equivalent orderings of the correlation functions involving the displacement

$$\langle D(\tau_1)D(\tau_2)\bar{D}(\tau_3)\bar{D}(\tau_4) \rangle, \quad \langle D(\tau_1)\bar{D}(\tau_2)D(\tau_3)\bar{D}(\tau_4) \rangle, \quad (5.4.1)$$

and the relevant crossing equations can be obtained from eq. (5.2.18) upon setting  $\Delta_D = 2$ . The leading non-identity defect primaries in the  $D \times \bar{D}$  OPE are denoted  $(D\bar{D})^\pm$  in the conventions of section 5.2.2, while the leading primary in the  $D \times D$  OPE is denoted  $D^2$ .

**Gap bounds.** We start computing the upper bound on the scaling dimension of the leading  $\mathcal{S}$ -parity even scalar  $\Delta_{(D\bar{D})^+}$  as we vary  $\Delta_{D^2}$  and  $\Delta_{(D\bar{D})^-}$ . The result is shown in the 3d plot of figure 5.1(a), where the light-red shaded region represents the ‘agnostic’ bound obtained imposing the same gap on the dimension of the  $\mathcal{S}$ -parity odd and  $\mathcal{S}$ -parity even scalars. The term ‘agnostic’ here refers to the fact that by holding  $\Delta_{(D\bar{D})^+} = \Delta_{(D\bar{D})^-}$  we are putting a bound on the lowest-lying singlet, whether it is parity-even or parity-odd. In order to help visualizing the constant- $\Delta_{(D\bar{D})^+}$  slices, we included figure 5.1(b). There are three notable regions in figure 5.1(a):

- I. This is the region with the weakest  $\Delta_{(D\bar{D})^-}$  gap assumptions, i.e.  $\Delta_{(D\bar{D})^-} \simeq 0 \div 3$ . In this region the upper bound is smooth: it is saturated by the ‘agnostic’ bound for both small and large values of  $\Delta_{D^2}$ , with a cross-over behavior at around  $\Delta_{D^2} \simeq 6$ . For low values of  $\Delta_{D^2}$ , the agnostic bound approaches the GFF value for a real fermion  $\Delta_{(D\bar{D})} = 2\Delta_D + 1 = 5$ . This is because a single real GFF satisfies the crossing equations for a single complex scalar as long as the gap in the charged sector is  $\Delta_{D^2} < 2\Delta_D = 4$ , see e.g. [110].



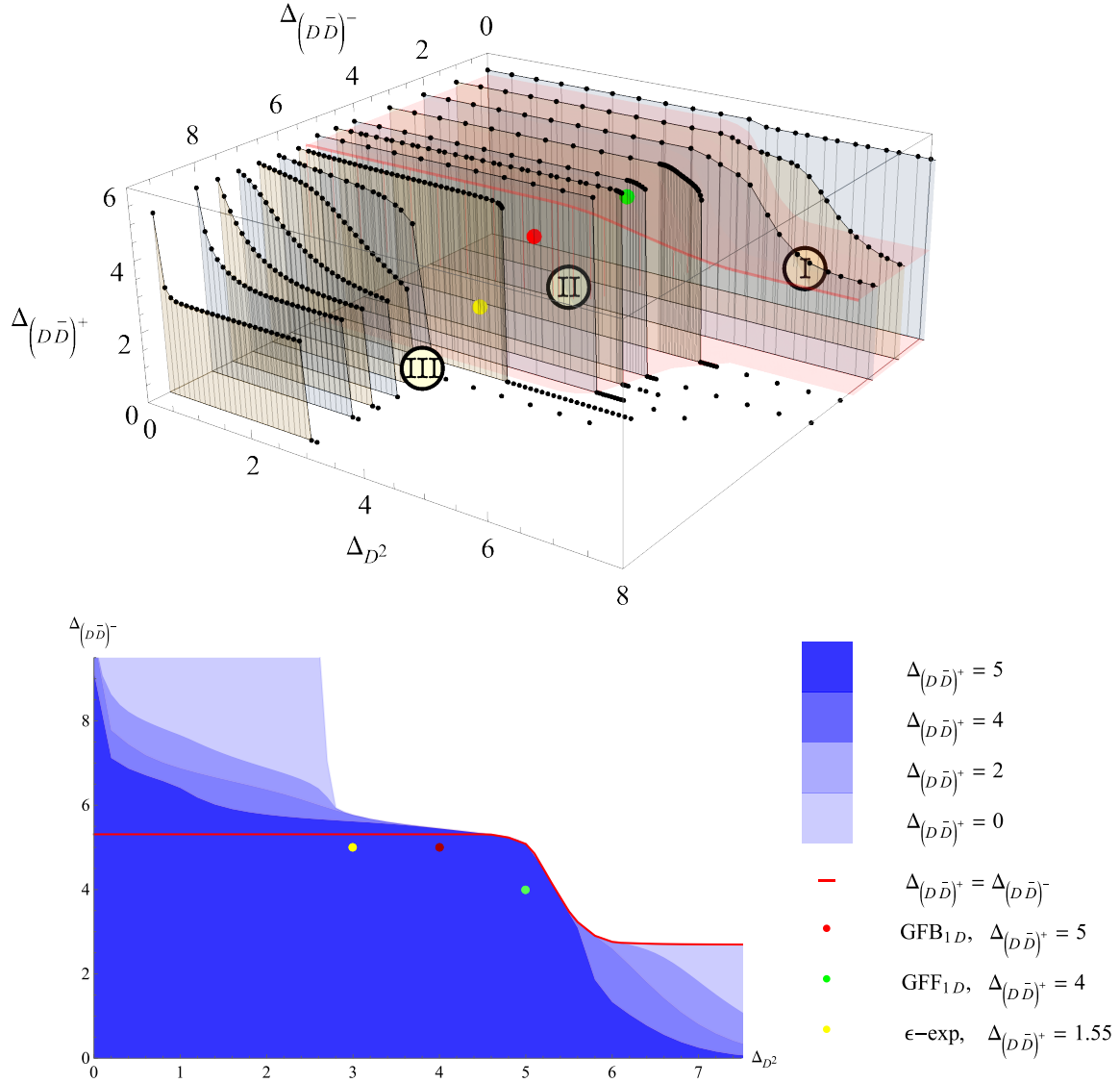


Figure 5.1: (a) Upper bounds on the dimension of the  $\mathcal{S}$ -parity even scalar  $(D\bar{D})^+$  as a function of the  $\mathcal{S}$ -parity odd operator  $(D\bar{D})^-$  and the leading charged operator  $D^2$ . (b) Projection of the three-dimensional allowed region in the  $(\Delta_{(D\bar{D})^-}, \Delta_{D^2})$  plane for different values of  $\Delta_{(D\bar{D})^+}$ . All points are computed with  $\Lambda = 33, P = 53$ . The green and red dots correspond to the GFF and GFB solutions respectively. The yellow dot is the extrapolation to  $\epsilon = 1$  of the  $\epsilon$ -expansion predictions for the magnetic line defect. The solid red line in (b) is the ‘agnostic’ bound for  $\Delta_{(D\bar{D})^+} = \Delta_{(D\bar{D})^-}$ .

- II. This is the region with intermediate values of  $\Delta_{(D\bar{D})^-} \simeq 3 \div 5$ . The upper bound remains constant for  $\Delta_{D^2} \lesssim 6$ , while it drops to zero for  $\Delta_{D^2} \gtrsim 6$ . These vertical drops can be interpreted as an upper bound on the dimension of  $\Delta_{D^2}$  as a function on the gap on  $\Delta_{(D\bar{D})^-}$ . As we increase the gap on  $\Delta_{(D\bar{D})^-}$ , the upper bound on  $\Delta_{D^2}$  becomes stronger. This region includes the GFF and GFB solutions – see eq. (5.2.20)– which are indicated in the figure by green and red dots respectively, as well as the (extrapolated)  $\varepsilon$ -expansion prediction for the magnetic line defect – see eqs. (5.3.14) and (5.3.65) – which is  $(\Delta_{D^2}, \Delta_{(D\bar{D})^-}, \Delta_{(D\bar{D})^+}) \simeq (3, 5, 1.55)$  and is marked in yellow. Interestingly, the yellow dot is close to saturating the upper bound on  $\Delta_{(D\bar{D})^-}$ , as can be seen more clearly from figure 5.1(b). The  $U(1)_F$  monodromy defect should also live in this region, and it would be interesting to verify this by computing e.g. the correlator  $\langle D\bar{D}\bar{D}\bar{D} \rangle$  at the first non-trivial order in the  $\varepsilon$ -expansion.
- III. This is the region with the strongest  $\Delta_{(D\bar{D})^-}$  gap assumptions, i.e.  $\Delta_{(D\bar{D})^-} \simeq 5 \div 8$ . As we enter this region from region II, we observe that for values  $6 \lesssim \Delta_{(D\bar{D})^-} \lesssim 7$ , the convexity of the bound changes and a plateau starts forming as we move towards small values of  $\Delta_{D^2}$ . If we increase  $\Delta_{(D\bar{D})^-}$  further, the plateau terminates around  $(\Delta_{D^2}, \Delta_{(D\bar{D})^+}) \simeq (2.7, 2.7)$ . The plateau happens to have the same height  $\Delta_{(D\bar{D})^+} \simeq 2.7$  as the bound for large  $\Delta_{D^2}$  in region I. This indicates that there is a universal upper bound  $\Delta_{(D\bar{D})^+} \simeq 2.7$  when increasing the gaps on the dimensions of all other operators.

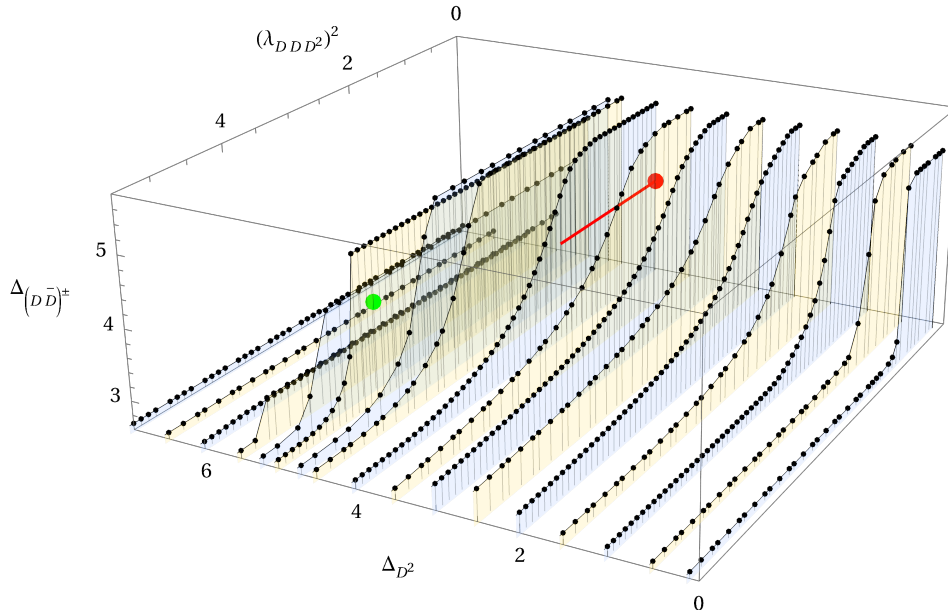


Figure 5.2: Bounds on the dimension of the first singlet in the  $D \times \bar{D}$  OPE as a function of the gap on the dimension  $\Delta_{D^2}$  and the OPE coefficient  $(\lambda_{DDD^2})^2$  of the first charged operator in the  $D \times D$  OPE. The parity-even and -odd singlets are set to have the same gap:  $\Delta_{(D\bar{D})^+} = \Delta_{(D\bar{D})^-}$ . The green and red dots correspond to the solutions for GFF and GFB, respectively.  $\Lambda = 49, P = 69$ .

**Including the OPE coefficient of  $D^2$ .** The light-red curve in figure 5.1 shows a family of solutions to crossing that maximize the gap on the lowest-lying operator in the

singlet channel. This curve looks rather smooth in figure 5.1. To further investigate this family of solutions, we repeat the gap maximization procedure but this time we keep  $\Delta_{(\text{D}\bar{\text{D}})^+} = \Delta_{(\text{D}\bar{\text{D}})^-}$  and varying both  $\Delta_{\text{D}^2}$  and the (squared) OPE coefficient  $(\lambda_{\text{D}\bar{\text{D}}\text{D}^2})^2$ . This OPE coefficient is the most straightforward to implement, and a similar choice was made in [74, 32]. The results are shown in figure 5.2, whose features we now describe. The free theory solutions are marked in the figure by green (GFF) and red (GFB) dots. We recall that these free theory solutions are given in eqs. (5.2.19) and (5.2.20), where it is shown that the OPE coefficients depend on the parameter  $\alpha$ , which is  $\alpha = -1$  for GFF and  $\alpha = 1$  for GFB. The red line in the figure represents the solutions for intermediate  $\alpha \in (-1, 1)$ ; it is well inside the allowed region and appears to be parallel to the upper bound. The GFF solution lies outside the red line, which can be understood from the fact that for an anti-commuting fermion  $\psi_a$ , the leading symmetric traceless representation in the  $\psi_a \times \phi_b$  OPE is  $\psi_a \partial_\tau \psi_b$  and has scaling dimension  $2\Delta_\psi + 1 = 5$ , while for a boson  $\phi_a$  it is  $\phi_a \phi_b$  and has scaling dimension  $2\Delta_\phi = 4$ . A family of rising kinks appears for values around  $\Delta_{\text{D}^2} \simeq 5$ , i.e. close to the GFF solution. Although we have not studied the evolution of these kinks when increasing the number of derivatives, it is plausible that they can be explained by the vicinity of the GFF solution. For  $\Delta_{\text{D}^2} \gtrsim 5$ , the bound on  $\Delta_{(\text{D}\bar{\text{D}})^\pm}$  quickly drops to the value  $\Delta_{(\text{D}\bar{\text{D}})^\pm} \simeq 2.7$ . For  $\Delta_{\text{D}^2} \lesssim 5$ , the kinks move towards smaller values of  $(\lambda_{\text{D}\bar{\text{D}}\text{D}^2})^2$  until around  $\Delta_{\text{D}^2} \simeq 4$  and below, the upper bound becomes completely smooth. The magnetic line defect lies well inside the allowed region, since for this defect the first parity-even singlet has dimension  $\Delta_{(\text{D}\bar{\text{D}})^+} \simeq 1.55$ .

### Single-correlator with the tilt operator

Next, we consider the four-point functions of the tilt operator  $t$ . We recall that  $t$  is a defect primary of scaling dimension  $\Delta_t = 1$ , transforming as a vector of  $O(2)_F$  and neutral under  $SO(2)_T$  (see section 5.2.2). This means that unlike the displacement bootstrap, here we are imposing the existence of a global symmetry  $O(2)_F$ , although we cannot distinguish between one-dimensional conformal defects with different co-dimension. In the complex notation of section 5.2.2, the two non-equivalent orderings along the line are

$$\langle t(\tau_1)t(\tau_2)\bar{t}(\tau_3)\bar{t}(\tau_4) \rangle, \quad \langle t(\tau_1)\bar{t}(\tau_2)t(\tau_3)\bar{t}(\tau_4) \rangle. \quad (5.4.2)$$

The leading non-identity defect primaries in the  $t \times \bar{t}$  OPE are denoted  $(t\bar{t})^\pm$  in the conventions of section 5.2.2, while the leading primary in the  $t \times t$  OPE is denoted  $t^2$ . The bootstrap equations can be obtained from eq. (5.2.18), setting  $\Delta_t = 1$  as external dimensions.

**Gap bounds.** Here we ask the same question as for the single-correlator displacement bootstrap, namely what is the upper bound on the scaling dimension of the leading  $\mathcal{S}$ -parity even scalar  $\Delta_{(t\bar{t})^+}$  as we vary  $\Delta_{t^2}$  and  $\Delta_{(t\bar{t})^-}$ . The results are shown in the 3d plot of figure 5.3(a), where the light-red shaded region represents the ‘agnostic’ bound obtained by imposing the same gap on the  $\mathcal{S}$ -parity odd and  $\mathcal{S}$ -parity even scalars, and in figure 5.3(b). Not surprisingly, these plots show many similarities with those in figure 5.1 because we used the same crossing equations, although for different external scaling dimensions. What changes is the interpretation of the results. There are three notable regions in 5.3(a):

- I. This is the region with the weakest  $\Delta_{(t\bar{t})^-}$  gap assumptions, i.e.  $\Delta_{(t\bar{t})^-} \simeq 0 \div 1.5$ . In this region the upper bound is saturated by the ‘agnostic’ bound for both small

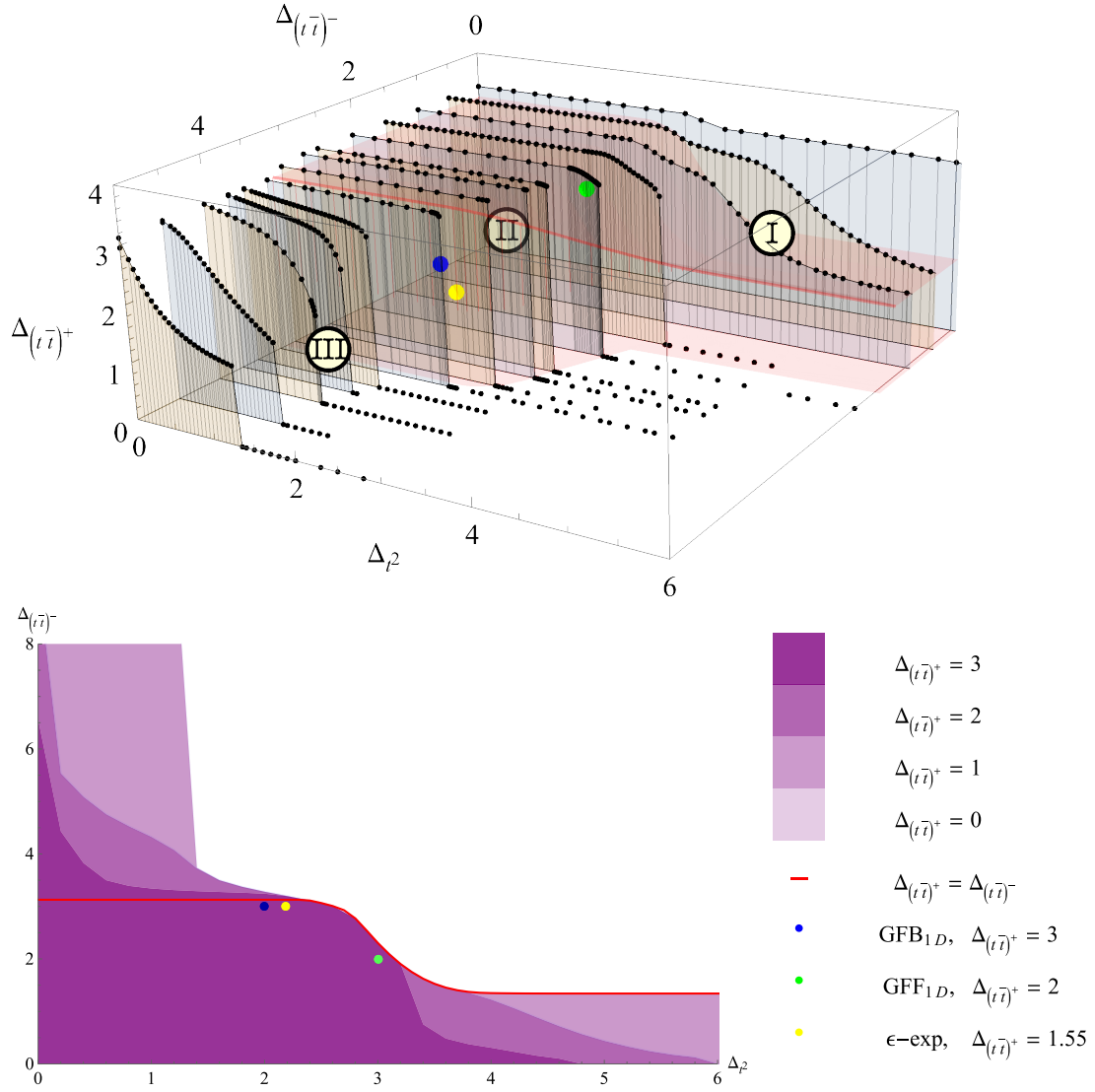


Figure 5.3: Bounds on the maximal gap on the dimension of the  $\mathcal{S}$ -parity even scalar  $(t\bar{t})^+$  (a) or  $\mathcal{S}$ -parity odd scalar  $(t\bar{t})^-$  (b) vs. the  $\mathcal{S}$ -parity odd (a) or even (b) scalar gap vs. the gap on the leading charged operator  $t^2$ .  $\Lambda = 33, P = 53$ . The green and blue dots correspond to the solutions for GFF and GFB, respectively. The yellow dot is the 1-loop  $\epsilon$ -expansion prediction for the magnetic line defect discussed in section 5.3.2. The solid red line in (b) is the ‘agnostic’ bound for  $\Delta_{(t\bar{t})^+} = \Delta_{(t\bar{t})^-}$ .

and large values of  $\Delta_{t^2}$ , which approaches the GFF bound for a real fermion  $\Delta_{(t\bar{t})} = 2\Delta_t + 1 = 3$  for  $\Delta_{t^2} < 2$  (cf. previous discussion in the displacement bootstrap). At around  $\Delta_{t^2} \simeq 3$ , the bound drops but remains smooth.

II. This is the region with intermediate values of  $\Delta_{(t\bar{t})^-} \simeq 1.5 \div 3.5$ . For  $\Delta_{t^2} \lesssim 3$ , the upper bound still approaches the GFF bound at  $\Delta_{(t\bar{t})} = 3$ . For  $\Delta_{t^2} \gtrsim 3$  the bound drops to zero, with increasingly sharper drops until  $\Delta_{(t\bar{t})^-} = 3$ , after which the drops remain but become smoother. As we noted previously, these vertical drops are due to the existing upper bound on  $\Delta_{t^2}$ , as a function of  $\Delta_{(t\bar{t})^-}$ . This region also contains the GFF (green) and GFB (blue) solutions – see eqs. (5.2.19) and (5.2.20) –, as well as the  $\varepsilon$ -expansion results  $(\Delta_{t^2}, \Delta_{(t\bar{t})^-}, \Delta_{(t\bar{t})^+}) \simeq (2 + 2/11, 3, 1.55)$  for the magnetic line defect (see section 5.3.2) which are shown as a yellow dot.<sup>12</sup> The  $\varepsilon$ -expansion results are close to saturating the bootstrap bound at  $\Delta_{(t\bar{t})^-} \simeq 3.2$ , which can be most clearly seen in figure 5.3(b). It would be very interesting to know the sign of the  $\mathcal{O}(\varepsilon^2)$  correction to the scaling dimension of  $(t\bar{t})^-$  in the magnetic line defect.

III. This is the region with the largest  $\Delta_{(t\bar{t})^-}$  gap, i.e.  $\Delta_{(t\bar{t})^-} \simeq 3.5 \div 5$ . The convexity of the bound changes for  $4 \lesssim \Delta_{(t\bar{t})^-} \lesssim 5$ . The plateau that was clearly visible in the same region in figure 5.1 also appears here once we move towards small values of  $\Delta_{t^2}$ , but it is less pronounced. For higher  $\Delta_{(t\bar{t})^-}$ , the plateau again terminates around  $(\Delta_{t^2}, \Delta_{(t\bar{t})^+}) \simeq (1.35, 1.35)$ . This is the same height  $\Delta_{(t\bar{t})^+} \simeq 1.35$  as the bound for large  $\Delta_{t^2}$  in region I, which can again be thought of as a universal upper bound on  $\Delta_{(t\bar{t})^+}$ . These kinks are reflected in figure 5.3(b) around  $\Delta_{t^2} \sim 1.35$ . The bound on  $\Delta_{(t\bar{t})^-}$  becomes infinite for  $\Delta_{(t\bar{t})^+} \lesssim 2$  and  $\Delta_{t^2} \lesssim 1.35$ , while it is saturated by the agnostic  $\Delta_{(t\bar{t})^+} = \Delta_{(t\bar{t})^-}$  bound for  $\Delta_{t^2} > 1.35$ .

**Including the OPE coefficient of  $t^2$ .** The  $\varepsilon$ -expansion results for the magnetic line defect from section 5.3.2 are close to saturating the bound in figure 5.3. However, since we do not know the sign of the  $\mathcal{O}(\varepsilon^2)$  correction on  $\Delta_{(t\bar{t})^-}$ , we cannot predict if the point will move closer or further away from the bound. Let us focus on the agnostic bound and impose the same gap on  $\Delta_{(t\bar{t})^+}$  and  $\Delta_{(t\bar{t})^-}$ . Similarly to what we did for the displacement bootstrap, we look for bounds on  $\Delta_{(t\bar{t})^\pm}$  as a function of  $(\lambda_{ttt^2})^2$  – the (squared) OPE coefficient of the first charged operator  $t^2$  – and  $\Delta_{t^2}$ . The results are shown in figure 5.4. The free theory solutions shown in green (GFF), and blue (GFB) – see eqs. (5.2.19) and (5.2.20) – are close to saturating the bound. Again, the GFF solution ( $\alpha = -1$ ) is disconnected from the GFB solution ( $\alpha = 1$ ) and the solution for  $\alpha \in (-1, 1)$  (cf. previous discussion). The  $\varepsilon$ -expansion result up to  $\mathcal{O}(\varepsilon)$  for the magnetic line defect given by  $((\lambda_{ttt^2})^2, \Delta_{t^2}, \Delta_{(t\bar{t})}) \simeq (2 - \frac{4}{11}, 2 + \frac{2}{11}, 1.55)$  – see eqs. (5.3.14), (5.3.17), (5.3.53) – and marked with the yellow dot in the figure is below the upper bound. There are additional kinks for  $2 \lesssim \Delta_{t^2} \lesssim 4$  around  $(\lambda_{ttt^2})^2 \simeq 2$ , one of which gets saturated by the GFF solution. For  $\Delta_{t^2} \gtrsim 4$  the bound becomes horizontal and settles at  $\Delta_{(t\bar{t})^\pm} \simeq 1.35$ .

<sup>12</sup>Here, the leading  $\mathcal{S}$ -parity even singlet is  $(t\bar{t})^+ = \phi_1$ , with scaling dimension  $\simeq 1.55$ , see eq. (5.2.19).

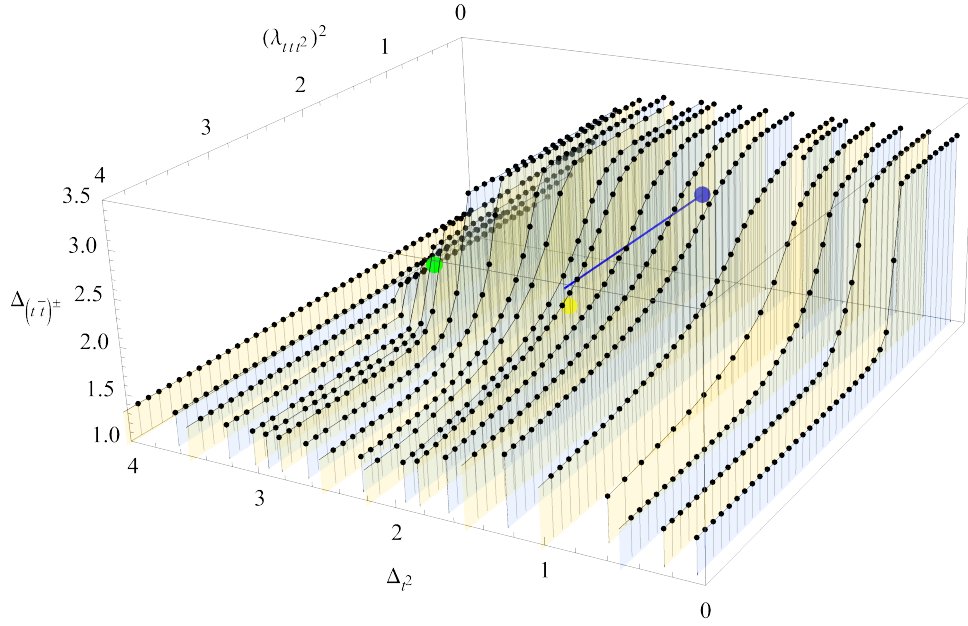


Figure 5.4: Bounds on the dimension of the first singlet in the  $t \times \bar{t}$  OPE as a function of the gap on the dimension  $\Delta_{t^2}$  and the OPE coefficient  $(\lambda_{tt^2})^2$  of the first operator charged under  $O(2)_F$  in the  $t \times t$  OPE. The gaps on the dimension of the parity-even and -odd operators are set to be equal. The free theory solutions GFF (green), GFB (blue), and their interpolation (blue), presented in eqs. (5.2.19) and (5.2.20) are also shown, as is the  $\varepsilon$ -expansion result for the magnetic line defect discussed in section 5.3.2 (yellow).  $\Lambda = 49, P = 69$ .

### Mixed-correlator with tilt and displacement

After having analyzed the single correlators of either the tilt or the displacement operators, we consider mixed correlators that involve both at the same time:

$$\langle D(\tau_1)\bar{D}(\tau_2)D(\tau_3)\bar{D}(\tau_4) \rangle, \quad \langle t(\tau_1)\bar{t}(\tau_2)t(\tau_3)\bar{t}(\tau_4) \rangle, \quad \langle D(\tau_1)\bar{D}(\tau_2)t(\tau_3)\bar{t}(\tau_4) \rangle. \quad (5.4.3)$$

plus all other non-equivalent orderings. This is the natural system of correlators to study the magnetic line defect for the  $O(3)$  vector model, which features a tilt operator in the vector representation of  $O(2)_F$ , as well as a displacement in the vector of  $SO(2)_T$ . The bootstrap equations can be found in eq. (5.2.22).

**Gap bounds.** There are several operators one can study with these crossing equations. On the one hand, we have the leading non-identity  $\mathcal{S}$ -parity even primary  $\mathcal{O}^+$  which appears both in the  $t \times \bar{t}$  and the  $D \times \bar{D}$  OPEs. On the other hand, there are the leading  $\mathcal{S}$ -parity odd primaries  $(t\bar{t})^-$  and  $(D\bar{D})^-$ , which are in general different to each other. Finally, there is the lowest-lying  $O(2)_F \times SO(2)_T$  vector in the  $t \times D$  channel

$$t \times D \sim (tD)^\pm + \dots, \quad (5.4.4)$$

where the superscript  $\pm$  denotes the  $\mathcal{S}$  parity of the operator. In figure 5.5 we compute the upper bound on  $\Delta_{\mathcal{O}^+}$ , while assuming gaps on the scaling dimensions of  $(t\bar{t})^-$ ,  $(tD)^\pm$  keeping  $\Delta_{(tD)^+} = \Delta_{(tD)^-}$ . We take all other gaps to be very close to the unitarity bound, concretely we set them to  $\Delta > 0.001$ . If we are interested in the most ‘agnostic’ bound with  $\Delta_{\mathcal{O}^+} = \Delta_{(t\bar{t})^-}$ , then the allowed region shrinks to the light-red region of figure 5.5,

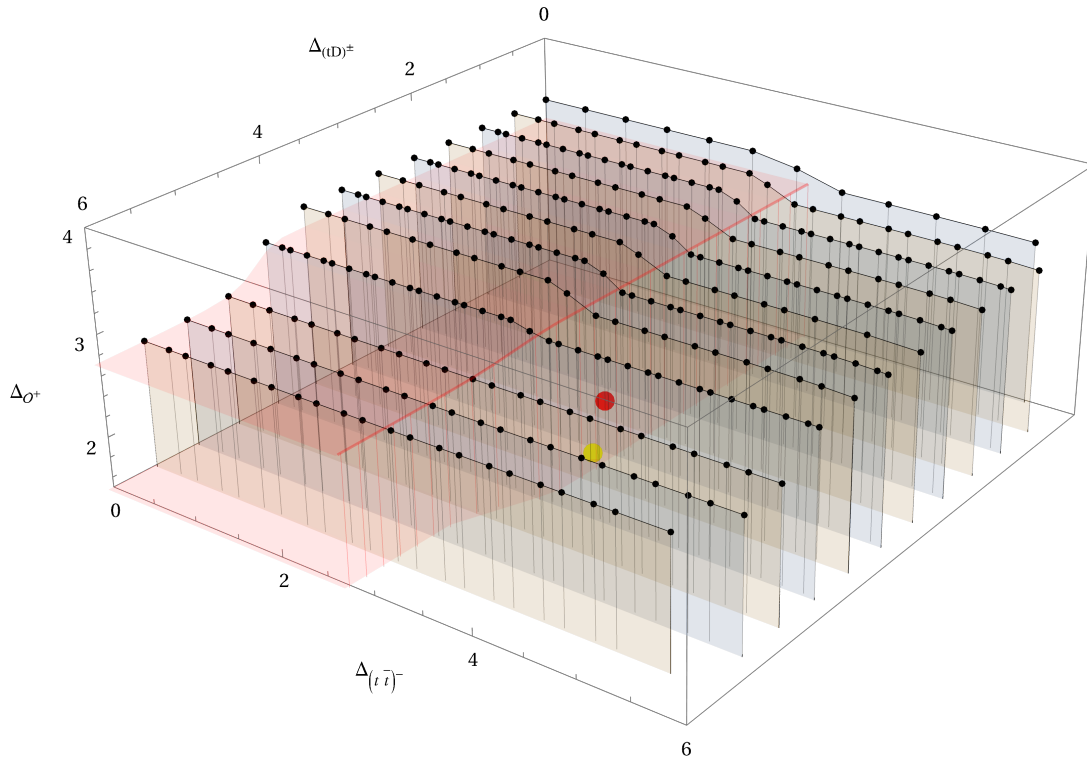


Figure 5.5: Bounds on the dimension of the first  $\mathcal{S}$ -parity even singlet  $\mathcal{O}^+$  in the  $t \times \bar{t}$  and the  $D \times \bar{D}$  OPEs as a function of the scaling dimension of  $(tD)^\pm$  and  $(\bar{t}\bar{t})^-$ . The GFB solution, given in eq. (5.2.25), is shown in red. The  $\varepsilon$ -expansion results for the magnetic line defect are given in yellow. The light-shaded region represents the results for the agnostic bound  $\Delta_{(\bar{t}\bar{t})^+} = \Delta_{(\bar{t}\bar{t})^-}$ .  $\Lambda = 33, P = 63$ .

which contains both the GFB (red dot) and the  $\varepsilon$ -expansion result for the magnetic line defect. The latter is far from saturating the upper bound and it seems hard to make progress without further assumptions. We will come back to this issue in section 5.4.3. The bounds are very uniform and show two drops, one in the  $\Delta_{(\bar{t}\bar{t})^-}$  direction around  $\Delta_{(\bar{t}\bar{t})^-} \simeq 3$  and one in the  $\Delta_{(tD)^\pm}$  direction around  $\Delta_{(tD)^\pm} \simeq 5$ . For  $\Delta_{(tD)^\pm} \gtrsim 5$  the bound on  $\Delta_{\mathcal{O}^+}$  becomes flat and approaches the value  $\Delta_{\mathcal{O}^+} \simeq 2.7$ , a result we already found in the single-correlator bootstrap of the displacement operator of section 5.4.1. In the upper ‘cubic-shaped’ region we have that  $\Delta_{\mathcal{O}^+} \lesssim 3.4$ , which approaches the bound for a real GFF  $\Delta_{\mathcal{O}^+} = 3$ .

**Including one OPE coefficient.** In sections 5.4.1 and 5.4.1 we have seen that including one OPE coefficient leads to interesting bounds. We repeat this strategy here and bound  $(\lambda_{tD(tD)^+})^2$  while varying the gap  $\Delta_{(tD)^\pm}$  in the agnostic region  $\Delta_{(\bar{t}\bar{t})^+} = \Delta_{(\bar{t}\bar{t})^-}$ . It turns out that  $(\lambda_{tD(tD)^+})^2$  is unbounded for  $\Delta_{\mathcal{O}^+} \lesssim 2.7$ . Above this value and for  $\Delta_{\mathcal{O}^+} \lesssim 3.4$  there exists an upper bound which is shown in figure 5.6, while for  $\Delta_{\mathcal{O}^+} \gtrsim 3.4$  the upper bound  $(\lambda_{tD(tD)^+})^2$  becomes negative, consistently with the results shown in figure 5.5. Since we are assuming a gap on the lowest operator  $\Delta_{(tD)^\pm}$ , but do not make any assumptions on the scaling dimension of the next operator in the  $t \times D$  OPE, the lower bound on  $(\lambda_{tD(tD)^+})^2$  is at zero. The  $\varepsilon = 1$  solution of the  $\varepsilon$ -expansion for the magnetic line defect is not shown, since it lies far within the bounds in the region where the OPE coefficient  $(\lambda_{tD(tD)^+})^2$  is unbounded.

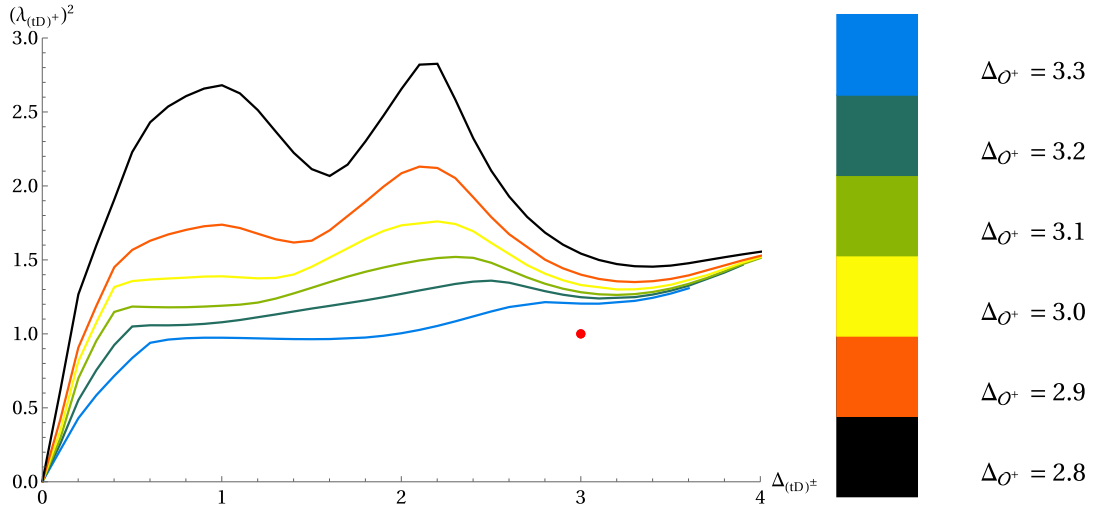


Figure 5.6: Bounds on  $(\lambda_{(tD)^+})^2$  as a function of the scaling dimension of  $\Delta_{(tD)^+}$  and of the scaling dimension of the first parity-even singlet  $\Delta_{O^+}$ . The gap on the dimension  $\Delta_{(tD)^-}$  is set to  $\Delta_{(tD)^+}$ , and all other gaps are set to 0.001. The GFB solution given in eq. (5.2.25) is marked by the red dot.  $\Lambda = 33, P = 63$ .

## 5.4.2 Bootstrapping the monodromy line defect in the $O(2)$ model

The approach adopted so far was agnostic, in that we bounded CFT data without committing to any particular model. In this section we pursue a complementary approach, and combine the numerical bootstrap with the  $\varepsilon$ -expansion with the goal of bootstrapping the monodromy defect in the  $O(2)$  model. Recall from section 5.3.1 two universal features of this monodromy defect: (i) for generic values of the parameter  $v \in [0, 1)$  the flavor symmetry of the model is  $SO(2)_F$ , which gets enhanced to  $O(2)_F$  for  $v = 0, \frac{1}{2}$ ; (ii) the defect spectrum contains a family of  $\mathcal{S}$ -parity even defect primaries  $\Psi_s$  with  $SO(2)_F$  charge  $v$  and transverse spin  $s \in \mathbb{Z} + v$ . These two features can be combined in our numerical bootstrap problem as follows. First, we consider a system of correlation functions that involve the lowest-lying operator with  $SO(2)_F$  charge  $r = v$  and its partner with charge  $r = 1 - v$ . By charge conservation, the non-zero correlation functions are

$$\begin{aligned} \langle \Psi_v(\tau_1) \bar{\Psi}_v(\tau_2) \Psi_v(\tau_3) \bar{\Psi}_v(\tau_4) \rangle, \quad \langle \Psi_{1-v}(\tau_1) \bar{\Psi}_{1-v}(\tau_2) \Psi_{1-v}(\tau_3) \bar{\Psi}_{1-v}(\tau_4) \rangle, \\ \langle \Psi_v(\tau_1) \bar{\Psi}_{1-v}(\tau_2) \Psi_{1-v}(\tau_3) \bar{\Psi}_v(\tau_4) \rangle, \end{aligned} \quad (5.4.5)$$

which lead to the crossing equations presented in eq. (5.2.24). Although for general  $v$  the monodromy defect is not invariant under  $O(2)_F$  symmetry, but only under  $SO(2)_F$  symmetry, we can use the same crossing equations in both cases. The justification for this appeared in [19], but we repeat it here for convenience. The tensor  $\epsilon_{ij}$  is invariant under  $SO(2)$  but not under  $O(2)$ , so the antisymmetric representation is isomorphic to the singlet representation for  $SO(2)$  but not for  $O(2)$ . However, this does not lead to additional relations in the crossing equations, because even when the singlet and antisymmetric representations are isomorphic, we can distinguish them since they contain  $\mathcal{S}$ -parity even and odd operators respectively.

Second, we input the scaling dimensions of  $\Psi_s$  using the predictions from the  $\varepsilon$ -expansion in eq. (5.3.7), extrapolated to  $\varepsilon = 1$ . With this input, we put an upper bound



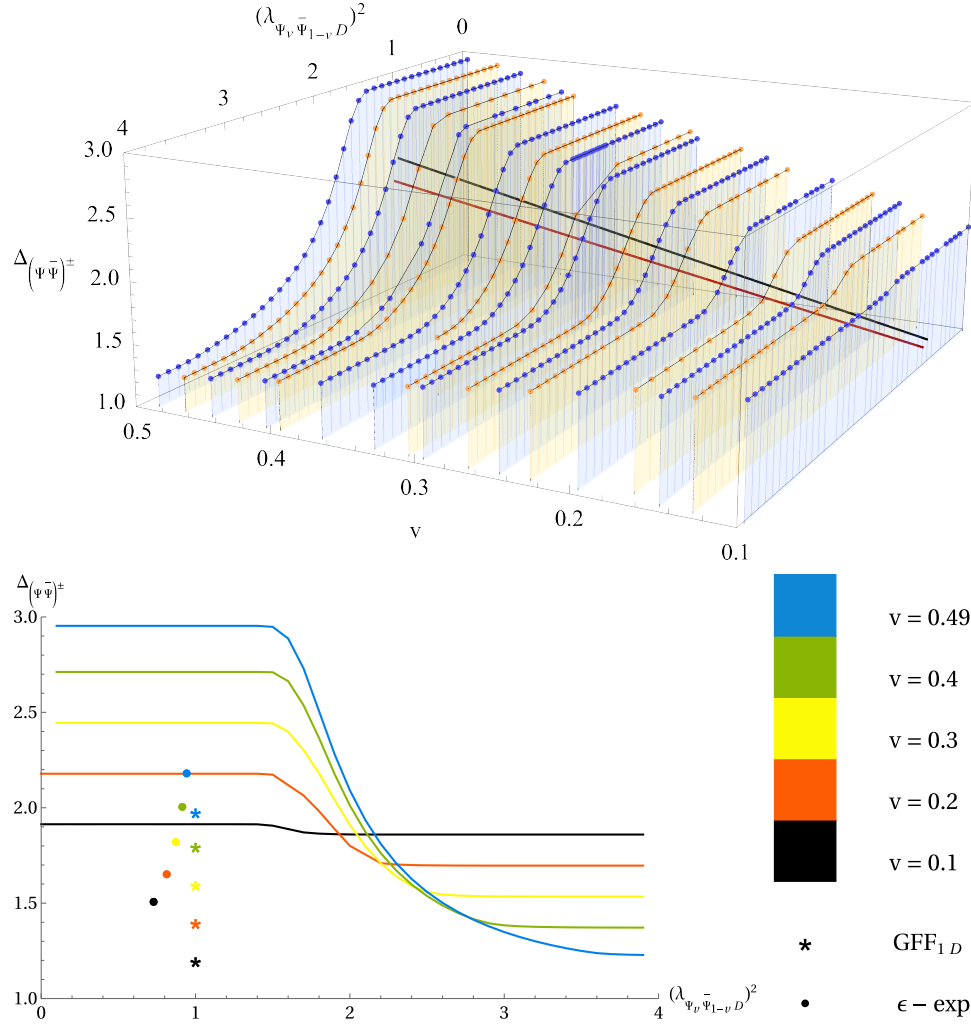


Figure 5.7: Bounds on the dimension of the first singlet in the  $\Psi_s \times \bar{\Psi}_s$  OPE  $\Delta_{(\Psi\bar{\Psi})^+}$  versus the OPE coefficient of the displacement operator and the monodromy  $v$ . The gaps on the dimension of the lowest-lying operators in all other channels is set to the unitarity bound. Parity-even and odd operators are set to have the same gaps. The gray line corresponds to the  $\epsilon$ -expansion results.  $\Lambda = 21, P = 41$ .

to the dimension of the lowest-lying operator in  $\Psi_s \times \bar{\Psi}_s$ , i.e.

$$\Psi_s \times \bar{\Psi}_s = \mathbb{1} + (\Psi\bar{\Psi})^\pm + \dots, \quad s = v, \text{ or } v - 1. \quad (5.4.6)$$

Note that  $(\Psi\bar{\Psi})^\pm$  is a singlet under  $SO(2)_T \times SO(2)_F$ , and it could be either  $\mathcal{S}$ -parity even or  $\mathcal{S}$ -parity odd. For the  $\Psi_v \times \bar{\Psi}_{v-1}$  OPE we assume the lowest-lying operator is the displacement operator, which is  $\mathcal{S}$ -parity even. We will further assume that there is no operator in the  $\mathcal{S}$ -parity odd channel with dimension smaller than the displacement, namely:

$$(\Psi_v \times \bar{\Psi}_{v-1})^+ = D + \dots, \quad (\Psi_v \times \bar{\Psi}_{v-1})^- = (\Psi_v \bar{\Psi}_{v-1})^- + \dots, \quad \Delta_{(\Psi_v \bar{\Psi}_{v-1})^-} \geq 2. \quad (5.4.7)$$

These assumptions are true in the  $\varepsilon$ -expansion, where one can see at leading order that the displacement operator appears in the OPE with the expected dimension  $\Delta_D = 2$ , see appendix D for more details.

In figure 5.7 we plot the upper bound on  $\Delta_{(\Psi\bar{\Psi})^\pm}$  as a function of the  $SO(2)_F$  charge  $v$  and the OPE coefficient of the displacement operator  $(\lambda_{\Psi_v \bar{\Psi}_{1-v} D})^2$ . Let us stress that  $v$  enters the crossing equations through the dimension of the external operators, which we take to be the  $\varepsilon$ -expansion prediction (5.3.7). Furthermore, since the crossing equations in eq. (5.4.5) are invariant under  $v \leftrightarrow 1 - v$ , it suffices to consider the range  $0 < v \leq 1/2$ , where the limiting case  $v = 1/2$  corresponds to the  $\mathbb{Z}_2$  twist defect studied in [74]. In the figure we observe a family of drops as we move along the  $(\lambda_{\Psi_v \bar{\Psi}_{1-v} D})^2$  direction, and as we increase  $v$  towards  $v = 1/2$  these drops become sharper and move slightly to the right. It is promising that the  $\varepsilon$ -expansion results are above and left of the free theory solutions, because this makes it possible for the theoretical prediction to saturate the bound. However, for the results with  $\Lambda = 21$  derivatives shown in figure 5.7(b), both the  $\varepsilon$ -expansion result and the free theory solution are still somewhat far from saturating the numerical bound.

One possibility that we explore in figure 5.8 is whether increasing the number of derivatives can bring the bound closer to the analytical prediction. For concreteness we focus on  $v = 1/3$ ,<sup>13</sup> and we increase the number of derivatives to  $\Lambda = 33$ . We observe that the kink moves slightly towards the left of the plot, but remains somewhat far from the analytical prediction. Another possibility is that one needs to consider less agnostic gap assumptions in the channels besides  $\Psi_v \times \bar{\Psi}_{1-v}$ , or perhaps higher-order corrections from the  $\varepsilon$ -expansion are needed to reconcile theory and numerics. In either case, this provides a good motivation for a more detailed study of monodromy defects using the  $\varepsilon$ -expansion, to which we hope to come back in future work.

### 5.4.3 Bootstrapping the localized magnetic field line defect

This section studies the magnetic line defect of [84] in the bulk  $O(3)$  CFT, combining the numerical bootstrap with the  $\varepsilon$ -expansion results of section 5.3.2. There are two features of the magnetic line defect which are important in our analysis: (i) the model is invariant under a  $O(2)_F \subset O(3)$  flavor symmetry and, (ii) the defect spectrum features a tilt operator  $t$  transforming in the vector representation of  $O(2)_F$ . To exploit these

<sup>13</sup>The choice  $v = 1/3$  is particularly interesting for its connection to half-BPS defects in superconformal field theories. For example, we expect that the monodromy defect for the Wess-Zumino model [78] preserves supersymmetry whenever  $v = 1/3$ .

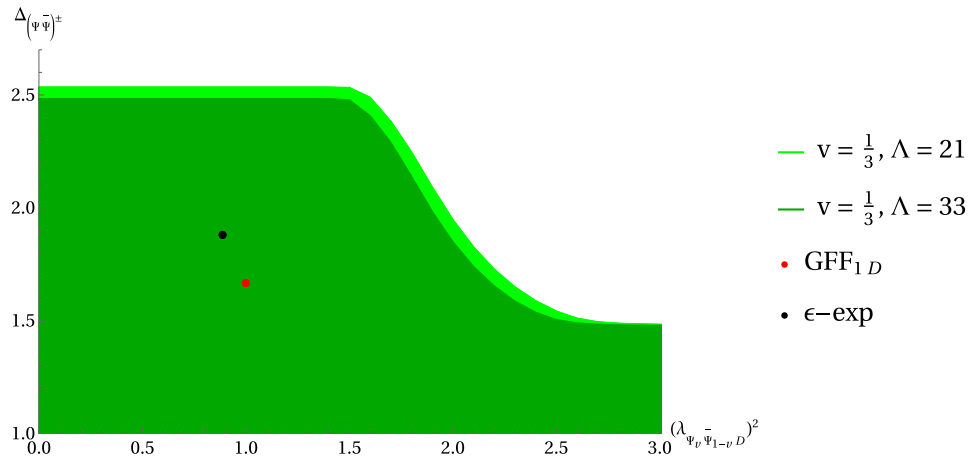


Figure 5.8: Bounds on the dimension of the first singlet in the  $\Psi_s \times \bar{\Psi}_s$  OPE  $\Delta_{(\Psi\bar{\Psi})^\pm}$  versus the OPE coefficient of the displacement operator  $(\lambda_{\Psi_v \bar{\Psi}_{1-v} D})^2$ .  $v = \frac{1}{3}$  and the gaps on the dimension of the lowest-lying operators in all other channels are set to the unitarity bound. Parity-even and odd operators are set to have the same gaps.  $\Lambda = 21, P = 41$  and  $\Lambda = 33, P = 53$ .

features, we consider a bootstrap problem involving the tilt  $t$  and the lowest-dimension neutral scalar  $\phi_1$ , so we consider the correlation functions

$$\begin{aligned} &\langle \phi_1(\tau_1)\phi_1(\tau_2)\phi_1(\tau_3)\phi_1(\tau_4) \rangle, \quad \langle t(\tau_1)\bar{t}(\tau_2)t(\tau_3)\bar{t}(\tau_4) \rangle, \\ &\langle \phi_1(\tau_1)\phi_1(\tau_2)t(\tau_3)\bar{t}(\tau_4) \rangle, \end{aligned} \quad (5.4.8)$$

plus all other non-equivalent orderings. The corresponding crossing equations are given in eq. (5.2.23).<sup>14</sup> There are five OPE channels that enter in our discussion

$$\begin{aligned} \phi_1 \times \phi_1 &\sim \mathbb{1} + \phi_1 + s_- + \dots, \quad (t \times \bar{t})^+ \sim \mathbb{1} + \phi_1 + s_- + \dots, \\ (t \times \bar{t})^- &\sim A + \dots, \quad t \times t \sim T + \dots, \quad t \times \phi_1 \sim t + V + \dots, \end{aligned} \quad (5.4.9)$$

where further details on the operators exchanged can be found in section 5.3.2. Note that the external operators are exchanged in some of the fusion channels, which allows us to impose the extra relations  $\lambda_{\phi_1 \bar{t} t} = \lambda_{\bar{t} \phi_1 t}$  in the crossing equations. Furthermore, we impose the following gaps

$$\Delta_{s_-} = 2.36, \quad \Delta_A = 3, \quad \Delta_T = 2.18, \quad \Delta_V = 3.18, \quad (5.4.10)$$

where the values are the  $\mathcal{O}(\epsilon)$  results for the scaling dimensions from eqs. (5.3.15), (5.3.16) and (5.3.17). With these assumptions we bound the scaling dimensions of  $\phi_1$  and  $t$ . Although we could also fix the scaling dimensions of  $t$  and  $\phi_1$  using the perturbative calculation (in particular,  $t$  has protected dimension  $\Delta_t = 1$ ), we keep them unfixed to see how they are constrained by the numerics. This logic is inspired by the search for the Ising model island, where (physically motivated) gap assumptions led to constraints on the external operators  $\sigma$  and  $\epsilon$  [187]. Our results are presented in figure 5.9, where the allowed values in the  $(\Delta_t, \Delta_{\phi_1})$  plane are shown in green.

<sup>14</sup>Since we are not including the displacement operator, this system of correlation functions is agnostic about the co-dimension of the line defect. It will enter only implicitly via our gap assumptions which are determined by the  $\epsilon$ -expansion results of section 5.3.2. The inclusion of the displacement operator is more involved. Nevertheless, it is an interesting extension and we will leave it for future work.

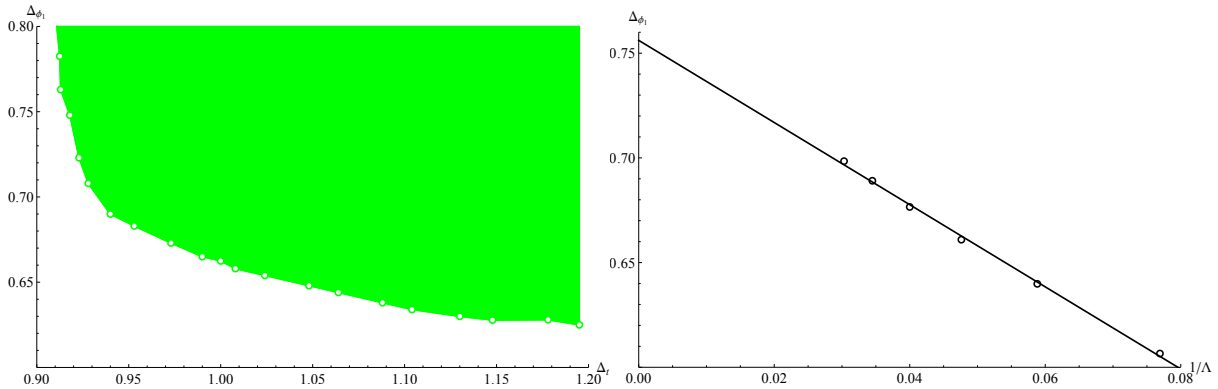


Figure 5.9: Bootstrapping the  $O(3)$ -breaking line defect. In (a), bounds on the scaling dimensions  $\Delta_{\phi_1}$  and  $\Delta_t$  for  $\Lambda = 21$ ,  $P = 41$ . The gaps are given in eq. (5.4.10). Allowed values of  $(\Delta_t, \Delta_{\phi_1})$  are given in green. In (b), the bound on  $\Delta_{\phi_1}$  for  $\Delta_t = 1$  as a function of the number of derivatives  $\Lambda$ , for which a fit is performed.

The lower bound for  $t$  is strikingly close to 1, the numerics seems to be rediscovering the tilt. For this value of  $\Delta_t$ , the bound goes up and cuts out a corner. It should also be noted that there are numerical instabilities in the region with large  $\Delta_{\phi_1}$  outside the range of figure 5.9(a). The lower bound on  $\Delta_{\phi_1}$  is on the other hand weaker, its value being nowhere close to the Padé extrapolation of  $\Delta_{\phi_1} \simeq 1.55$  (and it is even further away from the crude  $\varepsilon$ -expansion result  $\Delta_{\phi_1} = 2 + \mathcal{O}(\varepsilon^2)$ ). It is nevertheless a non-trivial numerical result that such a lower bound exists at all. Note that the magnetic line defect has no relevant operators [84], so  $\Delta_{\phi_1} > 1$  should be expected. Our  $\mathcal{O}(\varepsilon)$  assumptions allow for a weaker numerical bound on  $\Delta_{\phi_1}$ . For the physically interesting value  $\Delta_t = 1$ , figure 5.9(b) displays an extrapolation to infinite number of derivatives of the lower bound, which converges to

$$\Delta_{\phi_1} \gtrsim 0.76. \quad (5.4.11)$$

Again, we cannot completely rule out the region with  $\Delta_{\phi_1} \leq 1$ . It could be that our numerics is not strong enough to rule out the presence of relevant operators, so we should either change our assumptions or include more external operators to the system of eq. (5.4.8). Another possibility which we cannot rule out is the existence of alternative models consistent with our assumptions but with one relevant scalar in the spectrum. Definitely, we think this result calls for a more systematic investigation, which nowadays can be efficiently performed with the help of the *Navigator Function* [127, 128] in order to search for bootstrap islands in a large parameter space. Finally, one may wonder if our gap assumptions allow for upper bounds on  $\Delta_{\phi_1}$  as well. Clearly,  $\Delta_{\phi_1}$  cannot be bigger than  $\simeq 2.36$ , which is when the next operator  $\Delta_{s_-}$  appears, see eq. (5.4.10). Below this threshold there seems to be no upper bound, at least with the current number of derivatives.

**Bounds on OPE coefficients.** Having constrained the region  $(\Delta_{\phi_1}, \Delta_t)$ , we now set  $\Delta_t$  to its physical value of 1, but continue to treat  $\Delta_{\phi_1}$  as an external parameter. The goal is to bound the OPE coefficients  $(\lambda_{t\bar{t}\phi_1})^2$  and  $(\lambda_{\phi_1\phi_1\phi_1})^2$  as functions of  $\Delta_{\phi_1}$ , which in turn were computed in the  $\varepsilon$ -expansion in section 5.3.2, see eqs. (5.3.14) and (5.3.46).

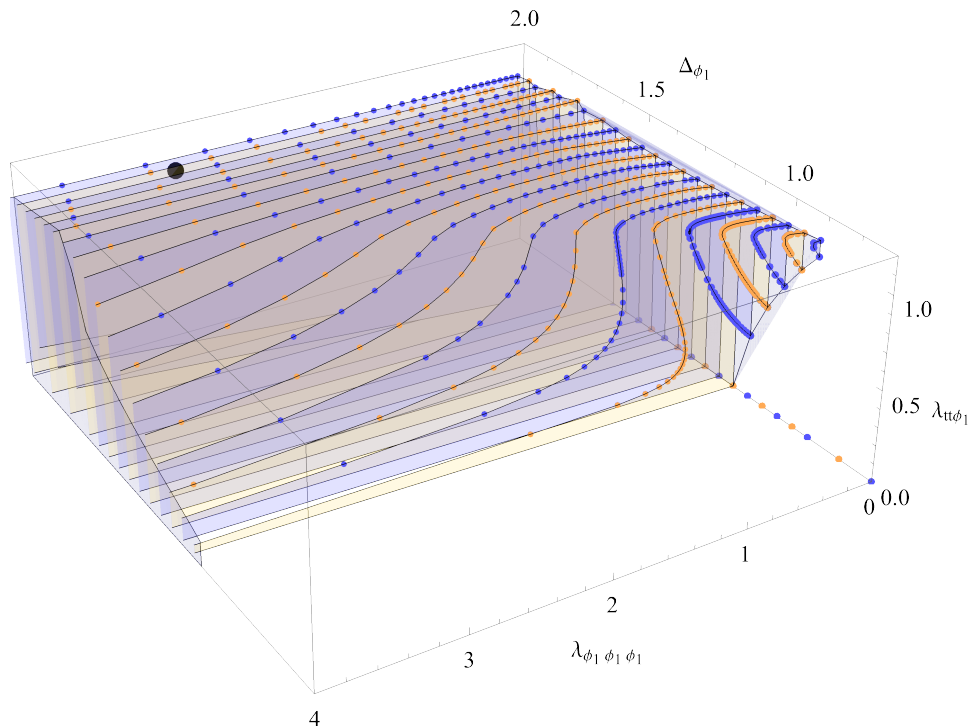


Figure 5.10: Bounds on the OPE coefficients  $\lambda_{t\bar{t}\phi_1}$  and  $\lambda_{\phi_1\phi_1\phi_1}$  as a function of the gap  $\Delta_{\phi_1}$  for the  $O(3)$ -breaking magnetic line defect. The black dot is the prediction from the  $\varepsilon$ -expansion. The gaps are given in eq. (5.4.10).  $\Lambda = 21, P = 41$ .

To this end, we employ the strategy developed in [187], i.e. we introduce the OPE angle  $\theta$  defined as

$$\tan \theta = \frac{\lambda_{\phi_1\phi_1\phi_1}}{\lambda_{t\bar{t}\phi_1}}, \quad (5.4.12)$$

and we search for upper and lower bounds on the quantity  $(\lambda_{\phi_1\phi_1\phi_1})^2 + (\lambda_{t\bar{t}\phi_1})^2$  as a function of  $\theta \in [0, \pi)$  and of  $\Delta_{\phi_1}$ . For concreteness we restrict to the case where  $0 \leq \theta < \frac{\pi}{2}$  (i.e.  $\lambda_{\phi_1\phi_1\phi_1}\lambda_{t\bar{t}\phi_1} \geq 0$ ), which is also compatible with the leading  $\varepsilon$ -expansion prediction. The numerics is of course sensitive to the relative sign only. The results in figure 5.10 show that for any value of the OPE coefficients  $\lambda_{\phi_1\phi_1\phi_1}$  and  $\lambda_{t\bar{t}\phi_1}$ , there is an excluded region which is fully consistent with the lower bound from figure 5.9(a). However, as it turns out, for  $\lambda_{\phi_1\phi_1\phi_1}/\lambda_{t\bar{t}\phi_1} \geq 0$ , the excluded region is larger and exists for  $\Delta_{\phi_1} \lesssim 0.9$ , while for  $\lambda_{\phi_1\phi_1\phi_1}/\lambda_{t\bar{t}\phi_1} \leq 0$ , only values up to  $\Delta_{\phi_1} \lesssim 0.7$  are excluded. For values between  $0.7 \lesssim \Delta_{\phi_1} \lesssim 1.1$ , the upper and lower bounds on  $\lambda_{t\bar{t}\phi_1}$  approach each other until they meet, after which the upper bound goes to zero. This means that certain values of the OPE coefficient  $\lambda_{\phi_1\phi_1\phi_1}$  are ruled out by the numerical bootstrap, even though the corresponding  $\Delta_{\phi_1}$  values are allowed in figure 5.9(a). For  $\Delta_{\phi_1} \gtrsim 1.1$ , the bound on  $\lambda_{t\bar{t}\phi_1}$  is always positive. There is an intriguing feature visible starting around  $\Delta_{\phi_1} \lesssim 0.9$  and continuing until  $\Delta_{\phi_1} \simeq 1.4$ , where the projection onto the  $(\lambda_{\phi_1\phi_1\phi_1}, \lambda_{t\bar{t}\phi_1})$  plane shows a pronounced cusp, see figure 5.11(a). For higher values of  $\Delta_{\phi_1}$  this feature disappears and the plot becomes smooth. For the quadrant where the OPE coefficients have opposite sign this cusp is not present. In order to better understand this feature, we have plotted two slices of the three-dimensional plot in figure 5.11. For figure 5.11(a) we have chosen the value  $\Delta_{\phi_1} = 1.2$  somewhat arbitrarily, in order to highlight a region where the cusp is clearly visible. It appears around  $\lambda_{\phi_1\phi_1\phi_1} \simeq 0.9$ , although its position shifts depending

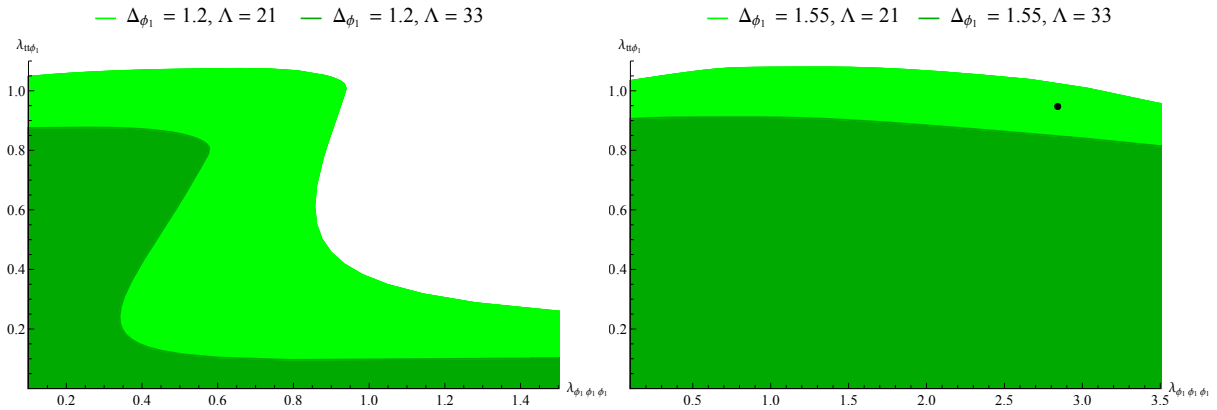


Figure 5.11: Bootstrapping the  $O(3)$ -breaking magnetic line defect. Upper bounds on the OPE coefficient  $\lambda_{\phi_1\phi_1\phi_1}$  as a function of  $\lambda_{t\bar{t}\phi_1}$ .  $\Lambda = 21, P = 41$  and  $\Lambda = 33, P = 63$ . In (a) the external scalar has dimension  $\Delta_{\phi_1} = 1.2$ . In (b) the external scalar has dimension  $\Delta_{\phi_1} = 1.55$ . The  $\varepsilon$ -expansion result is shown by the black dot.

on the value of  $\Delta_{\phi_1}$  and the number of derivatives. In figure 5.11(b) we have chosen  $\Delta_{\phi_1} = 1.55$ , which corresponds to the best estimate of the conformal dimension of  $\phi_1$  using a Padé approximation [84]. For this value of  $\Delta_{\phi_1}$  the features from figure 5.11(a) are gone and the bound is smooth. We have added in figure 5.11(b) the prediction coming from the  $\varepsilon$ -expansion for reference. We should warn the reader that this prediction is valid up to  $\mathcal{O}(\varepsilon)$ , for which  $\Delta_{\phi_1} = 2$ . Our numerical plot was obtained with a different set of assumptions, in particular for  $\Delta_{\phi_1} = 1.55$ , which explains why the dot is outside the numerical exclusion region. One possibility is that the cusp is also present for  $\Delta_{\phi_1} \simeq 1.55$ , but was lost due to numerical precision. Indeed from figure 5.11(a) the feature becomes more pronounced when we jump from  $\Lambda = 21$  to  $\Lambda = 33$  derivatives. It would be remarkable if the numerics could be pushed, such that figure 5.11(b) starts looking more like figure 5.11(a). The position of the cusp would then be a good candidate for the magnetic line defect.

# Chapter 6

## Line defect correlators in fermionic CFTs

### 6.1 Introduction

Our journey started with SCFTs in the presence of a boundary, through line defects with additional global symmetry in bosonic theories, which have a wider range of physical and experimental applications. Now, we move on to study line defects in non-supersymmetric CFTs that include scalar and fermionic fields in  $d = 4 - \varepsilon$  dimensions: the Yukawa CFTs. They are known to describe phase transitions in Dirac and Weyl semimetals, and can be used to e.g. study phase transitions in graphene and surfaces of topological insulators [197]. There are three models most studied in the literature: the Gross–Neveu–Yukawa model, the Nambu–Jona-Lasinio–Yukawa model, and the chiral Heisenberg model. They have an interacting fixed point in  $4 - \varepsilon$  dimensions, and exist for an arbitrary number of Dirac fermions  $N_f$ . They differ by the number of scalars in the model, and subsequently the additional global symmetry they preserve on top of the  $U(N_f)$  symmetry of the fermions.

The *Gross–Neveu–Yukawa* (GNY) model contains a single real scalar and  $N_f$  Dirac fermions. It has a perturbative fixed point in  $4 - \varepsilon$  and is expected to flow to the same three-dimensional universality class as the classic Gross–Neveu (GN) model. The GN model is a fermionic CFT with a four-fermion interaction originally formulated in  $d$  dimensions displaying asymptotic freedom in the large- $N_f$  limit [198], and is believed to have a non-trivial interacting fixed point in  $2 + \varepsilon$  dimensions. In  $d > 2$  dimensions, the GN model is renormalizable in the large- $N_f$  limit [199], but not for finite  $N_f$ . The GNY model can therefore be considered a UV-completion of the GN model [200, 201].<sup>1</sup>

If we consider a complex scalar and  $N_f$  Dirac fermions we obtain the *Nambu–Jona-Lasinio–Yukawa* (NJLY) model. Similarly to the GNY model, the NJLY model can be thought of as a UV completion of the Nambu–Jona-Lasinio (NJL) model [203], a purely fermionic model which exhibits asymptotic freedom in the large- $N_f$  limit and has the same symmetries as QCD. Similarly to the discussion above, in  $d = 3$  both the NJL and NJLY models are expected to describe the same universality class.<sup>2</sup>

With three real scalars we have the *chiral Heisenberg* (cH) model, which has an  $O(3)$

---

<sup>1</sup>For a specific number of fermions,  $N_f = 1/4$ , the interacting fixed point in  $d = 3$  exhibits emergent supersymmetry (SUSY) [173, 202]

<sup>2</sup>This model shows emergent SUSY as well, now for  $N_f = 1/2$  [174]. The SCFT in  $d = 3$  is the Wess-Zumino model with minimal SUSY ( $\mathcal{N} = 2$ ), which was considered with a boundary in chapter 4.

symmetry in addition to the  $U(N_f)$  symmetry of the fermions. This model has been studied less than the GNY and NJLY models in the literature, it is however expected to describe the antiferromagnetic critical point on graphene [204]. The cH model also has a  $d = 2 + \varepsilon$  description known as the  $SU(2)$ -Gross–Neveu model, where the fermion bilinear is contracted with a Pauli matrix (see for example [205]).

It was recently pointed out that all these models admit line defects that can be studied perturbatively [89, 90]. In the  $4 - \varepsilon$  description, the defect is given by an exponential of a scalar field integrated along a line. In  $d = 4$  a free scalar has dimension  $\Delta_\phi = 1$ , which makes the defect coupling marginal, and is therefore a good candidate for describing a non-trivial defect CFT in  $d = 4 - \varepsilon$  dimensions. In [89] (see also [90]) it was shown that this is indeed the case.

It was also pointed out in [89], that the GN model in  $2 + \varepsilon$  dimensions admits a natural line defect defined as the exponential of a fermion bilinear. In  $d = 2$  a free fermion has dimension  $\Delta_\psi = \frac{1}{2}$  and the defect coupling is again marginal. In  $2 + \varepsilon$  dimensions one can find a non-trivial defect CFT which is expected to be in the same universality class as the defect CFT in  $4 - \varepsilon$  dimensions described above. Most likely, this  $d = 2 + \varepsilon$  picture of the defect can also be generalized to the NJL and the cH models discussed above. For the chiral Heisenberg model, the defect will be given by the exponential of a fermion bilinear, similar to the GN model description. In the NJL model one can construct two fermion bilinears:  $\sim \bar{\psi}\psi$ ,  $\bar{\psi}\gamma_5\psi$ , and the defect will be given by an exponential of both these terms, neatly matching the  $4 - \varepsilon$  analysis of [90]. In this work however, we will focus exclusively on the  $4 - \varepsilon$  expansion.

The line defect considered here is closely related to the localized magnetic field or pinning line defect for the  $O(N)$  models studied in [81–85], and discussed in section 5.3. We focus on four-point functions on the defect, and two-point functions of bulk operators outside the defect. For the magnetic line defect in the  $O(N)$ -model, perturbative correlators were calculated in [85–88]. The results of this paper generalize the analysis of  $O(N)$  models to include fermions.

Notice that in our setup the defect remains one-dimensional, while the bulk is allowed to change dimension. It is also possible to keep the codimension fixed and to allow the defect to change dimension, as is the case for monodromy defects [73, 74]. We will not consider monodromy defects here, for interesting recent progress see for example [79]. Interpolating between different dimensions and/or codimensions poses several challenges, as it is not clear how to represent correlators across dimensions. This problem was recently tackled in the context of BCFT [65] (see also [59, 63]). However, for higher codimension defects the analysis is more involved. We will not study fermions across dimensions in this chapter, but we discuss possible future directions in section 7.

The outline of this chapter is as follows. In section 6.2 we discuss the fixed point of the line defect in generalized Yukawa CFTs, and compute the two-loop  $\beta$ -function of the defect scalar. In section 6.3 we focus on operators on the defect and compute two-, three-, and four-point correlators of scalars and fermions. We check that our results are consistent with an expansion of the four-point function in conformal blocks. In section 6.4, we move to bulk operators in the presence of the defect, and study one- and two-point functions for the scalars. In this section we also sketch the diagrams that contribute to two-point functions of fermions in the presence of the line.



## 6.2 Yukawa CFTs with a line defect

We are studying a general class of Yukawa models with  $N_f$  fermions and  $O(N)$  flavor symmetry. These theories are described by the following action in  $d$ -dimensional Euclidean space, with  $2 < d < 4$ :

$$S = \int d^d x \left( \frac{1}{2} \partial_\mu \phi^a \partial_\mu \phi^a + i \bar{\psi}^i \not{\partial} \psi^i + g \bar{\psi}^i \Sigma^a \phi^a \psi^i + \frac{\lambda}{4!} ((\phi^a)^2)^2 \right), \quad (6.2.1)$$

with  $\mu = 0, \dots, d-1$  with  $x^0 = \tau$  the Euclidean time direction,  $i = 1, \dots, N_f$  the flavor index of the (Dirac) spinors,  $a = 1, \dots, N$  the index of the  $O(N)$  symmetry,  $\not{\partial} = \gamma^\mu \partial^\mu$  and  $\bar{\psi} = \psi^\dagger \gamma^0$ . There are  $d$   $\gamma$ -matrices, which obey the (Euclidean) Clifford algebra  $\{\gamma^\mu, \gamma^\nu\} = 2\delta^{\mu\nu}$  in  $d$  dimensions, for which our conventions are gathered in appendix F.

The matrix  $\Sigma^a$  is a  $4 \times 4$ -matrix that defines how the field  $\phi^a$  interacts with fermions. A choice of  $\Sigma^a$  for a given  $N$  corresponds of a choice of model, and in this work we focus on the ones listed in appendix G for  $N = 1, 2, 3$ . The fermions here are defined as 4-component spinors, and we will use  $A, B = 1, \dots, 4$  as the matrix indices of  $\Sigma^a$  and  $\gamma^\mu$ . There is some ambiguity on how to take  $\Sigma$  and  $\gamma$  across dimensions. Here we will do so by assuming that the following identities hold:

$$\text{tr} \Sigma^a \gamma^\mu \Sigma^b \gamma^\nu = 4 \delta^{ab} \delta^{\mu\nu}, \quad (6.2.2)$$

$$\gamma^\mu \Sigma^a \gamma^\nu \Sigma^a \gamma^\rho = N (\delta^{\mu\nu} \gamma^\rho + \delta^{\nu\rho} \gamma^\mu - \delta^{\mu\rho} \gamma^\nu + i \epsilon^{\sigma\mu\nu\rho} \gamma^\sigma \gamma^5). \quad (6.2.3)$$

In all of the models mentioned above, we choose the matrix  $\Sigma^1$  to be

$$\Sigma^1 = \mathbf{1}. \quad (6.2.4)$$

On the other hand, we keep the matrices  $\Sigma^{\hat{a}=2, \dots, N}$  arbitrary, i.e. the fields  $\phi^{\hat{a}}$  can behave as *scalars* or *pseudoscalars*:

$$\Sigma^{\hat{a}} \gamma^\mu = +\gamma^\mu \Sigma^{\hat{a}}, \text{ if } \phi^{\hat{a}} \text{ is a scalar}, \quad (6.2.5)$$

$$\Sigma^{\hat{a}} \gamma^\mu = -\gamma^\mu \Sigma^{\hat{a}}, \text{ if } \phi^{\hat{a}} \text{ is a pseudoscalar}. \quad (6.2.6)$$

It is clear that  $\phi^1$  behaves as a scalar since (6.2.4) trivially commutes with all  $\gamma$ -matrices. For the NJLY model ( $N = 2$ ),  $\phi^2$  is a pseudoscalar, while for the chiral Heisenberg model ( $N = 3$ ) all the fields  $\phi^a$  are scalars.

The  $\beta$ -functions of the couplings in eq. (6.2.1) are known to several loop orders for each model [206]. For general Yukawa and scalar couplings, they can be found up to two loops in (the appendix of) [174]. We will use their conventions in the rest of this paper. For the purpose of writing our results for the three Yukawa models presented in appendix G in a compact way, we will write the  $\beta$ -functions in terms of the number of scalars  $N = 1, 2, 3$ . In this parametrization, setting  $N_f \rightarrow 0$  will give results that can be compared with the  $O(N)$  model. However, the exact  $\beta$ -function depends on the chosen Yukawa couplings that appear in the Lagrangian in eq. (6.2.1), and the parametrization of  $N$  should be considered with care and not be extended to  $N > 3$ . Below, we only list the expressions up to  $\mathcal{O}(\varepsilon)$ .

The  $\beta$ -functions are given by [207–209]

$$\beta_\lambda = -\varepsilon \lambda + \frac{1}{(4\pi)^2} \left( 8g^2 \lambda N_f - 48g^4 N_f + \frac{N+8}{3} \lambda^2 \right) + \mathcal{O}(\lambda^3, g^6, \lambda^2 g^2, \lambda g^4), \quad (6.2.7)$$

$$\beta_g = -\varepsilon \frac{g}{2} + \frac{\kappa_1 g^3}{(4\pi)^2} + \mathcal{O}(g^5), \quad (6.2.8)$$

where  $1 \leq N \leq 3$ . The Wilson-Fisher-Yukawa (WFY) fixed point can be reached for the following values of the couplings at one loop in  $\varepsilon := 4 - d$ :

$$\frac{\lambda_\star}{(4\pi)^2} = \frac{3\kappa_2\varepsilon}{2\kappa_1(N+8)} + \mathcal{O}(\varepsilon^2), \quad \frac{g_\star^2}{(4\pi)^2} = \frac{\varepsilon}{2\kappa_1} + \mathcal{O}(\varepsilon^2), \quad (6.2.9)$$

where we see that  $g \sim \mathcal{O}(\sqrt{\varepsilon})$ , while  $\lambda \sim \mathcal{O}(\varepsilon)$ . Furthermore, we have defined

$$\kappa_1 := 2N_f - N + 4, \quad (6.2.10)$$

$$\kappa_2 := 2(4 - N) - \kappa_1 + \sqrt{12(N^2 + 16) + \kappa_1(\kappa_1 + 12(N + 4))}. \quad (6.2.11)$$

Note that all the dependency on  $N_f$  is contained in  $\kappa_1$ .

### 6.2.1 Feynman rules

We collect in this section the Feynman rules associated to the action (6.2.1). The free propagators in  $d$  dimensions are given by

$$\text{----} := \langle \phi_a(x_1)\phi_b(x_2) \rangle_{\lambda=g=0} = \delta^{ab} I_{12}, \quad (6.2.12)$$

$$\text{---}\rightarrow := \delta^{ij} \not{\partial}_1 I_{12}, \quad (6.2.13)$$

where we have defined the scalar propagator function in  $d = 4 - \varepsilon$  dimensions:

$$I_{ij} := \frac{\Gamma(1 - \varepsilon/2)}{4\pi^{2-\varepsilon/2} x_{ij}^{2(1-\varepsilon/2)}}, \quad (6.2.14)$$

with  $x_{ij} := x_i - x_j$ . For  $d = 4$  we have

$$I_{12} = \frac{1}{4\pi^2 x_{12}^2}. \quad (6.2.15)$$

The scalar propagator satisfies the Green's equation

$$\partial_i^2 I_{ij} = -\delta^{(d)}(x_{ij}), \quad (6.2.16)$$

where  $\delta^{(d)}(x)$  refers to the  $d$ -dimensional Dirac delta function.

The interaction terms yield the following vertices:

$$\begin{array}{c} \diagup \bullet \diagdown \\ \diagdown \bullet \diagup \end{array} := -\lambda_0 \int d^d x_5 I_{15} I_{25} I_{35} I_{45}, \quad (6.2.17)$$

$$\begin{array}{c} \diagdown \bullet \diagup \\ \diagup \bullet \diagdown \\ | \end{array} := -g_0 \int d^d x_4 \not{\partial}_1 I_{14} \Sigma^a \not{\partial}_4 I_{34} I_{24}. \quad (6.2.18)$$

Note that one has to add a factor  $1/n!$  when  $n$  vertices of the same kind are being inserted, and that symmetry factors have to be taken into account.

### 6.2.2 Bulk renormalization

The couplings, as well as the (bulk) scalars  $\phi^a$  and fermions  $\psi^i, \bar{\psi}^i$  get renormalized. We can define the *bare* couplings and fields as

$$\lambda_0 = \mu^\varepsilon \lambda Z_\lambda, \quad g_0 = \mu^{\frac{\varepsilon}{2}} g Z_g, \quad \phi_0 = Z_\phi \phi, \quad \psi_0 = Z_\psi \psi, \quad (6.2.19)$$

where we have introduced rescaled couplings  $g \rightarrow \mu^{\frac{\epsilon}{2}}g, \lambda \rightarrow \mu^\epsilon\lambda$  to ensure that the couplings in the renormalized Lagrangian are dimensionless. The expressions for the renormalization factors  $Z_i$  up to  $\mathcal{O}(\epsilon^2)$  can be found in appendix G.

The renormalization factors allow us to obtain the anomalous dimensions  $\gamma_\phi, \gamma_\psi$  for the scalar and fermionic fields, which are given here to first order in the couplings:

$$\gamma_\phi = \frac{d \log Z_\phi}{d \log \mu} = \frac{2g^2 N_f}{(4\pi)^2} + \mathcal{O}(\lambda^2, g^4, \lambda g^2), \quad (6.2.20)$$

$$\gamma_\psi = \frac{d \log Z_\psi}{d \log \mu} = \frac{g^2 N}{2(4\pi)^2} + \mathcal{O}(\lambda^2, g^4, \lambda g^2). \quad (6.2.21)$$

This leads to the following values for the conformal dimensions evaluated at the WFY fixed point defined in eq. (6.2.9):

$$\Delta_\phi = 1 - \frac{\epsilon}{2} + \gamma_\phi = 1 - \epsilon \frac{4 - N}{2\kappa_1} + \mathcal{O}(\epsilon^2), \quad (6.2.22)$$

$$\Delta_\psi = \frac{3}{2} - \frac{\epsilon}{2} + \gamma_\psi = \frac{3}{2} - \frac{\epsilon}{4} \left( 2 - \frac{N}{\kappa_1} \right) + \mathcal{O}(\epsilon^2). \quad (6.2.23)$$

Furthermore, we will need the normalization of the two-point function, which is given by

$$\langle \phi^a(x_1) \phi^b(x_2) \rangle = \frac{\delta^{ab} \mathcal{N}_\phi^2}{(x_{12}^2)^{\Delta_\phi}}, \quad (6.2.24)$$

with

$$\mathcal{N}_\phi = \sqrt{\frac{\Gamma\left(\frac{d}{2}\right)}{2(d-2)\pi^{d/2}}} - \epsilon \frac{(\kappa_1 + N - 4)(1 + \aleph)}{8\pi \kappa_1} + \mathcal{O}(\epsilon^2), \quad (6.2.25)$$

where we have defined the following combination:

$$\aleph := 1 + \log \pi + \gamma_E, \quad (6.2.26)$$

with  $\gamma_E = 0.57722\dots$  the Euler-Mascheroni constant.

### 6.2.3 Defect fixed point

One can define a defect CFT by adding a scalar line to the action (6.2.1), in the same way as in the  $O(N)$  model [81]. This was shown in [89] for the GNY model, and generalized to the NJLY and chiral Heisenberg models in [90]. More precisely,

$$S_{\text{defect}} := S_0 + h_0 \int_{-\infty}^{\infty} d\tau \phi^1(\tau). \quad (6.2.27)$$

Here  $h_0$  is the bare coupling of the defect, which extends in the Euclidean time direction  $\tau$ , and  $S_0$  is the bulk action in terms of the bare couplings  $\lambda_0$  and  $g_0$ . The defect introduces a new vertex

$$\text{---} \underset{\bullet}{\vdots} \text{---} \equiv -h_0 \int_{-\infty}^{\infty} d\tau_2 I_{12}, \quad (6.2.28)$$

with  $\tau_2$  the point on the line, and where one should note that only  $\phi^1$  and not  $\phi^{\hat{a}}, \hat{a} = 2, \dots, N$  nor the fermions  $\psi^i, \bar{\psi}^j$  couple to the defect. As for the bulk Feynman rules,

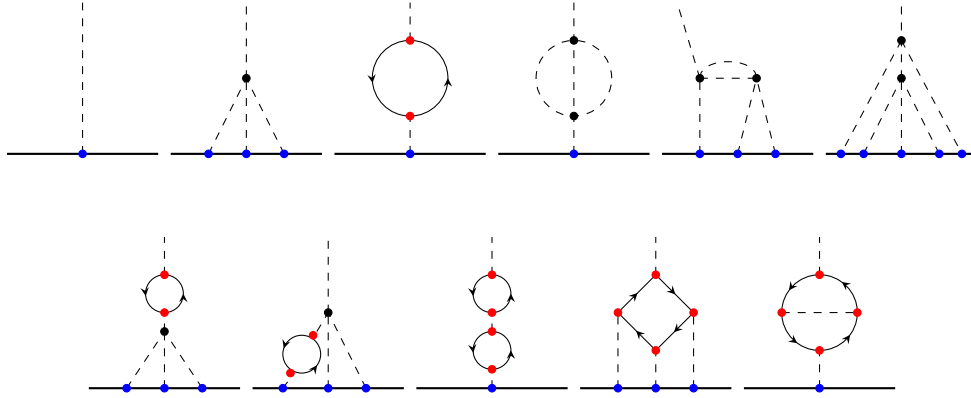


Figure 6.1: Diagrams contributing to the one-point function  $\langle\langle \phi^a \rangle\rangle$  up to  $\mathcal{O}(\varepsilon^2)$ . The defect is denoted by a solid line, scalars by a dotted line, and fermions by solid arrowed lines. Bulk scalar couplings  $\lambda_0$  are represented by a black dot, bulk Yukawa couplings  $g_0$  by a red dot and defect couplings  $h_0$  by a blue dot.

one should add a factor  $1/n!$  when  $n$  vertices are inserted, and symmetry factors have to be accounted for.

We can renormalize the defect coupling in a similar way to the bulk couplings. We define the bare coupling  $h_0$  in terms of the renormalized coupling  $h$  as

$$h_0 = \mu^{\frac{\varepsilon}{2}} h Z_h, \quad (6.2.29)$$

where  $Z_h$  is given in appendix G, and can be computed by extracting the divergences from the one-point function of the renormalized scalar  $\phi^a$  and requiring that it is finite:

$$\langle\langle \phi^a(x) \rangle\rangle = \text{finite}. \quad (6.2.30)$$

Note that the one-point function of a single fermion  $\psi^i$  is zero. The Feynman diagrams that contribute to the one-point function of  $\phi^a$  up to  $\mathcal{O}(\varepsilon^2)$  are given in figure 6.1. It is important to keep in mind that we are working perturbatively in the two bulk couplings  $\lambda$  and  $g$ , since they are  $\mathcal{O}(\varepsilon)$  and  $\mathcal{O}(\sqrt{\varepsilon})$  respectively at the WFY fixed point, but we need to keep diagrams up to all orders in the defect coupling  $h$  since it is of order  $\mathcal{O}(1)$ . There are however only a finite number of possible diagrams per order in  $\lambda$  and  $g$ . The diagrams in figure 6.1 involving only scalar four-point couplings  $\lambda$  (black dots) and defect couplings  $h$  (blue dots) are the same as for the line defect in the  $O(N)$  model and were already computed in [81]. The diagrams in figure 6.1 that include the Yukawa coupling  $g$  (red dots) were recently computed in [90]. Here we will give the corresponding  $\beta$ -function for  $h$  up to  $\mathcal{O}(\varepsilon^2)$ , which match the ones in [90].

Some of the diagrams in figure 6.1 are completely cancelled by the wavefunction renormalizations of  $\phi^a$  and  $\psi^i$ , while others do contribute to the defect counterterms.

We can compute the  $\beta$ -function  $\beta_h$  from the divergent part of the diagrams and we obtain:

$$\begin{aligned} \beta_h = & -\frac{\varepsilon h}{2} + \frac{1}{(4\pi)^2} \left( \frac{\lambda h^3}{6} \right) + \frac{1}{(4\pi)^4} \left\{ \lambda^2 h \left( \frac{(2+N)}{36} - \frac{h^2(N+8)}{35} - \frac{h^4}{12} \right) - \lambda g^2 h^3 N_f \right. \\ & \left. + g^4 h \left( -\frac{(N+4)N_f}{2} + h^2 4N_f \left( 1 - \frac{\pi^2}{6} \right) \right) \right\} + \mathcal{O}(\lambda^3, g^6, \lambda^2 g^2, \lambda g^4). \end{aligned} \quad (6.2.31)$$

Using the values for  $\lambda$  and  $g$  at the WFY fixed point in eq. (6.2.9), we find the corresponding defect fixed point

$$h_\star^2 = -\frac{2(N-4)(N+8)}{\kappa_2} + \mathcal{O}(\varepsilon), \quad (6.2.32)$$

where the  $\mathcal{O}(\varepsilon)$  term is given in appendix G for  $N = 1, 2, 3$ . If we include the finite part of the one-point function, we can extract the one-point function coefficient  $a_\phi$ :

$$\langle\langle \phi(x) \rangle\rangle = \frac{a_\phi}{|x^\perp|^{1+\gamma_\phi}}, \quad a_\phi^2 = -\frac{(N-4)(N+8)}{2\kappa_2} + \mathcal{O}(\varepsilon). \quad (6.2.33)$$

The  $\mathcal{O}(\varepsilon)$  term is lengthy and given in the attached Mathematica notebook.

### 6.3 Correlators of defect operators

The bulk operators give rise to a plethora of defect operators. In this section we will consider correlation functions between the lowest-lying defect operators. The lowest-lying scalars are the first scalars appearing in the bulk-to-defect expansion of  $\phi^a$ , and are labelled in the following as  $\hat{\phi}^1$  and  $t^{\hat{a}}$ , with  $\hat{a} = 2, \dots, N$ . These correspond to the two scalar operators of length 1 that arise due to the breaking of  $O(N)$  symmetry in the bulk to  $O(N-1)$  symmetry on the defect, namely  $\phi^1$  couples to the defect while  $\phi^{\hat{a}}$  does not. The conformal dimension of  $\hat{\phi}^1$  was computed in [89] for the GNY model up to  $\mathcal{O}(\varepsilon)$ . It can be extracted from the  $\beta$ -function of the defect coupling at the fixed point:

$$\Delta_{\hat{\phi}^1} = 1 + \frac{\partial\beta_h}{\partial h}\Big|_{h=h_\star} = 1 + \frac{(4-N)\varepsilon}{\kappa_1} + \mathcal{O}(\varepsilon^2), \quad (6.3.1)$$

which agrees with [89] for the case  $N = 1$  corresponding to the pure GNY model. In this section, we will extend their results to general  $N$ , as well as compute additional defect correlators. The operator  $t^{\hat{a}}$  (the *tilt* operator) has protected conformal dimension

$$\Delta_t = 1. \quad (6.3.2)$$

Note that for the GNY model, there will be no tilt operator, but only  $\hat{\phi}^1 \equiv \hat{\phi}$  on the defect.

Besides the tilt there is another scalar defect operator with protected conformal dimension, namely the displacement operator  $D$ . It is related to the bulk stress-energy tensor through the Ward identity

$$\partial_\mu T^{\mu\nu} = \delta^{d-1}(x^\perp) D_{\hat{\mu}}, \quad \hat{i} = 1, \dots, d-1, \quad (6.3.3)$$

and has transverse spin  $s = 1$  and conformal dimension

$$\Delta_D = 2. \quad (6.3.4)$$

The expansion of the bulk fermion on the defect gives us the defect Dirac fermions  $\hat{\psi}, \hat{\bar{\psi}}$  with conformal dimension

$$\Delta_{\hat{\psi}} = \frac{3-\varepsilon}{2} + \gamma_{\hat{\psi}}. \quad (6.3.5)$$

The anomalous dimension  $\gamma_{\hat{\psi}}$  can be extracted from the two-point function.

Below we will compute correlation functions between these operators and extract the corresponding defect CFT data.

### 6.3.1 Two-point functions

We will start by computing the two-point functions between the defect operators to obtain their anomalous dimensions and normalization constants.

#### Two-point functions of scalars

We consider first the two-point functions  $\langle \hat{\phi}^1(\tau_1) \hat{\phi}^1(\tau_2) \rangle$  and  $\langle t^{\hat{a}}(\tau_1) t^{\hat{b}}(\tau_2) \rangle$ . The two-point function of arbitrary (defect) scalars  $\hat{\phi}^a$  takes the general form

$$\langle \hat{\phi}^a(\tau_1) \hat{\phi}^b(\tau_2) \rangle = \mathcal{N}_{\hat{\phi}}^2 \frac{\delta^{ab}}{\tau_{12}^{2\Delta_{\hat{\phi}}}}, \quad (6.3.6)$$

with  $\tau_{12} := \tau_1 - \tau_2$ , and where  $\mathcal{N}_{\hat{\phi}}$  and  $\Delta_{\hat{\phi}}$  correspond respectively to the normalization constant and to the scaling dimensions given in eqs. (6.3.1) and (6.3.2).

In terms of Feynman diagrams, this two-point function can be expressed as

$$\langle \hat{\phi}^a(\tau_1) \hat{\phi}^b(\tau_2) \rangle = \text{[tree-level propagator]} + \text{[fermion loop]} + \text{[defect diagram]} + \mathcal{O}(\varepsilon^2), \quad (6.3.7)$$

In the first diagram, the two external operators are connected through a single tree-level propagator. The second diagram corresponds to the bulk self-energy and consists of an internal fermion loop and two bulk Yukawa vertices (represented by red dots), while the third one is special to the defect theory and involves two integrals along the line (represented by blue dots) as well as a bulk four-scalar vertex (the black dot).

The fermion loop diagram is easy to compute and reads

$$\begin{aligned} \text{[fermion loop]} &= g_0^2 N_f \text{tr} \Sigma^a \Sigma^b B_{12} \\ &= -\frac{g_0^2 N_f}{4\pi^2} \delta^{ab} I_{12} \left( \frac{1}{\varepsilon} + \aleph + \log \tau_{12}^2 + \mathcal{O}(\varepsilon^2) \right), \end{aligned} \quad (6.3.8)$$

where we have made use of the rules given in eq. (6.2.3). The integral  $B_{12}$  is defined in eq. (H.0.23) and solved in eq. (H.0.24), while the function  $I_{12}$  corresponds to the scalar propagator and is defined in eq. (6.2.14). Finally, the constant  $\aleph$  arising from dimensional regularization is defined in eq. (6.2.26). The expressions for the two other diagrams can be found in [85].

Requiring that the sum of the diagrams is finite allows us to compute the renormalization factors for  $\hat{\phi}^1$  and  $t^{\hat{a}}$ :

$$\langle \hat{\phi}^a(\tau_1) \hat{\phi}^b(\tau_2) \rangle = \frac{1}{Z_{\hat{\phi}}^2} \langle \hat{\phi}_0^a(\tau_1) \hat{\phi}_0^b(\tau_2) \rangle = \text{finite}, \quad (6.3.9)$$

and leads to

$$Z_{\hat{\phi}^1} = 1 - \frac{1}{\varepsilon} \frac{\lambda h^2 + 8g^2 N_f}{64\pi^2} + \mathcal{O}(\varepsilon^{-2}), \quad (6.3.10)$$

$$Z_t = 1 - \frac{1}{\varepsilon} \frac{\lambda h^2 - 24g^2 N_f}{192\pi^2} + \mathcal{O}(\varepsilon^{-2}). \quad (6.3.11)$$

As a sanity check, we can read the scaling dimensions from the renormalization factors:

$$\Delta_{\hat{\phi}^1} = \mu \frac{\partial \log Z_{\hat{\phi}^1}}{\partial \mu} = 1 + \varepsilon \frac{4 - N}{\kappa_1} + \mathcal{O}(\varepsilon^2), \quad (6.3.12)$$

$$\Delta_t = \mu \frac{\partial \log Z_t}{\partial \mu} = 1 + \mathcal{O}(\varepsilon^2), \quad (6.3.13)$$

which agree with the results given in eqs. (6.3.1) and (6.3.2).

The normalization constants can now be extracted from the finite two-point functions, and we find for the two scalars

$$\mathcal{N}_{\hat{\phi}^1}^2 = \frac{1}{4\pi^2} \left\{ 1 - \frac{\varepsilon}{2} \left( 2 + \frac{(N-4)(1-2\aleph)}{\kappa_1} \right) + \mathcal{O}(\varepsilon^2) \right\}, \quad (6.3.14)$$

$$\mathcal{N}_t^2 = \frac{1}{4\pi^2} \left\{ 1 - \frac{\varepsilon}{2} \left( 2 + \frac{N-4}{\kappa_1} \right) + \mathcal{O}(\varepsilon^2) \right\}, \quad (6.3.15)$$

where  $\kappa_1$  depends on  $N_f$  and  $N$  and is defined in eq. (6.2.10).

### Two-point function of the displacement

We continue with the two-point function of the displacement. The displacement has transverse spin  $s = 1$  and can be constructed by taking a transverse derivative of the field  $\hat{\phi}^1$ :

$$D_i = \partial_i^\perp \hat{\phi}^1, \quad (6.3.16)$$

while there exist additional operators  $\partial_i^\perp t^{\hat{a}}$  that correspond to taking the transverse derivative of the tilt. The latter will not be considered here for brevity, but its correlators can be computed in a similar way as the displacement correlators.

Because we can write the displacement as in eq. (6.3.16), the diagrams that contribute to the two-point function are the same as for  $\hat{\phi}_a$  and are given in eq. (6.3.7). For the evaluation of the diagrams, we need to first take the derivatives with respect to  $x_1^\perp, x_2^\perp$  and then send  $x_1^\perp, x_2^\perp \rightarrow 0$ . This leads to the following expressions for the diagrams:

$$\begin{aligned} \text{Diagram} &= \frac{1}{2} g_0^2 N_f \text{tr} \Sigma^a \Sigma^b B_{12} \\ &= -\frac{1}{2} \frac{g_0^2 N_f}{4\pi^2} I_{12} \delta^{ab} \left( \frac{1}{\varepsilon} + \aleph + \log \tau_{12}^2 + \mathcal{O}(\varepsilon^2) \right). \end{aligned} \quad (6.3.17)$$

The other diagrams were computed in [85].

We can compute the renormalization factor for the displacement in the usual way, by requiring that the two-point function is finite. This results in

$$Z_D = 1 - \frac{1}{(4\pi)^2 \varepsilon} \left( \frac{\lambda h^2}{12} + 2N_f g^2 \right) + \mathcal{O}(\varepsilon^{-2}). \quad (6.3.18)$$

As a check, we compute the anomalous dimension of D and find:

$$\Delta_D = \mu \frac{\partial \log Z_D}{\partial \mu} = 2 + \mathcal{O}(\varepsilon^2), \quad (6.3.19)$$

where the  $\mathcal{O}(\varepsilon)$  contributions cancel as expected. We can extract the proper normalization from the finite parts of the diagrams and obtain

$$\mathcal{N}_D^2 = \frac{1}{2\pi^2} \left\{ 1 - \varepsilon \left( 1 - \frac{N-4}{6\kappa_1} \right) + \mathcal{O}(\varepsilon^2) \right\}. \quad (6.3.20)$$

### Two-point functions of fermions

Let us now turn our attention to the fermions. In  $1d$ , the two-point function of Dirac fermions takes the form

$$\langle \hat{\psi}^i(\tau_1) \hat{\psi}^j(\tau_2) \rangle = \mathcal{N}_\psi^2 \frac{\bar{s}_1 \gamma^0 s_2}{\tau_{12}^2 \Delta_\psi} \delta^{ij}, \quad (6.3.21)$$

where we have used the polarization spinors  $\bar{s}_1^A, s_2^B$  as defined in eq. (F.0.8) in order to avoid cluttering.

The diagrams involved are:

$$\begin{aligned} \langle \hat{\psi}^i(\tau_1) \hat{\psi}^j(\tau_2) \rangle &= \text{diag}_1 + \text{diag}_2 \\ &+ \text{diag}_3 + \text{diag}_4 + \mathcal{O}(\varepsilon^2). \end{aligned} \quad (6.3.22)$$

As noted in [89], the second diagram is zero at order  $\mathcal{O}(\varepsilon)$ . This can be easily checked in the following way:

$$\begin{aligned} \text{diag}_2 &= \delta^{ij} g_0 h_0 \bar{s}_1 \int d\tau_3 \int d^d x_4 \phi_4 I_{14} \Sigma^1 \phi_4 I_{24} I_{34} s_2 \\ &= \delta^{ij} \pi^2 (\bar{s}_1 \gamma^0 s_2) g_0 h_0 I_{12} \int d\tau_3 \tau_{13} \tau_{23} I_{13} I_{23} \\ &= 0 + \mathcal{O}\left(\varepsilon^{\frac{3}{2}}\right), \end{aligned} \quad (6.3.23)$$

where in the second line we have used the  $4d$  fermionic star-triangle relationship given in eq. (H.0.17), to which the corrections towards  $d = 4 - \varepsilon$  are of order  $\mathcal{O}(\varepsilon)$  while  $g \sim \mathcal{O}(\sqrt{\varepsilon})$ .

The third diagram can be computed as follows:

$$\begin{aligned} \text{diag}_3 &= g_0^2 \delta^{ij} \bar{s}_1 \int d^d x_3 \int d^d x_4 \phi_1 I_{13} \Sigma^a \phi_3 I_{34} \Sigma^a \phi_4 I_{24} I_{34} s_2 \\ &= 2g_0^2 N \delta^{ij} \bar{s}_1 \phi_2 B_{12} s_2 \\ &= \frac{g_0^2 N}{32\pi^4} \frac{\bar{s}_1 \gamma^0 s_2}{\tau_{12}^3} \delta^{ij} \left\{ \frac{1}{\varepsilon} + \aleph - 1 + \log \tau_{12}^2 + \mathcal{O}(\varepsilon) \right\}. \end{aligned} \quad (6.3.24)$$

Here we have again made use of the rules given in eq. (6.2.3) in order to be able to rewrite the integral as a derivative of  $B_{12}$ .

The fourth diagram is more involved and reads

$$\text{diag}_4 = g_0^2 h_0^2 \delta^{ij} \bar{s}_1 \int d\tau_3 \int d\tau_4 \int d^d x_5 \int d^d x_6 \phi_1 I_{15} \Sigma^1 \phi_5 I_{56} \Sigma^1 \phi_6 I_{26} I_{35} I_{46} s_2, \quad (6.3.25)$$

with  $\Sigma^1 = 1$ . The easiest way to compute it is to apply another slashed derivative on the integral and compare the result to an ansatz. We define

$$J_{12} := \int d\tau_3 \int d\tau_4 \int d^d x_5 \int d^d x_6 \phi_1 I_{15} \phi_5 I_{56} \phi_6 I_{26} I_{35} I_{46}, \quad (6.3.26)$$

and assume that

$$J_{12} = \frac{\gamma^0}{\tau_{12}^2} \left\{ \frac{A}{\varepsilon} + B + C \log \tau_{12}^2 \right\}. \quad (6.3.27)$$



We then compute

$$\hat{\phi}_1 J_{12} = - \int d\tau_3 \int d\tau_4 I_{13} \hat{\phi}_1 \hat{\phi}_2 Y_{124}, \quad (6.3.28)$$

where we have used  $\hat{\phi}_1 \hat{\phi}_1 = \mathbb{1} \partial_1^2$  and  $\partial_1^2 I_{15} = -\delta^{(d)}(x_{15})$ . After applying the identity (H.0.17), we find

$$\hat{\phi}_1 J_{12} = \frac{3}{16\pi^6} \mathbb{1} + (\text{quadratic divergences}), \quad (6.3.29)$$

from which we can read:

$$A = C = 0, \quad B = -\frac{1}{16\pi^6}. \quad (6.3.30)$$

We see that this diagram is finite (after dropping the quadratic divergences) and so it contributes only to the normalization constant.

In the same way as for the scalars, we define a renormalization factor  $Z_{\hat{\psi}}$  such that

$$\langle \hat{\psi}^i(\tau_1) \hat{\psi}^j(\tau_2) \rangle = \frac{1}{Z_{\hat{\psi}}^2} \langle \hat{\psi}_0^i(\tau_1) \hat{\psi}_0^j(\tau_2) \rangle = \text{finite}, \quad (6.3.31)$$

for which we find

$$Z_{\hat{\psi}} = 1 - \frac{g^2 N}{32\pi^2 \varepsilon} + \mathcal{O}(\varepsilon^{-2}), \quad (6.3.32)$$

which agrees with the renormalization factor for the bulk given in eq. (G.0.4).

The scaling dimension gives

$$\Delta_{\hat{\psi}} = \frac{3}{2} - \frac{\varepsilon}{4} \left( 2 - \frac{N}{\kappa_1} \right) + \mathcal{O}(\varepsilon^2), \quad (6.3.33)$$

while the normalization constant reads

$$\mathcal{N}_{\hat{\psi}}^2 = -\frac{1}{2\pi^2} \left\{ 1 - \frac{\varepsilon}{2\kappa_1} \left( 2\kappa_1 - \aleph \left( 1 - \frac{N}{2\kappa_1} \right) + \frac{4}{\pi^2} \frac{(N-4)(N+8)}{\kappa_1 \kappa_2} \right) + \mathcal{O}(\varepsilon^2) \right\}. \quad (6.3.34)$$

Note that the renormalization factor as well the scaling dimension agree with the bulk computation, as the diagrams contributing to these results are the same<sup>3</sup>.

### 6.3.2 Three-point functions

We now compute three-point functions between the lowest-lying operators. This gives us various defect OPE coefficients, which can be compared with the OPE coefficients coming from the conformal block expansion of the four-point function.

#### Three-point functions of scalars

The three-point function between three defect scalars  $\hat{\phi}^{a,b,c}$ , where  $\hat{\phi}^a = \{\hat{\phi}^1, t^{\hat{a}}\}$ , is given by a single Feynman diagram up to  $\mathcal{O}(\varepsilon)$ :

$$\begin{aligned} \langle \hat{\phi}^a(\tau_1) \hat{\phi}^b(\tau_2) \hat{\phi}^c(\tau_3) \rangle &= \text{Diagram} + \mathcal{O}(\varepsilon^2) \\ &= \mathcal{N}_{\hat{\phi}^a} \mathcal{N}_{\hat{\phi}^b} \mathcal{N}_{\hat{\phi}^c} \frac{\lambda_{\hat{\phi}^a \hat{\phi}^b \hat{\phi}^c}}{\tau_{12}^{2\Delta_{abc}} \tau_{23}^{2\Delta_{bca}} \tau_{13}^{2\Delta_{cab}}}, \end{aligned} \quad (6.3.35)$$

<sup>3</sup>This agreement is expected to be lifted at higher orders of  $\varepsilon$ .

where we have defined  $\Delta_{abc} := \frac{1}{2}(\Delta_{\hat{\phi}^a} + \Delta_{\hat{\phi}^b} - \Delta_{\hat{\phi}^c})$ .

This diagram was already evaluated in [85], and results in the following OPE coefficients:

$$\lambda_{\hat{\phi}^1 \hat{\phi}^1 \hat{\phi}^1} = \frac{3\pi\varepsilon(4\kappa_1 - N_f)\sqrt{2(4-N)(N+8)\kappa_2}}{8\kappa_1^2(N+8)} + \mathcal{O}(\varepsilon^2), \quad (6.3.36)$$

$$\lambda_{tt\hat{\phi}^1} = \frac{\lambda_{\hat{\phi}^1 \hat{\phi}^1 \hat{\phi}^1}}{3} + \mathcal{O}(\varepsilon^2). \quad (6.3.37)$$

Since the OPE coefficients start at  $\mathcal{O}(\varepsilon)$ , they will only appear at order  $\mathcal{O}(\varepsilon^2)$  in the four-point function of scalars.

### Three-point functions involving $\hat{\phi}^2$

The first scalar operators that appear in the OPE  $\hat{\phi}^a \times \hat{\phi}^a$ ,  $\hat{\phi}^a = \{\hat{\phi}^1, t^{\hat{a}}\}$ , after  $\hat{\phi}^1$  itself, are the degenerate operators  $s_{\pm}$ . These operators have dimension close to 2, and can be constructed from  $(\hat{\phi}^1)^2$  and  $(\hat{\phi}^{\hat{a}})^2$ . In order to find the correct anomalous dimensions we need to require that the three-point functions involving  $\hat{\phi}$  and  $s_{\pm}$  are finite. The diagrams that contribute up to  $\mathcal{O}(\varepsilon)$  are

$$\begin{aligned} \langle \hat{\phi}^a(\tau_1) \hat{\phi}^b(\tau_2) \hat{\phi}^c \hat{\phi}^c(\tau_3) \rangle &= \text{[diagram 1]} + \text{[diagram 2]} + \text{[diagram 3]} + \text{[diagram 4]} + \mathcal{O}(\varepsilon^2) \\ &= \mathcal{N}_{\hat{\phi}^a}^2 \mathcal{N}_{s_{\pm}} \frac{\lambda_{\hat{\phi}^a \hat{\phi}^a s_{\pm}}}{\tau_{12}^{2\Delta_{abc^2}} \tau_{23}^{2\Delta_{bc^2a}} \tau_{13}^{2\Delta_{ac^2b}}}. \end{aligned} \quad (6.3.38)$$

The first three diagrams have been computed in [85], while the last one is the wavefunction renormalization. Requiring that this three-point function is finite in  $\varepsilon$  gives a renormalization matrix  $Z_s$  that has a lengthy expression and is given in a Mathematica notebook. The anomalous dimension can be computed by diagonalizing this matrix and taking the derivative:

$$\gamma_{s_{\pm}} = \frac{\varepsilon(-4(N+8)(-\kappa_1 + N - 4) + \kappa_2(N+4) \pm \kappa_3)}{4\kappa_1(N+8)} + \mathcal{O}(\varepsilon^2), \quad (6.3.39)$$

where we have defined

$$\kappa_3 := \sqrt{\kappa_2^2 N^2 + 8\kappa_2(N-4)(N-2)(N+8) + 16(N-4)^2(N+8)^2}. \quad (6.3.40)$$

We obtain the conformal dimension as  $\Delta_{s_{\pm}} = 2 - \varepsilon + \gamma_{s_{\pm}}$ .

To complete the computation of the OPE coefficients, we also need the normalization of the two-point functions  $\langle s_{\pm}(\tau_1) s_{\pm}(\tau_2) \rangle$ . From the two-point function, we get

$$\mathcal{N}_{s_{\pm}}^2 = \pm \frac{(N-1)(\kappa_2(N-2) + 4(N-4)(N+8) \pm \kappa_3)}{16\pi^4 \kappa_3} + \mathcal{O}(\varepsilon). \quad (6.3.41)$$

We have only displayed the  $\mathcal{O}(1)$  term here, while the  $\mathcal{O}(\varepsilon)$  term is once again long and given in the Mathematica notebook. We checked that the operators are now properly normalized, such that  $\langle s_+(\tau_1) s_-(\tau_2) \rangle = 0$ .

Putting everything together, we can now extract the OPE coefficients, for which we find:

$$\lambda_{\hat{\phi}^1 \hat{\phi}^1 s_{\pm}} = \pm \frac{2\kappa_2 \sqrt{N-1}}{\sqrt{\kappa_3^2 \pm (\kappa_2(N-2) + 4(N-4)(N+8))\kappa_3}} + \mathcal{O}(\varepsilon), \quad (6.3.42)$$

$$\lambda_{t^{\hat{a}} t^{\hat{b}} s_{\pm}} = \delta^{\hat{a}\hat{b}} \frac{\sqrt{\kappa_3 \pm \kappa_2(N-2) + 4(N-4)(N+8)}}{\sqrt{\kappa_3} \sqrt{N-1}} + \mathcal{O}(\varepsilon). \quad (6.3.43)$$

The  $\mathcal{O}(\varepsilon)$  terms can be found in the attached Mathematica notebook.

### Three-point functions of two fermions and one scalar

An example of a mixed correlator is the three-point function  $\langle \hat{\psi}^i(\tau_1) \hat{\psi}^j(\tau_2) \hat{\phi}^a(\tau_3) \rangle$ , which is given at leading order by

$$\begin{aligned} \langle \hat{\psi}^i(\tau_1) \hat{\psi}^j(\tau_2) \hat{\phi}^a(\tau_3) \rangle &= \text{diagram} + \mathcal{O}(\varepsilon) \\ &= \mathcal{N}_{\hat{\psi}}^2 \mathcal{N}_{\hat{\phi}^a} \frac{\delta^{ij} (\bar{s}_1 \gamma^0 \Sigma^a s_2) \lambda_{\hat{\psi} \hat{\psi} \hat{\phi}^a}}{\tau_{12}^{2\Delta_{\hat{\psi} \hat{\psi} a}} \tau_{23}^{2\Delta_{\hat{\psi} a \hat{\psi}}} \tau_{13}^{2\Delta_{a \hat{\psi} \hat{\psi}}}}, \end{aligned} \quad (6.3.44)$$

with  $\Delta_{ijk}$  following the same convention as given below eq. (6.3.35).

At order  $\mathcal{O}(\sqrt{\varepsilon})$  we have a single diagram contributing. It is easy to evaluate this diagram using the usual commutation rules for  $\Sigma^a$  as well as the fermionic star-triangle identity given in eq. (H.0.17). The results differ depending on the nature of the field  $\phi^a$ :

$$\text{diagram} = \pm \mathcal{N}_{\hat{\psi}}^2 \mathcal{N}_{\hat{\phi}^a} g_0 \delta^{ij} (\bar{s}_1 \Sigma^a \gamma^0 s_2) \frac{1}{64\pi^4 \tau_{12}^2 \tau_{23} \tau_{31}}, \quad (6.3.45)$$

where the sign is  $-$  for  $\phi^a$  scalar and  $+$  for  $\phi^a$  pseudoscalar. After inserting the normalization constants derived in section 6.3.1 we find that the OPE coefficient is

$$\lambda_{\hat{\psi} \hat{\psi} \hat{\phi}^a} = \pm \frac{\sqrt{\varepsilon}}{4\sqrt{2}\kappa_1} + \mathcal{O}(\varepsilon). \quad (6.3.46)$$

### 6.3.3 Four-point functions

Let us now turn our attention to the four-point functions, which are the first correlators in our list to have non-trivial kinematics. These correlators can be expanded in  $1d$  conformal blocks to obtain defect CFT data, which we can compare with the OPE coefficients computed in the previous section. We start by considering correlators of purely scalar operators, before moving on to fermions and concluding with an example of a mixed correlator including both scalars and fermions.

#### Four-point functions of scalars

We start this section by the four-point functions of scalars. Such correlators depend kinematically on a single cross-ratio  $\chi$ , which we define as<sup>4</sup>

$$\chi := \frac{\tau_{12}\tau_{34}}{\tau_{13}\tau_{24}}. \quad (6.3.47)$$

<sup>4</sup>In higher  $d$ , four-point functions depend on *two* cross-ratios  $\chi$  and  $\bar{\chi}$ . In  $1d$  the second cross-ratio is not independent of  $\chi$  and becomes  $\bar{\chi} = 1 - \chi$ .

Four-point functions of scalars take the following form:

$$\langle \hat{\phi}^a(\tau_1) \hat{\phi}^b(\tau_2) \hat{\phi}^c(\tau_3) \hat{\phi}^d(\tau_4) \rangle = \mathcal{N}_{\hat{\phi}^a} \mathcal{N}_{\hat{\phi}^b} \mathcal{N}_{\hat{\phi}^c} \mathcal{N}_{\hat{\phi}^d} \mathcal{K}_4 f^{abcd}(\chi). \quad (6.3.48)$$

with the conformal prefactor

$$\mathcal{K}_4 := \frac{1}{\tau_{12}^{\Delta_{\hat{\phi}^a} + \Delta_{\hat{\phi}^b}} \tau_{34}^{\Delta_{\hat{\phi}^c} + \Delta_{\hat{\phi}^d}}} \left( \frac{\tau_{24}}{\tau_{14}} \right)^{\Delta_{\hat{\phi}^a} - \Delta_{\hat{\phi}^b}} \left( \frac{\tau_{14}}{\tau_{13}} \right)^{\Delta_{\hat{\phi}^a} - \Delta_{\hat{\phi}^b}}. \quad (6.3.49)$$

In terms of Feynman diagrams, the four-point function of arbitrary scalars is given up to  $\mathcal{O}(\varepsilon)$  by

$$\langle \hat{\phi}^a(\tau_1) \hat{\phi}^b(\tau_2) \hat{\phi}^c(\tau_3) \hat{\phi}^d(\tau_4) \rangle = \begin{array}{c} \text{---} \text{---} \text{---} \text{---} \\ \text{---} \text{---} \end{array} + \begin{array}{c} \text{---} \text{---} \text{---} \text{---} \\ \text{---} \text{---} \end{array} + \begin{array}{c} \text{---} \text{---} \text{---} \text{---} \\ \text{---} \text{---} \end{array} + \mathcal{O}(\varepsilon^2), \quad (6.3.50)$$

where the first diagrams are products of two-point functions, and the last one was computed in [85].

Adding all diagrams in eq. (6.3.50), we obtain the following unit-normalized results:

$$f^{1111}(\chi) = 1 + \chi^{2\Delta_{\hat{\phi}^1}} + \left( \frac{\chi}{1-\chi} \right)^{2\Delta_{\hat{\phi}^1}} + \frac{3\varepsilon\kappa_2}{\kappa_1(N+8)} \left( \chi \log(1-\chi) + \frac{\chi^2}{1-\chi} \log \chi \right) + \mathcal{O}(\varepsilon^2), \quad (6.3.51)$$

$$f^{1\hat{a}1\hat{b}}(\chi) = \delta^{\hat{a}\hat{b}} \chi^{\Delta_{\hat{\phi}^1} + \Delta_{\hat{t}}} + \varepsilon \delta^{\hat{a}\hat{b}} \frac{\kappa_2}{\kappa_1(N+8)} \left( \chi \log(1-\chi) + \frac{\chi^2}{1-\chi} \log \chi \right) + \mathcal{O}(\varepsilon^2), \quad (6.3.52)$$

$$\begin{aligned} f^{\hat{a}\hat{b}\hat{c}\hat{d}}(\chi) &= \delta^{\hat{a}\hat{b}} \delta^{\hat{c}\hat{d}} + \delta^{\hat{a}\hat{c}} \delta^{\hat{b}\hat{d}} \chi^2 + \delta^{\hat{a}\hat{d}} \delta^{\hat{b}\hat{c}} \frac{\chi^2}{(1-\chi)^2} \\ &+ \varepsilon (\delta^{\hat{a}\hat{b}} \delta^{\hat{c}\hat{d}} + \delta^{\hat{a}\hat{c}} \delta^{\hat{b}\hat{d}} + \delta^{\hat{a}\hat{d}} \delta^{\hat{b}\hat{c}}) \frac{\kappa_2}{\kappa_1(N+8)} \left( \chi \log(1-\chi) + \frac{\chi^2}{1-\chi} \log \chi \right) + \mathcal{O}(\varepsilon^2), \end{aligned} \quad (6.3.53)$$

where  $\kappa_1$  and  $\kappa_2$  are defined in eqs. (6.2.10) and (6.2.11). Other orderings of  $\hat{\phi}^1$  and  $\hat{t}^{\hat{a}}$  are not given here but can be computed in the same way straightforwardly from (6.3.50). The last correlator  $f^{\hat{a}\hat{b}\hat{c}\hat{d}}(\chi)$  can be decomposed into a scalar ( $S$ ), an antisymmetric ( $A$ ), and a traceless symmetric ( $T$ ) contribution:

$$\begin{aligned} f_S^{\hat{a}\hat{b}\hat{c}\hat{d}}(\chi) &= \frac{N}{N-1} \frac{\chi^2}{(1-\chi)^2} (2 + \chi(\chi-2)) \\ &+ \varepsilon \frac{\kappa_2(N+1)}{\kappa_1(N-1)(N+8)} \frac{\chi}{1-\chi} (\chi \log \chi + (1-\chi) \log(1-\chi)) + \mathcal{O}(\varepsilon^2), \end{aligned} \quad (6.3.54)$$

$$\begin{aligned} f_T^{\hat{a}\hat{b}\hat{c}\hat{d}}(\chi) &= \frac{\chi^2}{(1-\chi)^2} (2 + \chi(\chi-2)) \\ &+ \varepsilon \frac{2\kappa_2}{\kappa_1(N+8)} \frac{\chi}{1-\chi} (\chi \log \chi + (1-\chi) \log(1-\chi)) + \mathcal{O}(\varepsilon^2), \end{aligned} \quad (6.3.55)$$

$$f_A^{\hat{a}\hat{b}\hat{c}\hat{d}}(\chi) = \frac{(2-\chi)\chi^3}{2(1-\chi)^2} + \mathcal{O}(\varepsilon^2). \quad (6.3.56)$$

We can expand these four-point functions in the  $1d$  conformal blocks

$$g_{\Delta}^{\Delta_{ij}, \Delta_{kl}}(\chi) = \chi^{\Delta} {}_2F_1(\Delta - \Delta_{ij}, \Delta + \Delta_{kl}; 2\Delta; \chi), \quad g_{\Delta} := g_{\Delta}^{0,0}, \quad (6.3.57)$$

where  $\Delta_{ij} = \Delta_i - \Delta_j$  are the conformal dimensions of the external operators.

The first operators in the  $\hat{\phi}^1 \times \hat{\phi}^1$  OPE are the degenerate operators  $s_{\pm}$ . They can be unmixed, which we have done in section 6.3.2 in order to obtain the anomalous dimensions  $\gamma_{s_{\pm}}$  and the OPE coefficients  $\lambda_{\hat{\phi}^a \hat{\phi}^a s_{\pm}}$ . However, in the conformal block expansion we will only see the *average* of the conformal data for this operator, and we find

$$f^{1111}(\chi) = 1 + \left(2 - \frac{3\kappa_2\varepsilon}{\kappa_1(N+8)}\right) g_2(\chi) + \varepsilon \left(\frac{3\kappa_2 + 4(N+8)(4-N)}{\kappa_1(N+8)}\right) \partial_{\Delta} g_2(\chi) + \dots, \quad (6.3.58)$$

$$(\Delta_{s_+} - 2)\lambda_{\hat{\phi}^1 \hat{\phi}^1 s_+}^2 + (\Delta_{s_-} - 2)\lambda_{\hat{\phi}^1 \hat{\phi}^1 s_-}^2 = \varepsilon \frac{3\kappa_2 + 4(N+8)(4-N)}{\kappa_1(N+8)} + \mathcal{O}(\varepsilon^2), \quad (6.3.59)$$

$$\lambda_{\hat{\phi}^1 \hat{\phi}^1 s_+}^2 + \lambda_{\hat{\phi}^1 \hat{\phi}^1 s_-}^2 = 2 - \frac{3\kappa_2\varepsilon}{\kappa_1(N+8)} + \mathcal{O}(\varepsilon^2). \quad (6.3.60)$$

This is also the case for the correlators  $f_S^{\hat{a}\hat{b}\hat{c}\hat{d}}(\chi)$  and  $f^{11\hat{a}\hat{b}}(\chi)$ , which contain in addition information on the OPE coefficients  $\lambda_{ts_{\pm}}$ . The OPE coefficients given in eq. (6.3.43) neatly obey these relations.

From the other correlators we can obtain the OPE coefficients and anomalous dimensions of  $\hat{V}^{\hat{a}}$  appearing in  $\hat{\phi}^1 \times t^{\hat{a}}$ , and  $\hat{T}^{\hat{a}\hat{b}}$  and  $\hat{A}^{\hat{a}\hat{b}}$ , which are respectively a traceless symmetric and antisymmetric operator appearing in  $t^{\hat{a}} \times t^{\hat{b}}$ .

$$\Delta_{\hat{V}} = 2 + \varepsilon \frac{2(\kappa_2 + (4-N)(N+8))}{(N+8)\kappa_1} + \mathcal{O}(\varepsilon^2), \quad \lambda_{t\hat{\phi}^1 \hat{V}}^2 = 1 - \varepsilon \frac{\kappa_2}{\kappa_1(N+8)} + \mathcal{O}(\varepsilon^2), \quad (6.3.61)$$

$$\Delta_{\hat{T}} = 2 + \varepsilon \frac{\kappa_2}{\kappa_1(8+N)} + \mathcal{O}(\varepsilon^2), \quad \lambda_{t\hat{T}}^2 = 2 - \varepsilon \frac{2\kappa_2}{\kappa_1(N+8)} + \mathcal{O}(\varepsilon^2), \quad (6.3.62)$$

$$\Delta_{\hat{A}} = 3 + \mathcal{O}(\varepsilon^2), \quad \lambda_{t\hat{A}} = 1 + \mathcal{O}(\varepsilon^2). \quad (6.3.63)$$

Setting  $N_f \rightarrow 0$ , we obtain the results for the  $O(N)$  model found in [84, 85] which provides a final check for our results.

### Four-point functions of the displacement

We consider now the four-point function of the displacement. Similarly to the two-point function, the diagrams contributing to this four-point function are the same as for the four-point function of scalars, and are shown in eq. (6.3.50). Again, we will take the derivative with respect to the transverse coordinates  $\partial_j^{\perp}$ ,  $j = 1, \dots, 4$ , and then set  $x_j^{\perp} \rightarrow 0$ ,  $j = 1, \dots, 4$ . The diagrams not involving fermions were already computed for the  $O(N)$  model in [85], while the fermionic diagram is the renormalization of the wavefunction. Adding all the diagrams and using the proper renormalization, we find the

correlators up to  $\mathcal{O}(\varepsilon)$ :

$$\begin{aligned}
\langle D_i(\tau_1)D_j(\tau_2)D_k(\tau_3)D_l(\tau_4) \rangle &= \delta_{ij}\delta_{kl} + \delta_{ik}\delta_{jl}\chi^4 + \delta_{il}\delta_{jk}\frac{\chi^4}{(1-\chi)^4} \\
&+ \varepsilon(\delta_{il}\delta_{jk} + \delta_{ik}\delta_{jl} + \delta_{ij}\delta_{kl})\frac{\kappa_2}{10\kappa_1(N+8)}\frac{\chi}{(1-\chi)^3} \\
&\times (2\chi(1-\chi)(\chi(1-\chi)-1) + \chi^3(\chi(5-2\chi)-5)\log\chi \\
&\quad - (1-\chi)^3(2\chi^2 + \chi + 2)\log(1-\chi)) \\
&+ \mathcal{O}(\varepsilon^2).
\end{aligned} \tag{6.3.64}$$

### Four-point functions of fermions

We now turn our attention to correlators involving four elementary fermions, identical up to their flavor index. This correlator is given by

$$\begin{aligned}
\langle \hat{\psi}^i(\tau_1)\hat{\psi}^j(\tau_2)\hat{\psi}^k(\tau_3)\hat{\psi}^l(\tau_4) \rangle &= \text{diagram 1} + \text{diagram 2} + \text{diagram 3} \\
&+ \text{diagram 4} + \text{diagram 5} + \mathcal{O}(\varepsilon^{\frac{3}{2}}) \\
&= \frac{\mathcal{N}_{\hat{\psi}}^4}{\tau_{12}^{2\Delta_{\hat{\psi}}}\tau_{34}^{2\Delta_{\hat{\psi}}}} \left( f_{12,34}^{ijkl}(\chi) - \frac{\chi^3}{(1-\chi)^3} f_{14,32}^{ilkj}(1-\chi) \right),
\end{aligned} \tag{6.3.65}$$

where the second term follows by crossing symmetry, and where the flavor structure is encoded in  $f_{12,34}^{ijkl}$ . The subscripts indicate the dependency on the polarization spinors  $\bar{s}_1, s_2, \bar{s}_3, s_4$ . We have omitted the product of two-point functions that gives zero at this order (see section 6.3.1). The disconnected part of the correlator is easy to compute and give

$$\begin{aligned}
\langle \hat{\psi}^i(\tau_1)\hat{\psi}^j(\tau_2)\hat{\psi}^k(\tau_3)\hat{\psi}^l(\tau_4) \rangle_{\text{disc.}} &= \langle \hat{\psi}^i(\tau_1)\hat{\psi}^j(\tau_2) \rangle \langle \hat{\psi}^k(\tau_3)\hat{\psi}^l(\tau_4) \rangle \\
&+ \langle \hat{\psi}^i(\tau_1)\hat{\psi}^l(\tau_4) \rangle \langle \hat{\psi}^k(\tau_3)\hat{\psi}^j(\tau_2) \rangle \\
&= \frac{1}{\tau_{12}^{2\Delta_{\hat{\psi}}}\tau_{34}^{2\Delta_{\hat{\psi}}}} \left\{ (\bar{s}_1\gamma^0 s_2)(\bar{s}_3\gamma^0 s_4)\delta^{ij}\delta^{kl} \right. \\
&\quad \left. - \frac{\chi^3}{(1-\chi)^3} (\{s_2, j, \chi\} \leftrightarrow \{s_4, l, 1-\chi\}) \right\}.
\end{aligned} \tag{6.3.66}$$

The connected part consists of two diagrams:

$$\langle \hat{\psi}^i(\tau_1)\hat{\psi}^j(\tau_2)\hat{\psi}^k(\tau_3)\hat{\psi}^l(\tau_4) \rangle_{\text{conn.}} = \text{diagram 1} + \text{diagram 2}. \tag{6.3.67}$$

These diagrams belong to a new class that we have not encountered yet and that we name *H-diagrams*. They can be expressed as

$$\text{diagram 1} = g_0^2 \delta^{ij} \delta^{kl} (\bar{s}_1 \Sigma^a \not{\partial}_1 \not{\partial}_2 s_2) (\bar{s}_3 \Sigma^a \not{\partial}_3 \not{\partial}_4 s_4) H_{12,34}, \tag{6.3.68}$$

where we used the rules defined in eqs. (6.2.4) and (6.2.6) in order to move the  $\Sigma$ -matrices in front, and where the integral  $H_{12,34}$  is defined in eq. (H.0.3) and has not been solved analytically yet. It is however possible to solve the integral thanks to the derivatives in

front, as shown in (H.0.19)-(H.0.21). The second diagram can be calculated analogously, and we obtain the following unit-normalized correlator:

$$\begin{aligned}
f_{12,34}^{ijkl}(\chi) &= \delta^{ij} \delta^{kl} (\bar{s}_1 \gamma^0 s_2) (\bar{s}_3 \gamma^0 s_4) \\
&+ \frac{\varepsilon}{64\kappa_1} \delta^{ij} \delta^{kl} (\bar{s}_1 \Sigma^a \gamma^0 s_2) (\bar{s}_3 \Sigma^a \gamma^0 s_4) \\
&\times \frac{\chi}{(1-\chi)^2} \left( (1-\chi)(2-\chi) + \chi^2(2-\chi) \log \chi + \chi(1-\chi)^2 \log(1-\chi) \right) \\
&+ \mathcal{O}(\varepsilon^2).
\end{aligned} \tag{6.3.69}$$

We can extract new defect CFT data from this correlator by expanding it in the  $1d$  blocks of eq. (6.3.57). Since we have  $N_f$  fermions, there is a  $U(N_f)$  flavor symmetry and we need to decompose the fermions in the singlet ( $S$ ) and adjoint (Adj) representations:

$$f^{ijkl}(\chi) = \delta^{ij} \delta^{kl} f_S(\chi) + \left( \delta^{il} \delta^{jk} - \frac{\delta^{ij} \delta^{kl}}{N_f} \right) f_{\text{Adj}}(\chi), \tag{6.3.70}$$

$$\begin{aligned}
f_S(\chi) &= \frac{4 + (\kappa_1 + N)(\chi - 1)^3 - 2\chi((\chi - 6)\chi + 6)}{(\chi - 1)^3(\kappa_1 + N - 4)} + \frac{\kappa_1 + N}{(\kappa_1 + N - 4)} \\
&+ \frac{\chi\varepsilon}{64\kappa_1(\chi - 1)^2(\kappa_1 + N - 4)} \left\{ 2(\kappa_1 - 4 + N) - \chi(14 + 3\kappa_1 + 3N) \right. \\
&+ \chi^2(\kappa_1 + N - 2) - \chi^2(\chi(\kappa_1 + N - 2) - 2(\kappa_1 + N - 3)) \log \chi \\
&\left. + (\chi - 1)^2(\chi(\kappa_1 + N - 2) + 2) \log(1 - \chi) \right\},
\end{aligned} \tag{6.3.71}$$

$$\begin{aligned}
f_{\text{Adj}}(\chi) &= \frac{\chi^3}{(\chi - 1)^3} + \frac{\varepsilon\chi}{64\kappa_1(\chi - 1)^2} \left\{ \chi(1 + \chi) + (1 + \chi)(1 - \chi)^2 \log(1 - \chi) \right. \\
&\left. + (1 - \chi)\chi^2 \log \chi \right\}.
\end{aligned} \tag{6.3.72}$$

Let us decompose the singlet sector in the conformal blocks. For the first few operators, we find

$$\begin{aligned}
f_S(\chi) &= g_0(\chi) + \frac{\varepsilon}{32\kappa_1} g_1(\chi) - \left( \frac{1}{N_f} - \frac{\varepsilon(17 - 2N - 2\kappa_1)}{384\kappa_1 N_f} \right) g_3(\chi) \\
&- \frac{\varepsilon(3 - N - \kappa_1)}{64\kappa_1 N_f} \partial_{\Delta} g_3(\chi) + \dots
\end{aligned} \tag{6.3.73}$$

The absence of a conformal block  $g_{\Delta=2}(\chi)$  indicates that

$$\lambda_{\hat{\psi}\hat{\psi}s_{\pm}} = \mathcal{O}(\varepsilon), \tag{6.3.74}$$

such that the squared OPE coefficients only contribute at  $\mathcal{O}(\varepsilon^2)$ . We can read off  $\lambda_{\hat{\psi}\hat{\psi}\hat{\phi}^1}^2$  as the coefficient in front of the block  $g_{\Delta=1}(\chi)$ , which matches the expression in eq. (6.3.46).

### Four-point functions of fermions and scalars

In this section we will compute the mixed correlator with two Dirac fermions  $\hat{\psi}^i, \hat{\psi}^j$  and two elementary scalars  $\phi^a, \phi^b$ . The correlator takes the following form:

$$\langle \hat{\psi}^i(\tau_1) \hat{\psi}^j(\tau_2) \hat{\phi}^a(\tau_3) \hat{\phi}^b(\tau_4) \rangle = \frac{\mathcal{N}_{\hat{\psi}}^2 \mathcal{N}_{\hat{\phi}}^2}{\tau_{12}^{2\Delta_{\hat{\psi}}} \tau_{34}^{2\Delta_{\hat{\phi}}}} \delta^{ij} f^{ab}(\chi), \quad (6.3.75)$$

with the kinematical cross-ratio  $\chi$  defined in eq. (6.3.47), and where the  $O(N)$  tensor structure is encoded in  $f^{ab}$ . As before, the disconnected part of the correlator is easy to obtain and consists of only one non-zero term:

$$\begin{aligned} \langle \hat{\psi}^i(\tau_1) \hat{\psi}^j(\tau_2) \hat{\phi}^a(\tau_3) \hat{\phi}^b(\tau_4) \rangle_{\text{disc.}} &= \langle \hat{\psi}^i(\tau_1) \hat{\psi}^j(\tau_2) \rangle \langle \hat{\phi}^a(\tau_3) \hat{\phi}^b(\tau_4) \rangle \\ &= \frac{(\bar{s}_1 \gamma^0 s_2)}{\tau_{12}^{2\Delta_{\hat{\psi}}} \tau_{34}^{2\Delta_{\hat{\phi}}}} \delta^{ij} \delta^{ab}. \end{aligned} \quad (6.3.76)$$

The connected part consists of two fermion-scalar  $H$ -diagrams:

$$\langle \hat{\psi}^i(\tau_1) \hat{\psi}^j(\tau_2) \hat{\phi}^a(\tau_3) \hat{\phi}^b(\tau_4) \rangle_{\text{conn.}} = \text{Diagram 1} + \text{Diagram 2}. \quad (6.3.77)$$

After using the rules defined in eqs. (6.2.4) and (6.2.6) in order to commute the  $\Sigma$ -matrices, we find that the first diagram gives

$$\text{Diagram 1} = \pm g_0^2 \delta^{ij} (\bar{s}_1 \Sigma^a \Sigma^b F_{13,24} s_2), \quad (6.3.78)$$

with  $+$  if  $\phi^a$  is a scalar and  $-$  if it is a pseudoscalar<sup>5</sup>, and where the integral  $F_{13,24}$  is defined in eq. (H.0.15) and solved in eq. (H.0.18). Putting everything together, the unit-normalized correlator reads

$$\begin{aligned} f^{ab}(\chi) &= \delta^{ab} (\bar{s}_1 \cdot s_2) \\ &\pm (\bar{s}_1 \Sigma^a \Sigma^b s_2) \frac{\varepsilon}{8\kappa_1} \frac{\chi}{(1-\chi)^2} (\chi^3 \log \chi - (1-\chi)^2 (2+\chi) \log(1-\chi)) \\ &+ \mathcal{O}(\varepsilon^2). \end{aligned} \quad (6.3.79)$$

We expand this correlator in the  $1d$  blocks of eq. (6.3.57) for the case of equal external scalars, such that

$$\Sigma^a = \Sigma^b, \quad \Sigma^a \Sigma^b = \mathbf{1}. \quad (6.3.80)$$

We find:

$$f^{aa}(\chi) = g_0(\chi) + \frac{\varepsilon}{4\kappa_1} g_2(\chi) + \frac{19\varepsilon}{240\kappa_1} g_4(\chi) - \frac{\varepsilon}{8\kappa_1} \partial_{\Delta} g_4(\chi) + \dots, \quad (6.3.81)$$

where we emphasize that no sum is implied by the repetition of indices on the left-hand side. Since the correlator and the block expansion have the same expression for  $\hat{\phi}^1$  and  $t^{\hat{a}}$ , we find the same relations for the OPE coefficients  $\lambda_{\hat{\phi}^1 \hat{\phi}^1 \mathcal{O}}$  and  $\lambda_{t\hat{a} \mathcal{O}}$ , which we will denote as  $\lambda_{\hat{\phi}^a \hat{\phi}^a \mathcal{O}}$  for brevity.

<sup>5</sup>In this formulation, the index  $b$  can be kept arbitrary since we have to commute  $\Sigma^b$  with  $\gamma$ -matrices twice.



From the block expansion we see that for  $s_{\pm}$ , which has dimension  $\Delta_{s_{\pm}} \sim 2$ , we obtain

$$\lambda_{\hat{\psi}\hat{\psi}s_+} \lambda_{\hat{\phi}^a\hat{\phi}^a s_+} + \lambda_{\hat{\psi}\hat{\psi}s_-} \lambda_{\hat{\phi}^a\hat{\phi}^a s_-} = \frac{\varepsilon}{4\kappa_1}, \quad (6.3.82)$$

$$(\Delta_{s_+} - 2)\lambda_{\hat{\psi}\hat{\psi}s_+} \lambda_{\hat{\phi}^a\hat{\phi}^a s_+} + (\Delta_{s_-} - 2)\lambda_{\hat{\psi}\hat{\psi}s_-} \lambda_{\hat{\phi}^a\hat{\phi}^a s_-} = 0. \quad (6.3.83)$$

Using the expressions for  $\Delta_{s_{\pm}}$  and  $\lambda_{\hat{\phi}^1\hat{\phi}^1 s_{\pm}}, \lambda_{tt s_{\pm}}$  in eqs. (6.3.39) and (6.3.43), we can extract the OPE coefficients involving the fermions:

$$\lambda_{\hat{\psi}\hat{\psi}s_{\pm}} = \varepsilon \frac{(N\kappa_2 - 4(N-4)(N+8) \pm \kappa_3) \sqrt{\kappa_3 \pm 4(N-4)(N+8) \pm (N-2)\kappa_2}}{16\kappa_1\kappa_2\sqrt{\kappa_3}\sqrt{N-1}} + \mathcal{O}(\varepsilon^2). \quad (6.3.84)$$

As expected from the conformal block expansion in eq. (6.3.73), the OPE coefficients start at  $\mathcal{O}(\varepsilon)$ .

## 6.4 Correlators of bulk operators with a defect

The three- and four-point functions of scalars and fermions on the defect provided us with important defect data. In addition, we can also study bulk operators in the presence of the line defect, and obtain new data such as bulk-to-defect OPE coefficients. In this section we study two-point functions of bulk and defect operators, as well as two-point functions of bulk scalars. At the end of the section we give a short outlook on how to generalize our analysis to the case of fermionic operators.

### 6.4.1 One-point functions

**Squared scalar.** We computed the one-point function of  $\phi^a$  in section 6.2 to extract the  $\beta$ -function of the defect coupling. The coefficient of this one-point function,  $a_{\phi}$ , will appear in the bulk channel expansion of the two-point function of  $\phi^a$  in the presence of the line defect. One-point function coefficients of other operators will appear as well, the first one being the one-point function of  $\phi^2$  and the traceless symmetric tensor  $T^{ab} = \phi^a\phi^b - \frac{\delta^{ab}}{N}(\phi^c)^2$ .<sup>6</sup> These observables were computed for the  $O(N)$  model in [84]. At  $\mathcal{O}(\varepsilon)$  there are four diagrams that contribute:

$$\langle\langle \phi_a \phi_b(x) \rangle\rangle = \text{diag}_1 + \text{diag}_2 + \text{diag}_3 + \text{diag}_4 + \mathcal{O}(\varepsilon^2). \quad (6.4.1)$$

The diagrams not including any fermionic contributions were computed in [84, 86, 87], while the diagram with the fermionic loop cancels the wavefunction renormalization of  $\phi^a$ . In order to compute the one-point function coefficient, we need the renormalization factor, anomalous dimension, and normalization factor of  $\phi^2$  and  $T^{ab}$ . The anomalous dimensions for the GNY and NJLY models can be found in [174], while the others can be obtained from computing the corrections to the propagator  $\langle\phi^a\phi^b(x_1)\phi^c\phi^d(x_2)\rangle$ . Generalized for

<sup>6</sup>Note that  $T^{ab}$  does not appear for the GNY model, where  $N = 1$ .

$N = 1, 2, 3$ , we find for  $\phi^2$  up to  $\mathcal{O}(\varepsilon)$  [174, 206]

$$Z_{\phi^2} = 1 - \frac{1}{\varepsilon(4\pi)^2} \left( \frac{\lambda(N+2)}{3} + 4g^2 N_f \right) + \mathcal{O}\left(\frac{1}{\varepsilon^2}\right), \quad (6.4.2)$$

$$\gamma_{\phi^2} = \frac{\lambda(N+2)}{3(4\pi)^2} + \frac{4g^2 N_f}{(4\pi)^2} + \mathcal{O}(\lambda^2, g^4, \lambda g^2), \quad (6.4.3)$$

$$\mathcal{N}_{\phi^2} = \frac{\Gamma\left(\frac{d}{2}\right) \sqrt{2N}}{2\pi^{\frac{d}{2}}(d-2)} \left\{ 1 - \varepsilon \left( \frac{2(\aleph+1)(N+8)(\kappa_1+N-4) + \kappa_2 \aleph(N+2)}{4\kappa_1(N+8)} \right) + \mathcal{O}(\varepsilon^2) \right\}. \quad (6.4.4)$$

For  $T^{ab}$ , we obtain the following results:

$$Z_T = 1 - \frac{1}{\varepsilon(4\pi)^2} \left( \frac{2\lambda}{3} + 4g^2 N_f \right) + \mathcal{O}\left(\frac{1}{\varepsilon^2}\right), \quad (6.4.5)$$

$$\gamma_T = \frac{2\lambda}{3(4\pi)^2} + \frac{4g^2 N_f}{(4\pi)^2} + \mathcal{O}(\lambda^2, g^4, \lambda g^2), \quad (6.4.6)$$

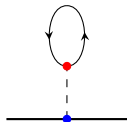
$$\mathcal{N}_{\phi^2} = \frac{\Gamma\left(\frac{d}{2}\right)}{\sqrt{2}\pi^{\frac{d}{2}}(d-2)} \left\{ 1 - \varepsilon \left( \frac{(\aleph+1)(N+8)(\kappa_1+N-4) + \kappa_2 \aleph}{2\kappa_1(N+8)} \right) + \mathcal{O}(\varepsilon^2) \right\}, \quad (6.4.7)$$

from which we can extract the one-point function coefficients  $a_{\phi^2}$  and  $a_T$ :

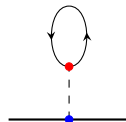
$$a_{\phi^2} = \frac{(4-N)(N+8)}{2\kappa_2\sqrt{2N}} + \mathcal{O}(\varepsilon), \quad a_T = \frac{(4-N)(N+8)}{2\kappa_2\sqrt{2}} + \mathcal{O}(\varepsilon). \quad (6.4.8)$$

The  $\mathcal{O}(\varepsilon)$ -terms are lengthy and can be found in the attached Mathematica notebook.

**Fermion bilinear.** Another interesting one-point function is  $\langle\langle \bar{\psi}^i \psi^i(x) \rangle\rangle$ , which appears in the two-point function  $\langle\langle \bar{\psi}^i(x_1) \psi^j(x_2) \rangle\rangle$ . In this case,  $\bar{\psi}^i \psi^i$  is not a conformal primary, but rather a conformal descendant of  $\phi$ . This can be seen from its conformal dimension being  $\Delta_\phi + 2 + \mathcal{O}(\varepsilon^2)$  [174]. The one-point function can be computed through Feynman diagrams, and receives a contribution at  $\mathcal{O}(\sqrt{\varepsilon})$ :

$$\langle\langle \bar{\psi}^i \psi^i(x) \rangle\rangle = \text{Diagram} + \mathcal{O}(\varepsilon). \quad (6.4.9)$$


This egg-shaped diagram is new and has the following expression:

$$\text{Diagram} = \mathcal{N}_{\bar{\psi}\psi} \frac{g_0 h_0 N_f}{16\pi^3 |x^\perp|^3} s^1 \text{tr} \Sigma^1. \quad (6.4.10)$$


Hence, the one-point function coefficient can be written as

$$\langle\langle \bar{\psi}^i \psi^i(x) \rangle\rangle = \frac{a_{\bar{\psi}\psi}}{|x^\perp|^{\Delta_{\bar{\psi}\psi}}}, \quad a_{\bar{\psi}\psi} = -\frac{\sqrt{(4-N)(N+8)} 8\pi^2 N_f}{\sqrt{\kappa_1 \kappa_2} (4\pi)^2} \sqrt{\varepsilon} + \mathcal{O}(\varepsilon). \quad (6.4.11)$$

### 6.4.2 Bulk-to-defect two-point functions

The correlators of a bulk and a defect operator give us the OPE coefficients of the bulk-to-defect OPE. The fundamental bulk scalar  $\phi^a$  can be decomposed into  $\hat{\phi}^1$  and  $t^{\hat{a}}$ , and the two-point function between these operators is given by the following diagrams:

$$\langle\langle \phi^a(x_1) \hat{\phi}^b(\tau_2) \rangle\rangle = \text{---} + \text{---} + \text{---} + \mathcal{O}(\varepsilon^2). \quad (6.4.12)$$

The first diagram does not involve any integration, while the second is a self-energy correction. The third diagram is less trivial, and was computed in [86]. Adding all diagrams and the proper renormalization terms, we obtain the following bulk-to-defect OPE coefficients:

$$\langle\langle \phi^a(x_1) \hat{\phi}^1(\tau_2) \rangle\rangle = \frac{\delta^{a1} \mathcal{N}_\phi \mathcal{N}_{\hat{\phi}^1} \hat{b}_{\phi \hat{\phi}^1}}{(\hat{x}_{12}^2)^{\hat{\Delta}_{\hat{\phi}^1}} |x_1^\perp|^{\Delta_\phi - \hat{\Delta}_{\hat{\phi}^1}}}, \quad \hat{b}_{\phi \hat{\phi}^1} = 1 + \varepsilon \frac{3(4-N)(\log 2 - 1)}{2\kappa_1} + \mathcal{O}(\varepsilon^2), \quad (6.4.13)$$

$$\langle\langle \phi^a(x_1) t^{\hat{b}}(\tau_2) \rangle\rangle = \frac{\delta^{a\hat{b}} \mathcal{N}_\phi \mathcal{N}_t \hat{b}_{\phi t}}{(\hat{x}_{12}^2)^{\hat{\Delta}_t} |x_1^\perp|^{\Delta_\phi - \hat{\Delta}_t}}, \quad \hat{b}_{\phi t} = 1 + \varepsilon \frac{(4-N)(\log 2 - 1)}{2\kappa_1} + \mathcal{O}(\varepsilon^2). \quad (6.4.14)$$

### 6.4.3 Two-point functions of bulk scalars

In the presence of a defect, the two-point function of bulk operators is no longer fixed by kinematics. Instead, it depends on two *defect cross-ratios* determined by the distance to the defect and the distance between the bulk operators. The scalar two-point function then takes the form

$$\langle\langle \phi^a(x_1) \phi^b(x_2) \rangle\rangle = \frac{\mathcal{N}_\phi^2 \mathcal{F}^{ab}(r, w)}{|x_1^\perp|^{\Delta_\phi} |x_2^\perp|^{\Delta_\phi}}, \quad (6.4.15)$$

where  $\mathcal{F}^{ab}(r, w)$  is a function of the cross-ratios

$$r + \frac{1}{r} = \frac{\tau_{12}^2 + (x_1^\perp)^2 + (x_2^\perp)^2}{|x_1^\perp| |x_2^\perp|}, \quad w + \frac{1}{w} = \frac{2x_1^\perp \cdot x_2^\perp}{|x_1^\perp| |x_2^\perp|}. \quad (6.4.16)$$

It is sometimes convenient to switch to different cross-ratios  $z, \bar{z}$ , which are related to  $r, w$  as

$$z = rw, \quad \bar{z} = \frac{r}{w}. \quad (6.4.17)$$

The diagrams contributing to this two-point function, up to  $\mathcal{O}(\varepsilon)$ , are shown in figure 6.2. They consist of diagrams we already encountered when computing the one-point function of  $\phi^a$ , of diagrams coming from the wavefunction renormalization in the bulk, and one non-trivial one.

The non-trivial diagram is the X-shaped diagram, which was computed for a line

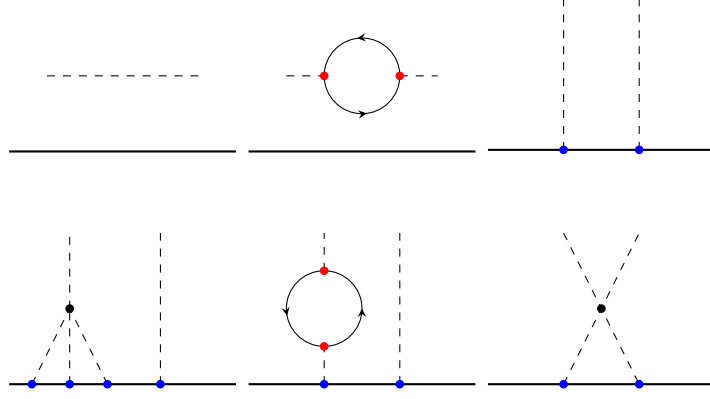


Figure 6.2: Contributions to the two-point function  $\langle\langle \phi^a(x_1)\phi^b(x_2) \rangle\rangle$  up to  $\mathcal{O}(\varepsilon)$ . The defect is denoted by a solid line, scalars by a dotted line, and fermions by solid arrowed lines. Bulk scalar couplings  $\lambda_0$  are represented by a black dot, bulk Yukawa couplings  $g_0$  by a red dot and defect couplings  $h_0$  by a blue dot.

defect in the  $O(N)$  model in [86, 87]. Evaluating it in  $d = 4$  gives:

$$\begin{aligned}
 \text{Diagram} &= -\frac{\lambda_0 h_0^2 \Gamma\left(\frac{d}{2}\right)^4}{32\pi^{2d}(d-2)^4} \int \frac{d\tau_3 d\tau_4 d^d x_5}{(\hat{x}_{35}^2)^{\frac{d-2}{2}} (\hat{x}_{45}^2)^{\frac{d-2}{2}} (x_{15}^2)^{\frac{d-2}{2}} (x_{25}^2)^{\frac{d-2}{2}}} \\
 &= \frac{3\lambda_0 h_0^2 H(r, w)}{768\pi^4 |x_1^\perp| |x_2^\perp|} + \mathcal{O}(\varepsilon^2),
 \end{aligned} \tag{6.4.18}$$

where  $H(r, w)$  contains one unevaluated integral over a Schwinger parameter  $\alpha$  [86]:

$$H(r, w) = -\int_0^\infty d\alpha \sqrt{\frac{z\bar{z}}{(\alpha+1)(\alpha+z\bar{z})(\alpha+z)(\alpha+\bar{z})}} \tanh^{-1} \sqrt{\frac{(\alpha+z)(\alpha+\bar{z})}{(\alpha+1)(\alpha+z\bar{z})}}. \tag{6.4.19}$$

Even though the integral is unevaluated, the series expansions in the bulk and defect channels are known.

Adding all diagrams in figure 6.2 and properly renormalizing them, we obtain:

$$\mathcal{F}^{ab}(r, w) = \delta^{ab} \xi^{-\Delta_\phi} + \delta^{a1} \delta^{b1} a_\phi^2 + \varepsilon(\delta^{ab} + 2\delta^{a1} \delta^{b1}) \frac{3(4-N)}{4\kappa_1} H(r, w) + \mathcal{O}(\varepsilon^2). \tag{6.4.20}$$

Here,  $a_\phi$  is the one-point function coefficient given in eq. (6.2.33). We see that the general form is the same as in [86, 87], except for additional fermionic contributions to the coefficient in front of  $H(r, w)$ . We can expand this expression in bulk and defect conformal blocks to extract CFT data, and check with the explicit calculations in the previous sections.

### Defect channel

In the defect channel, the correlator  $\mathcal{F}^{ab}(r, w)$  contains two types of operators:  $O(N)$ -singlets  $\hat{\mathcal{O}}_{s,n}^S$  and  $O(N)$ -vectors  $\hat{\mathcal{O}}_{s,n}^V$ . Their conformal dimensions are given by

$$\Delta_{\hat{\mathcal{O}}_{s,n}^{S,V}} = \Delta_\phi + s + n + \gamma_{\hat{\mathcal{O}}_{s,n}^{S,V}}. \tag{6.4.21}$$

These operators are in general degenerate, except for  $n = 0$ , where they can be expressed as derivatives of  $\hat{\phi}^1$  and  $t$ :

$$\hat{\mathcal{O}}_{s,0}^S \sim \partial_{i_1}^\perp \cdots \partial_{i_s}^\perp \hat{\phi}_1, \quad \hat{\mathcal{O}}_{s,0}^S \sim \partial_{i_1}^\perp \cdots \partial_{i_s}^\perp t_{\hat{a}}, \quad (6.4.22)$$

where  $i_n = 1, \dots, d-1$  are the directions transverse to the defect. For higher  $n$ , one needs to solve a mixing problem. This has been done in [84, 85] for the  $O(N)$  model and repeated in section 6.3.2 for the case  $n = 1, s = 0$  to obtain the anomalous dimension  $\gamma_{s\pm}$ . For general  $n > 0, s$  we will give the averaged CFT data.

The correlator  $\mathcal{F}^{ab}(r, w)$  can be decomposed in the two symmetry channels  $S$  (singlet) and  $V$  (vector):

$$\mathcal{F}^{ab}(r, w) = \delta^{a1} \delta^{b1} \hat{\mathcal{F}}_S(r, w) + (\delta^{ab} - \delta^{a1} \delta^{b1}) \hat{\mathcal{F}}_V(r, w), \quad (6.4.23)$$

$$\hat{\mathcal{F}}_S(r, w) = a_\phi^2 + \frac{1}{\xi^{\Delta_\phi}} + \varepsilon \frac{3(4-N)}{4\kappa_1} H(r, w), \quad \hat{\mathcal{F}}_V(r, w) = \frac{1}{\xi^{\Delta_\phi}} + \varepsilon \frac{(4-N)}{4\kappa_1} H(r, w). \quad (6.4.24)$$

Each of the channels can be composed in defect conformal blocks, which are known in closed form [47]:

$$\mathcal{F}(z, \bar{z}) = \sum_{\mathcal{O}} 2^{-s} \hat{b}_{\mathcal{O}\mathcal{O}}^2 \hat{f}_{\hat{\Delta},s}(z, \bar{z}), \quad (6.4.25)$$

$$\hat{f}_{\hat{\Delta},s}(z, \bar{z}) = (z\bar{z})^{\frac{\hat{\Delta}}{2}} \left(\frac{\bar{z}}{z}\right)^{\frac{s}{2}} {}_2F_1\left(\frac{p}{2}, \hat{\Delta}; \hat{\Delta} + 1 - \frac{p}{2}; z\bar{z}\right) {}_2F_1\left(-s, \frac{q}{2} - 1; 2 - \frac{q}{2} - s; \frac{z}{\bar{z}}\right), \quad (6.4.26)$$

where  $p = 1$  is the dimension of the defect,  $q = d - 1$  the codimension,  $s$  is the transverse spin and we have switched variables from  $r, w$  to  $z, \bar{z}$  using the definition in eq. (6.4.17). The factor of  $2^{-s}$  ensures that the blocks have a convenient normalization.

To expand the correlator in terms of these blocks, we need to know how to decompose the function  $H(r, w)$ . It turns out there is an elegant expression found in [86, 87]:

$$H(r, w) = \sum_{s=0}^{\infty} \left( \frac{H_s - H_{s-\frac{1}{2}}}{s + \frac{1}{2}} - \frac{1}{(s + \frac{1}{2})^2} + \frac{1}{s + \frac{1}{2}} \partial_{\hat{\Delta}} \right) \hat{f}_{s+1,s}(r, w). \quad (6.4.27)$$

The derivative of the block gives us the anomalous dimension of the corresponding operator, and hence eq. (6.4.27) provides a straightforward way to extract defect CFT data.

The constant terms in eq. (6.4.24) correspond to the defect identity given by  $\hat{f}_{0,0}(r, w)$ . This leaves us with the factors  $\xi^{-\Delta_\phi}$ , whose expansion in defect blocks is well known [51].

Combining all the pieces together we are ready to extract the CFT data. Let us start with the singlet channel. Expanding in conformal blocks gives us

$$\hat{\mathcal{F}}_S(r, w) = a_\phi^2 \hat{f}_{0,0}(r, w) + \sum_{s=0}^{\infty} 2^{-s} \hat{b}_{\phi\hat{\mathcal{O}}_{s,0}^S}^2 \hat{f}_{\hat{\Delta}_{\hat{\mathcal{O}}_{s,0}^S},s}(r, w) + \mathcal{O}(\varepsilon^2), \quad (6.4.28)$$

where up to  $\mathcal{O}(\varepsilon)$  only operators with  $n = 0$  appear. Combining eq. (6.4.28) and eq. (6.4.24), and using the expression in eq. (6.4.27), we obtain the following OPE coefficients:

$$\hat{b}_{\phi\hat{\mathcal{O}}_{s,0}^S} = 2^{\frac{s}{2}} \left\{ 1 + \frac{\varepsilon}{4\kappa_1} \left( \frac{6(N-4)}{(2s+1)^2} - \frac{(\kappa_1(2s+1) + 3(N-4))}{(2s+1)} H_s + 3(N-4) H_{s-\frac{1}{2}} \right) + \mathcal{O}(\varepsilon^2) \right\}. \quad (6.4.29)$$

For  $s = 0$ , we see that this matches exactly the bulk-to-defect OPE coefficient  $\hat{b}_{\phi\hat{\phi}_1}$  given in eq. (6.4.14). As stated above, to extract the anomalous dimension we only have to look at the derivative term in eq. (6.4.27). This results in

$$\begin{aligned}\Delta_{\hat{\mathcal{O}}_{s,0}^S} &= \Delta_\phi + s + n + \frac{3(4-N)\varepsilon}{4\kappa_1\left(s + \frac{1}{2}\right)} + \mathcal{O}(\varepsilon^2) \\ &= 1 + s + \frac{(N-4)(s-1)\varepsilon}{\kappa_1(2s+1)} + \mathcal{O}(\varepsilon^2).\end{aligned}\tag{6.4.30}$$

For  $s = 0$ , this matches with  $\Delta_{\hat{\phi}_1}$  given in eq. (6.3.1), while for  $s = 1$  this should give us the dimension of the displacement  $\Delta_D = 2$ . Indeed, we see that for  $s = 1$ , the  $\mathcal{O}(\varepsilon)$  correction is zero and the dimension is protected and equal to 2.

We are ready to move on to the vector channel. The expansion in conformal blocks results in

$$\hat{\mathcal{F}}_V(r, w) = \sum_{s=0}^{\infty} 2^{-s} \hat{b}_{\phi\hat{\mathcal{O}}_{s,0}^V}^2 \hat{f}_{\hat{\Delta}_{\hat{\mathcal{O}}_{s,0}^V}, s}(r, w) + \mathcal{O}(\varepsilon^2),\tag{6.4.31}$$

where we see that also here up to  $\mathcal{O}(\varepsilon)$ , only the  $n = 0$  family of operators appears. The defect identity is not present in this case. We will follow the same procedure as for the singlet channel, and extract the bulk-to-defect OPE coefficients

$$\hat{b}_{\phi\hat{\mathcal{O}}_{s,0}^V} = 2^{\frac{s}{2}} \left\{ 1 + \frac{\varepsilon(N-4)}{4\kappa_1} \left( \frac{2s+3}{(2s+1)^2} + \frac{2sH_s + H_{s-\frac{1}{2}}}{(2s+1)} \right) + \mathcal{O}(\varepsilon^2) \right\}.\tag{6.4.32}$$

We can now compare this for  $s = 0$  with  $\hat{b}_{\phi t}$  in eq. (6.4.14) and find a perfect match. The anomalous dimensions are once again read off from the derivative term in the expansion of  $H(r, w)$ , and result in the following conformal dimensions:

$$\hat{\Delta}_{\hat{\mathcal{O}}_{s,0}^V} = \Delta_\phi + s + n + \frac{\varepsilon(4-N)}{4\kappa_1\left(s + \frac{1}{2}\right)} + \mathcal{O}(\varepsilon^2) = 1 + s + \frac{\varepsilon(N-4)s}{\kappa_1(2s+1)} + \mathcal{O}(\varepsilon^2).\tag{6.4.33}$$

As a check, we see that for  $s = 0$  the  $\mathcal{O}(\varepsilon)$  term disappears and we find the protected dimension of the tilt  $\Delta_t = 1$ .

## Bulk channel

In the bulk channel, the operators that appear in the  $\phi^a \times \phi^b$  OPE are  $O(N)$  singlets  $\mathcal{O}_{\ell,n}^S$ , where the first one is  $\phi^2$ , and traceless symmetric representations  $\mathcal{O}_{\ell,n}^T$ , the first one of which is  $T^{ab}$ . The operators in the lowest twist family after  $\phi^2$  and  $T^{ab}$  can be written as

$$\mathcal{O}_{\ell,0}^S \sim \partial_{\mu_1} \cdots \partial_{\mu_\ell} (\phi^a)^2, \quad \mathcal{O}_{\ell,0}^T \sim \partial_{\mu_1} \cdots \partial_{\mu_\ell} \left( \phi^a \phi^b - \frac{\delta^{ab}}{N} (\phi^c)^2 \right),\tag{6.4.34}$$

where  $\ell \geq 2$ . In the free theory, they are the higher-spin currents and hence their conformal dimension and OPE coefficients are protected up to  $\mathcal{O}(\varepsilon)$  and given by the conformal dimension of  $\phi$  and their spin. The CFT data is given by

$$\Delta_{\mathcal{O}_{\ell,0}^{S,T}} = 2\Delta_\phi + \ell + \mathcal{O}(\varepsilon^2),\tag{6.4.35}$$

$$\lambda_{\phi\phi\mathcal{O}_{\ell,0}^S}^2 = \frac{2^{\ell+1}(\Delta_\phi)_\ell^2}{N\ell!(2\Delta_\phi + \ell - 1)_\ell} + \mathcal{O}(\varepsilon^2),\tag{6.4.36}$$

$$\lambda_{\phi\phi\mathcal{O}_{\ell,0}^T}^2 = N\lambda_{\phi\phi\mathcal{O}_{\ell,0}^S}^2 + \mathcal{O}(\varepsilon^2).\tag{6.4.37}$$

Operators with  $n > 0$  are not protected up to this order, and are also degenerate. The correlator can be decomposed in the two symmetry channels as:

$$\mathcal{F}^{ab}(r, w) = \delta^{ab} \mathcal{F}_S(r, w) + \left( \delta^{a1} \delta^{b1} - \frac{\delta^{ab}}{N} \right) \mathcal{F}_T(r, w), \quad (6.4.38)$$

$$\mathcal{F}_S(r, w) = \frac{1}{\xi^{\Delta_\phi}} + \frac{a_\phi^2}{N} + \frac{\varepsilon(4-N)(N-2)}{4N\kappa_1} H(r, w), \quad (6.4.39)$$

$$\mathcal{F}_T(r, w) = a_\phi^2 + \frac{\varepsilon(4-N)}{2\kappa_1} H(r, w). \quad (6.4.40)$$

The decomposition in bulk channel blocks is more difficult, since they are not known in closed form. One should also keep in mind that the correlator gets multiplied by a factor of  $\xi^{\Delta_\phi}$  coming from the prefactor. However, as pointed out, eq. (6.4.20) has a similar form to the correlator  $\langle\langle \phi^a \phi^b \rangle\rangle$  computed for the  $O(N)$  model in [86, 87], and we can reuse known results. In particular, they found an expression for  $H(r, w)$  in terms of bulk blocks as well:

$$\xi H(r, w) = (\partial_\Delta - 1 - \log 2) f_{2,0}^0(r, w) + \mathcal{O}(\varepsilon), \quad (6.4.41)$$

where  $f_{\Delta,\ell}^{\Delta_{12}}(r, w)$  are the bulk channel conformal blocks, which are known as a double sum [47, 137].

From eq. (6.4.41) we see that  $H(r, w)$  only corrects  $\phi^2$ , hence, for the CFT data of the other operators we can directly use the results from [86, 87]. The other terms in eq. (6.4.40), after multiplication with  $\xi^{\Delta_\phi}$ , are a constant term that corresponds to the bulk identity  $f_{0,0}^0(r, w)$ , and a term proportional to  $\xi^{\Delta_\phi}$ , whose expansion in bulk blocks is given in equation (167) of [86]. Putting everything together, the expansion of  $\mathcal{F}_{S,T}$  in blocks can be written as follows:

$$\begin{aligned} \xi^{\Delta_\phi} \mathcal{F}_S(r, w) &= 1 + \lambda_{\phi\phi\phi^2} a_{\phi^2} f_{\Delta_{\phi^2},0} + \sum_{\ell=2,4,\dots}^{\infty} 2^{-\ell} \lambda_{\phi\phi\mathcal{O}_{\ell,0}^S} a_{\mathcal{O}_{\ell,0}^S} f_{2\Delta_\phi+\ell,\ell}^0 \\ &\quad + \sum_{\ell=0,2,\dots}^{\infty} 2^{-\ell} \overline{\lambda_{\phi\phi\mathcal{O}_{\ell,1}^S} a_{\mathcal{O}_{\ell,1}^S}} f_{2\Delta_\phi+\ell+2,\ell}^0 + \mathcal{O}(\varepsilon^2), \end{aligned} \quad (6.4.42)$$

$$\begin{aligned} \xi^{\Delta_\phi} \mathcal{F}_T(r, w) &= \lambda_{\phi\phi T} a_T f_{\Delta_T,0} + \sum_{\ell=2,4,\dots}^{\infty} 2^{-\ell} \lambda_{\phi\phi\mathcal{O}_{\ell,0}^T} a_{\mathcal{O}_{\ell,0}^T} f_{2\Delta_\phi+\ell,\ell}^0 \\ &\quad + \sum_{\ell=0,2,\dots}^{\infty} 2^{-\ell} \overline{\lambda_{\phi\phi\mathcal{O}_{\ell,1}^T} a_{\mathcal{O}_{\ell,1}^T}} f_{2\Delta_\phi+\ell+2,\ell}^0 + \mathcal{O}(\varepsilon^2), \end{aligned} \quad (6.4.43)$$

where the bar indicates an average over CFT data since mixing needs to be solved before one is able to extract the individual OPE and one-point coefficients. We can now extract the CFT data of all operators except  $\phi^2$  and  $T$ . For the  $O(N)$  singlets, using eq. (6.4.37), we extract the following one-point functions of twist-two operators:

$$\begin{aligned} a_{\mathcal{O}_{\ell,0}^S} &= \frac{(4-N)(N+8)\Gamma\left(\frac{\ell+1}{2}\right)^2 \sqrt{\frac{2^{1-\ell}\Gamma(\frac{\ell+1}{2})}{N\Gamma(\frac{\ell+1}{2})}}}{\pi^{\frac{3}{4}} \kappa_2 \ell^2 \Gamma\left(\frac{\ell}{2}\right)^2} \left\{ 1 + \varepsilon \left( -\frac{2\kappa_2 a_\phi^{(1)}}{(N-4)(N+8)} \right. \right. \\ &\quad \left. \left. + \frac{(N-4)}{2\kappa_1} \left( 2H_{\frac{\ell-1}{2}} + H_{2\ell} - 2H_\ell - H_{\ell-\frac{1}{2}} + 2\log 2 \right) \right) + \mathcal{O}(\varepsilon^2) \right\}, \end{aligned} \quad (6.4.44)$$

where  $a_\phi^{(1)}$  is the  $\mathcal{O}(\varepsilon)$  correction to  $a_\phi$ , which can be found in the attached Mathematica notebook. The averaged CFT data for the higher-twist  $n = 1$  operators is given by

$$\overline{\lambda_{\phi\phi\mathcal{O}_{\ell,1}^S} a_{\mathcal{O}_{\ell,1}^S}} = \varepsilon \frac{(\ell+1)^2(4-N)(N+8)\Gamma\left(\frac{\ell+1}{2}\right)^3}{64\pi\kappa_2 N \Gamma\left(\frac{\ell}{2}+2\right)\Gamma\left(\ell+\frac{3}{2}\right)} + \mathcal{O}(\varepsilon^2). \quad (6.4.45)$$

For the traceless symmetric operators, we find the following conformal dimensions and OPE coefficients:

$$a_{\mathcal{O}_{\ell,0}^T} = \frac{(4-N)(N+8)\Gamma\left(\frac{\ell+1}{2}\right)^2 \sqrt{\frac{2^{1-\ell}\Gamma(\ell+1)}{\Gamma(\ell+\frac{1}{2})}}}{\pi^{\frac{3}{4}}\kappa_2 \ell^2 \Gamma\left(\frac{\ell}{2}\right)^2} \left\{ 1 + \varepsilon \left( -\frac{2\kappa_2 a_\phi^{(1)}}{(N-4)(N+8)} + \frac{(N-4)\left(2H_{\frac{\ell-1}{2}} - 2H_\ell + H_{2\ell} - H_{\ell-\frac{1}{2}} + \log(4)\right)}{2\kappa_1} \right) \right\} + \mathcal{O}(\varepsilon^2) \quad (6.4.46)$$

$$\overline{\lambda_{\phi\phi\mathcal{O}_{\ell,1}^T} a_{\mathcal{O}_{\ell,1}^T}} = \varepsilon \frac{(\ell+1)^2(N+8)\Gamma\left(\frac{\ell+1}{2}\right)^3}{128\pi\Gamma\left(\frac{\ell}{2}+2\right)\Gamma\left(\ell+\frac{3}{2}\right)} + \mathcal{O}(\varepsilon^2). \quad (6.4.47)$$

To compare the expansion in eq. (6.4.43) with the one-point functions of  $\phi^2$  and  $T_{ab}$  computed in section 6.4.1, we need to know the bulk OPE coefficients  $\lambda_{\phi\phi\phi^2}$  and  $\lambda_{\phi\phi T}$ . These can be easily calculated and are given by

$$\lambda_{\phi\phi\phi^2} = \delta^{ab} \left( \sqrt{\frac{2}{N}} - \frac{\varepsilon\kappa_2(N+2)}{2\sqrt{2N}\kappa_1(N+8)} + \mathcal{O}(\varepsilon^2) \right), \quad (6.4.48)$$

$$\lambda_{\phi\phi T} = \sqrt{2} - \frac{\varepsilon\kappa_2}{\sqrt{2}\kappa_1(N+8)} + \mathcal{O}(\varepsilon^2). \quad (6.4.49)$$

With these OPE coefficients and the one-point functions in eq. (6.4.8), we can check the block expansion in eq. (6.4.43) and see that it indeed reproduces the desired conformal data of  $\phi^2$  and  $T^{ab}$ .

#### 6.4.4 Towards two-point functions of bulk fermions

We conclude this section by commenting on how to generalize the two-point function analysis when the external operators are fermions. This is an interesting problem as the  $\varepsilon$ -expansion was originally designed to capture physics in three dimensions, however four-dimensional fermions are very different objects compared to three-dimensional fermions. In order to understand how fermionic correlators in  $d = 3$  are encoded in the  $\varepsilon$ -expansion, we can start by calculating them in perturbation theory. We will not bring this calculation to completion in this section, as the diagrams involved are a lot more challenging than the ones we have studied so far. Nevertheless we sketch out the computation, and in the conclusion we discuss in more detail possible future directions.

The disconnected part of the correlator corresponds to the wavefunction renormalization of the bulk fermion, and the diagrams are the first and third ones shown in figure 6.3. The Feynman diagrams contributing to the connected part of the fermionic two-point function  $\langle\langle \bar{\psi}^i(x_1)\psi^j(x_2) \rangle\rangle$  up to  $\mathcal{O}(\varepsilon)$  are given in figure 6.3 (second and fourth diagrams).



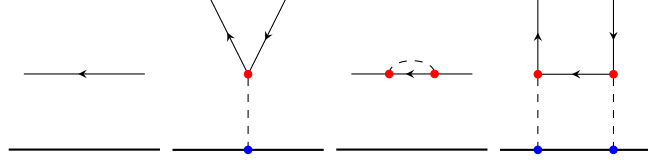


Figure 6.3: Contributions to the two-point function  $\langle\langle \bar{\psi}^i(x_1)\psi^j(x_2) \rangle\rangle$  up to  $\mathcal{O}(\varepsilon)$ . The defect is denoted by a solid line, scalars by a dotted line, and fermions by solid arrowed lines. Bulk Yukawa couplings  $g_0$  are represented by a red dot and defect couplings  $h_0$  by a blue dot. The first and third diagrams correspond to the *disconnected* part of the correlator, while the second and fourth are *connected* and are the diagrams which make the correlator different to a defectless two-point function.

The Y-diagram in figure 6.3 is the first connected diagram at  $\mathcal{O}(g) \sim \mathcal{O}(\sqrt{\varepsilon})$ . It is given by

$$\begin{aligned}
 \begin{array}{c} \diagup \\ \diagdown \\ \cdot \\ \vdots \\ \cdot \\ \text{---} \end{array} &= \bar{s}_1^A s_2^B \mathcal{N}_\psi^2 g_0 h_0 \delta^{ij} \int d\tau_3 \int d^4 x_4 \not{x}_1 I_{14} \Sigma^1 \not{x}_2 I_{24} I_{34} \\
 &= -\frac{\pi g_0 h_0 \delta^{ij}}{8(|x_1^\perp| + |x_2^\perp|)} \bar{s}_1 \left( \frac{\not{x}_1 \not{x}_2}{|x_1^\perp| |x_2^\perp|} + \mathbb{1} \right) s_2,
 \end{aligned} \tag{6.4.50}$$

where we have used the fermionic star-triangle identity given in eq. (H.0.17). The remaining one-dimensional integral is trivial to compute.

At  $\mathcal{O}(\varepsilon)$  we have one H-diagram that connects scalar insertions on the line to the external fermions through two Yukawa vertices. This diagram contains a challenging ten-dimensional (finite) integral that we will only solve partially for now. We will however provide a solution for the  $4d$  bulk integral, i.e. before performing the  $\tau_3, \tau_4$  integrals. After Wick contractions the diagram gives

$$\begin{array}{c} \uparrow \\ \cdot \\ \leftarrow \\ \cdot \\ \vdots \\ \cdot \\ \text{---} \end{array} = -g_0^2 h_0^2 \bar{s}_1 \int d\tau_3 \int d\tau_4 \int d^4 x_5 \int d^4 x_6 \not{x}_1 I_{15} \Sigma^1 \not{x}_5 I_{56} \Sigma^1 \not{x}_6 I_{26} I_{35} I_{46} s_2.$$

(6.4.51)

We set  $\Sigma^1 = \mathbb{1}$  as in eq. (6.2.4), and one four-dimensional integral can be lifted by using the fermionic star-triangle identity given in eq. (H.0.17). We then have

$$\begin{array}{c} \uparrow \\ \cdot \\ \leftarrow \\ \cdot \\ \vdots \\ \cdot \\ \text{---} \end{array} = \pi^2 g^2 h^2 \bar{s}_1 \not{x}_1 \int d\tau_3 \int d\tau_4 I_{24} \left( \int d^4 x_5 \not{x}_5 I_{15} I_{25} I_{35} I_{45} \right) \not{x}_2 s_2.$$

(6.4.52)

The tensor integral between the brackets can be solved by applying tensor decomposition. There exists many automated tools to perform this step, and here we use the package X [210]. We find

$$J_{123;4} := \int d^4 x_5 \not{x}_5 I_{15} I_{25} I_{35} I_{45} = \frac{2}{\phi_K} j_{123;4}, \tag{6.4.53}$$

with  $\phi_K$  the Kibble function defined as

$$\phi_K := \Phi_{1234} + \Phi_{1324} + \Phi_{1423} + \Psi_{123} + \Psi_{124} + \Psi_{134} + \Psi_{234}, \quad (6.4.54)$$

$$\Phi_{1234} = -\frac{1}{64\pi^6 I_{12} I_{34}} \left( \frac{1}{I_{12}} + \frac{1}{I_{34}} - \frac{1}{I_{13}} - \frac{1}{I_{14}} - \frac{1}{I_{23}} - \frac{1}{I_{24}} \right), \quad (6.4.55)$$

$$\Psi_{123} = -\frac{1}{64\pi^6 I_{12} I_{13} I_{23}}, \quad (6.4.56)$$

and with

$$j_{123;4} := f_{1234} X_{1234} + \not{g}_{123;4} Y_{123} + \not{g}_{124;3} Y_{124} + \not{g}_{134;2} Y_{134} + \not{g}_{234;1} Y_{234}. \quad (6.4.57)$$

The  $X$ - and  $Y$ -integrals are defined in eq. (H.0.3) and solved in eqs. (H.0.4) and (H.0.8). The prefactor function  $f_{1234}$  can be expressed in terms of propagators and read

$$f_{1234} = a_{1234} \not{x}_1 + a_{2341} \not{x}_2 + a_{3412} \not{x}_3 + (a_{4123} - 1) \not{x}_4, \quad (6.4.58)$$

with

$$a_{1234} := -\frac{1}{I_{23} I_{24} I_{34}} \left( 2 + \frac{I_{24} I_{34}}{I_{14} I_{23}} + \frac{I_{23} I_{34}}{I_{13} I_{24}} + \frac{I_{23} I_{24}}{I_{12} I_{34}} \right. \\ \left. - I_{34} \left( \frac{1}{I_{13}} + \frac{1}{I_{14}} \right) - I_{24} \left( \frac{1}{I_{12}} + \frac{1}{I_{14}} \right) - I_{23} \left( \frac{1}{I_{12}} + \frac{1}{I_{13}} \right) \right). \quad (6.4.59)$$

The function  $\not{g}_{123;4}$  can also be expressed in an elegant way as

$$\not{g}_{123;4} := b_{123;4} \not{x}_1 + b_{231;4} \not{x}_2 + b_{312;4} \not{x}_3 + c_{123} \not{x}_4, \quad (6.4.60)$$

with

$$b_{123;4} := \frac{1}{I_{23}} \left( \frac{1}{I_{12}} + \frac{1}{I_{13}} - \frac{1}{I_{23}} + \frac{1}{I_{24}} + \frac{1}{I_{34}} - \frac{2}{I_{14}} \right) - \left( \frac{1}{I_{12}} - \frac{1}{I_{13}} \right) \left( \frac{1}{I_{24}} - \frac{1}{I_{23}} \right), \quad (6.4.61)$$

$$c_{123} := \frac{1}{I_{12}^2} + \frac{1}{I_{13}^2} + \frac{1}{I_{23}^2} - 2 \left( \frac{1}{I_{12} I_{13}} + \frac{1}{I_{12} I_{23}} + \frac{1}{I_{13} I_{23}} \right). \quad (6.4.62)$$

This is as far as we can go for now and we are left with a difficult two-dimensional integral as well as a slashed derivative with respect to  $x_1$ . We note however that this integral can efficiently be computed numerically.

There is another path that one can take in order to try and solve this integral. Instead of computing the bulk integrals, one could start with the *defect* integral over  $\tau_3, \tau_4$  and use e.g. Schwinger parametrization for computing the remaining eight-dimensional integral. This approach was indeed useful for the computation of the  $X$ -diagram in the scalar two-point case, however here it is not clear at present how these 8 integrals could be solved efficiently.

# Chapter 7

## Conclusion

In this thesis we studied a special class of extended objects in conformal field theories, called *conformal defects*, using various approaches such as the  $\epsilon$ -expansion and the modern conformal bootstrap. After an introduction to the basics of CFTs in chapter 2 and conformal defects in chapter 3, we started our journey through the main results of this thesis with the most symmetry-constrained case of superconformal boundaries in  $3d$   $\mathcal{N} = 2$  superconformal theories in chapter 4. There are two possible choices characterized by  $2d$   $\mathcal{N} = (0, 2)$  and  $\mathcal{N} = (1, 1)$  boundary algebras. After performing a careful superspace analysis of correlators involving chiral fields, we observed in section 4.4 that the  $\mathcal{N} = (1, 1)$  choice can be analytically continued in the spacetime dimension. This allowed us to compute superconformal blocks across dimensions and opened the door for the  $\epsilon$ -expansion bootstrap in our supersymmetric setup. We proved uniqueness of the first two orders in  $\epsilon$ , and confirmed our general prediction for one specific model using perturbation theory.

In the next chapter 5, we moved on to defects with higher codimension and without supersymmetry, which have interesting physical applications. We studied  $O(2)$  line defects in a  $3d$  bulk CFT with  $SO(2)$  flavor symmetry – the monodromy defect – or  $O(3)$  flavor symmetry – the magnetic line defect – using the conformal bootstrap. After writing the corresponding crossing equations we applied the numerical machinery in order to obtain exclusion bounds valid for generic  $1d$  defect CFTs. We concentrated mostly on two canonical operators: the displacement and the tilt. The displacement operator is truly universal in that it controls the breaking of translations due to the presence of the conformal defect. The tilt operator can exist when a conformal defect breaks a bulk global symmetry, which is still quite a generic phenomenon.

After obtaining general bounds that constrain the landscape of  $1d$  theories, we changed gears and focused on two models of interest: the monodromy defect studied in [76, 77, 79], and the magnetic line defect described in [84]. In order to guide the numerics we complemented our bootstrap analysis with explicit analytic calculations in the  $\epsilon$ -expansion. For the monodromy defect, the results had already appeared in [76, 77], while for the magnetic line defect most of the calculations presented in section 5.3.2 are new.

For the monodromy defect we have kept the gap assumptions to a minimum, using the dimension of the external operators from the  $\epsilon$ -expansion results and imposing the existence of the displacement operator. Hence the numerical results are quite general, and they are fully consistent with the analytical data. The results for the magnetic line defect are more constraining. By imposing gaps coming from the  $\epsilon$ -expansion, the allowed region for certain OPE coefficients shows a series of intriguing cusps. The location of these cusps

however, does not match the best numerical estimates of the conformal dimension of the scalar field  $\Delta_{\phi_1} \simeq 1.55$ . Nevertheless, we consider this result an encouraging sign. Ways in which our methods can be improved include higher order terms in the  $\varepsilon$ -expansion, and higher precision in the numerics. The hope is that with these improvements, the region where the magnetic line defect is expected to sit will be constrained even further.

Many applications of CFTs in condensed matter physics involve the presence of fermions. Chapter 6 is dedicated to the study of defect correlators for line defects in fermionic models using the  $\varepsilon$ -expansion. Our setup is a natural generalization of the localized magnetic field line defect for the  $O(N)$  models studied as one of the examples in chapter 5. Indeed, the definition of the defect as the integral of a scalar along a line is identical to this defect. The main difference is the presence of fermions in the bulk, which induce new fermionic excitations on the  $1d$  defect.

We calculated a host of  $1d$  correlators, putting special emphasis on the new fermionic excitations. Closed-form expressions for four-point functions on the line were obtained in terms of the unique  $1d$  cross-ratio. These correlators can be used to easily extract CFT data by means of a conformal block expansion, and can also be used as input in the numerical bootstrap. The numerical bootstrap for magnetic line defects was initiated in [85]. The numerical bootstrap plots should accommodate the models studied in this paper, where the numbers of fermions  $N_f$  is a free parameter. One can also use the data calculated here to steer the numerics, and hopefully solve particular models of interest using the numerical bootstrap machinery.

In addition to correlators constrained to the line, we also studied how excitations in the bulk are modified by the presence of the defect. We focused on two-point functions, which have non-trivial kinematics and depend on two conformal invariants. For  $O(N)$  models this analysis had been done recently in [86, 87]. Due to the similarity of the Feynman diagram calculation, we could recycle several of their results, in particular the non-trivial integral presented in eq. (6.4.19).

Conformal defects give access to a host of new conformal data that can be computed perturbatively, or constrained using nonperturbative methods such as the conformal bootstrap. Combining these two approaches can provide guidance in the infinite-dimensional parameter space of the crossing equations for the conformal bootstrap, and help to find stronger bounds. One could also try using alternative approaches, such as Mellin space [57], analytic functionals [32] or the equations of motion method of [169].

Instead of studying a boundary in a  $3d\mathcal{N} = 2$  SCFT, one can also consider a  $1/2$ -BPS monodromy defect. This setup was bootstrapped in the  $\varepsilon$ -expansion in [78] using the defect inversion formula. The bulk  $R$ -symmetry is broken to a  $U(1)$  symmetry on the defect, which is comparable to the  $O(2)$  symmetry on the line considered in chapter 5. It would be interesting to study this defect using the numerical bootstrap, as we did in chapter 5. The monodromy defect now contains a displacement as well as a tilt operator due to the breaking of the  $R$ -symmetry, which in turn sit inside protected multiplets of the superconformal algebra. Together with the fundamental fields with transverse spin related to the charge of the monodromy, one can study mixed correlators with three external operators as has been done in [211, 23, 212] in the context of  $O(2)$  and  $O(3)$  models. A similar setup could be applied to a non-supersymmetric monodromy defect that breaks the bulk  $O(N)$  flavor symmetry.

Furthermore, the numerical results of chapter 5 could be extended to line defects with  $O(N)$  flavor symmetry. In addition to the analytical tools used in this work, we would gain access to the large- $N$  expansion, giving us perturbative results in a different

regime to compare with the numerics. At the same time, these line defects could break a bulk  $O(N + M)$  symmetry to a defect  $O(N)$  symmetry, where  $N, M \in \mathbb{Z}$ . In this generalization, the tilt will no longer be a vector under  $O(2)$  flavour symmetry, but will be part of another representation.

The results of chapter 6 for the chiral Heisenberg model ( $N = 3$ ) should also be captured by the numerical bootstrap results of chapter 5. In fact, the cusp found in section 5.4 could correspond to a line defect in a fermionic theory instead, for a certain number of fermions  $N_f$ . It would be interesting to explore this further and add correlators of fermions to the ones of the tilt and fundamental scalar considered at the moment. This would hopefully add additional constraints that can be used to carve out a region corresponding to line defects in Yukawa CFTs and distinguish them from  $O(N)$  line defects.

It is known that critical exponents for the Yukawa and  $O(N)$  CFTs can be computed perturbatively in the  $d = 2 + \tilde{\varepsilon}$  expansion in addition to the  $d = 4 - \varepsilon$  expansion, leading to the same interacting fixed point in three dimensions. For a line defect in the Gross–Neveu–Yukawa model, this was shown to be the case as well in [89]. The advantage is that having access to both the  $d = 4 - \varepsilon$  and the  $d = 2 + \tilde{\varepsilon}$  expansion can be used to obtain a two-sided Padé approximation for the conformal data, hence improving the  $\varepsilon$ -expansion results obtained so far. A technical difficulty, however, is that one would need to sum an infinite number of Feynman diagrams already at first order in  $\tilde{\varepsilon}$ .

A direct extension to the research in chapter 6, where we ended with the two-point functions of scalars in the presence of a line, is to study two-point functions of fermions. This analysis comes with several conceptual and technical challenges. The question of how to analytically continue fermions across dimensions has not been studied systematically, and a naive counting of tensor structures already shows disagreement between three and four dimensions. This problem opens several avenues for future research. On the one hand there is the explicit perturbative calculation, which we sketched at the end of section 6.4. Regardless if one knows how to interpolate fermions across dimensions, the Yukawa models studied here are well-defined perturbative CFTs, and correlators involving fermions exist and can be calculated. On the other hand, one can also study the kinematics of fermion correlators at a more fundamental level, understanding for example the structure of conformal blocks and how they depend on the spacetime dimension  $d$ . We should point out that, even though in this paper we focused on a line defect, the questions raised above are relevant for standard CFTs without defects. For example, the following *bulk* four-point function  $\langle \psi\psi\phi\phi \rangle$  already exhibits interesting non-trivial behavior across dimensions [213]. To our knowledge this type of correlator has never been studied using the  $\varepsilon$ -expansion.

There are other setups which are similar to the localized magnetic field line defect considered in chapters 5 and 6 which could be studied in the  $\varepsilon$ -expansion or using bootstrap techniques. An example is the same defect in theories with upper critical dimension  $d_c = 6$ , where it would correspond to a surface defect. This defect was recently studied in [102–105], for a defect not breaking the  $O(N)$  symmetry in the bulk. Another related setup is a Wilson line in gauge theories, such as QED. Such a defect was recently studied in [214]. This defect has some resemblance to a line defect in fermionic theories, and could also be tackled with either the conformal bootstrap or the  $\varepsilon$ -expansion.

A longer term goal is to include multipoint correlators in the bootstrap analyses presented in this thesis; this is a program that has been underexplored, although significant progress can be made using Calogero–Sutherland technology [215], and multipoint corre-

lators have been studied for operators on a Wilson line in  $\mathcal{N} = 4$  SYM [216, 217] and in the presence of a boundary [68, 52, 218]. Finally, the study of free theories in the presence of interacting defects has gotten some attention recently; in particular the results of [68] suggest the existence of a new conformal boundary condition for the free scalar field. It would be interesting to repeat their analysis in a supersymmetric setup or in a setup with fermions, either for boundaries or higher codimension defects.

# Appendix A

## Details on three-dimensional boundaries

### A.1 Conventions

In section 4.3 we work in Lorenzian signature with mostly plus metric  $\eta_{\mu\nu} = \text{diag}(-1, +1, +1)$ . The gamma matrices are defined in terms of the identity matrix  $\mathbf{1}$  and Pauli matrices  $\sigma^i$  as

$$(\gamma^\mu)_{\alpha\beta} \equiv (-\mathbf{1}_{\alpha\beta}, (\sigma^3)_{\alpha\beta}, (\sigma^1)_{\alpha\beta}), \quad (\gamma^\mu)_\alpha{}^\beta = (\gamma^\mu)_{\alpha\gamma} \epsilon^{\gamma\beta}, \quad (\gamma^\mu)^{\alpha\beta} = \epsilon^{\alpha\gamma} (\gamma^\mu)_\gamma{}^\beta. \quad (\text{A.1.1})$$

With these conventions the gamma matrices are real and symmetric. Here and in what follows we are raising and lowering spinor indices as  $\theta^\alpha = \epsilon^{\alpha\beta} \theta_\beta$  and  $\theta_\alpha = \epsilon_{\alpha\beta} \theta^\beta$ , where

$$\epsilon^{12} = 1, \quad \epsilon_{12} = -1. \quad (\text{A.1.2})$$

The contraction of two spinors is defined as  $\theta^2 = \epsilon_{\alpha\beta} \theta^\alpha \theta^\beta$ . Finally, the spacetime Levi-Civita tensor is defined by:

$$\epsilon_{012} = -1, \quad \epsilon^{012} = 1. \quad (\text{A.1.3})$$

### A.2 Superconformal algebra

The three dimensional Lorentz group  $SO(2, 1)$  is generated by  $\mathcal{M}_{\mu\nu}$ . A generic element of the algebra  $\mathcal{J}$  contains vector indices  $\mu, \nu, \lambda, \dots$  and spinor indices  $\alpha, \beta, \dots$ , and each of them transforms under rotations as:

$$\begin{aligned} [\mathcal{M}_{\mu\nu}, \mathcal{J}_{\lambda\dots}] &= i(\eta_{\mu\lambda} \mathcal{J}_{\nu\dots} - \eta_{\nu\lambda} \mathcal{J}_{\mu\dots}), \\ [\mathcal{M}_{\mu\nu}, \mathcal{J}_{\alpha\dots}] &= +\frac{i}{2} \epsilon_{\mu\nu\lambda} (\gamma^\lambda)_\alpha{}^\beta \mathcal{J}_{\beta\dots}, \\ [\mathcal{M}_{\mu\nu}, \mathcal{J}^{\alpha\dots}] &= -\frac{i}{2} \epsilon_{\mu\nu\lambda} (\gamma^\lambda)^\alpha{}_\beta \mathcal{J}^{\beta\dots}. \end{aligned} \quad (\text{A.2.1})$$

With these identities it is easy to write down any commutator involving  $\mathcal{M}_{\mu\nu}$ . The rest of the  $3d$  conformal algebra is:

$$[\mathcal{D}, \mathcal{P}_\mu] = i\mathcal{P}_\mu, \quad [\mathcal{D}, \mathcal{K}_\mu] = -i\mathcal{K}_\mu, \quad [\mathcal{K}_\mu, \mathcal{P}_\nu] = -2i(\mathcal{M}_{\mu\nu} + \eta_{\mu\nu} \mathcal{D}). \quad (\text{A.2.2})$$

The  $3d$   $\mathcal{N} = 2$  superconformal algebra is given by  $OSP(2|4)$ . Besides the conformal and  $R$ -symmetry generators, it contains four Poincaré supercharges and four superconformal supercharges that anticommute as

$$\begin{aligned} \{\mathcal{Q}_\alpha, \bar{\mathcal{Q}}_\beta\} &= 2(\gamma^\mu)_{\alpha\beta} \mathcal{P}_\mu, \quad \{\mathcal{S}^\alpha, \bar{\mathcal{S}}^\beta\} = 2(\gamma^\mu)^{\alpha\beta} \mathcal{K}_\mu, \\ \{\mathcal{Q}_\alpha, \bar{\mathcal{S}}^\beta\} &= -i(2\delta_\alpha{}^\beta (\mathcal{D} + i\mathcal{R}) - \epsilon^{\mu\nu\lambda} (\gamma_\lambda)_\alpha{}^\beta \mathcal{M}_{\mu\nu}), \\ \{\bar{\mathcal{Q}}_\alpha, \mathcal{S}^\beta\} &= -i(2\delta_\alpha{}^\beta (\mathcal{D} - i\mathcal{R}) - \epsilon^{\mu\nu\lambda} (\gamma_\lambda)_\alpha{}^\beta \mathcal{M}_{\mu\nu}). \end{aligned} \quad (\text{A.2.3})$$

The commutation relations between the conformal group and the supercharges are

$$\begin{aligned} [\mathcal{D}, \mathcal{Q}_\alpha] &= \frac{1}{2}i\mathcal{Q}_\alpha, & [\mathcal{D}, \mathcal{S}^\alpha] &= -\frac{1}{2}i\mathcal{S}^\alpha, & [\mathcal{K}_\mu, \mathcal{Q}_\alpha] &= (\gamma_\mu)_{\alpha\beta}\mathcal{S}^\beta, & [\mathcal{P}_\mu, \mathcal{S}^\alpha] &= -(\gamma_\mu)^{\alpha\beta}\mathcal{Q}_\beta, \\ [\mathcal{D}, \bar{\mathcal{Q}}_\alpha] &= \frac{1}{2}i\bar{\mathcal{Q}}_\alpha, & [\mathcal{D}, \bar{\mathcal{S}}^\alpha] &= -\frac{1}{2}i\bar{\mathcal{S}}^\alpha, & [\mathcal{K}_\mu, \bar{\mathcal{Q}}_\alpha] &= (\gamma_\mu)_{\alpha\beta}\bar{\mathcal{S}}^\beta, & [\mathcal{P}_\mu, \bar{\mathcal{S}}^\alpha] &= -(\gamma_\mu)^{\alpha\beta}\bar{\mathcal{Q}}_\beta. \end{aligned} \quad (\text{A.2.4})$$

Lastly, all generators are neutral under  $R$ -symmetry, except the eight supercharges:

$$[\mathcal{R}, \mathcal{Q}_\alpha] = -\mathcal{Q}_\alpha, \quad [\mathcal{R}, \bar{\mathcal{Q}}_\alpha] = \bar{\mathcal{Q}}_\alpha, \quad [\mathcal{R}, \mathcal{S}^\alpha] = -\mathcal{S}^\alpha, \quad [\mathcal{R}, \bar{\mathcal{S}}^\alpha] = \bar{\mathcal{S}}^\alpha. \quad (\text{A.2.5})$$

### A.3 Differential operators

In this appendix we present the action of our generators in terms of differential operators in superspace. We consider an operator  $\mathcal{O}(z)$  of dimension  $\Delta$  and charge  $r$  that transforms under rotations in a representation dictated by matrices  $s_{\mu\nu}$ , which satisfy the same commutation relations as  $\mathcal{M}_{\mu\nu}$ . Then, the generators of the algebra act as:

$$[\mathcal{D}, \mathcal{O}(z)] = i \left( \Delta + x^\mu \partial_\mu + \frac{1}{2}\theta^\alpha \partial_\alpha + \frac{1}{2}\bar{\theta}^\alpha \bar{\partial}_\alpha \right) \mathcal{O}(z), \quad (\text{A.3.1})$$

$$\begin{aligned} [\mathcal{K}_\mu, \mathcal{O}(z)] &= \left( -2i\Delta x_\mu - 2ix_\mu x^\nu \partial_\nu + ix^2 \partial_\mu \right. \\ &\quad - ix_\mu (\theta^\alpha \partial_\alpha + \bar{\theta}^\alpha \bar{\partial}_\alpha) + i\epsilon_{\mu\nu\rho} (\gamma^\nu)_{\alpha\beta} x^\rho (\theta^\alpha \partial_\beta + \bar{\theta}^\alpha \bar{\partial}_\beta) \\ &\quad + (\gamma_\mu)_{\alpha\beta} \theta^\alpha \bar{\theta}^\beta (\theta^\gamma \partial_\gamma - \bar{\theta}^\gamma \bar{\partial}_\gamma) - \frac{i}{2}\theta^2 \bar{\theta}^2 \partial_\mu \\ &\quad \left. - 2r(\gamma_\mu)_{\alpha\beta} \theta^\alpha \bar{\theta}^\beta - 2x^\nu s_{\mu\nu} - i\eta_{\mu\nu} \epsilon^{\nu\rho\sigma} s_{\rho\sigma} \theta^\alpha \bar{\theta}_\alpha \right) \mathcal{O}(z), \end{aligned} \quad (\text{A.3.2})$$

$$[\mathcal{M}_{\mu\nu}, \mathcal{O}(z)] = \left( \frac{i}{2}\epsilon_{\mu\nu\rho} (\gamma^\rho)_{\alpha\beta} (\theta^\alpha \partial_\beta + \bar{\theta}^\alpha \bar{\partial}_\beta) + ix_\mu \partial_\nu - ix_\nu \partial_\mu + s_{\mu\nu} \right) \mathcal{O}(z), \quad (\text{A.3.3})$$

$$[\mathcal{R}, \mathcal{O}(z)] = (\bar{\theta}^\alpha \bar{\partial}_\alpha - \theta^\alpha \partial_\alpha + r) \mathcal{O}(z), \quad (\text{A.3.4})$$

$$\begin{aligned} [\mathcal{S}^\alpha, \mathcal{O}(z)] &= \left( -i(\gamma_\mu)^{\alpha\beta} x^\mu \partial_\beta + \bar{\theta}^\alpha x^\mu \partial_\mu + \frac{1}{2}(\gamma^\mu)^{\alpha\beta} (\gamma^\nu)_{\beta\gamma} \bar{\theta}^\gamma (x_\mu \partial_\nu - x_\nu \partial_\mu) \right. \\ &\quad - \theta^\alpha \bar{\theta}^\beta \partial_\beta + \bar{\theta}^\alpha \theta^\beta \partial_\beta - 2\bar{\theta}^\alpha \bar{\theta}^\beta \bar{\partial}_\beta \\ &\quad \left. - i(\gamma^\mu)_{\beta\gamma} \theta^\beta \bar{\theta}^\gamma \bar{\theta}^\alpha \partial_\mu + 2\Delta \bar{\theta}^\alpha - 2r\bar{\theta}^\alpha + i\epsilon^{\mu\nu\rho} (\gamma_\rho)_\beta^\alpha \bar{\theta}^\beta s_{\mu\nu} \right) \mathcal{O}(z), \end{aligned} \quad (\text{A.3.5})$$

$$\begin{aligned} [\bar{\mathcal{S}}^\alpha, \mathcal{O}(z)] &= \left( i(\gamma^\mu)^{\alpha\beta} x_\mu \bar{\partial}_\beta - \theta^\alpha x^\mu \partial_\mu - \frac{1}{2}(\gamma^\mu)^{\alpha\beta} (\gamma^\nu)_{\beta\gamma} \theta^\gamma (x_\mu \partial_\nu - x_\nu \partial_\mu) \right. \\ &\quad + \bar{\theta}^\alpha \theta^\beta \bar{\partial}_\beta - \theta^\alpha \bar{\theta}^\beta \bar{\partial}_\beta + 2\theta^\alpha \theta^\beta \partial_\beta \\ &\quad \left. + i(\gamma^\mu)_{\beta\gamma} \bar{\theta}^\beta \theta^\gamma \theta^\alpha \partial_\mu - 2\Delta \theta^\alpha - 2r\theta^\alpha - i\epsilon^{\mu\nu\rho} (\gamma_\rho)_\beta^\alpha \theta^\beta s_{\mu\nu} \right) \mathcal{O}(z). \end{aligned} \quad (\text{A.3.6})$$



# Appendix B

## Non-supersymmetric conformal blocks

In this appendix, we derive the non-supersymmetric bulk and boundary blocks for bulk two-point functions and bulk-boundary-boundary correlators.

### B.1 Two-point function

The conformal blocks for a two-point function were first derived in [149] but we will follow [46] in our approach.

**Bulk channel.** The bulk-channel blocks can be found by acting on the two-point function (4.2.7) with the bulk Casimir operator:

$$\mathcal{C}_{\text{bulk,bos}}^{(12)} = -\mathcal{D}^2 - \frac{1}{2} \{\mathcal{K}^\mu, \mathcal{P}_\mu\} + \frac{1}{2} \mathcal{M}^{\mu\nu} \mathcal{M}_{\mu\nu}. \quad (\text{B.1.1})$$

The differential operators are well known, but they can also be obtained from section A.3 by setting all Grassmann coordinates to zero. The Casimir eigenvalue is  $C_{\Delta,\ell} = \Delta(\Delta - d) + \ell(\ell + d - 2)$ , but only operators with  $\ell = 0$  can appear in the bulk OPE. For the bulk channel, it is convenient to define the blocks in terms of  $g_\Delta^{\Delta_{12}}(\xi) = \xi^{(\Delta_1 + \Delta_2)/2} f_\Delta^{\Delta_{12}}(\xi)$ . The resulting differential equation is

$$\frac{(\mathcal{C}_{\text{bulk,bos}} - C_{\Delta,\ell}) \langle \phi_1(x_1) \phi_2(x_2) \rangle}{(2x_1^\perp)^{-\Delta_1} (2x_2^\perp)^{-\Delta_2} \xi^{-(\Delta_1 + \Delta_2)/2}} = \left[ 4\xi^2 (\xi + 1) \partial_\xi^2 + 2\xi(2\xi - d + 2) \partial_\xi - (\Delta(\Delta - d) + \Delta_{12}^2 \xi) \right] g_\Delta^{\Delta_{12}}(\xi) = 0, \quad (\text{B.1.2})$$

which is solved by

$$g_\Delta^{\Delta_{12}}(\xi) = \xi^{\Delta/2} {}_2F_1\left(\frac{\Delta + \Delta_{12}}{2}, \frac{\Delta - \Delta_{12}}{2}; \Delta + 1 - \frac{d}{2}; -\xi\right). \quad (\text{B.1.3})$$

Whenever the superscript  $\Delta_{12}$  is omitted, it is assumed that  $\Delta_{12} = 0$ .

**Boundary channel.** In the boundary channel, the conformal blocks are eigenfunctions of the boundary Casimir that acts on a single point

$$\hat{\mathcal{C}}_{\text{non-susy}}^{(1)} = -\mathcal{D}^2 - \frac{1}{2} \{\mathcal{K}^a, \mathcal{P}_a\} + \frac{1}{2} \mathcal{M}^{ab} \mathcal{M}_{ab}, \quad (\text{B.1.4})$$

where the index  $a, b$  runs only on directions parallel to the boundary. The eigenvalue of the boundary Casimir is  $\hat{C}_{\Delta,j} = \Delta(\Delta - d + 1) + j(j + d - 1)$ , but once more we have

to take  $j = 0$  because only scalar operators appear in the BOE of a bulk scalar. The resulting differential equation is

$$\frac{\left(\hat{C}_{\text{non-susy}} - \hat{C}_{\Delta,0}\right) \langle \phi_1(x_1) \phi_2(x_2) \rangle}{(2x_1^\perp)^{-\Delta_1} (2x_2^\perp)^{-\Delta_2}} = \left[ \xi(\xi + 1) \partial_\xi^2 + \frac{d}{2} (2\xi + 1) \partial_\xi - \hat{\Delta}(\hat{\Delta} - d + 1) \right] \hat{f}_{\hat{\Delta}}(\xi) = 0, \quad (\text{B.1.5})$$

which is solved by

$$\hat{f}_{\hat{\Delta}}(\xi) = \xi^{-\hat{\Delta}} {}_2F_1\left(\hat{\Delta}, \hat{\Delta} - \frac{d}{2} + 1; 2\hat{\Delta} - d + 2; -\frac{1}{\xi}\right). \quad (\text{B.1.6})$$

## B.2 Three-point bosonic blocks

In this section we restrict to  $d = 3$ . We start with considering the bosonic correlator

$$\langle \mathcal{O}_1(x) \hat{\mathcal{O}}_{2,j}(0) \hat{\mathcal{O}}_3(\infty) \rangle = \frac{(x^a \omega_a)^j}{(x^\perp)^{\Delta_1 + \hat{\Delta}_{23}} |x^a|^j} \mathcal{F}^{\text{3pt}}(\chi), \quad \chi = \frac{|x^a|^2}{(x^\perp)^2}, \quad (\text{B.2.1})$$

where the second operator has parallel spin  $j$ . We used index-free notation to contract all vector indices, and  $\omega_a$  is a null-vector. We need to evaluate the eigenvalue equation

$$\hat{C}_{\text{bos}}^{(1)} \langle \mathcal{O}_1(x) \hat{\mathcal{O}}_{2,j}(0) \hat{\mathcal{O}}_3(\infty) \rangle = \hat{C}_{\hat{\Delta},0} \langle \mathcal{O}_1(x) \hat{\mathcal{O}}_{2,j}(0) \hat{\mathcal{O}}_3(\infty) \rangle, \quad (\text{B.2.2})$$

where  $\hat{C}_{\hat{\Delta},0}$  is the boundary Casimir eigenvalue when the parallel spin of the exchanged operator is zero. This gives us the differential equation

$$\left[ 4\chi(\chi + 1) \partial_\chi^2 + 4 \left( (\hat{\Delta}_{23} + 2)\chi + 1 \right) \partial_\chi - \hat{\Delta}(\hat{\Delta} - 2) + \hat{\Delta}_{23}(\hat{\Delta}_{23} + 2) - \frac{j^2}{\chi} \right] \hat{f}_{\hat{\Delta},j}^{\text{3pt},\hat{\Delta}_{23}} = 0. \quad (\text{B.2.3})$$

The solution to eq. (B.2.3) is once more given by a hypergeometric function

$$\hat{f}_{\hat{\Delta},j}^{\text{3pt},\hat{\Delta}_{23}}(\chi) = \chi^{-\frac{1}{2}(\hat{\Delta} + \hat{\Delta}_{23})} {}_2F_1\left(\frac{1}{2} \left( \hat{\Delta} + \hat{\Delta}_{23} - j \right), \frac{1}{2} \left( \hat{\Delta} + \hat{\Delta}_{23} + j \right); \hat{\Delta}; -\frac{1}{\chi}\right). \quad (\text{B.2.4})$$

# Appendix C

## More on blocks across dimensions

In this appendix, we provide more details on the derivation of the superconformal blocks in any number of dimension. In section 4.4 we showed that the supersymmetric part of the Casimir acting on a two-point function can be written in terms of  $Q$  supercharges acting on the two-point function. Our current goal is to find equivalent expressions where the supercharges are replaced by a differential operator, for example

$$\langle 0 | [Q_{\dot{\alpha}}^-, \phi_1(x_1)] [Q_{\alpha}^+, \bar{\phi}_2(x_2)] | 0 \rangle \sim \mathcal{D}_x \langle 0 | \phi_1(x_1) \bar{\phi}_2(x_2) | 0 \rangle. \quad (\text{C.0.1})$$

It was proposed in [154] that this can be achieved with supersymmetric Ward identities. Here we give a quick summary of the strategy. In our setup the supercharges  $\mathcal{Q}_A$  and  $\mathcal{S}_A$  are preserved by the boundary, so the following Ward identities are satisfied:

$$\begin{aligned} \langle 0 | \{Q_1^{\text{bdy}}, [Q_1^-, \phi_1(x_1)] \bar{\phi}_2(x_2)\} | 0 \rangle &= 0, & \langle 0 | \{S_1^{\text{bdy}}, [Q_1^-, \phi_1(x_1)] \bar{\phi}_2(x_2)\} | 0 \rangle &= 0, \\ \langle 0 | \{Q_1^{\text{bdy}}, [Q_2^-, \phi_1(x_1)] \bar{\phi}_2(x_2)\} | 0 \rangle &= 0, & \langle 0 | \{S_1^{\text{bdy}}, [Q_2^-, \phi_1(x_1)] \bar{\phi}_2(x_2)\} | 0 \rangle &= 0. \\ \langle 0 | \{Q_2^{\text{bdy}}, [Q_1^-, \phi_1(x_1)] \bar{\phi}_2(x_2)\} | 0 \rangle &= 0, \end{aligned} \quad (\text{C.0.2})$$

There are other Ward identities that can be considered, but these five are sufficient for our purposes. At this point, it is hard to continue without an explicit matrix representation for the Clifford algebra, so we focus on  $d = 3$  where  $\Sigma_\mu = (\sigma_3, \sigma_1, \sigma_2)$ . Let us consider explicitly the simplest Ward identity to show how to replace the supercharges with differential operators in the general case. With elementary manipulations we find:

$$\begin{aligned} 0 &= \langle 0 | \{Q_2^{\text{bdy}}, [Q_1^-, \phi_1(x_1)] \bar{\phi}_2(x_2)\} | 0 \rangle \\ &= \langle 0 | \{Q_2^{\text{bdy}}, [Q_1^-, \phi_1(x_1)]\} \bar{\phi}_2(x_2) | 0 \rangle - \langle 0 | [Q_1^-, \phi_1(x_1)] [Q_2^{\text{bdy}}, \bar{\phi}_2(x_2)] | 0 \rangle \\ &= \langle 0 | \{[Q_2^+, Q_1^-], \phi_1(x_1)\} \bar{\phi}_2(x_2) | 0 \rangle - \langle 0 | [Q_1^-, \phi_1(x_1)] [Q_2^+, \bar{\phi}_2(x_2)] | 0 \rangle. \end{aligned} \quad (\text{C.0.3})$$

In our conventions  $\{Q_2^+, Q_1^-\} = P_2 + iP_3$  and also  $[P_\mu, \mathcal{O}(x)] = -i\partial_\mu \mathcal{O}(x)$ , so we conclude

$$\langle 0 | [Q_1^-, \phi_1(x_1)] [Q_2^+, \bar{\phi}_2(x_2)] | 0 \rangle = (-i\partial_2 + \partial_3) \langle 0 | \phi_1(x_1) \bar{\phi}_2(x_2) | 0 \rangle. \quad (\text{C.0.4})$$

The other Ward identities can be manipulated identically, but unlike the example we showed they do not decouple, so one has to solve a simple linear system of equations to obtain the terms we are interested in.

These steps can be automated in `Mathematica` and applied to all cases of interest in  $d = 3, 4$ . The resulting differential operators  $\mathcal{D}_x$  depend on  $x_i^\mu$  and  $\partial_{\mu,i}$  and take a complicated looking form. However, we know that the Casimir operator  $C_{\text{bulk/bdy,susy}}$  has to respect conformal invariance, so when we combine all the contributing terms, the result has to be a differential operator of the cross-ratio  $\xi$ . Indeed, in  $d = 3, 4$  we find the following results:

$$\begin{aligned} ix_{12}^\mu \bar{\Sigma}_\mu^{\dot{\alpha}\alpha} \langle 0 | [Q_{\dot{\alpha}}^-, \phi_1(x_1)] [Q_{\alpha}^+, \bar{\phi}_2(x_2)] | 0 \rangle &\rightarrow (4\xi\partial_\xi - 2(\Delta_1 + \Delta_2))\mathcal{G}(\xi), \\ ix_1^\perp \langle 0 | \{Q_1^-, [Q_2^-, \phi_1(x_1)]\} \bar{\phi}_2(x_2) | 0 \rangle &\rightarrow (-\xi\partial_\xi - \Delta_1)\mathcal{F}(\xi), \\ ix_1^\perp \langle 0 | \{Q_1^-, [Q_2^-, \phi_1(x_1)]\} \phi_2(x_2) | 0 \rangle &\rightarrow (-(\xi + 1)\partial_\xi - \Delta_1)\mathcal{F}(\xi). \end{aligned} \quad (\text{C.0.5})$$

From these results we can obtain (4.4.10), (4.4.13) and (4.4.18). Although the intermediate differential operators were complicated, the final result takes a remarkably simple form. Perhaps one could find a more direct method of obtaining these results, and at the same time make it more manifest that the result is indeed independent of  $d$ .

# Appendix D

## More data on the $O(N)$ monodromy defect in 3d

In this appendix, we give a more detailed explanation of the calculation of the dimensions and OPE coefficients given in section 5.3.1 and computed in [77].

### D.1 OPE coefficients with the displacement operator

The displacement operator appears in the OPE of two defect modes  $\Psi_v \times \bar{\Psi}_{v-1} \sim D + \dots$ . Hence, we are interested in the correlators involving these defect modes, which are

$$\begin{aligned} & \langle \Psi_v(\vec{x}_1) \bar{\Psi}_v(\vec{x}_2) \Psi_v(\vec{x}_3) \bar{\Psi}_v(\vec{x}_4) \rangle, \quad \langle \Psi_{1-v}(\vec{x}_1) \bar{\Psi}_{1-v}(\vec{x}_2) \Psi_{1-v}(\vec{x}_3) \bar{\Psi}_{1-v}(\vec{x}_4) \rangle, \\ & \langle \Psi_v(\vec{x}_1) \bar{\Psi}_{1-v}(\vec{x}_2) \Psi_{1-v}(\vec{x}_3) \bar{\Psi}_v(\vec{x}_4) \rangle. \end{aligned} \quad (\text{D.1.1})$$

The results for the single-operator correlators were already computed in [74] for a  $\mathbb{Z}_2$  monodromy defect. For correlators with two operators  $\Psi_1$  and  $\Psi_2$ , the anomalous dimensions of the operators appearing in the OPEs are computed in [77], and from their results also the OPE coefficients can be readily derived.<sup>1</sup> The anomalous dimensions and first-order corrections to the OPE coefficients appear in the four-point correlator as

$$\begin{aligned} & \langle \Psi_{\alpha+v}(\vec{x}_1) \bar{\Psi}_{\alpha-s+v}(\vec{x}_2) \Psi_{\beta-s+v}(\vec{x}_3) \bar{\Psi}_{\beta+v}(\vec{x}_4) \rangle \in \sum_m (|\lambda_{\Psi\bar{\Psi}\mathcal{O}_\alpha}^{(0)s,m}|^2 + \varepsilon |\lambda_{\Psi\bar{\Psi}\mathcal{O}_\alpha}^{(1)s,m}|^2) \\ & \times \left( \delta_{\alpha\beta} + \frac{\varepsilon}{2} \Delta_{\alpha\beta}^{s,m} \partial_m \right) W_{d-2+s+2m,0}(\vec{x}_i), \end{aligned} \quad (\text{D.1.3})$$

where

$$W_{\Delta,\ell}(\vec{x}_i) = \left( \frac{\vec{x}_{24}^2}{\vec{x}_{14}^2} \right)^{\frac{1}{2}\Delta_{12}} \left( \frac{\vec{x}_{14}^2}{\vec{x}_{13}^2} \right)^{\frac{1}{2}\Delta_{34}} \frac{G_{\Delta,\ell}(u,v)}{\vec{x}_{12}^{\frac{1}{2}(\Delta_1+\Delta_2)} \vec{x}_{34}^{\frac{1}{2}(\Delta_3+\Delta_4)}}, \quad (\text{D.1.4})$$

and  $G_{\Delta,\ell}$  are the conformal blocks as defined in [186]. The variables  $\alpha, \beta$  in eq. (D.1.3) refer to degeneracies between operators that have the same tree-level conformal dimension and  $SO(2)_T$  spin. For the correlator of interest to us, we set  $s = 1$  and since  $\alpha, \beta = 0, 1, \dots, s-1 = 0$  [77], we will not have to worry about said degeneracies.

The anomalous dimensions will receive contributions from the logarithmic term of the four-point correlator, and from the  $\mathcal{O}(\varepsilon)$  term of the dimension of the external operators.

<sup>1</sup>Note that our conventions differ slightly from those used in [77]; in particular, we normalize the two-point function as

$$\langle \bar{\Psi}_{s_1}(\vec{x}_1) \Psi_{s_2}(\vec{x}_2) \rangle_0 = \frac{\delta_{s_1,s_2}}{\vec{x}_{12}^{2\Delta_{s_1}}}, \quad (\text{D.1.2})$$

without an extra factor of  $\mathcal{C}_{\Delta_{s_1}}$  that was present in [77]. This does not have any impact on the anomalous dimensions, but needs to be taken into account when computing the OPE coefficients.

The anomalous dimension of the external operators was given in eq. 5.3.7, and gives a contribution of

$$\Delta^{(1);\text{disc}} = \Delta_{s_1}^{(1)} + \Delta_{s_2}^{(1)} = \frac{v(v-1)(N+2)}{2(N+8)} \left( \frac{1}{|s_1|} + \frac{1}{|s_2|} \right) \quad (\text{D.1.5})$$

to the anomalous dimension of the operators appearing in their OPEs. At tree level, the four-point correlator is given by the free theory discussed in eq. (5.2.25). At  $\mathcal{O}(\varepsilon)$ , one can compute the correction to the correlator through a contact Witten diagram with the four defect modes  $\Psi_{s_i}$  as external operators. These diagrams are described by the well-known D-functions [219, 220, 118]. The first-order correction to the correlator in eq. (D.1.3) is given by [77]

$$\langle \Psi_v(\vec{x}_1) \bar{\Psi}_{v-1}(\vec{x}_2) \Psi_{v-1}(\vec{x}_3) \bar{\Psi}_v(\vec{x}_4) \rangle_1 = -\pi \lambda_* \times D_{\Delta_{\Psi_v}, \Delta_{\Psi_{v-1}}, \Delta_{\Psi_{v-1}}, \Delta_{\Psi_v}}(\vec{x}_i), \quad (\text{D.1.6})$$

where  $\lambda_* \sim \mathcal{O}(\varepsilon)$  is given in eq. (5.3.6). The D-function can be expanded in conformal blocks as [221, 222]:

$$D_{\Delta_{s_1}, \Delta_{s_2}, \Delta_{s_3}, \Delta_{s_4}}(\vec{x}_i) = \sum_m P_1^{(12)}(m, 0) W_{\Delta_m, 0}(\vec{x}_i) + \sum_n P_1^{(34)}(n, 0) W_{\Delta_n, 0}(\vec{x}_i). \quad (\text{D.1.7})$$

Note that since  $\lambda_* \sim \mathcal{O}(\varepsilon)$ , we can evaluate the conformal blocks at  $p = d - 2 = 2$ , and the dimensions  $\Delta_m = \Delta_{s_1} + \Delta_{s_2} + 2m$  contribute at tree level. The coefficients  $P_1(m, 0)$  are given in [77].

When  $\Delta_{s_1} + \Delta_{s_2} - \Delta_{s_3} - \Delta_{s_4} = 2k, k \in \mathbb{Z}$ , where  $\Delta_{s_i}$  are evaluated at tree level, the coefficients have a divergence and hence contribute to the anomalous dimension. For the correlator we study,  $\Delta_v + \Delta_{v-1} - \Delta_{v-1} - \Delta_v = 0$ . In this case, the D-function can be written as [77]:

$$\begin{aligned} D_{\Delta_{s_1}, \Delta_{s_2}, \Delta_{s_3}, \Delta_{s_4}}(\vec{x}_i) &= \sum_m \frac{\pi \left( \prod_{i=1}^4 (\Delta_{s_i})_m \right) (\Delta_{s_1} + \Delta_{s_2} + 2m - 1)_{-m}^2}{2(m!)^2 (\Delta_{s_1} + \Delta_{s_2} + 2m - 1)} \left( \frac{2}{\Delta_{s_1} + \Delta_{s_2} + 2m - 1} \right. \\ &\quad \left. + 2H^m - 2H^{m+\Delta_{s_1}+\Delta_{s_2}-2} + 4H^{2m+\Delta_{s_1}+\Delta_{s_2}-2} - \sum_{i=1}^4 H^{m+\Delta_{s_i}-1} - \partial_m \right) W_{\Delta_{s_1}+\Delta_{s_2}+2m, 0}(\vec{x}_i), \end{aligned} \quad (\text{D.1.8})$$

where  $H^m$  are harmonic numbers. Setting  $s_1 = s_4 = v$ ,  $s_2 = s_3 = v - 1$ , we can extract the contribution to the anomalous dimension from the logarithmic part:

$$\Delta^{(1);\text{con}} = \frac{4}{10(2+2m)}, \quad (\text{D.1.9})$$

and the  $\mathcal{O}(\varepsilon)$  correction to the OPE coefficients from the non-divergent part, for  $m = 0$ :

$$|\lambda_{\Psi_v \bar{\Psi}_{v-1} \mathcal{O}_{0,0}^{1,0}}^{(1)}|^2 = \frac{(N+2)(2H^{1-v} + 2H^v - 3)}{2N(N+8)}. \quad (\text{D.1.10})$$

Combining the contribution in eq. (D.1.9) and the contribution in eq. (D.1.5), we get

$$\Delta_{0,0}^{1,m} = \frac{1}{5(1+m)} - \frac{1}{5}, \quad (\text{D.1.11})$$

such that indeed, for  $m = 0$ ,  $\Delta_{0,0}^{1,0} = 0$  and the displacement, a protected operator, does not get any anomalous dimension.

OPE	$s$	$\Delta^{(1)}$	$\lambda^{(1)}$
$\Psi_v \times \bar{\Psi}_{v-1}$	1	$\frac{N+2}{(N+8)(2+2m)} - \frac{(N+2)}{2(N+8)}$	$\frac{(N+2)(2H^{1-v}+2H^v-3)}{2N(N+8)}$
$\Psi_{v-1} \times \bar{\Psi}_{v-1}$	0	$\frac{2(N+2)}{(N+8)(3-2v)} - \frac{(N+2)v}{(N+8)}$	$\frac{2(N+2)(2H^{1-v}-H^{2-2v})}{(3-2v)N(N+8)} - \frac{2(N+2)}{(3-2v)^2N(N+8)}$
$\Psi_v \times \bar{\Psi}_v$	0	$\frac{2(N+2)}{(N+8)(1+2v)} + \frac{(N+2)(v-1)}{(N+8)}$	$\frac{2(N+2)(2H^v-H^{2v})}{(1+2v)N(N+8)} - \frac{2(N+2)}{(1+2v)^2N(N+8)}$

Table D.1: The  $\varepsilon$ -expansion results for various operators,  $m = 0$ 

## D.2 The leading singlet

The anomalous dimension of the first singlet in the  $\Psi_v \times \bar{\Psi}_v$ , or the  $\Psi_{v-1} \times \bar{\Psi}_{v-1}$  OPE, and its OPE coefficient, can be computed in the same way as for the  $\Psi_v \times \bar{\Psi}_{v-1}$  OPE. We still do not encounter degeneracies. The correction coming from the anomalous dimensions of the external operators is now given by

$$2\Delta_{s_i}^{(1);\text{disc}} = \frac{v(v-1)(N+2)}{(N+8)} \frac{1}{|s_i|}, \quad (\text{D.2.1})$$

and the tree-level dimensions and OPE coefficients of the operators in the  $\Psi_{s_i} \times \bar{\Psi}_{s_i}$  OPE are given by the free theory results described in eq. (5.2.19). The first-order correction to the correlator is given by

$$\langle \Psi_{s_i}(\vec{x}_1) \bar{\Psi}_{s_i}(\vec{x}_2) \Psi_{s_i}(\vec{x}_3) \bar{\Psi}_{s_i}(\vec{x}_4) \rangle_1 = -2\pi\lambda_* \times D_{\Delta_{s_i}, \Delta_{s_i}, \Delta_{s_i}, \Delta_{s_i}}(\vec{x}_i), \quad (\text{D.2.2})$$

and we can use the same conformal block expansion of the D-functions in eq. (D.1.7). Since all external dimensions are equal, the relation  $\Delta_{s_1} + \Delta_{s_2} - \Delta_{s_3} - \Delta_{s_4} = 2k$ ,  $k \in \mathbb{Z}$  holds. Hence, the coefficients  $P_1(m, 0)$  have a divergence and the D-function is given by eq. (D.1.8). We extract the contributions to the anomalous dimensions from the logarithmic part of eq. (D.1.8) and obtain

$$\Delta_v^{(1);\text{con}} = \frac{2(N+2)}{(N+8)(1+2v)}, \quad \Delta_{v-1}^{(1);\text{con}} = \frac{2(N+2)}{(N+8)(3-2v)}. \quad (\text{D.2.3})$$

The  $\mathcal{O}(\varepsilon)$  corrections to the OPE coefficients is now given by

$$|\lambda_{\Psi_v \bar{\Psi}_v \mathcal{O}_0}^{(1)}|^2 = \frac{2(N+2)(2H^v - H^{2v})}{(1+2v)N(N+8)} - \frac{2(N+2)}{(1+2v)^2N(N+8)}, \quad (\text{D.2.4})$$

$$|\lambda_{\Psi_{v-1} \bar{\Psi}_{v-1} \mathcal{O}_0}^{(1)}|^2 = \frac{2(N+2)(2H^{1-v} - H^{2-2v})}{(3-2v)N(N+8)} - \frac{2(N+2)}{(3-2v)^2N(N+8)}. \quad (\text{D.2.5})$$

Adding the results from eq. (D.2.3) and eq. (D.2.1), we obtain the following anomalous dimensions:

$$\Delta_{0,0}^{0,m} |_{s_i=v} = \frac{2(N+2)}{(N+8)(1+2v)} + \frac{(N+2)(v-1)}{(N+8)}, \quad (\text{D.2.6})$$

$$\Delta_{0,0}^{0,m} |_{s_i=v-1} = \frac{2(N+2)}{(N+8)(3-2v)} - \frac{(N+2)v}{(N+8)}. \quad (\text{D.2.7})$$

All results are summarized in table 5.1. We have only considered the  $\Psi_{s_1} \times \bar{\Psi}_{s_2}$  channel. One can also consider the  $\Psi_{s_1} \times \Psi_{s_2}$  channel, which contains operators of the form  $\mathcal{O}_\alpha^{s,m} = \Psi_{\alpha+v}(\bar{\partial}^2)^m \Psi_{s-\alpha-v}$  that have fractional spin  $s = s_1 + s_2 = k + 2v \in \mathbb{Z} + 2v$ . Since the anomalous dimensions have been given in [77] and we have shown how to obtain the OPE coefficients from their results, we will not repeat the calculation for this channel in this work.





# Appendix E

## Crossing vectors for $O(2)$ line defects

In this appendix, we give explicit formulas for the vectors that enter the crossing equations.

### E.1 One complex scalar

The crossing vectors for eq. (5.2.18) read

$$\vec{V}_{\Delta,S}^{\phi\bar{\phi}} = \begin{pmatrix} F_{-,\Delta} \\ (-1)^S F_{-,\Delta} \\ (-1)^S F_{+,\Delta} \end{pmatrix}, \quad \vec{V}_{\Delta}^{\phi\phi} = \begin{pmatrix} 0 \\ F_{-,\Delta} \\ -F_{+,\Delta} \end{pmatrix}, \quad (\text{E.1.1})$$

where the shorthand notation  $F_{\pm,\Delta} = F_{\pm,\Delta}^{\phi\phi\phi\phi}(\xi)$  is understood.

### E.2 Tilt and displacement

The crossing equations for the tilt and displacement in eq. (5.2.22) are written in terms of the following crossing vectors:

$$\vec{V}_{\Delta}^+ = \begin{pmatrix} \begin{pmatrix} F_{-,\Delta}^{tt,tt} & 0 \\ 0 & 0 \end{pmatrix} \\ \begin{pmatrix} F_{-,\Delta}^{tt,tt} & 0 \\ 0 & 0 \end{pmatrix} \\ \begin{pmatrix} F_{+,\Delta}^{tt,tt} & 0 \\ 0 & 0 \end{pmatrix} \\ \begin{pmatrix} 0 & 0 \\ 0 & F_{-,\Delta}^{DD,DD} \end{pmatrix} \\ \begin{pmatrix} 0 & 0 \\ 0 & F_{-,\Delta}^{DD,DD} \end{pmatrix} \\ \begin{pmatrix} 0 & 0 \\ 0 & F_{+,\Delta}^{DD,DD} \end{pmatrix} \\ 0 \\ \begin{pmatrix} 0 & \frac{1}{2} \\ \frac{1}{2} & 0 \end{pmatrix} F_{-,\Delta}^{tt,DD} \\ \begin{pmatrix} 0 & \frac{1}{2} \\ \frac{1}{2} & 0 \end{pmatrix} F_{+,\Delta}^{tt,DD} \end{pmatrix}, \quad \vec{V}_{\Delta}^{t\bar{t},-} = \begin{pmatrix} F_{-,\Delta}^{tt,tt} \\ -F_{-,\Delta}^{tt,tt} \\ -F_{+,\Delta}^{tt,tt} \\ 0 \\ 0 \\ 0 \\ 0 \\ 0 \\ 0 \end{pmatrix}, \quad \vec{V}_{\Delta}^{D\bar{D},-} = \begin{pmatrix} 0 \\ 0 \\ 0 \\ F_{-,\Delta}^{DD,DD} \\ -F_{-,\Delta}^{DD,DD} \\ -F_{+,\Delta}^{DD,DD} \\ 0 \\ 0 \\ 0 \end{pmatrix}, \quad (\text{E.2.1})$$

$$\vec{V}_{\Delta}^{tt} = \begin{pmatrix} 0 \\ F_{-\Delta}^{tt,tt} \\ -F_{+\Delta}^{tt,tt} \\ 0 \\ 0 \\ 0 \\ 0 \\ 0 \\ 0 \end{pmatrix}, \quad \vec{V}_{\Delta}^{DD} = \begin{pmatrix} 0 \\ 0 \\ 0 \\ 0 \\ F_{-\Delta}^{DD,DD} \\ -F_{+\Delta}^{DD,DD} \\ 0 \\ 0 \\ 0 \end{pmatrix}, \quad \vec{V}_{\Delta,S}^{tD} = \begin{pmatrix} 0 \\ 0 \\ 0 \\ 0 \\ 0 \\ 0 \\ (-1)^S F_{-\Delta}^{tD,tD} \\ F_{-\Delta}^{Dt,tD} \\ -F_{+\Delta}^{Dt,tD} \end{pmatrix}. \quad (\text{E.2.2})$$

### E.3 One real and one complex scalar

The crossing equations for one real scalar  $\phi_1$  and one complex scalar  $\phi_2$  appear in eq. (5.2.23), with crossing vectors

$$\vec{V}_{\Delta}^{+} = \begin{pmatrix} \begin{pmatrix} F_{-\Delta}^{11,11} & 0 \\ 0 & 0 \end{pmatrix} \\ \begin{pmatrix} 0 & 0 \\ 0 & F_{-\Delta}^{22,22} \end{pmatrix} \\ \begin{pmatrix} 0 & 0 \\ 0 & F_{-\Delta}^{22,22} \end{pmatrix} \\ \begin{pmatrix} 0 & 0 \\ 0 & F_{+\Delta}^{22,22} \end{pmatrix} \\ 0 \\ \begin{pmatrix} 0 & \frac{1}{2} \\ \frac{1}{2} & 0 \end{pmatrix} F_{-\Delta}^{11,22} \\ \begin{pmatrix} 0 & \frac{1}{2} \\ \frac{1}{2} & 0 \end{pmatrix} F_{+\Delta}^{11,22} \end{pmatrix}, \quad \vec{V}_{\Delta}^{-} = \begin{pmatrix} 0 \\ F_{-\Delta}^{22,22} \\ -F_{-\Delta}^{22,22} \\ -F_{+\Delta}^{22,22} \\ 0 \\ 0 \\ 0 \end{pmatrix}, \quad (\text{E.3.1})$$

$$\vec{V}_{\Delta}^{22} = \begin{pmatrix} 0 \\ 0 \\ F_{-\Delta}^{22,22} \\ -F_{+\Delta}^{22,22} \\ 0 \\ 0 \\ 0 \end{pmatrix}, \quad \vec{V}_{\Delta,S}^{12} = \begin{pmatrix} 0 \\ 0 \\ 0 \\ 0 \\ (-1)^S F_{-\Delta}^{12,12} \\ F_{-\Delta}^{21,12} \\ -F_{+\Delta}^{21,12} \end{pmatrix}. \quad (\text{E.3.2})$$

Here we are using  $F_{\pm,\Delta}^{ij,kl} = F_{\pm,\Delta}^{\phi_i\phi_j,\phi_k\phi_l}(\xi)$ , and we do not distinguish between  $\phi_2$  and  $\bar{\phi}_2$  because they have the same scaling dimension.

## E.4 Two complex scalars

The crossing equations for two complex scalars given in eq. (5.2.24) are written in terms of the following crossing vectors:

$$\vec{V}_{\Delta,S} = \begin{pmatrix} \begin{pmatrix} F_{-,\Delta}^{11,11} & 0 \\ 0 & 0 \end{pmatrix} \\ \begin{pmatrix} (-1)^S F_{-,\Delta}^{11,11} & 0 \\ 0 & 0 \end{pmatrix} \\ \begin{pmatrix} (-1)^S F_{+,\Delta}^{11,11} & 0 \\ 0 & 0 \end{pmatrix} \\ \begin{pmatrix} 0 & 0 \\ 0 & F_{-,\Delta}^{22,22} \end{pmatrix} \\ \begin{pmatrix} 0 & 0 \\ 0 & (-1)^S F_{-,\Delta}^{22,22} \end{pmatrix} \\ \begin{pmatrix} 0 & 0 \\ 0 & (-1)^S F_{+,\Delta}^{22,22} \end{pmatrix} \\ 0 \\ 0 \\ \begin{pmatrix} 0 & \frac{1}{2} \\ \frac{1}{2} & 0 \end{pmatrix} F_{-,\Delta}^{11,22} \\ \begin{pmatrix} 0 & \frac{1}{2} \\ \frac{1}{2} & 0 \end{pmatrix} F_{+,\Delta}^{11,22} \\ \begin{pmatrix} 0 & \frac{1}{2} \\ \frac{1}{2} & 0 \end{pmatrix} (-1)^S F_{-,\Delta}^{11,22} \\ \begin{pmatrix} 0 & \frac{1}{2} \\ \frac{1}{2} & 0 \end{pmatrix} (-1)^S F_{+,\Delta}^{11,22} \end{pmatrix}, \quad \vec{V}_{\Delta}^{11} = \begin{pmatrix} 0 \\ F_{-,\Delta}^{11,11} \\ -F_{+,\Delta}^{11,11} \\ 0 \\ 0 \\ 0 \\ 0 \\ 0 \\ 0 \\ 0 \\ 0 \\ 0 \\ 0 \end{pmatrix}, \quad \vec{V}_{\Delta}^{22} = \begin{pmatrix} 0 \\ 0 \\ 0 \\ 0 \\ F_{-,\Delta}^{22,22} \\ -F_{+,\Delta}^{22,22} \\ 0 \\ 0 \\ 0 \\ 0 \\ 0 \\ 0 \\ 0 \end{pmatrix}, \quad (\text{E.4.1})$$

$$\vec{V}_{\Delta,S}^{1\bar{2}} = \begin{pmatrix} 0 \\ 0 \\ 0 \\ 0 \\ 0 \\ 0 \\ (-1)^S F_{-,\Delta}^{12,12} \\ -(-1)^S F_{+,\Delta}^{1\bar{2},12} \\ F_{-,\Delta}^{21,12} \\ -F_{+,\Delta}^{2\bar{1},12} \\ 0 \\ 0 \end{pmatrix}, \quad \vec{V}_{\Delta,S}^{12} = \begin{pmatrix} 0 \\ 0 \\ 0 \\ 0 \\ 0 \\ 0 \\ (-1)^S F_{-,\Delta}^{12,12} \\ (-1)^S F_{+,\Delta}^{1\bar{2},12} \\ 0 \\ 0 \\ F_{-,\Delta}^{21,12} \\ -F_{+,\Delta}^{2\bar{1},12} \end{pmatrix}. \quad (\text{E.4.2})$$



# Appendix F

## Spinor conventions

In this appendix we describe our conventions for the spinor fields. In the action given in eq. (6.2.1), the fermions are presented as Dirac fields, which can be decomposed into two basic Weyl spinors as follows:

$$\psi^A = \begin{pmatrix} \chi^\alpha \\ \xi^{\dagger\dot{\alpha}} \end{pmatrix}, \quad \bar{\psi}^A = \begin{pmatrix} \xi^\alpha & \chi_{\dot{\alpha}}^\dagger \end{pmatrix}, \quad (\text{F.0.1})$$

with  $\alpha, \dot{\alpha} = 1, 2$ . The Weyl spinors are two-component vectors defined as

$$\chi = \begin{pmatrix} \chi_1 \\ \chi_2 \end{pmatrix}, \quad \xi^\dagger = (\xi_1 \ \xi_2). \quad (\text{F.0.2})$$

Spinors with an undotted index  $\alpha$  transform as left-handed spinors  $(1, 0)$ , while right-handed spinors  $(0, 1)$  are complex conjugates of the  $(1, 0)$  representation and carry a dotted index  $\dot{\alpha}$ . The dot is here to indicate the transformation property, i.e.

$$\chi_{\dot{\alpha}}^\dagger = (\chi_\alpha)^\dagger. \quad (\text{F.0.3})$$

Indices can be raised and lowered in the following way:

$$\chi^\alpha = \epsilon^{\alpha\beta} \chi_\beta = -\epsilon^{\beta\alpha} \chi_\beta, \quad (\text{F.0.4})$$

which implies

$$\chi^\alpha \xi_\alpha = -\chi_\alpha \xi^\alpha. \quad (\text{F.0.5})$$

Here the tensor  $\epsilon^{\alpha\beta}$  is defined as

$$\epsilon^{12} = -\epsilon^{21} = \epsilon_{21} = -\epsilon_{12} = +1, \quad (\text{F.0.6})$$

and a similar definition can be formulated for dotted indices:

$$\epsilon_{\dot{\alpha}\dot{\beta}} = \epsilon_{\alpha\beta}, \quad \epsilon^{\dot{\alpha}\dot{\beta}} = \epsilon^{\alpha\beta}. \quad (\text{F.0.7})$$

For external operators it is convenient to use polarization spinors  $s^A, \bar{s}^A$  in order to avoid cluttering of the indices. We define

$$\psi^i(s, \tau) := s^A \psi^{i,A}(\tau), \quad \bar{\psi}^i(s, \tau) := \bar{s}^A \bar{\psi}^{i,A}(\tau), \quad (\text{F.0.8})$$

and a similar definition holds for the Weyl fermions as well.

The four-dimensional (Euclidean)  $\gamma$ -matrices are defined in the chiral representation as

$$(\gamma^\mu)^{AB} := \begin{pmatrix} 0 & (\sigma^\mu)_{\alpha\dot{\beta}} \\ (\bar{\sigma}^\mu)^{\dot{\alpha}\beta} & 0 \end{pmatrix}, \quad (\text{F.0.9})$$

where we have introduced

$$(\sigma^\mu)_{\alpha\dot{\beta}} := (\sigma^0, i\sigma^i), \quad (\bar{\sigma}^\mu)^{\dot{\alpha}\beta} := (\sigma^0, -i\sigma^i). \quad (\text{F.0.10})$$

The Pauli matrices  $\sigma^0, \sigma^i$  are defined as

$$\sigma^0 = \mathbb{1}_2, \quad \sigma^1 = \begin{pmatrix} 0 & 1 \\ 1 & 0 \end{pmatrix}, \quad \sigma^2 = \begin{pmatrix} 0 & -i \\ i & 0 \end{pmatrix}, \quad \sigma^3 = \begin{pmatrix} 1 & 0 \\ 0 & -1 \end{pmatrix}. \quad (\text{F.0.11})$$

The  $\gamma$ -matrices satisfy the Euclidean Clifford algebra

$$\{\gamma^\mu, \gamma^\nu\}^{AB} = 2\delta^{\mu\nu} \mathbb{1}^{AB}, \quad (\text{F.0.12})$$

and we can define an additional  $\gamma$ -matrix as

$$(\gamma^5)^{AB} := \begin{pmatrix} \mathbb{1}_{\alpha\beta} & 0 \\ 0 & -\mathbb{1}_{\dot{\alpha}\dot{\beta}} \end{pmatrix}. \quad (\text{F.0.13})$$

This definition ensures that  $\gamma^5$  satisfies the following properties:

$$\{\gamma^5, \gamma^\mu\} = 0 \quad (\gamma^5)^\dagger = \gamma^5, \quad (\gamma^5)^2 = \mathbb{1}. \quad (\text{F.0.14})$$

# Appendix G

## More details on the $\beta$ -functions for Yukawa CFTs

The general  $\beta$ -function for the bulk coupling constants  $\lambda_{ijkl}, \Gamma_i$ , as well as the anomalous dimensions, was given in the appendix of [174] up to  $\mathcal{O}(\varepsilon^2)$ . The renormalization constants up to  $\mathcal{O}(\varepsilon^2)$ , are:

$$\begin{aligned}
Z_\lambda = 1 &+ \frac{1}{(4\pi)^2\varepsilon} \left( \frac{(N+8)\lambda}{3} + 8N_f g^2 - \frac{4(N+8)N_f g^2 \lambda}{6(4\pi)^2} - \frac{12N_f g^4}{\lambda} + \frac{12N_f g^6}{\pi^2 \lambda} \right. \\
&+ \frac{4(12-5N)N_f g^4}{2(4\pi)^2} - \frac{(14+3N)\lambda^2}{6(4\pi)^2} \Big) \\
&+ \frac{1}{(4\pi)^4 \varepsilon^2} \left( -96N_f(4+4N_f-N) \frac{g^6}{\lambda} + 4(N+8)N_f g^2 \lambda \right. \\
&+ \left. 12N_f(4N_f-2(N+4))g^4 + \frac{(N+8)^2}{9}\lambda^2 \right) + \mathcal{O}(\lambda^3, g^6, \lambda^2 g^2, \lambda g^4), \tag{G.0.1}
\end{aligned}$$

$$\begin{aligned}
Z_g = 1 &+ \frac{1}{(4\pi)^2\varepsilon} \left( \kappa_1 g^2 - \frac{N+2}{3(4\pi)^2} g^2 \lambda - \frac{9N^2-40N-32+24\kappa_1}{8(4\pi)^2} g^4 + \frac{N+2}{72(4\pi)^2} \lambda^2 \right) \\
&+ \frac{1}{(4\pi)^4 \varepsilon^2} \left( \frac{(N+2)(5\kappa_1-32)}{72(4\pi)^2} g^2 \lambda^2 + \frac{3\kappa_1^2}{2} g^4 \right) \\
&+ \mathcal{O}(\lambda^3, g^6, \lambda^2 g^2, \lambda g^4), \tag{G.0.2}
\end{aligned}$$

$$\begin{aligned}
Z_\phi = 1 &+ \frac{1}{(4\pi)^2\varepsilon} \left( -2N_f g^2 + \frac{4(N+4)N_f}{8(4\pi)^2} g^4 - \frac{N+2}{72(4\pi)^2} \lambda^2 \right) + \frac{1}{(4\pi)^4 \varepsilon^2} \left( \frac{(N-4)^2 - \kappa_1^2}{2} g^4 \right) \\
&+ \mathcal{O}(\lambda^3, g^6, \lambda^2 g^2, \lambda g^4), \tag{G.0.3}
\end{aligned}$$

$$\begin{aligned}
Z_\psi = 1 &+ \frac{1}{(4\pi)^2\varepsilon} \left( -\frac{N}{2} g^2 + \frac{N(7N+6(\kappa_1-4))}{16(4\pi)^2} g^4 \right) - \frac{1}{(4\pi)^4 \varepsilon^2} \left( \frac{N(N-4\kappa_1)}{8} g^4 \right) \\
&+ \mathcal{O}(\lambda^3, g^6, \lambda^2 g^2, \lambda g^4). \tag{G.0.4}
\end{aligned}$$

The  $\beta$ -function for the defect coupling was computed up to  $\mathcal{O}(\varepsilon^2)$  in [90]. The

corresponding renormalization factor is given by

$$\begin{aligned}
Z_h = 1 + \frac{1}{(4\pi)^2 \varepsilon} & \left\{ \frac{\lambda h^2}{12} - \frac{g^2 \lambda h^2 N_f}{3(4\pi)^2} - \frac{(\pi^2 - 6) g^4 h^2 2N_f}{9(4\pi)^2} \right. \\
& \left. - \frac{g^4(N+4)N_f}{4(4\pi)^2} + g^2 2N_f + \lambda^2 \left( -\frac{h^2(N+8)}{108(4\pi)^2} - \frac{h^4}{48(4\pi)^2} + \frac{N+2}{72(4\pi)^2} \right) \right\} \\
& + \frac{1}{(4\pi)^4 \varepsilon^2} \left\{ \frac{g^2 \lambda h^2 N_f}{2} - \frac{g^4 h^2 4N_f}{3} + g^4(6N_f + 8 - 2NN) + \lambda^2 \left( \frac{h^2(N+8)}{108} + \frac{h^4}{96} \right) \right\}.
\end{aligned} \tag{G.0.5}$$

Let us look at each model individually.

## G.1 Gross–Neveu–Yukawa model ( $N = 1$ )

We will start with considering the GNY model, which contains a single scalar field  $\phi$  and  $N_f$  fermions. Hence, the matrix  $\Sigma^a = \Sigma^1$  in eq. (6.2.1), which corresponds to  $\Gamma_i$  in [174], is given by the identity matrix:

$$\Sigma = \mathbf{1}, \quad \Gamma_1 = g_1 \mathbf{1}_{N_f \times N_f} \otimes \mathbf{1}. \tag{G.1.1}$$

The  $\beta$ -functions up to  $\mathcal{O}(\varepsilon^2)$  were computed in [207] and we adopted the same convention as [174]:

$$\begin{aligned}
\beta_\lambda^{\text{GNY}} = -\varepsilon \lambda + \frac{1}{(4\pi)^2} & (8g^2 \lambda N_f - 48g^4 N_f + 3\lambda^2) \\
& - \frac{1}{(4\pi)^4} \left( -12g^2 \lambda^2 N_f + 28g^4 \lambda N_f + 384g^6 N_f - \frac{17\lambda^3}{3} \right) + \mathcal{O}(\lambda^3, g^6, \lambda^2 g^2, \lambda g^4),
\end{aligned} \tag{G.1.2}$$

$$\beta_g^{\text{GNY}} = -g \frac{\varepsilon}{2} + \frac{1}{(4\pi)^2} \left( \frac{g^3(4N_f + 6)}{2} \right) + \frac{1}{(4\pi)^4} \left( -2g^3 \lambda - \frac{3}{4} g^5(16N_f + 3) + \frac{g\lambda^2}{12} \right) + \mathcal{O}(g^6). \tag{G.1.3}$$

The Wilson-Fisher-Yukawa (WFY) fixed point can be reached for the following values of the couplings at one loop in  $\varepsilon := 4 - d$ :

$$(g_\star^{\text{GNY}})^2 = (4\pi)^2 \left( \frac{\varepsilon}{2\kappa_1} + \frac{\varepsilon^2(2\kappa_1(\kappa_2 + 288) + 15(4\kappa_2 - 99))}{432\kappa_1^3} + \mathcal{O}(\varepsilon^3) \right), \tag{G.1.4}$$

$$\begin{aligned}
\lambda_\star^{\text{GNY}} = (4\pi)^2 & \left\{ \frac{\varepsilon \kappa_2}{6\kappa_1} + \frac{\varepsilon^2}{216\kappa_1^3(\kappa_1 + \kappa_2 - 6)} \left( -12\kappa_1^3(\kappa_2 - 36) \right. \right. \\
& \left. \left. + 2\kappa_1^2(97\kappa_2 + 72) + 15\kappa_1(47\kappa_2 - 1188) - 2925\kappa_2 + 40500 \right) + \mathcal{O}(\varepsilon^3) \right\}.
\end{aligned} \tag{G.1.5}$$



The  $\beta$ -function for  $h \equiv h_1$  is given by

$$\begin{aligned} \beta_h^{\text{GNY}} &= -\frac{h\varepsilon}{2} + \frac{1}{(4\pi)^2} \left( 2g^2 h N_f + \frac{\lambda h^3}{6} \right) \\ &+ \frac{1}{(4\pi)^4} \left( 4g^4 h^3 N_f - g^2 \lambda h^3 N_f - \frac{2}{3} \pi^2 g^4 h^3 N_f - \frac{5}{2} g^4 h N_f - \frac{\lambda^2 h^5}{12} - \frac{\lambda^2 h^3}{4} + \frac{\lambda^2 h}{12} \right) \\ &+ \mathcal{O}(\lambda^3, g^6, \lambda^2 g^2, \lambda g^4), \end{aligned} \tag{G.1.6}$$

leading to the following fixed point at  $\mathcal{O}(\varepsilon)$ :

$$\begin{aligned} (h_\star^{\text{GNY}})^2 &= \frac{54}{\kappa_2} + \frac{\varepsilon}{2\kappa_1^2 \kappa_2^2 (4\kappa_1(\kappa_2 - 54) + (\kappa_2 - 24)\kappa_2 + 648)} \left\{ (\kappa_1(149\kappa_1 - 816) + 1125)\kappa_2^3 \right. \\ &+ 3(\kappa_1(-216\pi^2(\kappa_1 - 3) + \kappa_1(105\kappa_1 - 302) + 1545) - 4500)\kappa_2^2 \\ &- 216(\kappa_1(3\pi^2(\kappa_1 - 6)(\kappa_1 - 3) + \kappa_1(69\kappa_1 - 112) + 171) - 1125)\kappa_2 \\ &\left. + 69984(\kappa_1 - 6)(\kappa_1 - 3)\kappa_1 \right\} + \mathcal{O}(\varepsilon^2). \end{aligned} \tag{G.1.7}$$

## G.2 Nambu–Jona-Lasinio–Yukawa model ( $N = 2$ )

When we extend the number of scalars to a real scalar and a real pseudoscalar, or one complex scalar, and keep the number of fermions arbitrary at  $N_f$ , we obtain the NJLY model. The matrix  $\Sigma^a = \Sigma^1, \Sigma^2$  is now given by  $\Sigma^1 = \mathbf{1}, \Sigma^2 = i\gamma_5$ . The  $\beta$ -functions for  $\lambda$  and  $g$  are given up to two loop orders by [174]:

$$\begin{aligned} \beta_\lambda^{\text{NJLY}} &= -\varepsilon\lambda + \frac{1}{(4\pi)^2} \left( \frac{10}{3}\lambda^2 + 8N_f\lambda g^2 - 48N_f g^4 \right) \\ &- \frac{1}{(4\pi)^4} \left( \frac{20}{3}\lambda^2 - 384N_f g^6 - 8N_f\lambda g^4 + \frac{40}{3}N_f g^2 \lambda^2 \right) \\ &+ \mathcal{O}(\lambda^3, g^6, \lambda^2 g^2, \lambda g^4), \end{aligned} \tag{G.2.1}$$

$$\beta_g^{\text{NJLY}} = -\frac{\varepsilon}{2}g + \frac{1}{(4\pi)^2} (2N_f + 2) + \frac{1}{(4\pi)^4} \left( -\frac{8}{3}g^3\lambda + \frac{1}{9}g\lambda^2 + (7 - 12N_f)g^5 \right) + \mathcal{O}(g^7). \tag{G.2.2}$$

The zeros of these  $\beta$ -functions give us the fixed points  $\lambda_\star, g_\star$  of the NJLY model:

$$\begin{aligned} \frac{\lambda_\star^{\text{NJLY}}}{(4\pi)^2} &= \frac{3\kappa_2\varepsilon}{20\kappa_1} - \frac{9\varepsilon^2(3\kappa_1^3(\kappa_2 - 40) + \kappa_1^2(160 - 75\kappa_2) + \kappa_1(5000 - 219\kappa_2) + 674\kappa_2 - 9680)}{500\kappa_1^3(\kappa_1 + \kappa_2 - 4)} \\ &+ \mathcal{O}(\varepsilon^3), \end{aligned} \tag{G.2.3}$$

$$\frac{(g_\star^{\text{NJLY}})^2}{(4\pi)^2} = \frac{\varepsilon}{2\kappa_1} + \frac{\varepsilon^2(\kappa_1(\kappa_2 + 260) + 36\kappa_2 - 870)}{200\kappa_1^3} + \mathcal{O}(\varepsilon^3). \tag{G.2.4}$$

The defect  $\beta$ -function is given by

$$\begin{aligned} \beta_h^{\text{NJLY}} = & -\frac{\varepsilon h}{2} + \frac{1}{(4\pi)^2} \left( 2g^2 h N_f + \frac{\lambda h^3}{6} \right) \\ & + \frac{1}{(4\pi)^4} \left( 4g^4 h^3 N_f - 3g^4 h N_f - g^2 \lambda h^3 N_f - \frac{2}{3} \pi^2 g^4 h^3 N_f - \frac{\lambda^2 h^5}{12} - \frac{5\lambda^2 h^3}{18} + \frac{\lambda^2 h}{9} \right) \\ & + \mathcal{O}(\lambda^3, g^6, \lambda^2 g^2, \lambda g^4), \end{aligned} \tag{G.2.5}$$

which has a fixed point for  $g_*$ ,  $\lambda_*$  and

$$\begin{aligned} (h_*^{\text{NJLY}})^2 = & \frac{40}{\kappa_2} + \frac{\varepsilon}{15\kappa_1^2 \kappa_2^2 (4\kappa_1(\kappa_2 - 60) + (\kappa_2 - 16)\kappa_2 + 480)} \left\{ 6(\kappa_1(187\kappa_1 - 1096) + 1452)\kappa_2^3 \right. \\ & + 2(\kappa_1(-2000\pi^2(\kappa_1 - 2) + 3\kappa_1(353\kappa_1 + 1620) + 3708) - 34848)\kappa_2^2 \\ & - 160(\kappa_1(25\pi^2(\kappa_1 - 4)(\kappa_1 - 2) + 3\kappa_1(179\kappa_1 - 72) + 2820) - 8712)\kappa_2 \\ & \left. + 288000(\kappa_1 - 4)(\kappa_1 - 2)\kappa_1 \right\} + \mathcal{O}(\varepsilon^2). \end{aligned} \tag{G.2.6}$$

### G.3 Chiral Heisenberg model ( $N = 3$ )

The last model we will consider is the chiral Heisenberg model. It contains three real scalars and the model is invariant under  $SO(3)$  rotations. The matrix  $\Sigma^a = \Sigma^1, \Sigma^2, \Sigma^3$  is given by the Pauli matrices  $\sigma_i$ :

$$\Sigma^a = \sigma_a \otimes \mathbf{1}_2. \tag{G.3.1}$$

The  $\beta$ -functions for  $\lambda$  and  $g$  up to  $\mathcal{O}(\varepsilon^2)$  were calculated in [208], together with various critical exponents. They are given by

$$\begin{aligned} \beta_\lambda^{\text{XH}} = & -\varepsilon \lambda + \frac{1}{(4\pi)^2} \left( 8g^2 \lambda N_f - 48g^4 N_f + \frac{11\lambda^2}{3} \right) \\ & - \frac{1}{(4\pi)^4} \left( -\frac{44}{3} g^2 \lambda^2 N_f - 12g^4 \lambda N_f + 384g^6 N_f - \frac{23\lambda^3}{3} \right) + \mathcal{O}(\lambda^3, g^6, \lambda^2 g^2, \lambda g^4), \end{aligned} \tag{G.3.2}$$

$$\beta_g^{\text{XH}} = -\frac{\varepsilon}{2} g + \frac{1}{(4\pi)^2} (2g^3 N_f + g^3) + \frac{1}{(4\pi)^4} \left( -\frac{10g^3 \lambda}{3} - 12g^5 N_f + \frac{47g^5}{4} + \frac{5g\lambda^2}{36} \right) + \mathcal{O}(g^7). \tag{G.3.3}$$

The corresponding WFY fixed points are

$$\begin{aligned} \frac{\lambda_*^{\text{XH}}}{(4\pi)^2} = & \frac{3\kappa_2 \varepsilon}{22\kappa_1} + \frac{\varepsilon^2}{10648\kappa_1^3(\kappa_1 + \kappa_2 - 2)} \left( -564\kappa_1^3(\kappa_2 - 44) \right. \\ & \left. + 6\kappa_1^2(2951\kappa_2 - 9064) + 57\kappa_1(1027\kappa_2 - 16412) - 74853\kappa_2 + 965052 \right) + \mathcal{O}(\varepsilon^3), \end{aligned} \tag{G.3.4}$$

$$\frac{(g_*^{\text{XH}})^2}{(4\pi)^2} = \frac{\varepsilon}{2\kappa_1} + \frac{\varepsilon^2(2\kappa_1(5\kappa_2 + 1232) + 420\kappa_2 - 8151)}{1936\kappa_1^3} + \mathcal{O}(\varepsilon^3). \tag{G.3.5}$$

The  $\beta$ -function of  $h$  is given by

$$\begin{aligned} \beta_h^{\text{CH}} = & -\frac{\varepsilon h}{2} + \frac{1}{(4\pi)^2} \left( 2g^2 h N_f + \frac{\lambda h^3}{6} \right) \\ & + \frac{1}{(4\pi)^4} \left( -g^2 \lambda h^3 N_f - \frac{2}{3} \pi^2 g^4 h^3 N_f + 4g^4 h^3 N_f - \frac{7}{2} g^4 h N_f - \frac{\lambda^2 h^5}{12} - \frac{11\lambda^2 h^3}{36} + \frac{5\lambda^2 h}{36} \right) \\ & + \mathcal{O}(\lambda^3, g^6, \lambda^2 g^2, \lambda g^4), \end{aligned} \tag{G.3.6}$$

with the corresponding fixed point

$$\begin{aligned} (h_\star^{\text{CH}})^2 = & \frac{22}{\kappa_2} + \frac{\varepsilon}{66\kappa_1^2 \kappa_2^2 (4\kappa_1(\kappa_2 - 66) + (\kappa_2 - 8)\kappa_2 + 264)} \left\{ \left( \kappa_1 (7947\kappa_1^2 + 98706\kappa_1 \right. \right. \\ & - 10648\pi^2(\kappa_1 - 1) - 18717) - 87732) \kappa_2^2 + 3(\kappa_1(1627\kappa_1 - 8928) + 7311) \kappa_2^3 \\ & - 88(\kappa_1(121\pi^2(\kappa_1 - 2)(\kappa_1 - 1) + 3\kappa_1(813\kappa_1 + 280) + 18753) - 21933) \kappa_2 \\ & \left. \left. + 383328(\kappa_1 - 2)(\kappa_1 - 1)\kappa_1 \right\} + \mathcal{O}(\varepsilon^2). \end{aligned} \tag{G.3.7}$$



# Appendix H

## Integrals

We gather in this appendix the integrals useful for the computations performed in this work. Integrals are computed using dimensional regularization with  $d = 4 - \varepsilon$ . In our perturbative computations, we encounter the following integrals:

$$Y_{123} := \int d^d x_4 I_{14} I_{24} I_{34}, \quad (\text{H.0.1})$$

$$X_{1234} := \int d^d x_5 I_{15} I_{25} I_{35} I_{45}, \quad (\text{H.0.2})$$

$$H_{12,34} := \int d^d x_5 \int d^d x_6 I_{15} I_{25} I_{36} I_{46} I_{56} = \int d^d x_5 I_{15} I_{25} Y_{345}, \quad (\text{H.0.3})$$

where  $I_{ij}$  corresponds to the scalar propagator in  $d$  dimensions (see eq. (6.2.14)). The three- and four-point massless integrals  $X$  and  $Y$  are finite in  $d = 4$  and have been solved analytically [223, 224]. The  $X$ -integral is given by

$$X_{1234} = \frac{I_{12} I_{34}}{16\pi^2} \chi \bar{\chi} D(\chi, \bar{\chi}), \quad (\text{H.0.4})$$

with the Bloch-Wigner function

$$D(\chi, \bar{\chi}) := \frac{1}{\chi - \bar{\chi}} \left( 2\text{Li}_2(\chi) - 2\text{Li}_2(\bar{\chi}) + \log \chi \bar{\chi} \log \frac{1 - \chi}{1 - \bar{\chi}} \right), \quad (\text{H.0.5})$$

and where the variables  $\chi, \bar{\chi}$  are defined via

$$\chi \bar{\chi} = \frac{I_{13} I_{24}}{I_{12} I_{34}}, \quad (1 - \chi)(1 - \bar{\chi}) = \frac{I_{13} I_{24}}{I_{14} I_{23}}. \quad (\text{H.0.6})$$

In the case where all the external points are aligned (here in the  $\tau$ -direction), the  $X$ -integral can be expressed as a special limit of the result above:

$$\begin{aligned} X_{1234} &= \frac{I_{12} I_{34}}{16\pi^2} \chi^2 D(\chi, \chi) \\ &= -\frac{I_{12} I_{34}}{8\pi^2} \frac{\chi}{1 - \chi} (\chi \log \chi + (1 - \chi) \log(1 - \chi)). \end{aligned} \quad (\text{H.0.7})$$

Note that in  $1d$ ,  $X_{1234}$  is one degree of transcendentality lower than in higher  $d$ , and that although the prefactor in eq. (H.0.5) implies a divergence in the limit  $\bar{\chi} \rightarrow \chi$ , it turns out to be compensated by the numerator.

The  $Y$ -integral can easily be obtained starting with  $X_{1234}$  and sending one of the external points to  $\infty$ :

$$Y_{123} = \lim_{x_4 \rightarrow \infty} 4\pi^2 x_4^2 X_{1234}. \quad (\text{H.0.8})$$

For the  $1d$  limit mentioned above, this gives

$$Y_{123} = -\frac{I_{12}}{8\pi^2} \left( \frac{\tau_{12}}{\tau_{13}} \log \frac{\tau_{12}}{\tau_{13}} + \frac{\tau_{23}}{\tau_{13}} \log \frac{\tau_{23}}{\tau_{13}} \right), \quad (\text{H.0.9})$$

with  $\tau_{ij} := \tau_i - \tau_j$ . It is also useful to consider derivatives of the  $Y$ -integral, e.g.

$$\partial_1^2 Y_{123} = -I_{12}I_{13}, \quad (\text{H.0.10})$$

$$(\partial_1 \cdot \partial_2) Y_{123} = \frac{1}{2} (I_{12}I_{13} + I_{12}I_{23} - I_{13}I_{23}). \quad (\text{H.0.11})$$

To the best of our knowledge there exists no analytical solution for the  $H$ -integral. However several identities relate derivatives of the  $H$ -integral to its  $X$  and  $Y$  siblings [225, 226]:

$$\partial_1^2 H_{12,34} = -I_{12}Y_{134}, \quad (\text{H.0.12})$$

$$(\partial_1 \cdot \partial_2) H_{12,34} = \frac{1}{2} [I_{12}(Y_{134} + Y_{234}) - X_{1234}]. \quad (\text{H.0.13})$$

Other combinations can be obtained by using

$$H_{12,34} = H_{21,34} = H_{12,43} = H_{34,12}. \quad (\text{H.0.14})$$

In our calculations we only encounter the  $H$ -integral in the following special "spinor" combinations:

$$(F_{13,24})^{AB} := (\not{\partial}_1(\not{\partial}_1 + \not{\partial}_3)\not{\partial}_2)^{AB} H_{13,24}, \quad (\text{H.0.15})$$

$$(G_{12,34})^{ABCD} := (\not{\partial}_1\not{\partial}_2)^{AB}(\not{\partial}_3\not{\partial}_4)^{CD} H_{12,34}, \quad (\text{H.0.16})$$

where we have written the matrix indices explicitly to avoid confusion.

The  $F$ -integral is finite and can be solved by using integration by parts, the fermionic star-triangle relation

$$\int d^d x_4 \not{\partial}_4 I_{14} I_{24} \not{\partial}_4 I_{34} = -4\pi^2 \not{x}_{12} \not{x}_{23} I_{12} I_{13} I_{23}, \quad (\text{H.0.17})$$

and going to a conformal frame. For the case where all the external points are aligned, this gives

$$\begin{aligned} F_{13,24} &\stackrel{\tau_4 \rightarrow \infty}{\sim} \frac{\gamma^0}{4} I_{34} \partial_{\tau_1} Y_{123} \\ &= \frac{\gamma^0}{\tau_{12}^3 \tau_{34}^2} \frac{1}{512\pi^6} \frac{\chi}{1-\chi} (\chi^2 \log \chi + (1+\chi)(1-\chi) \log(1-\chi)), \end{aligned} \quad (\text{H.0.18})$$

where we have suppressed the indices for compactness.

The  $G$ -integral is also finite and can be solved by observing that the correlator given in (6.3.68) for the case  $N = 1$  needs to have the following structure in terms of spinor matrices:

$$G_{12,34}^{ABCD} = \frac{(\gamma^0)^{AB} (\gamma^0)^{CD}}{\tau_{12}^3 \tau_{34}^2} g_{12,34}(\chi). \quad (\text{H.0.19})$$

This implies

$$g_{12,34}(\chi) = \frac{1}{4} \tau_{12}^3 \tau_{34}^3 (\partial_1 \cdot \partial_2) (\partial_3 \cdot \partial_4) H_{12,34}, \quad (\text{H.0.20})$$

which, after using the identities given in eqs. (H.0.11) and (H.0.13), turns into

$$g_{12,34}(\chi) = \frac{1}{2048\pi^6} \frac{\chi}{(1-\chi)^2} ((1-\chi)(2-\chi) + \chi^2(2-\chi) \log \chi + \chi(1-\chi)^2 \log(1-\chi)). \quad (\text{H.0.21})$$

The integrals described above are log-divergent in the limit where two external points coincide. In particular, we encounter repeatedly the integral  $Y_{112}$  in self-energy diagrams, which reads:

$$Y_{112} = -\frac{1}{32\pi^4\tau_{12}^2} \left( \frac{1}{\varepsilon} + \aleph + \log \tau_{12}^2 + \mathcal{O}(\varepsilon) \right). \quad (\text{H.0.22})$$

Another divergent integral that appears in two-point fermion loops is the following:

$$B_{12} := \int d^d x_3 \int d^d x_4 I_{13} I_{24} \not{\partial}_3 I_{34} \not{\partial}_3 I_{34}. \quad (\text{H.0.23})$$

This integral is easy to relate to  $Y_{112}$  by using  $\gamma$ -matrix identities and integration by parts:

$$\begin{aligned} B_{12} &= \frac{1}{2} \int d^d x_3 \int d^d x_4 I_{13} I_{24} \partial_3^2 I_{34}^2 \\ &= \frac{1}{2} Y_{112}, \end{aligned} \quad (\text{H.0.24})$$

where in the final result there is a  $4 \times 4$  identity matrix implied. Note that in the last line we have made use of Green's equation (6.2.16). In the course of the computation, a quadratic divergence dropped out as dimensional regularization is insensitive to it.





# Bibliography

- [1] N. Bogoliubov and D. Shirkov, *Problems in quantum field theory. i and ii*, *Uspekhi Fiz. Nauk* **55** (1955) 149–214.
- [2] E. C. G. Stueckelberg and A. Petermann, *The normalization group in quantum theory*, *Helv. Phys. Acta* **24** (1951) 317–319.
- [3] M. Gell-Mann and F. E. Low, *Quantum electrodynamics at small distances*, *Phys. Rev.* **95** (Sep, 1954) 1300–1312.
- [4] K. G. Wilson and J. Kogut, *The renormalization group and the  $\epsilon$  expansion*, *Physics Reports* **12** (1974), no. 2 75–199.
- [5] K. G. Wilson, *The renormalization group and critical phenomena*, *Rev. Mod. Phys.* **55** (Jul, 1983) 583–600.
- [6] J. Polchinski, *Scale and Conformal Invariance in Quantum Field Theory*, *Nucl.Phys.* **B303** (1988) 226.
- [7] V. Riva and J. L. Cardy, *Scale and conformal invariance in field theory: A Physical counterexample*, *Phys. Lett. B* **622** (2005) 339–342, [[hep-th/0504197](#)].
- [8] Y. Nakayama, *Scale invariance vs conformal invariance*, *Physics Reports* **569** (2015) 1–93. Scale invariance vs conformal invariance.
- [9] O. Schnetz, *Numbers and Functions in Quantum Field Theory*, *Phys. Rev. D* **97** (2018), no. 8 085018, [[arXiv:1606.08598](#)].
- [10] K. G. Wilson and M. E. Fisher, *Critical exponents in 3.99 dimensions*, *Phys. Rev. Lett.* **28** (Jan, 1972) 240–243.
- [11] J. Wess and B. Zumino, *A lagrangian model invariant under supergauge transformations*, *Physics Letters B* **49** (1974), no. 1 52–54.
- [12] T. Banks and A. Zaks, *On the phase structure of vector-like gauge theories with massless fermions*, *Nuclear Physics B* **196** (1982), no. 2 189–204.
- [13] L. Onsager, *Crystal statistics. i. a two-dimensional model with an order-disorder transition*, *Phys. Rev.* **65** (Feb, 1944) 117–149.
- [14] A. Polyakov, *Nonhamiltonian approach to conformal quantum field theory*, *Zh.Eksp.Teor.Fiz.* **66** (1974) 23–42.

- [15] S. Ferrara, A. Grillo, and R. Gatto, *Tensor representations of conformal algebra and conformally covariant operator product expansion*, *Annals Phys.* **76** (1973) 161–188.
- [16] A. Belavin, A. M. Polyakov, and A. Zamolodchikov, *Infinite Conformal Symmetry in Two-Dimensional Quantum Field Theory*, *Nucl.Phys.* **B241** (1984) 333–380.
- [17] R. Rattazzi, V. S. Rychkov, E. Tonni, and A. Vichi, *Bounding scalar operator dimensions in 4D CFT*, *JHEP* **0812** (2008) 031, [[arXiv:0807.0004](#)].
- [18] S. El-Showk, M. F. Paulos, D. Poland, S. Rychkov, D. Simmons-Duffin, *et al.*, *Solving the 3D Ising Model with the Conformal Bootstrap*, *Phys.Rev.* **D86** (2012) 025022, [[arXiv:1203.6064](#)].
- [19] F. Kos, D. Poland, D. Simmons-Duffin, and A. Vichi, *Bootstrapping the  $O(N)$  Archipelago*, *JHEP* **11** (2015) 106, [[arXiv:1504.07997](#)].
- [20] F. Kos, D. Poland, D. Simmons-Duffin, and A. Vichi, *Precision Islands in the Ising and  $O(N)$  Models*, *JHEP* **08** (2016) 036, [[arXiv:1603.04436](#)].
- [21] N. B. Agmon, S. M. Chester, and S. S. Pufu, *The M-theory Archipelago*, *JHEP* **02** (2020) 010, [[arXiv:1907.13222](#)].
- [22] R. S. Erramilli, L. V. Iliesiu, P. Kravchuk, A. Liu, D. Poland, and D. Simmons-Duffin, *The Gross-Neveu-Yukawa Archipelago*, [arXiv:2210.02492](#).
- [23] S. M. Chester, W. Landry, J. Liu, D. Poland, D. Simmons-Duffin, N. Su, and A. Vichi, *Carving out OPE space and precise  $O(2)$  model critical exponents*, [arXiv:1912.03324](#).
- [24] A. L. Fitzpatrick, J. Kaplan, D. Poland, and D. Simmons-Duffin, *The Analytic Bootstrap and AdS Superhorizon Locality*, *JHEP* **12** (2013) 004, [[arXiv:1212.3616](#)].
- [25] Z. Komargodski and A. Zhiboedov, *Convexity and Liberation at Large Spin*, *JHEP* **1311** (2013) 140, [[arXiv:1212.4103](#)].
- [26] S. Caron-Huot, *Analyticity in Spin in Conformal Theories*, *JHEP* **09** (2017) 078, [[arXiv:1703.00278](#)].
- [27] S. Hellerman, D. Orlando, S. Reffert, and M. Watanabe, *On the CFT Operator Spectrum at Large Global Charge*, *JHEP* **12** (2015) 071, [[arXiv:1505.01537](#)].
- [28] D. Jafferis, B. Mukhametzhanov, and A. Zhiboedov, *Conformal Bootstrap At Large Charge*, *JHEP* **05** (2018) 043, [[arXiv:1710.11161](#)].
- [29] D. Mazac, *Analytic bounds and emergence of AdS<sub>2</sub> physics from the conformal bootstrap*, *JHEP* **04** (2017) 146, [[arXiv:1611.10060](#)].
- [30] D. Mazac and M. F. Paulos, *The analytic functional bootstrap. Part I: 1D CFTs and 2D S-matrices*, *JHEP* **02** (2019) 162, [[arXiv:1803.10233](#)].
- [31] D. Mazac and M. F. Paulos, *The analytic functional bootstrap. Part II. Natural bases for the crossing equation*, *JHEP* **02** (2019) 163, [[arXiv:1811.10646](#)].

- [32] K. Ghosh, A. Kaviraj, and M. F. Paulos, *Charging up the functional bootstrap*, *JHEP* **10** (2021) 116, [arXiv:2107.00041].
- [33] K. Sen and A. Sinha, *On critical exponents without Feynman diagrams*, *J. Phys. A* **49** (2016), no. 44 445401, [arXiv:1510.07770].
- [34] R. Gopakumar, A. Kaviraj, K. Sen, and A. Sinha, *Conformal Bootstrap in Mellin Space*, *Phys. Rev. Lett.* **118** (2017), no. 8 081601, [arXiv:1609.00572].
- [35] R. Gopakumar, A. Kaviraj, K. Sen, and A. Sinha, *A Mellin space approach to the conformal bootstrap*, *JHEP* **05** (2017) 027, [arXiv:1611.08407].
- [36] P. Dey, K. Ghosh, and A. Sinha, *Simplifying large spin bootstrap in Mellin space*, *JHEP* **01** (2018) 152, [arXiv:1709.06110].
- [37] F. Dolan and H. Osborn, *Superconformal symmetry, correlation functions and the operator product expansion*, *Nucl. Phys. B* **629** (2002) 3–73, [hep-th/0112251].
- [38] C. Beem, M. Lemos, P. Liendo, W. Peelaers, L. Rastelli, and B. C. van Rees, *Infinite Chiral Symmetry in Four Dimensions*, *Commun. Math. Phys.* **336** (2015), no. 3 1359–1433, [arXiv:1312.5344].
- [39] S. M. Chester, J. Lee, S. S. Pufu, and R. Yacoby, *Exact Correlators of BPS Operators from the 3d Superconformal Bootstrap*, *JHEP* **03** (2015) 130, [arXiv:1412.0334].
- [40] J. M. Maldacena, *The Large  $N$  limit of superconformal field theories and supergravity*, *Int. J. Theor. Phys.* **38** (1999) 1113–1133, [hep-th/9711200].
- [41] K. G. Wilson, *Confinement of quarks*, *Phys. Rev. D* **10** (Oct, 1974) 2445–2459.
- [42] G. 't Hooft, *On the Phase Transition Towards Permanent Quark Confinement*, *Nucl. Phys. B* **138** (1978) 1–25.
- [43] A. Kapustin, *Wilson-'t Hooft operators in four-dimensional gauge theories and  $S$ -duality*, *Phys. Rev.* **D74** (2006) 025005, [hep-th/0501015].
- [44] D. Gaiotto, A. Kapustin, N. Seiberg, and B. Willett, *Generalized Global Symmetries*, *JHEP* **02** (2015) 172, [arXiv:1412.5148].
- [45] O. Aharony, N. Seiberg, and Y. Tachikawa, *Reading between the lines of four-dimensional gauge theories*, *JHEP* **08** (2013) 115, [arXiv:1305.0318].
- [46] P. Liendo, L. Rastelli, and B. C. van Rees, *The Bootstrap Program for Boundary  $CFT_d$* , *JHEP* **1307** (2013) 113, [arXiv:1210.4258].
- [47] M. Billò, V. Goncalves, E. Lauria, and M. Meineri, *Defects in conformal field theory*, *JHEP* **04** (2016) 091, [arXiv:1601.02883].
- [48] L. Bianchi, M. Meineri, R. C. Myers, and M. Smolkin, *Rényi entropy and conformal defects*, arXiv:1511.06713.
- [49] E. Lauria, M. Meineri, and E. Trevisani, *Radial coordinates for defect CFTs*, *JHEP* **11** (2018) 148, [arXiv:1712.07668].

- [50] E. Lauria, M. Meineri, and E. Trevisani, *Spinning operators and defects in conformal field theory*, [arXiv:1807.02522](#).
- [51] M. Lemos, P. Liendo, M. Meineri, and S. Sarkar, *Universality at large transverse spin in defect CFT*, *JHEP* **09** (2018) 091, [[arXiv:1712.08185](#)].
- [52] E. Lauria, P. Liendo, B. C. Van Rees, and X. Zhao, *Line and surface defects for the free scalar field*, [arXiv:2005.02413](#).
- [53] F. Gliozzi, P. Liendo, M. Meineri, and A. Rago, *Boundary and Interface CFTs from the Conformal Bootstrap*, *JHEP* **05** (2015) 036, [[arXiv:1502.07217](#)].
- [54] L. Rastelli and X. Zhou, *The Mellin Formalism for Boundary CFT<sub>d</sub>*, *JHEP* **10** (2017) 146, [[arXiv:1705.05362](#)].
- [55] M. de Leeuw, A. C. Ipsen, C. Kristjansen, K. E. Vardinghus, and M. Wilhelm, *Two-point functions in AdS/dCFT and the boundary conformal bootstrap equations*, *JHEP* **08** (2017) 020, [[arXiv:1705.03898](#)].
- [56] A. Bissi, T. Hansen, and A. Söderberg, *Analytic Bootstrap for Boundary CFT*, *JHEP* **01** (2019) 010, [[arXiv:1808.08155](#)].
- [57] A. Kaviraj and M. F. Paulos, *The Functional Bootstrap for Boundary CFT*, [arXiv:1812.04034](#).
- [58] D. Mazac, L. Rastelli, and X. Zhou, *An Analytic Approach to BCFT<sub>d</sub>*, [arXiv:1812.09314](#).
- [59] D. Carmi, L. Di Pietro, and S. Komatsu, *A Study of Quantum Field Theories in AdS at Finite Coupling*, *JHEP* **01** (2019) 200, [[arXiv:1810.04185](#)].
- [60] P. Dey and A. Söderberg, *On analytic bootstrap for interface and boundary CFT*, *JHEP* **07** (2021) 013, [[arXiv:2012.11344](#)].
- [61] P. Dey, T. Hansen, and M. Shpot, *Operator expansions, layer susceptibility and two-point functions in BCFT*, [arXiv:2006.11253](#).
- [62] A. Gimenez-Grau, P. Liendo, and P. van Vliet, *Superconformal boundaries in  $4 - \epsilon$  dimensions*, *JHEP* **04** (2021) 167, [[arXiv:2012.00018](#)].
- [63] S. Giombi, E. Helfenberger, and H. Khanchandani, *Fermions in AdS and Gross-Neveu BCFT*, *JHEP* **07** (2022) 018, [[arXiv:2110.04268](#)].
- [64] T. Nishioka, Y. Okuyama, and S. Shimamori, *Comments on epsilon expansion of the  $O(N)$  model with boundary*, *JHEP* **03** (2023) 051, [[arXiv:2212.04078](#)].
- [65] C. P. Herzog and V. Schaub, *Fermions in boundary conformal field theory: crossing symmetry and  $\epsilon$ -expansion*, *JHEP* **02** (2023) 129, [[arXiv:2209.05511](#)].
- [66] C. P. Herzog and V. Schaub, *The Tilting Space of Boundary Conformal Field Theories*, [arXiv:2301.10789](#).
- [67] J. L. Cardy, *Boundary Conditions, Fusion Rules and the Verlinde Formula*, *Nucl.Phys.* **B324** (1989) 581.

- [68] C. Behan, L. Di Pietro, E. Lauria, and B. C. Van Rees, *Bootstrapping boundary-localized interactions*, [arXiv:2009.03336](#).
- [69] C. Behan, L. Di Pietro, E. Lauria, and B. C. van Rees, *Bootstrapping boundary-localized interactions II. Minimal models at the boundary*, *JHEP* **03** (2022) 146, [[arXiv:2111.04747](#)].
- [70] J. Padayasi, A. Krishnan, M. A. Metlitski, I. A. Gruzberg, and M. Meineri, *The extraordinary boundary transition in the 3d  $O(N)$  model via conformal bootstrap*, [arXiv:2111.03071](#).
- [71] A. Antunes, *Conformal bootstrap near the edge*, *JHEP* **10** (2021) 057, [[arXiv:2103.03132](#)].
- [72] A. Bissi, P. Dey, J. Sisti, and A. Söderberg, *Interacting conformal scalar in a wedge*, *JHEP* **10** (2022) 060, [[arXiv:2206.06326](#)].
- [73] M. Billó, M. Caselle, D. Gaiotto, F. Gliozzi, M. Meineri, and R. Pellegrini, *Line defects in the 3d Ising model*, *JHEP* **07** (2013) 055, [[arXiv:1304.4110](#)].
- [74] D. Gaiotto, D. Mazac, and M. F. Paulos, *Bootstrapping the 3d Ising twist defect*, *JHEP* **1403** (2014) 100, [[arXiv:1310.5078](#)].
- [75] S. Yamaguchi, *The  $\epsilon$ -expansion of the codimension two twist defect from conformal field theory*, *PTEP* **2016** (2016), no. 9 091B01, [[arXiv:1607.05551](#)].
- [76] A. Söderberg, *Anomalous Dimensions in the WF  $O(N)$  Model with a Monodromy Line Defect*, *JHEP* **03** (2018) 058, [[arXiv:1706.02414](#)].
- [77] S. Giombi, E. Helfenberger, Z. Ji, and H. Khanchandani, *Monodromy defects from hyperbolic space*, *JHEP* **02** (2022) 041, [[arXiv:2102.11815](#)].
- [78] A. Gimenez-Grau and P. Liendo, *Bootstrapping Monodromy Defects in the Wess-Zumino Model*, [arXiv:2108.05107](#).
- [79] L. Bianchi, A. Chalabi, V. Procházka, B. Robinson, and J. Sisti, *Monodromy defects in free field theories*, *JHEP* **08** (2021) 013, [[arXiv:2104.01220](#)].
- [80] D. E. Berenstein, R. Corrado, W. Fischler, and J. M. Maldacena, *The Operator product expansion for Wilson loops and surfaces in the large  $N$  limit*, *Phys. Rev. D* **59** (1999) 105023, [[hep-th/9809188](#)].
- [81] A. Allais and S. Sachdev, *Spectral function of a localized fermion coupled to the Wilson-Fisher conformal field theory*, *Phys. Rev.* **B90** (2014), no. 3 035131, [[arXiv:1406.3022](#)].
- [82] A. Allais, *Magnetic defect line in a critical ising bath*, [arXiv:1412.3449](#).
- [83] F. P. Toldin, F. F. Assaad, and S. Wessel, *Critical behavior in the presence of an order-parameter pinning field*, *Physical Review B* **95** (jan, 2017).
- [84] G. Cuomo, Z. Komargodski, and M. Mezei, *Localized magnetic field in the  $O(N)$  model*, *JHEP* **02** (2022) 134, [[arXiv:2112.10634](#)].

- [85] A. Gimenez-Grau, E. Lauria, P. Liendo, and P. van Vliet, *Bootstrapping line defects with  $O(2)$  global symmetry*, *JHEP* **11** (2022) 018, [[arXiv:2208.11715](#)].
- [86] A. Gimenez-Grau, *Probing magnetic line defects with two-point functions*, [arXiv:2212.02520](#).
- [87] L. Bianchi, D. Bonomi, and E. de Sabbata, *Analytic bootstrap for the localized magnetic field*, [arXiv:2212.02524](#).
- [88] T. Nishioka, Y. Okuyama, and S. Shimamori, *The epsilon expansion of the  $O(N)$  model with line defect from conformal field theory*, *JHEP* **03** (2023) 203, [[arXiv:2212.04076](#)].
- [89] S. Giombi, E. Helfenberger, and H. Khanchandani, *Line Defects in Fermionic CFTs*, [arXiv:2211.11073](#).
- [90] W. H. Pannell and A. Stergiou, *Line Defect RG Flows in the  $\varepsilon$  Expansion*, [arXiv:2302.14069](#).
- [91] J. Barrat, P. Liendo, and P. van Vliet, *Line defect correlators in fermionic CFTs*, [arXiv:2304.13588](#).
- [92] A. Cavaglià, N. Gromov, J. Julius, and M. Preti, *Integrability and Conformal Bootstrap: One Dimensional Defect CFT*, [arXiv:2107.08510](#).
- [93] A. Cavaglià, N. Gromov, J. Julius, and M. Preti, *Bootstrability in defect CFT: integrated correlators and sharper bounds*, *JHEP* **05** (2022) 164, [[arXiv:2203.09556](#)].
- [94] A. Cavaglià, N. Gromov, J. Julius, and M. Preti, *Integrated correlators from integrability: Maldacena-Wilson line in  $\mathcal{N} = 4$  SYM*, *JHEP* **04** (2023) 026, [[arXiv:2211.03203](#)].
- [95] A. Gimenez-Grau and P. Liendo, *Bootstrapping line defects in  $\mathcal{N} = 2$  theories*, *JHEP* **03** (2020) 121, [[arXiv:1907.04345](#)].
- [96] M. F. Paulos and B. Zan, *A functional approach to the numerical conformal bootstrap*, *JHEP* **09** (2020) 006, [[arXiv:1904.03193](#)].
- [97] P. Liendo, Y. Linke, and V. Schomerus, *A Lorentzian inversion formula for defect CFT*, [arXiv:1903.05222](#).
- [98] J. Barrat, A. Gimenez-Grau, and P. Liendo, *A dispersion relation for defect CFT*, *JHEP* **02** (2023) 255, [[arXiv:2205.09765](#)].
- [99] L. Bianchi and D. Bonomi, *Conformal dispersion relations for defects and boundaries*, [arXiv:2205.09775](#).
- [100] L. Córdova, Y. He, and M. F. Paulos, *From conformal correlators to analytic  $S$ -matrices:  $CFT_1/QFT_2$* , *JHEP* **08** (2022) 186, [[arXiv:2203.10840](#)].
- [101] Z. Li, *Large  $N$  analytical functional bootstrap I: 1D CFTs and total positivity*, [arXiv:2301.01311](#).

- [102] D. Rodriguez-Gomez, *A scaling limit for line and surface defects*, *JHEP* **06** (2022) 071, [[arXiv:2202.03471](#)].
- [103] M. Trépanier, *Surface defects in the  $O(N)$  model*, [arXiv:2305.10486](#).
- [104] A. Raviv-Moshe and S. Zhong, *Phases of Surface Defects in Scalar Field Theories*, [arXiv:2305.11370](#).
- [105] S. Giombi and B. Liu, *Notes on a Surface Defect in the  $O(N)$  Model*, [arXiv:2305.11402](#).
- [106] S. Gukov and E. Witten, *Gauge Theory, Ramification, And The Geometric Langlands Program*, [hep-th/0612073](#).
- [107] A. Kapustin, K. Setter, and K. Vyas, *Surface Operators in Four-Dimensional Topological Gauge Theory and Langlands Duality*, [arXiv:1002.0385](#).
- [108] P. S. Howe, N. D. Lambert, and P. C. West, *The Selfdual string soliton*, *Nucl. Phys. B* **515** (1998) 203–216, [[hep-th/9709014](#)].
- [109] D. Gaiotto,  *$N=2$  dualities*, *JHEP* **08** (2012) 034, [[arXiv:0904.2715](#)].
- [110] M. F. Paulos, S. Rychkov, B. C. van Rees, and B. Zan, *Conformal Invariance in the Long-Range Ising Model*, [arXiv:1509.00008](#).
- [111] S. Giombi and H. Khanchandani,  *$O(N)$  models with boundary interactions and their long range generalizations*, *JHEP* **08** (2020), no. 08 010, [[arXiv:1912.08169](#)].
- [112] D. Simmons-Duffin, *The Conformal Bootstrap*, in *Proceedings, Theoretical Advanced Study Institute in Elementary Particle Physics: New Frontiers in Fields and Strings (TASI 2015): Boulder, CO, USA, June 1-26, 2015*, pp. 1–74, 2017. [arXiv:1602.07982](#).
- [113] S. Rychkov, *EPFL Lectures on Conformal Field Theory in  $D \leq 3$  Dimensions*. SpringerBriefs in Physics. 2016.
- [114] J. Penedones, *TASI lectures on AdS/CFT*, in *Theoretical Advanced Study Institute in Elementary Particle Physics: New Frontiers in Fields and Strings*, pp. 75–136, 2017. [arXiv:1608.04948](#).
- [115] D. Poland, S. Rychkov, and A. Vichi, *The Conformal Bootstrap: Theory, Numerical Techniques, and Applications*, *Rev. Mod. Phys.* **91** (2019) 015002, [[arXiv:1805.04405](#)].
- [116] P. A. M. Dirac, *Wave equations in conformal space*, *Annals of Mathematics* **37** (1936), no. 2 429–442.
- [117] M. S. Costa, J. Penedones, D. Poland, and S. Rychkov, *Spinning Conformal Correlators*, *JHEP* **1111** (2011) 071, [[arXiv:1107.3554](#)].
- [118] F. Dolan and H. Osborn, *Conformal four point functions and the operator product expansion*, *Nucl. Phys. B* **599** (2001) 459–496, [[hep-th/0011040](#)].

- [119] F. Dolan and H. Osborn, *Conformal partial waves and the operator product expansion*, *Nucl.Phys.* **B678** (2004) 491–507, [[hep-th/0309180](#)].
- [120] H. Kleinert and V. Schulte-Frohlinde, *Critical Properties of  $\phi^4$  theories*. World Scientific Publishing Company Incorporated, 2001.
- [121] E. Brézin, J. C. Le Guillou, and J. Zinn-Justin, *Perturbation theory at large order. i. the  $\varphi^{2N}$  interaction*, *Phys. Rev. D* **15** (Mar, 1977) 1544–1557.
- [122] S. Rychkov and Z. M. Tan, *The  $\epsilon$ -expansion from conformal field theory*, *J. Phys. A* **48** (2015), no. 29 29FT01, [[arXiv:1505.00963](#)].
- [123] J. Henriksson, *The critical  $O(N)$  CFT: Methods and conformal data*, *Phys. Rept.* **1002** (2023) 1–72, [[arXiv:2201.09520](#)].
- [124] W. Landry and D. Simmons-Duffin, *Scaling the semidefinite program solver SDPB*, [arXiv:1909.09745](#).
- [125] S. El-Showk and M. F. Paulos, *Bootstrapping Conformal Field Theories with the Extremal Functional Method*, *Phys. Rev. Lett.* **111** (2013), no. 24 241601, [[arXiv:1211.2810](#)].
- [126] S. El-Showk, M. F. Paulos, D. Poland, S. Rychkov, D. Simmons-Duffin, and A. Vichi, *Solving the 3d Ising Model with the Conformal Bootstrap II. c-Minimization and Precise Critical Exponents*, *J. Stat. Phys.* **157** (2014) 869, [[arXiv:1403.4545](#)].
- [127] M. Reehorst, S. Rychkov, D. Simmons-Duffin, B. Sirois, N. Su, and B. van Rees, *Navigator Function for the Conformal Bootstrap*, *SciPost Phys.* **11** (2021) 072, [[arXiv:2104.09518](#)].
- [128] M. Reehorst, *Rigorous bounds on irrelevant operators in the 3d Ising model CFT*, *JHEP* **09** (2022) 177, [[arXiv:2111.12093](#)].
- [129] M. Hogervorst, S. Rychkov, and B. C. van Rees, *Unitarity violation at the Wilson-Fisher fixed point in  $4-\epsilon$  dimensions*, *Phys. Rev. D* **93** (2016), no. 12 125025, [[arXiv:1512.00013](#)].
- [130] S. El-Showk, M. Paulos, D. Poland, S. Rychkov, D. Simmons-Duffin, and A. Vichi, *Conformal Field Theories in Fractional Dimensions*, *Phys. Rev. Lett.* **112** (2014) 141601, [[arXiv:1309.5089](#)].
- [131] T. Hartman, D. Mazac, D. Simmons-Duffin, and A. Zhiboedov, *Snowmass White Paper: The Analytic Conformal Bootstrap*, in *Snowmass 2021*, 2, 2022. [arXiv:2202.11012](#).
- [132] A. Bissi, A. Sinha, and X. Zhou, *Selected topics in analytic conformal bootstrap: A guided journey*, *Phys. Rept.* **991** (2022) 1–89, [[arXiv:2202.08475](#)].
- [133] S. El-Showk and M. F. Paulos, *Bootstrapping Conformal Field Theories with the Extremal Functional Method*, *Phys. Rev. Lett.* **111** (2013), no. 24 241601, [[arXiv:1211.2810](#)].



- [134] T. Hartman, D. Mazáč, and L. Rastelli, *Sphere Packing and Quantum Gravity*, *JHEP* **12** (2019) 048, [arXiv:1905.01319].
- [135] M. F. Paulos, *Analytic functional bootstrap for CFTs in  $d > 1$* , *JHEP* **04** (2020) 093, [arXiv:1910.08563].
- [136] A. J. Bray and M. Moore, *Critical behaviour of semi-infinite systems*, *Journal of Physics A: Mathematical and General* **10** (1977) 1927.
- [137] M. Isachenkov, P. Liendo, Y. Linke, and V. Schomerus, *Calogero-Sutherland Approach to Defect Blocks*, *JHEP* **10** (2018) 204, [arXiv:1806.09703].
- [138] F. Gliozzi, *More constraining conformal bootstrap*, *Phys.Rev.Lett.* **111** (2013) 161602, [arXiv:1307.3111].
- [139] F. Gliozzi and A. Rago, *Critical exponents of the 3d Ising and related models from Conformal Bootstrap*, *JHEP* **10** (2014) 042, [arXiv:1403.6003].
- [140] G. Cuomo, M. Mezei, and A. Raviv-Moshe, *Boundary conformal field theory at large charge*, *JHEP* **10** (2021) 143, [arXiv:2108.06579].
- [141] S. Coleman and J. Mandula, *All possible symmetries of the  $s$  matrix*, *Phys. Rev.* **159** (Jul, 1967) 1251–1256.
- [142] R. Haag, J. T. Łopuszański, and M. Sohnius, *All possible generators of supersymmetries of the  $s$ -matrix*, *Nuclear Physics B* **88** (1975), no. 2 257–274.
- [143] A. Gadde, S. Gukov, and P. Putrov, *Walls, Lines, and Spectral Dualities in 3d Gauge Theories*, *JHEP* **05** (2014) 047, [arXiv:1302.0015].
- [144] T. Okazaki and S. Yamaguchi, *Supersymmetric boundary conditions in three-dimensional  $N=2$  theories*, *Phys. Rev. D* **87** (2013), no. 12 125005, [arXiv:1302.6593].
- [145] F. Aprile and V. Niarchos,  *$\mathcal{N} = 2$  supersymmetric field theories on 3-manifolds with  $A$ -type boundaries*, *JHEP* **07** (2016) 126, [arXiv:1604.01561].
- [146] T. Dimofte, D. Gaiotto, and N. M. Paquette, *Dual boundary conditions in 3d SCFT's*, *JHEP* **05** (2018) 060, [arXiv:1712.07654].
- [147] S. Sugishita and S. Terashima, *Exact Results in Supersymmetric Field Theories on Manifolds with Boundaries*, *JHEP* **11** (2013) 021, [arXiv:1308.1973].
- [148] Y. Yoshida and K. Sugiyama, *Localization of 3d  $\mathcal{N} = 2$  Supersymmetric Theories on  $S^1 \times D^2$* , arXiv:1409.6713.
- [149] D. McAvity and H. Osborn, *Conformal field theories near a boundary in general dimensions*, *Nucl.Phys.* **B455** (1995) 522–576, [cond-mat/9505127].
- [150] P. Liendo and C. Meneghelli, *Bootstrap equations for  $\mathcal{N} = 4$  SYM with defects*, *JHEP* **01** (2017) 122, [arXiv:1608.05126].
- [151] R. Doobary and P. Heslop, *Superconformal partial waves in Grassmannian field theories*, *JHEP* **12** (2015) 159, [arXiv:1508.03611].

- [152] I. Buric, V. Schomerus, and E. Sobko, *Superconformal Blocks: General Theory*, [arXiv:1904.04852](#).
- [153] I. Burić, V. Schomerus, and E. Sobko, *The Superconformal Xing Equation*, [arXiv:2005.13547](#).
- [154] N. Bobev, S. El-Showk, D. Mazac, and M. F. Paulos, *Bootstrapping SCFTs with Four Supercharges*, *JHEP* **08** (2015) 142, [[arXiv:1503.02081](#)].
- [155] D. J. Binder and S. Rychkov, *Deligne Categories in Lattice Models and Quantum Field Theory, or Making Sense of  $O(N)$  Symmetry with Non-integer  $N$* , *JHEP* **04** (2020) 117, [[arXiv:1911.07895](#)].
- [156] A. Bilal, *Supersymmetric Boundaries and Junctions in Four Dimensions*, *JHEP* **11** (2011) 046, [[arXiv:1103.2280](#)].
- [157] I. Brunner, J. Schulz, and A. Tabler, *Boundaries and supercurrent multiplets in 3D Landau-Ginzburg models*, *JHEP* **06** (2019) 046, [[arXiv:1904.07258](#)].
- [158] C. Cordova, T. T. Dumitrescu, and K. Intriligator, *Multiplets of Superconformal Symmetry in Diverse Dimensions*, *JHEP* **03** (2019) 163, [[arXiv:1612.00809](#)].
- [159] N. Bobev, S. El-Showk, D. Mazac, and M. F. Paulos, *Bootstrapping the Three-Dimensional Supersymmetric Ising Model*, *Phys. Rev. Lett.* **115** (2015), no. 5 051601, [[arXiv:1502.04124](#)].
- [160] M. Baggio, N. Bobev, S. M. Chester, E. Lauria, and S. S. Pufu, *Decoding a Three-Dimensional Conformal Manifold*, *JHEP* **02** (2018) 062, [[arXiv:1712.02698](#)].
- [161] C. P. Herzog and A. Shrestha, *Two Point Functions in Defect CFTs*, [arXiv:2010.04995](#).
- [162] M. Cornagliotto, M. Lemos, and V. Schomerus, *Long Multiplet Bootstrap*, *JHEP* **10** (2017) 119, [[arXiv:1702.05101](#)].
- [163] N. Bobev, E. Lauria, and D. Mazac, *Superconformal Blocks for SCFTs with Eight Supercharges*, *JHEP* **07** (2017) 061, [[arXiv:1705.08594](#)].
- [164] A. Kaviraj, S. Rychkov, and E. Trevisani, *Random Field Ising Model and Parisi-Sourlas supersymmetry. Part I. Supersymmetric CFT*, *JHEP* **04** (2020) 090, [[arXiv:1912.01617](#)].
- [165] A. Kaviraj, S. Rychkov, and E. Trevisani, *Random Field Ising Model and Parisi-Sourlas Supersymmetry II. Renormalization Group*, [arXiv:2009.10087](#).
- [166] D. Poland and D. Simmons-Duffin, *Bounds on 4D Conformal and Superconformal Field Theories*, *JHEP* **05** (2011) 017, [[arXiv:1009.2087](#)].
- [167] F. A. Dolan and H. Osborn, *On short and semi-short representations for four-dimensional superconformal symmetry*, *Annals Phys.* **307** (2003) 41–89, [[hep-th/0209056](#)].

- [168] N. B. Agmon and Y. Wang, *Classifying Superconformal Defects in Diverse Dimensions Part I: Superconformal Lines*, [arXiv:2009.06650](#).
- [169] S. Giombi and H. Khanchandani, *CFT in AdS and boundary RG flows*, [arXiv:2007.04955](#).
- [170] L. F. Alday, J. Henriksson, and M. van Loon, *Taming the  $\epsilon$ -expansion with large spin perturbation theory*, *JHEP* **07** (2018) 131, [[arXiv:1712.02314](#)].
- [171] V. Procházka and A. Söderberg, *Composite operators near the boundary*, *JHEP* **03** (2020) 114, [[arXiv:1912.07505](#)].
- [172] L. F. Alday, *Solving CFTs with Weakly Broken Higher Spin Symmetry*, *JHEP* **10** (2017) 161, [[arXiv:1612.00696](#)].
- [173] S.-S. Lee, *Emergence of supersymmetry at a critical point of a lattice model*, *Phys. Rev. B* **76** (2007) 075103, [[cond-mat/0611658](#)].
- [174] L. Fei, S. Giombi, I. R. Klebanov, and G. Tarnopolsky, *Yukawa CFTs and Emergent Supersymmetry*, *PTEP* **2016** (2016), no. 12 12C105, [[arXiv:1607.05316](#)].
- [175] P. Townsend and P. van Nieuwenhuizen, *Dimensional Regularization and Supersymmetry at the Two Loop Level*, *Phys. Rev. D* **20** (1979) 1832.
- [176] C. P. Herzog, K.-W. Huang, I. Shamir, and J. Virrueta, *Superconformal Models for Graphene and Boundary Central Charges*, *JHEP* **09** (2018) 161, [[arXiv:1807.01700](#)].
- [177] H. Diehl, *Why boundary conditions do not generally determine the universality class for boundary critical behavior*, *Eur. Phys. J. B* **93** (2020), no. 10 195, [[arXiv:2006.15425](#)].
- [178] D. McAvity, *Integral transforms for conformal field theories with a boundary*, *J. Phys. A* **28** (1995) 6915–6930, [[hep-th/9507028](#)].
- [179] M. Shpot, *Boundary conformal field theory at the extraordinary transition: The layer susceptibility to  $O(\epsilon)$* , [arXiv:1912.03021](#).
- [180] C. P. Herzog and N. Kobayashi, *The  $O(N)$  model with  $\phi^6$  potential in  $\mathbb{R}^2 \times \mathbb{R}^+$* , *JHEP* **09** (2020) 126, [[arXiv:2005.07863](#)].
- [181] E. Eisenriegler and M. Stapper, *Critical behavior near a symmetry-breaking surface and the stress tensor*, *Phys. Rev. B* **50** (Oct, 1994) 10009–10026.
- [182] P. Liendo, C. Meneghelli, and V. Mitev, *Bootstrapping the half-BPS line defect*, *JHEP* **10** (2018) 077, [[arXiv:1806.01862](#)].
- [183] C. Behan, *Bootstrapping the long-range Ising model in three dimensions*, *J. Phys. A* **52** (2019), no. 7 075401, [[arXiv:1810.07199](#)].
- [184] N. Kobayashi and T. Nishioka, *Spinning conformal defects*, [arXiv:1805.05967](#).

- [185] C. P. Herzog and A. Shrestha, *Conformal surface defects in Maxwell theory are trivial*, *JHEP* **08** (2022) 282, [arXiv:2202.09180].
- [186] F. Dolan and H. Osborn, *Conformal Partial Waves: Further Mathematical Results*, arXiv:1108.6194.
- [187] F. Kos, D. Poland, and D. Simmons-Duffin, *Bootstrapping Mixed Correlators in the 3D Ising Model*, *JHEP* **11** (2014) 109, [arXiv:1406.4858].
- [188] D. Poland, D. Simmons-Duffin, and A. Vichi, *Carving Out the Space of 4D CFTs*, *JHEP* **05** (2012) 110, [arXiv:1109.5176].
- [189] A. L. Fitzpatrick and J. Kaplan, *Unitarity and the Holographic S-Matrix*, *JHEP* **10** (2012) 032, [arXiv:1112.4845].
- [190] M. Lemos and P. Liendo, *Bootstrapping  $\mathcal{N} = 2$  chiral correlators*, *JHEP* **01** (2016) 025, [arXiv:1510.03866].
- [191] F. Parisen Toldin, F. F. Assaad, and S. Wessel, *Critical behavior in the presence of an order-parameter pinning field*, *prb* **95** (Jan., 2017) 014401, [arXiv:1607.04270].
- [192] A. Allais, *Magnetic defect line in a critical Ising bath*, arXiv:1412.3449.
- [193] E. Panzer, *On hyperlogarithms and Feynman integrals with divergences and many scales*, *JHEP* **03** (2014) 071, [arXiv:1401.4361].
- [194] E. Panzer, *Feynman integrals and hyperlogarithms*. PhD thesis, Humboldt U., 2015. arXiv:1506.07243.
- [195] E. Panzer, *Algorithms for the symbolic integration of hyperlogarithms with applications to Feynman integrals*, *Comput. Phys. Commun.* **188** (2015) 148–166, [arXiv:1403.3385].
- [196] D. Simmons-Duffin, *A semidefinite program solver for the conformal bootstrap*, *JHEP* **06** (2015) 174, [arXiv:1502.02033].
- [197] B. Roy, V. Juričić, and I. F. Herbut, *Quantum superconducting criticality in graphene and topological insulators*, *Physical Review B* **87** (jan, 2013).
- [198] D. J. Gross and A. Neveu, *Dynamical Symmetry Breaking in Asymptotically Free Field Theories*, *Phys. Rev. D* **10** (1974) 3235.
- [199] D. J. Gross, *Applications of the Renormalization Group to High-Energy Physics*, *Conf. Proc. C* **7507281** (1975) 141–250.
- [200] A. Hasenfratz, P. Hasenfratz, K. Jansen, J. Kuti, and Y. Shen, *The Equivalence of the top quark condensate and the elementary Higgs field*, *Nucl. Phys. B* **365** (1991) 79–97.
- [201] J. Zinn-Justin, *Four fermion interaction near four-dimensions*, *Nucl. Phys. B* **367** (1991) 105–122.

- [202] T. Grover, D. N. Sheng, and A. Vishwanath, *Emergent Space-Time Supersymmetry at the Boundary of a Topological Phase*, *Science* **344** (2014), no. 6181 280–283, [arXiv:1301.7449].
- [203] Y. Nambu and G. Jona-Lasinio, *Dynamical Model of Elementary Particles Based on an Analogy with Superconductivity. 1.*, *Phys. Rev.* **122** (1961) 345–358.
- [204] L. Janssen and I. F. Herbut, *Antiferromagnetic critical point on graphene’s honeycomb lattice: A functional renormalization group approach*, *Phys. Rev. B* **89** (2014) 205403, [arXiv:1402.6277]. [Addendum: *Phys.Rev.B* 102, 199902 (2020)].
- [205] J. A. Gracey, *Large  $N$  critical exponents for the chiral Heisenberg Gross-Neveu universality class*, *Phys. Rev. D* **97** (2018), no. 10 105009, [arXiv:1801.01320].
- [206] N. Zerf, L. N. Mihaila, P. Marquard, I. F. Herbut, and M. M. Scherer, *Four-loop critical exponents for the Gross-Neveu-Yukawa models*, *Phys. Rev. D* **96** (2017), no. 9 096010, [arXiv:1709.05057].
- [207] L. Karkkainen, R. Lacaze, P. Lacock, and B. Petersson, *Critical behavior of the three-dimensional Gross-Neveu and Higgs-Yukawa models*, *Nucl. Phys. B* **415** (1994) 781–796, [hep-lat/9310020]. [Erratum: *Nucl.Phys.B* 438, 650–650 (1995)].
- [208] B. Rosenstein, H.-L. Yu, and A. Kovner, *Critical exponents of new universality classes*, *Phys. Lett. B* **314** (1993) 381–386.
- [209] I. F. Herbut, V. Juričić, and O. Vafek, *Relativistic mott criticality in graphene*, *Phys. Rev. B* **80** (Aug, 2009) 075432.
- [210] H. H. Patel, *Package-X 2.0: A Mathematica package for the analytic calculation of one-loop integrals*, *Comput. Phys. Commun.* **218** (2017) 66–70, [arXiv:1612.00009].
- [211] M. Go and Y. Tachikawa, *autoboot: A generator of bootstrap equations with global symmetry*, *JHEP* **06** (2019) 084, [arXiv:1903.10522].
- [212] S. M. Chester, W. Landry, J. Liu, D. Poland, D. Simmons-Duffin, N. Su, and A. Vichi, *Bootstrapping Heisenberg magnets and their cubic instability*, *Phys. Rev. D* **104** (2021), no. 10 105013, [arXiv:2011.14647].
- [213] J. Barrat, I. Buric, P. Liendo, V. Schomerus, and P. van Vliet, *Work in progress*.
- [214] O. Aharony, G. Cuomo, Z. Komargodski, M. Mezei, and A. Raviv-Moshe, *Phases of Wilson Lines in Conformal Field Theories*, *Phys. Rev. Lett.* **130** (2023), no. 15 151601, [arXiv:2211.11775].
- [215] I. Burić and V. Schomerus, *Defect Conformal Blocks from Appell Functions*, *JHEP* **05** (2021) 007, [arXiv:2012.12489].
- [216] J. Barrat, P. Liendo, G. Peveri, and J. Plefka, *Multipoint correlators on the supersymmetric Wilson line defect CFT*, *JHEP* **08** (2022) 067, [arXiv:2112.10780].

- [217] J. Barrat, P. Liendo, and G. Peveri, *Multipoint correlators on the supersymmetric Wilson line defect CFT II: Unprotected operators*, [arXiv:2210.14916](#).
- [218] J. Chen and X. Zhou, *Aspects of higher-point functions in BCFT<sub>d</sub>*, [arXiv:2304.11799](#).
- [219] E. D'Hoker, D. Z. Freedman, S. D. Mathur, A. Matusis, and L. Rastelli, *Graviton exchange and complete four point functions in the AdS / CFT correspondence*, *Nucl. Phys. B* **562** (1999) 353–394, [[hep-th/9903196](#)].
- [220] H. Liu and A. A. Tseytlin, *On four point functions in the CFT / AdS correspondence*, *Phys. Rev. D* **59** (1999) 086002, [[hep-th/9807097](#)].
- [221] E. Hijano, P. Kraus, E. Perlmutter, and R. Snively, *Witten Diagrams Revisited: The AdS Geometry of Conformal Blocks*, *JHEP* **01** (2016) 146, [[arXiv:1508.00501](#)].
- [222] C. B. Jepsen and S. Parikh, *Propagator identities, holographic conformal blocks, and higher-point AdS diagrams*, *JHEP* **10** (2019) 268, [[arXiv:1906.08405](#)].
- [223] N. I. Usyukina and A. I. Davydychev, *New results for two loop off-shell three point diagrams*, *Phys. Lett. B* **332** (1994) 159–167, [[hep-ph/9402223](#)].
- [224] N. I. Usyukina and A. I. Davydychev, *Two loop three point diagrams with irreducible numerators*, *Phys. Lett. B* **348** (1995) 503–512, [[hep-ph/9412356](#)].
- [225] B. Eden, P. S. Howe, C. Schubert, E. Sokatchev, and P. C. West, *Four point functions in N=4 supersymmetric Yang-Mills theory at two loops*, *Nucl. Phys. B* **557** (1999) 355–379, [[hep-th/9811172](#)].
- [226] B. Eden, P. S. Howe, C. Schubert, E. Sokatchev, and P. C. West, *Simplifications of four point functions in N=4 supersymmetric Yang-Mills theory at two loops*, *Phys. Lett. B* **466** (1999) 20–26, [[hep-th/9906051](#)].